Final Report

DESIGN AND PERFORMANCE EVALUATION OF A WIDEBAND FM SPREAD-SPECTRUM MULTIPLE-ACCESS SYSTEM

By

Richard H. Wachsman and Dr. Ahmad F. Ghais

July 1971

Prepared Under

Contract No. NAS5-20225

For

Goddard Space Flight Center
National Aeronautics and Space Administration
Greenbelt, Maryland 20771

ADVANCED INFORMATION PROCESSING

COMMUNICATIONS • DATA ACQUISITION • SIMULATION

TELEDYNE ADCOM

808 Memorial Drive Cambridge, Massachusetts 02139 Telephone: (617) 868-1000 TWX 710 320 0586

1. Report No.	2. Government Accession No.	3. Recipient's Catalog No.

4. Title and Subtitle
DESIGN AND PERFORMANCE EVALUATION OF A WIDEBAND FM SPREAD-SPECTRUM MULTIPLE-ACCESS SYSTEM

5. Report Date
July 1971

6. Performing Organization Code

7. Author(s)
Richard H. Wachsman & Dr. Ahmad F. Ghais

8. Performing Organization Report No.
G-181-F

9. Performing Organization Name and Address
Teledyne ADCOM
808 Memorial Drive
Cambridge, Massachusetts 02139

10. Work Unit No.

11. Contract or Grant No.
NAS5-20225

12. Sponsoring Agency Name and Address
Goddard Space Flight Center
National Aeronautics & Space Administration
Greenbelt, Maryland 20771(see 15):Monitor

13. Type of Report and Period Covered
Final Report
3/71 - 7/71

14. Sponsoring Agency Code

15. Supplementary Notes
Technical Officer: Howard Kingman, Code 813.2

16. Abstract

The system described performs the tracking and communications functions of a Tracking and Data Relay Satellite System (TDRS). The spread-spectrum signal format is achieved through wide deviation FM by a sinusoidal subcarrier unique to each multiple-access User. A compound phase-locked loop tracks carrier and subcarrier and demodulates data and ranging signals. Design parameters of User and ground terminals for TDRS are given. Acquisition procedures are described. Performance analyses are presented including the effects of noise, RFI, multipath and other Users.

17. Key Words (Selected by Author(s))	18. Distribution Statement
Tracking and Data Relay Satellite Spread-Spectrum, Multiple-Access Compound Phase-Locked Loop Multipath, Tracking	

19. Security Classif. (of this report)	20. Security Classif. (of this page)	21. No. of Pages	22. Price*
Unclassified	Unclassified	204	

TABLE OF CONTENTS

TABLE OF CONTENTS (Continued)

TABLE OF CONTENTS (Continued)

LIST OF ILLUSTRATIONS

LIST OF TABLES

1. INTRODUCTION AND SUMMARY

1.1 Introduction

This report comprises the Final Report covering studies performed under Contract NAS5-20225 for NASA/Goddard Space Flight Center, Greenbelt, Maryland. The scope and requirements of this study are defined in the contract work statement, which is reproduced below for reference.

(a) Scope: The objective of this contract is to design a wideband FM communication system for the Tracking and Data Relay System and to analytically determine its performance. Of the several varieties of wideband FM schemes discussed in the pertinent documents listed below, the most promising approach is to be selected.

(b) Pertinent Documents: The reports generated by ADCOM under contract NAS5-10797 are groundwork for performance under this contract.

(c) Requirements: This communication system encompasses both the up-link and down-link functions of tracking, command and telemetry between a ground terminal and VHF User spacecraft. For the purpose of this study, the TDRS Spacecraft can be considered to operate according to the "bent pipe" principle; therefore, design of such receiving and signal handling operations can be omitted. Other system functions, common to any TDRS system, such as RF transmit and receive, data coders and decoders, etc., can likewise be ignored.

The following parameters are fixed for the low data rate (VHF) TDRS communications.

1. Minimum effective on-axis TDRS antenna gain ... 16 dB.
2. User Antenna Gain ... 0 dB.
3. Down-link data rate ... 1 kb/s.
4. Up-link data rate ... 100 b/s per spacecraft (4 commands simultaneously requires 400 b/sec.)
5. Assume noiseless and interference free communications between TDRS and ground.

6. Down-link telemetry and ranging multiple access ... operations on 30 User spacecraft simultaneously (fewer than 30 might also be considered if appropriate). As many as 50 Users can be in view of the TDRS at one time.

7. Up-link multiple access command and ranging ... Command 4 User spacecraft simultaneously in the presence of R&R signal.

8. Down-link frequency band ... 2 MHz; 136 MHz to 138 MHz

9. Up-link frequency band ... Assume two MHz band at 150 MHz.

10. RFI and multipath environment ... As prescribed in the latest GSFC and ADCOM studies that exists just prior to the work on this task. The multipath and RFI models assumed shall be quantitatively described.

11. Down-link communication accuracy ... BER = 10^{-6}.

12. Up-link communication accuracy ... BER = 10^{-6}.

13. Tolerable link outage ... In the interest of achieving a feasible TDRS system a finite link outage probability will be tolerated. Total link failure shall not exceed 1 % in terms of time or 36 second out of each hour of operation. The outages on any particular User shall be less than 5 % or 3 minutes out of each hour. An outage is defined as that period of time a link operates below specifications and includes the period one minute after the outage ceases. This last requirement is included because data intervals of less than one minute have reduced value.

14. Acquisition time, ground and User ... 10 seconds maximum.

15. Location of User spacecraft ... randomly distributed, heights from 100 miles to 5,000 miles.

16. Range determination uncertainty ... less than 15 meters.

17. Range acquisition time ... less than 16 seconds.

18. Unambiguous range determinations ... less than 10,000 miles.

19. Range rate determination accuracy ... less than 10 cm/sec with an observation period of 1.0 seconds.

The results of the analysis shall determine:

1. Required User transmitter power.
2. Required TDRS transmitter power.
3. Margins of 1 and 2 based upon probability of RFI and Multipath.

1.2 Modulation Techniques for Spread-Spectrum Multiple-Access

Radio communication links between the TDRS and the User spacecraft will suffer from Multipath and radio frequency interferences. To combat these interferences it has been suggested that spread-spectrum signals be utilized on both the uplink and downlink. Spread-spectrum signals have the further benefit of enabling spread-spectrum multiple-access operation of the tracking and data relay system. Thus, the increased spectrum occupancy requirements of such signals would be at least partly offset by the ability to communicate simultaneously with several User spacecrafts over the same wideband channel.

Of the four types of spread-spectrum signals, namely:

- Pseudo-noise phase-modulated carrier,
- Frequency-hopping signal,
- Adaptive pulse burst,
- Wideband frequency-modulated carrier,

the latter has seen the least use in multiple-access applications. Under Contract NAS5-10797 for NASA/GSFC, Teledyne ADCOM has evolved several forms of a multiple-access system concept utilizing wideband FM signals for the TDRS application. The present study serves to identify and describe the design and performance of the most promising form of this system concept.

The wideband FM spread-spectrum multiple-access system was designed to provide the advantages of spread-spectrum techniques while exploiting the inherent narrowband nature of the information-bearing signals,

and without suffering certain disadvantages which often accompany spread-spectrum techniques.

1.3 The Wideband-FM Multiple-Access System

The wideband FM system studied in this report performs the functions of:

1. command data link from DAF to User,
2. telemetry data link from User to DAF,
3. multiple access to any one of several TDRS uplink signals by the User,
4. multiple access to any or all User downlink signals by the DAF,
5. two-way range and range rate measurement capability, and
6. resistance to RFI, multipath, and SSMA interference.

The data on both the uplink and the downlink are split-phase coded and PM modulated directly on the carrier with a deviation of 1 radian. Ranging is performed by utilizing sinusoidal range tones which PM modulate the uplink carrier. These tones are turned around in the User transponder and PM modulated on the coherently transponded downlink carrier. The highest frequency range tone is at 102.4 kHz. Three ambiguity resolution range tones at 6.4 kHz, 400 Hz, and 25 Hz provide ambuiguity resolution down to 12,000 kilometers. This is more than adequate for the TDRS application.

The uplink carrier is wideband FM modulated by a sinusoidal subcarrier whose frequency is selected to lie between 108 kHz and 136 kHz, such that the 4th and 5th order upper sidebands lie in relatively RFI-free portions of the uplink spectrum. The 4th order sideband will lie somewhere between 432 kHz and 544 kHz above the carrier frequency, and the 5th order sideband will correspondingly lie between 540 kHz and 680 kHz above the carrier frequency.

The width of the band of the spectrum which must be free of RFI is ±8 kHz about the 4th and 5th order sidebands. Condequently, it should be relatively easy to either find such bands or else create them by forcing certain RFI sources off the air. These RFI-free bands assure reliable acquisition of the wideband FM signal on the uplink. Once the signal is acquired, wideband FM compression in the User receiver provides processing gain against other RFI sources and multipath interference. The fact that only a relatively small fraction of the uplink RF bandwidth need be free of RFI in order to assure reliable acquisition is one of the advantages of the wideband FM spread-spectrum technique.

Identification of a particular TDRS transmission is achieved by assigning a unique subcarrier frequency to each TDRS. On the other hand, identification of a particular User transmission is achieved by assigning a unique combination of subcarrier and carrier frequencies to each User spacecraft. There are ten primary and ten auxiliary subcarrier frequencies to choose from, located in the range 110 - 141 kHz spaced by 3.2 kHz. Each User generates its own downlink subcarrier frequency independent of any uplink frequencies. There are three carrier frequencies (lower, middle and upper carrier bands), spaced by 25.6 kHz. Thus the number of simultaneous Users is, respectively, 60 and 30, according to whether or not the auxiliary subcarrier frequencies are used.

The modulation index is chosen to be 5.52 radians. This value of δ is a zero of $J_0(\delta)$, and means that there will be no discrete-carrier component in either the uplink or downlink RF spectrum. It also yields relatively high 4th and 5th order sidebands which are useful for acquisition. Finally, only sidebands up to sixth order need be transmitted with this value of modulation index.

A compound phase-locked loop is utilized in both the User and ground receivers, in which the subcarrier and the carrier are tracked. The tracked subcarrier is used to FM modulate the tracked carrier so as to generate a

wideband FM reference signal which is used to multiply the RF input signal in the input mixer. The modulation index is chosen so as to provide full compression of the wideband FM subcarrier at the output of this mixer. The actual receiver implementation utilizes a PM modulator followed by a frequency multiplier to achieve the proper modulation index.

Additional signal processing is performed by the ground receiver. The range measurement is performed by comparing the returned range and ambiguity tones against the original transmitted tones. The range rate measurement is performed on the coherent downlink carrier by comparison to the uplink carrier.

1.4 Summary of Results

The narrowband nature of the information-bearing signals in the TDRS system may be appreciated from the following observations:

1. The data bit rates are relatively small on both the forward (uplink) and the return (downlink) links, being either 100 BPS (normal mode) or 400 BPS (high data rate mode) on the uplink, and 1000 BPS on the downlink. These rates, particularly on the uplink, are low, compared to such parameters as the direct-path carrier doppler range, the relative multipath carrier doppler, the doppler dynamics between the User and earth-based RFI sources, and the bandwidth of narrowband earth-based RFI.
2. The range rate is determined by coherently transponding the carrier component. This carrier component is tracked by a phase-locked loop whose noise bandwidth is small (9 Hz on the uplink and 12.2 Hz on the downlink, single-sided) compared to the above-mentioned parameters.
3. Range measurements are performed with a set of coherently related sinusoidal range tones. These tones are tracked in very narrowband phase-locked loops.

The advantages of the narrowband nature of the information bearing signals is that straightforward filtering in the frequency domain may be used to combat multipath and RFI interference, provided that the receiver can lock up to the desired direct-path carrier. The wideband FM spread-spectrum

technique is ideally suited for this purpose. This technique also has the added advantage of providing simple multiple access capability while at the same time minimizing the effects of other-User interference - the so-called SSMA interference or system self-noise.

Unlike other spread-spectrum techniques which often suffer from

1. problems of acquisition,
2. susceptibility to any and all interference sources in the RF bandwidth,
3. cumulative effects of all interference sources in the RF band,
4. non-independence of the functions of data transmission ranging, and spread-spectrum, often to the detriment of each,
5. complex receiver implementation, particularly on board the User, and
6. constraints which reduce the flexibility of system modifications and improvements,

the wideband FM technique offers

1. relatively simple, reliable, and fast acquisition,
2. susceptibility to only a small fraction of the interference sources present in the RF bandwidth at any particular instant,
3. non-cumulative effects of interference sources except in certain rare situations,
4. processing gain against any and all interference sources,
5. relatively simple receiver implementation both on the User and on the ground,
6. the ability to separate the ranging, data, and spread-spectrum functions so that each may be optimized almost independently of the others, and
7. a flexibility in signal and receiver design which permits improvements in signal design and receiver implementation to be made with a minimum of interaction between the various communications functions, and which require a minimum of recomputation of system performance.

This last feature of the wideband FM technique permits changes in system requirements to be readily incorporated into the system design without the necessity of having to recompute all aspects of system performance. This is one feature of the wideband-FM spread-spectrum technique whose importance cannot be overestimated. In fact, several modifications were made in the system design during the present study which provided improved performance in one area or another without requiring extensive recalculations. In particular, improvements in the range turnaround channel were made in the noise analysis of Sec. 4, with additional improvements suggested in the improved system concept described in Appendix D.

The results of an additive noise analysis indicate that on both the uplink and the downlink the data bit error probability requirements set the threshold on signal-to-noise power density ratio. In addition, since the data is the widest bandwidth information signal, it is also the communications function most susceptible to multipath, SSMA, and RFI interference. The improved system concept described in Appendix D offers reduced susceptibility of the data to multipath, SSMA, and RFI interference and is an outgrowth of the analysis of the wideband FM system described in Sec. 2 and analyzed in Secs. 4, 5, 6, 7 and 8. The performance of this modified system may be readily analyzed by making minor modifications of the analyses presented in the above-mentioned sections of this report.

Analysis of CW interference effects indicates system susceptibility only when the RFI is located in certain narrow regions of the RF band. The system still has a moderate processing gain under these conditions, but the important result is that this "worst case" condition persists only for very short time intervals. This is because the doppler rate as observed at the User spacecraft on the terrestrial RFI is very different from that observed on the desired signal originating at the TDRS. Thus, the RFI will fall in the " worst" regions of the band relative to the desired signal components only for short periods, then will rapidly sweep off to be filtered out by various filters.

Again, the system is susceptible to narrowband RFI only when it is located in certain narrow regions of the RF band. The system has substantial processing gain under these conditions, enhanced by the ability to filter out large portions of the narrowband RFI spectrum that do not fall within the narrow regions of the RF band.

The multiple-access features of the system were specifically designed to minimize SSMA. Even under "worst case" conditions determined by various doppler shifts, it is not expected that more than one User will significantly interfere with another User. In this case, the system has sufficient processing gain to combat the resulting SSMA interference, for all reasonable ratios of received User signal powers.

Finally, multipath interference is rejected by similar mechanisms. Realtive doppler shifts of any appreciable magnitude are exploited to filter out the multipath interference. When the relative doppler is too low to permit filtering, the doppler rate is large causing this unfavorable condition to last only short intervals of time. The system still has a moderate processing gain, enhanced in the case of diffuse multipath by the ability to filter out portions of the multipath interference that does not fall within the "worst" narrow regions of the RF band.

1.5 Conclusions and Recommendations

The wideband FM system is a form of spread-spectrum multiple-access system employing wide-deviation sinusoidal subcarriers to achieve the desired-spectrum spreading. The concept encompasses the functions of tracking, command and telemetry, and is capable of accommodating many User spacecrafts and three or four relay satellites.

Analysis has indicated superior system performance in combatting the expected sources of disturbance, including random noise, multipath, RF interference, and interferences from other User spacecrafts or other relay satellites. Furthermore, the system concept offers many deployment and

operational advantages, such as flexibility in assignment of channels among different Users, and ease of handover from one relay satellite to another. Wideband FM is a highly effective and flexible approach to implementing the TDRS communications and tracking functions.

It is essential for GSFC to thoroughly evaluate the candidate TDRS system concepts prior to adoption of a specific approach for hardware implementation. Such evaluation includes paper design and performance evaluation of the concepts to meet practical requirements under the same ground rules.

The present study fulfills this requirement for the wideband FM system concept. However, we wish to emphasize that definite evaluation and comparison of candidate system concepts must be based, not only on paper design and analytical predictions of performance, but also and more importantly on experimental evaluations. Only an experimental evaluation can uncover the practical advantages and limitations of a given system concept.

Consequently, we strongly recommend that GSFC initiate an experimental evaluation program of the wideband FM system concept. Such a comprehensive program would yield, in a timely manner, sufficient information for a well-founded decision on the merits of the wideband FM system vis-a-vis other candidate concepts. Experimental evaluation of the wideband FM system is now urgently needed, in view of the on-going laboratory evaluation of other candidate concepts.

2. SYSTEM DESIGN

2.1 Wideband FM Spread-Spectrum Multiple-Access Techniques

The basic signal format used in this system concept, both on the uplink and the downlink, is as follows:

a) Ranging information is carried in a cluster of range tones designed to yield the desired range measurement accuracy and ambiguity resolution.

b) Data, viz., commands on the uplink and telemetry on the downlink, is carried by a split-phase signal which, along with the ranging sidetones, phase-modulates the carrier.

c) Spectrum-spreading is accomplished by frequency-modulating the VHF carrier by a sinusoidal subcarrier using a wide frequency deviation (modulation index = 5.52).

d) Identification of a particular TDRS transmission on the uplink is achieved by assigning a unique subcarrier frequency to that TDRS. Identification of a particular User spacecraft transmission on the downlink is achieved by assigning a unique combination of one of ten (primary) subcarrier frequencies and one of three carrier frequencies (lower, middle, and upper carrier bands). Auxiliary subcarrier frequency slots are available to increase the number of simultaneous Users to 60.

Straightforward means for accomplishing these modulation operations have been evolved, but their discussion will be deferred until Sec. 2.3.3.

Reception and separation of a desired signal in the presence of other wideband FM signals is based on utilizing the unique combination of carrier and subcarrier frequencies characterizing it. A compound phase-locked loop receiver, to be described shortly, locks on to both the carrier and the subcarrier by fully compressing the subcarrier modulation on the desired signal. Undesired interference components such as other wideband FM signals, multipath, or RFI disturbances are reduced in amplitude and

spread in spectrum by this wideband FM compression operation, thereby reducing their effects on receiver operation. In this manner, the spread-spectrum multiple-access advantage is realized in achieving disturbance-resistant communications with several User spacecrafts on the same frequency band.

2.2 System Configuration

The system configuration is described first for the simplified situation of a single User and a single TDRS. Figure 2.1 illustrates this situation. At the ground station data acquisition facility (DAF), the VHF signal is generated, modulated with the command data, then translated up to X-band for transmission to the TDRS. All frequencies, including the range tones, are obtained from the station master clock and frequency synthesizer. The TDRS operates on the received X-band signal according to the bent-pipe principle, coherently translating it back down to VHF for relay to the User spacecraft.

At the User transponder receiver, the compound phase-locked loop locks onto the carrier and the subcarrier, and yield the split-phase command signal for detection in the command extractor. The extracted uplink carrier frequency is multiplied in the transponder transmitter by the turnaround ratio (23/25) to generate the coherent downlink carrier. A new subcarrier for the downlink signal is generated by the transponder clock and frequency synthesizer. Thus the downlink subcarrier is not maintained coherent with the uplink subcarrier. The uplink range-tone cluster is filtered prior to remodulation on the downlink signal. The transponder transmitter combines the telemetry data, filtered range tones, subcarrier and turnaround carrier to generate the downlink VHF signal.

On the downlink the TDRS again operates on the bent-pipe principle to coherently translate the received VHF signal up to X-band for relay to the DAF. At the DAF the received X-band signal is translated back down to VHF

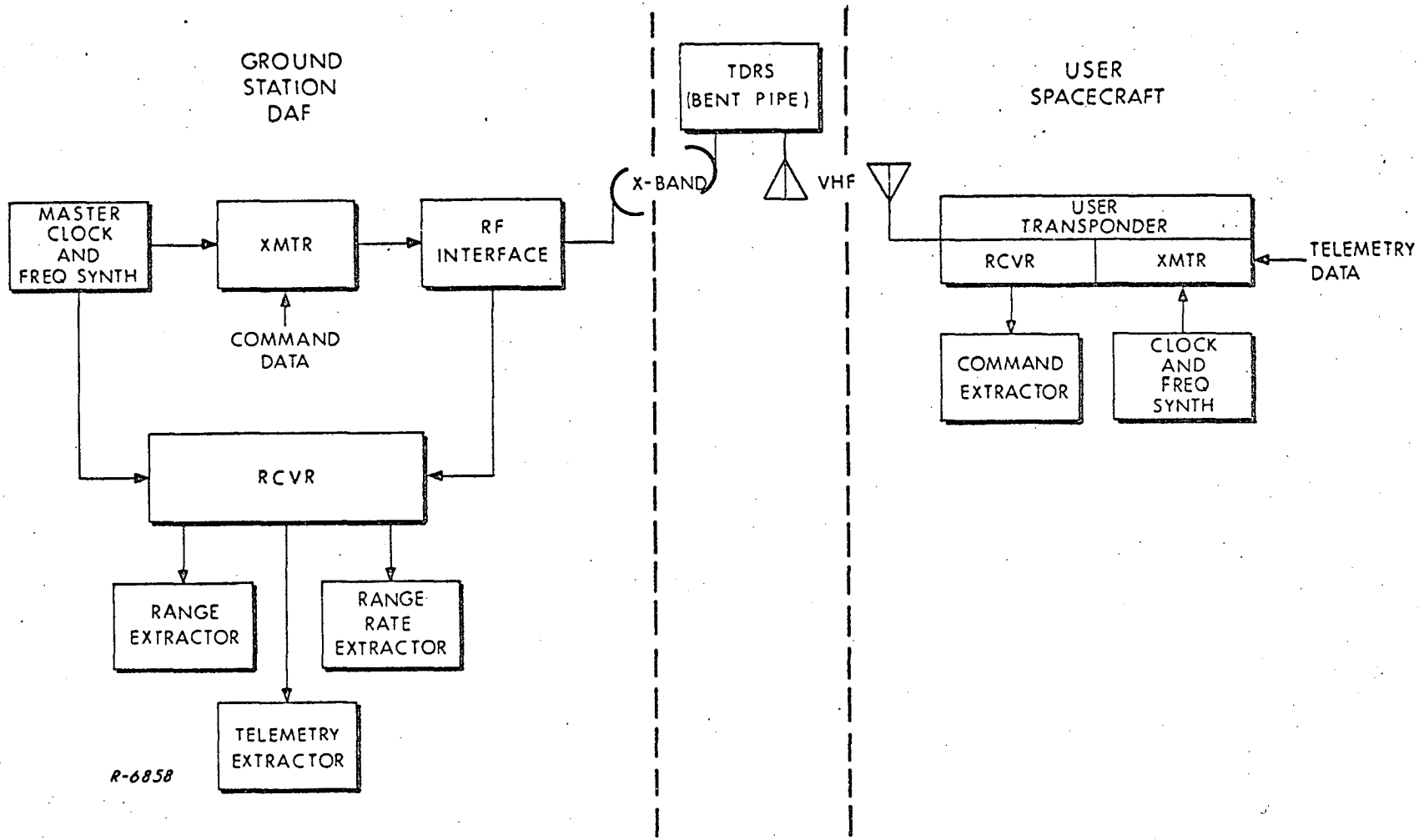

Fig. 2.1 System Configuration, Single User and Single TDRS

for processing in the VHF receiver. A compound phase-locked loop locks onto the carrier and subcarrier, yielding

a) The carrier frequency to the range rate extractor which measures the round-trip doppler.

b) The range tone cluster to the range extractor which measures the phase shifts on the various range tones.

c) The split-phase telemetry signal to the telemetry extractor for data detection.

The system configuration for the general situation of several TDRS's and many User spacecrafts is illustrated in Fig. 2.2. Three TDRS's are shown, designated A, B and C, although extension to four is straightforward. A DAF is dedicated to each TDRS, with a separate X-band link up and down. Each TDRS radiates its VHF signal to all User spacecrafts in view, using the common uplink carrier frequency but identified by its unique subcarrier frequency. This is indicated in Fig. 2.2 by lines going to User No. 1 only to reduce pictorial clutter. Each User's transponder receiver locks onto the uplink signal containing the subcarrier to which it is tuned as soon as it comes into view of the appropriate TDRS, and commences to detect commands. Commands intended for a particular User are identified by an address code unique to that User. Addressing of several Users is accomplished by a time-division multiplexing scheme (TDM).

The User downlink identification, based on its carrier and subcarrier frequency combination, is either preset or is selectable on command from the DAF. The carrier frequency offset of 25.6 kHz, when used, is derived from the downlink subcarrier frequency, and is removed on the ground prior to doppler processing. On the downlink, each TDRS receives signals from all User spacecrafts in view, and relays the full downlink VHF band down to its DAF. Each DAF is equipped with a bank of VHF receivers, one for each User addressed by the TDRS associated with that particular DAF.

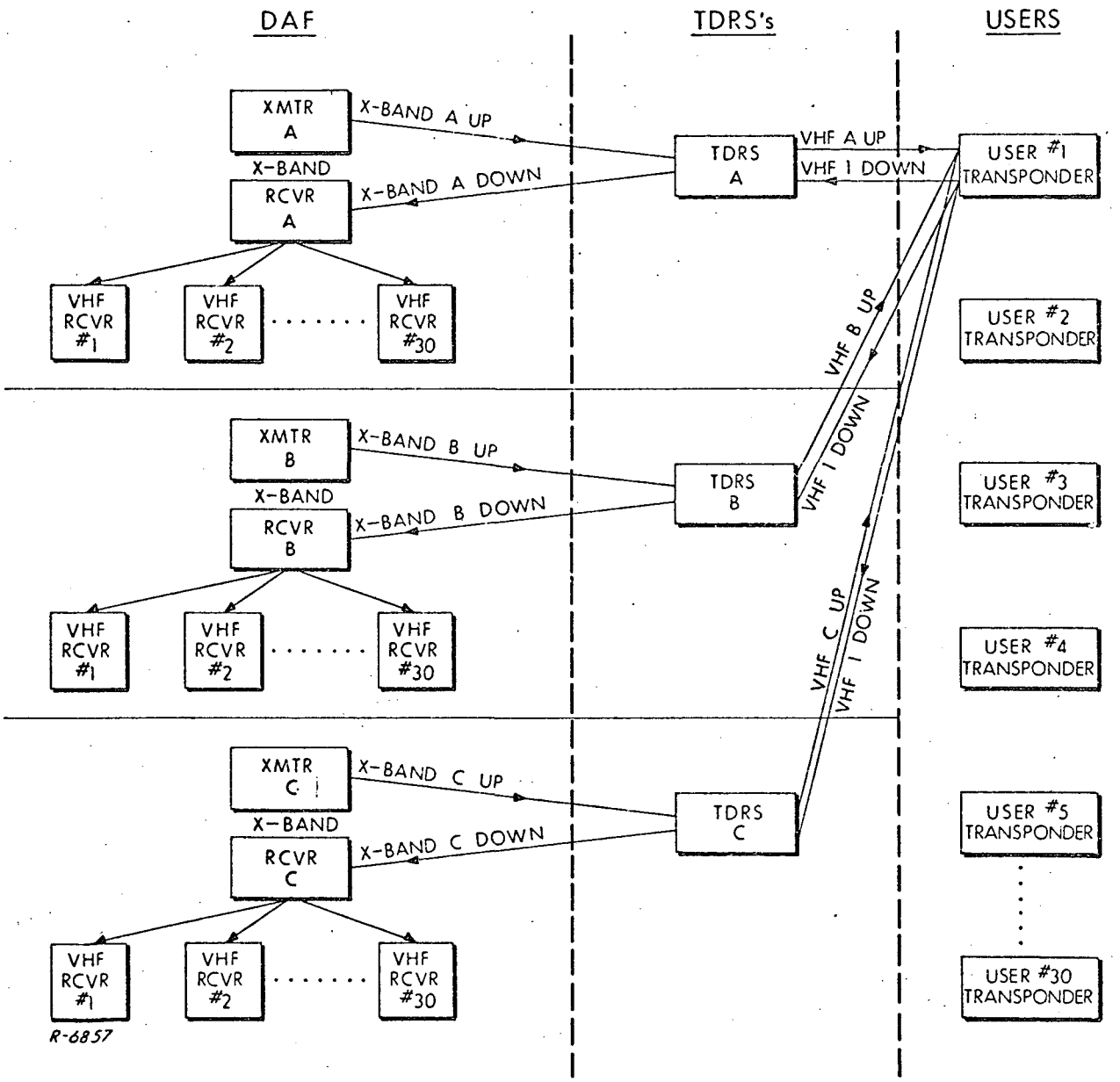

Fig. 2.2 Full System Configuration

2.3 DAF Transmitter

2.3.1 Functions

The functions of the DAF transmitter are:

1) To generate the wideband FM VHF signal,
2) To coherently translate it up to X-band, and
3) To transmit the X-band signal to the relay satellite.

2.3.2 Uplink VHF Signal Structure

The uplink wideband FM VHF signal consists of a VHF carrier which is simultaneously

1) PM Modulated by
   a) command data in the form of a split-phase binary signal, and
   b) ranging sidetones, and
2) Wideband FM Modulated by a sinusoidal subcarrier with a modulation index of 5.52.

The command data bit rate may be either 100 BPS or 400 BPS.

The ranging sidetones consist of a fine range tone at 102.4 kHz and ambiguity ranging sidetones clustered around 96.0 kHz as shown in Fig. 2.3. The ratio between the frequencies of successive range tones is 16. The range tone frequencies are listed in Table 2.1.

Table 2.1

Range Tone Frequencies

Range Tone	Frequency
Fine range tone	f_1 = 102.4 kHz
Medium-fine range tone	f_2 = 6.4 kHz
Medium-coarse range tone	f_3 = 400 Hz
Coarse range tone	f_4 = 25 Hz

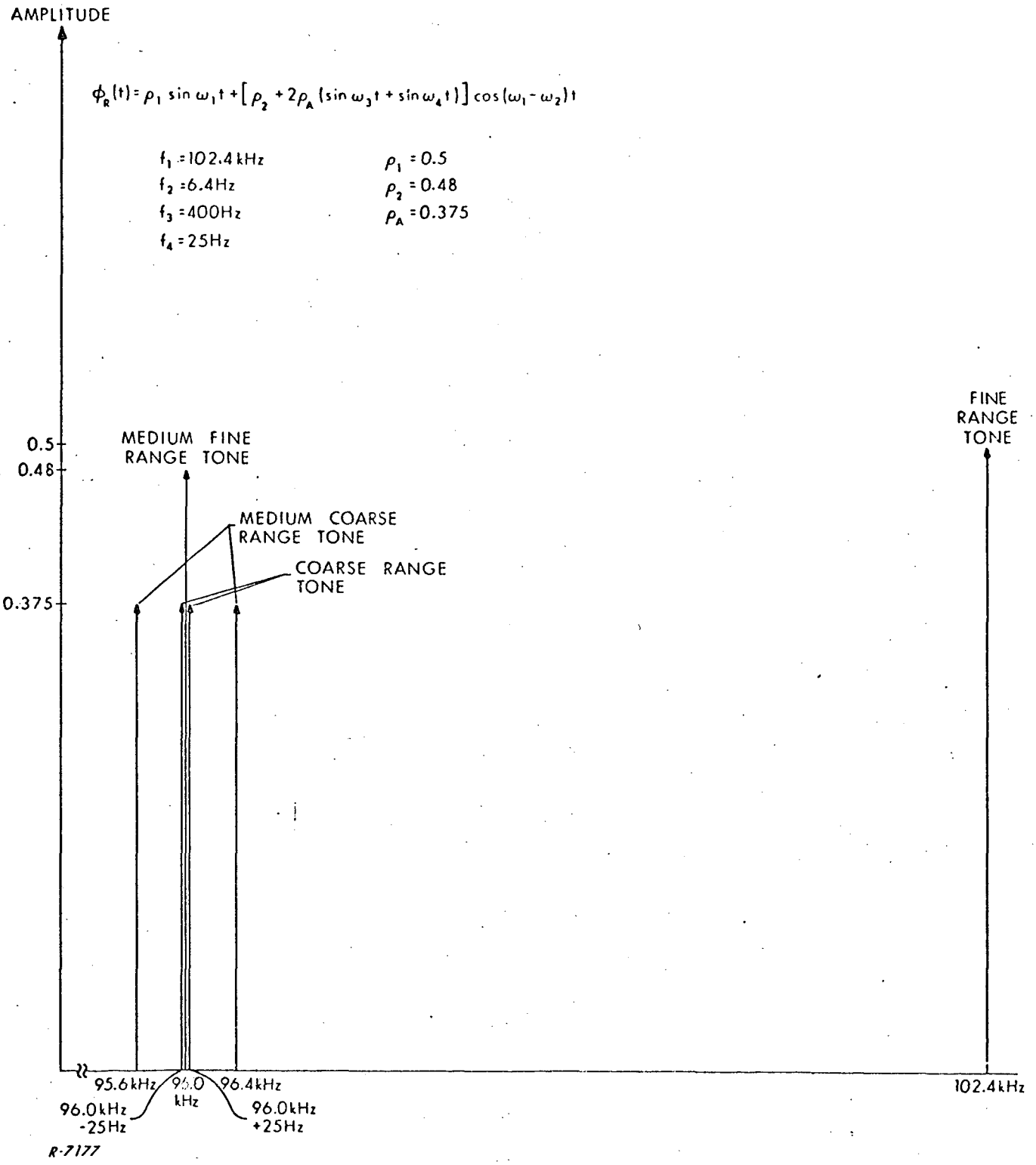

Fig. 2.3 Ranging Sidetone Signal Structure

The ranging sidetones are generated as indicated in Fig. 2.4. The ranging sidetone signal representation is

$$\phi_R(t) = \rho_1 \sin \omega_1 t + [\rho_2 + 2\rho_A(\sin \omega_3 t + \sin \omega_4 t)] \cos(\omega_1 - \omega_2)t \quad (2.1)$$

where

$$\rho_1 = 0.5, \ \rho_2 = 0.48, \text{ and } \rho_A = 0.375.$$

All relay satellites transmit at the same VHF carrier frequency of 148.9255 MHz. The signals from different relay satellites are distinguished in the TDRS-User VHF link by the unique subcarrier frequency assigned to each TDRS. For example, two relay satellites require two DAF transmitters, each with a different uplink subcarrier frequency. Subcarrier frequencies should be in excess of several kHz.

A plot of the distribution of the wideband FM signal power in the various sidebands for a modulation index of 5.52 is shown in Fig. 2.5. The fraction of the total signal power contained in the first six sidebands on either side of the carrier is 0.982. The power in the carrier is zero since $J_o(5.52) = 0$. As may be seen from Fig. 2.5, the largest sideband is the fourth order sideband, followed in order by the first, fifth, third, sixth, second, and seventh order sidebands. The fact that the fourth and fifth order sidebands are large is utilized in the design of the wideband FM compound PLL receiver acquisition aid system.

2.3.3 Uplink Signal Generation

The technique used to generate the uplink wideband FM VHF signal is to perform the PM modulation and the wideband FM modulation in separate channels and then combine these two modulated signals by a mixing operation. This permits optimum design of each type of modulator and ensures better control over the modulation indices.

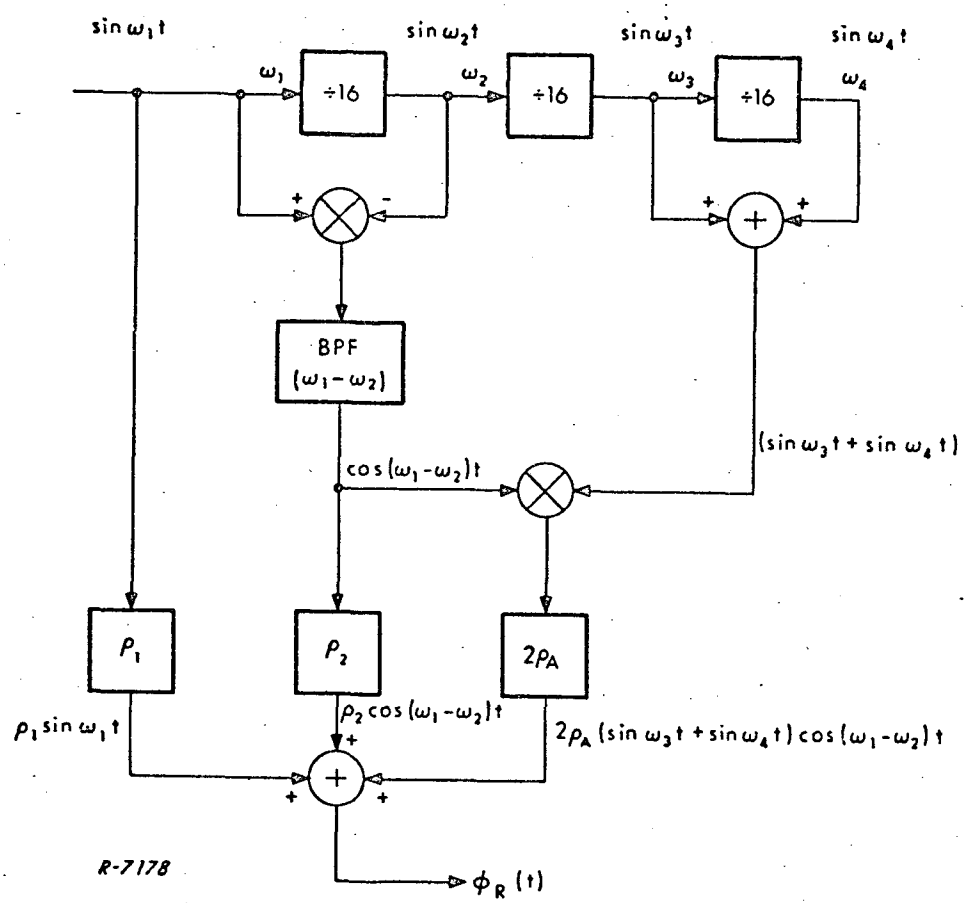

Fig. 2.4 Ranging Sidetone Signal Generator

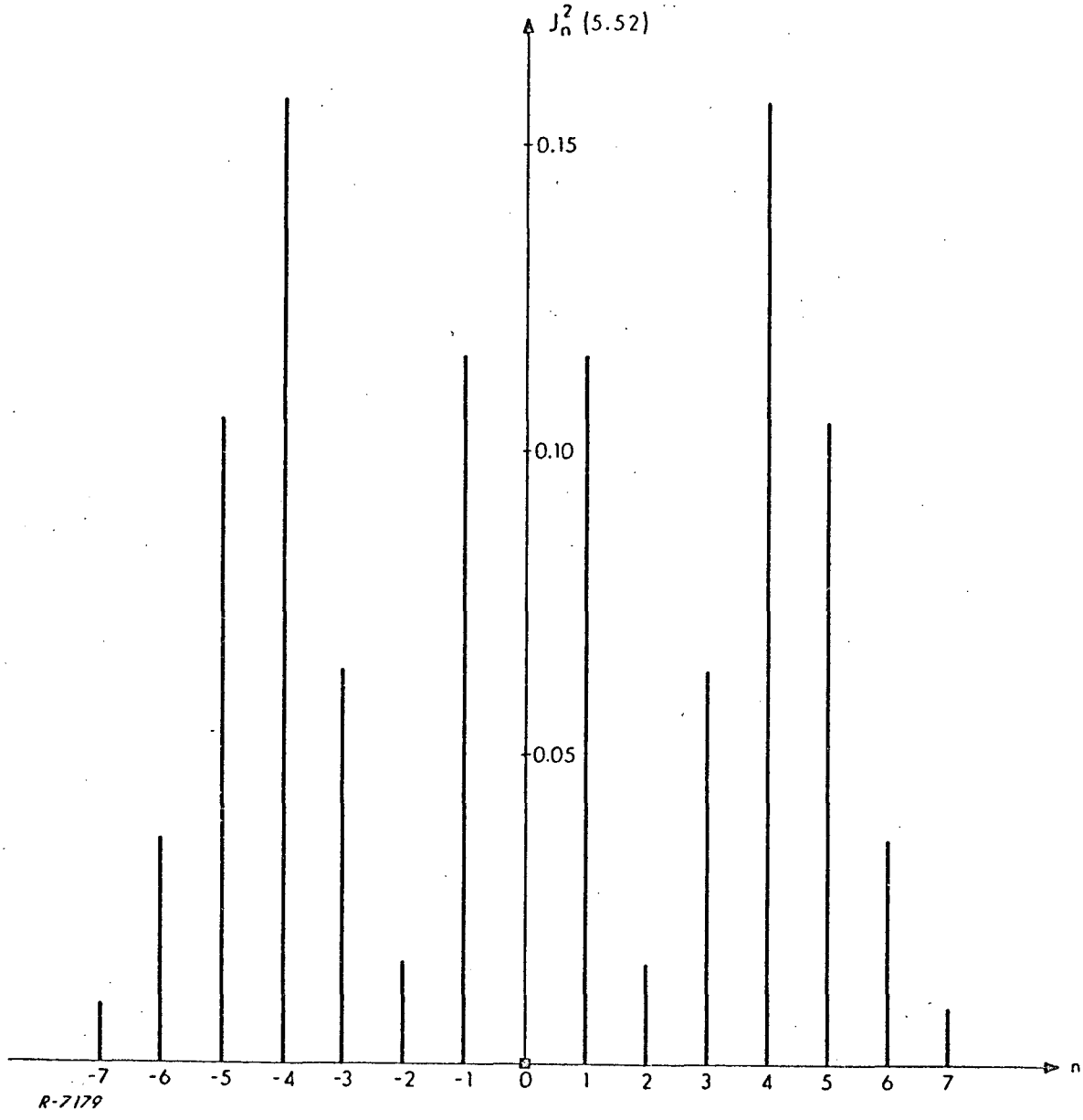

Fig. 2.5 Distribution of the Wideband FM Signal Power in the Various Subcarrier Sidebands for $\delta = 5.52$

A block diagram of the DAF transmitter is shown in Fig. 2.6.* A clock and frequency synthesizer generates the fine range tone frequency of 102.4 kHz, the command clock frequency, the subcarrier frequency, a reference frequency, f_o, at approximately 1 MHz, and an X-band reference frequency.

Commands originating at mission control are formatted at the DAF transmitter. The command formatter is synchronized by the command clock rate. The command signal generator converts the command signal from the command formatter into a split-phase command signal.

A range tone generator generates the ranging sidetones. The ranging sidetones and the split-phase command signal are added together and fed to the PM modulator. The output of the PM modulator, which operates at a frequency of 5 f_o, is frequency multiplied by 48. This brings the carrier frequency up to 240 f_o and the phase deviations of the carrier by the ranging sidetones and the command data up to their desired values.

A coherent wideband FM modulator FM modulates a carrier at 91 f_o with the subcarrier while at the same time maintaining coherence with the reference frequency f_o. This is implemented as shown in Fig. 2.7.

The FM modulator is made coherent with the reference frequency f_o by phase-locking the carrier component of an FM modulated VCO. The modulation index at this point is sufficiently small so that a large carrier component is maintained at the output of the VCO. The desired modulation index of 5.52 is obtained by frequency multiplying the VCO signal by 8 as shown. This also brings the carrier frequency up to 91 f_o. The PM and FM modulated carriers are mixed and the difference frequency component at 149 f_o = 148.9255 MHz becomes the desired VHF wideband FM signal.

*The frequency at the output of a mixer is denoted as either the sum or difference of the input frequencies in accordance with the polarity signs at the inputs to the mixer. This applies to all mixers shown in all figures.

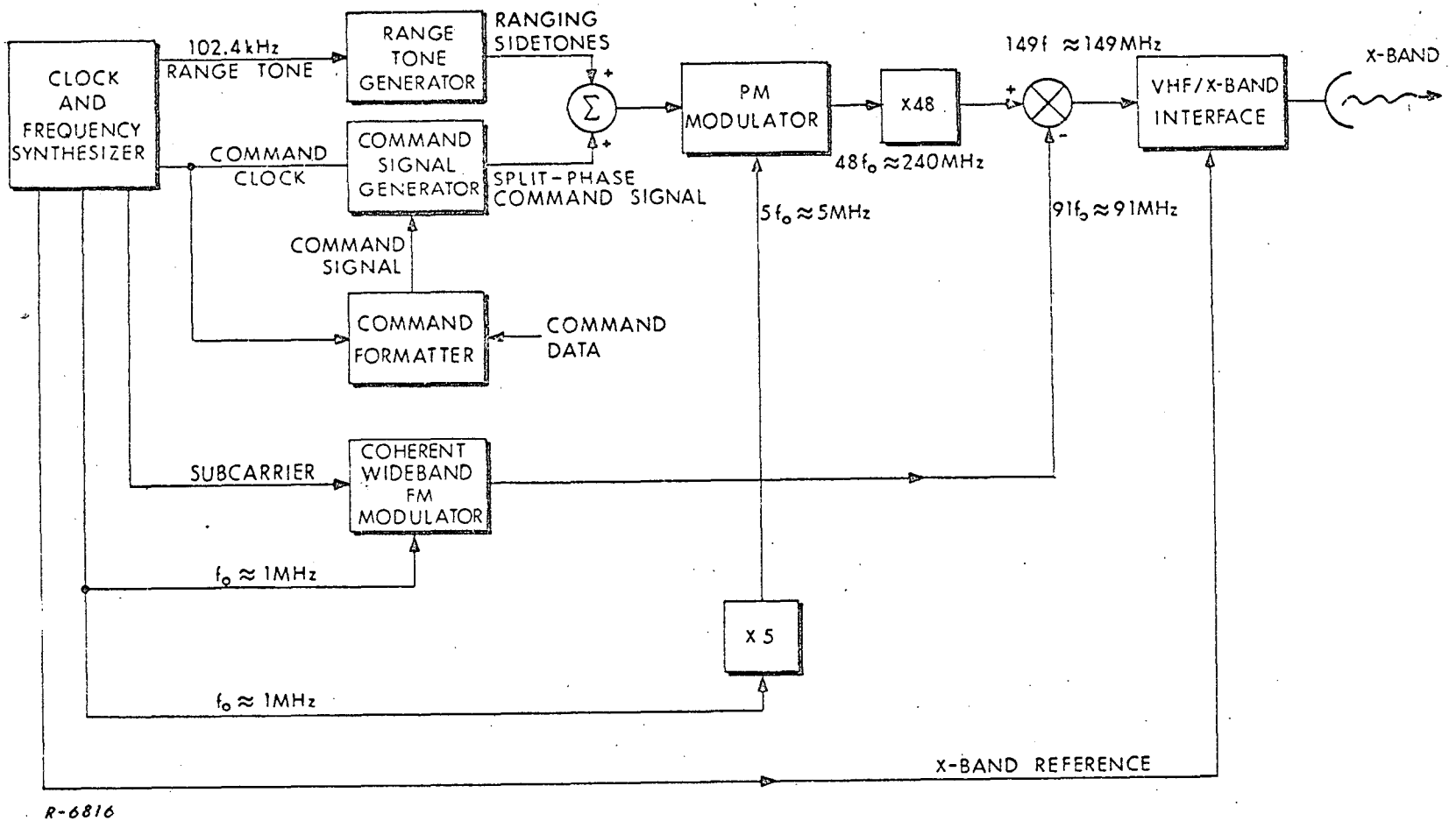

Fig. 2.6 DAF Transmitter

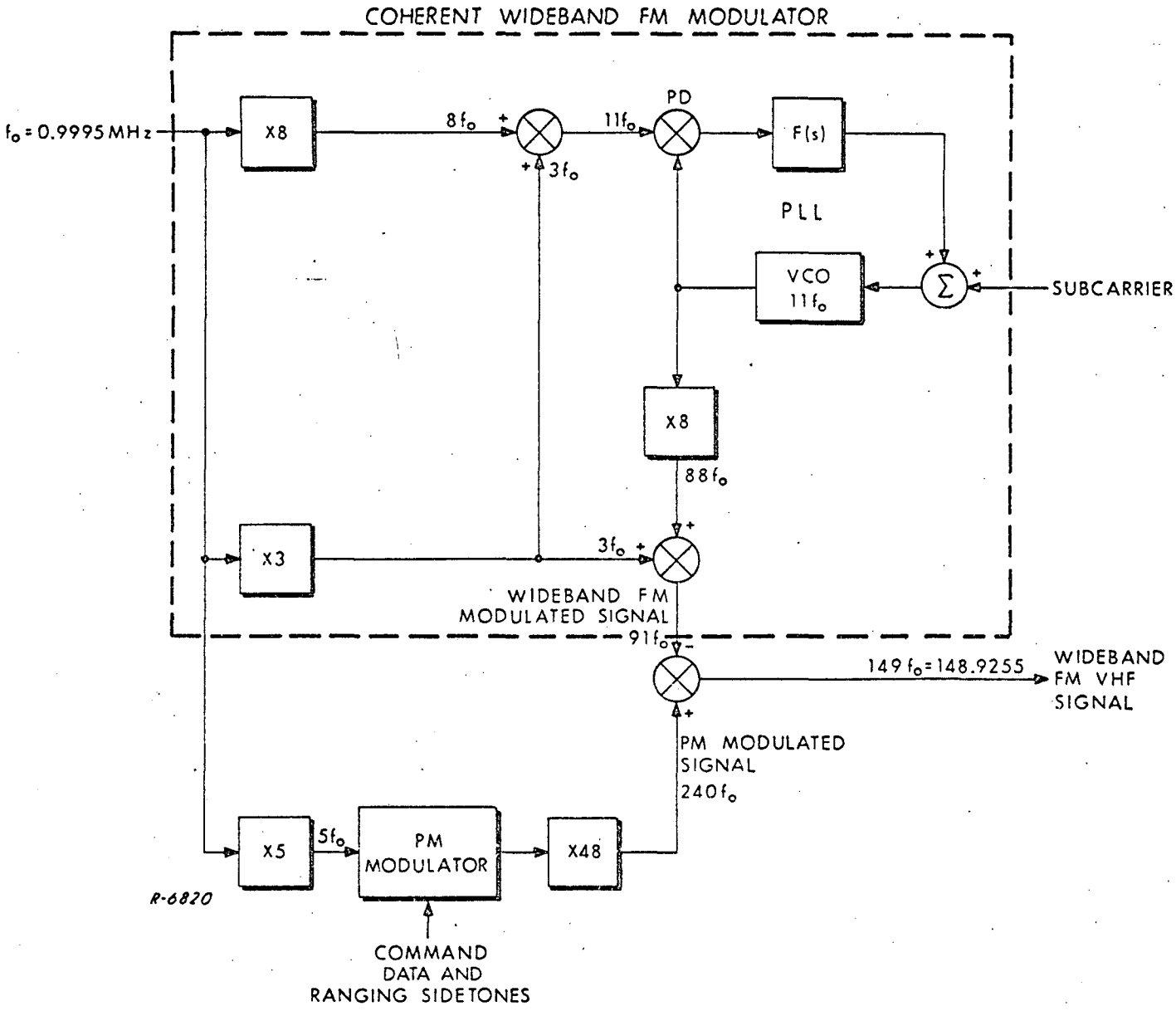

Fig. 2.7 DAF VHF Signal Generator

The carrier frequency of 148.9255 MHz is chosen because:

1) It places the uplink VHF carrier frequency very near the center of the uplink VHF band extending from 148.0 to 149.9 MHz.

2) It permits use of a simple User transponder turnaround ratio of 23/25.

3) With this turnaround ratio and uplink VHF carrier frequency, the downlink carrier frequency is 137.01146 MHz which is very near the center of the downlink VHF band extending from 136.0 to 138.0 MHz.

4) To achieve this uplink carrier frequency, f_o is chosen a 1 MHz minus 500 Hz = 999.5 kHz.

If it were necessary to place the carrier frequencies precisely in the center of the uplink and downlink VHF bands, a turnaround ratio of 137.0/148.95 would have to be used. This is rather difficult to achieve. Fortunately, this ratio, which is approximately 0.91977, is sufficiently close to 0.920 = 23/25 to permit the 23/25 turnaround ratio to be used with only slight tolerable shifts in the frequencies of the carriers from the desired center band values.

The uplink VHF signal is therefore

$$e_u(t) = \sin\left\{(149)\,2\pi f_o t + \delta \sin \omega_{sc} t + \phi_R(t) + \phi_D(t)\right\} \qquad (2.2)$$

where $\delta \sin \omega_{sc} t$ is the wideband FM subcarrier, $\phi_R(t)$ is the ranging sidetones signal, and $\phi_D(t)$ is the split-phase command data signal. The phase deviation of the data signal is 1 radian.

2.4 Relay Satellite

The relay satellite is presumed to function as a simple "bent-pipe" frequency translator from X-band to VHF. The effects of X-band DAF-to-TDRS doppler in the VHF link is presumed compensated for by some means. (See ADCOM Final Report G-95 entitled, "Communication Technique Studies for the Data Relay Satellite System," May 15, 1969, prepared for NASA/GSFC under Contract NAS5-10510, Mod 3.) Each TDRS relays all signals that it receives in the downlink VHF band.

2.5 User Transponder

2.5.1 Functions

The User transponder must perform the following functions:

1) Acquisition of the wideband FM signal.
2) Coherent carrier tracking and demodulation.
3) Extraction of the command data.
4) Filtering of the ranging sidetones.
5) Generation of the downlink subcarrier frequency.
6) Coherent turnaround of the uplink carrier, and generation of one of three downlink carrier frequencies.
7) PM modulation of the filtered ranging sidetones and the downlink telemetry split-phase data signal on the downlink carrier.
8) Wideband FM modulation of the downlink carrier by the downlink subcarrier, and
9) Handover of signal reception from one TDRS to another TDRS.

These functions are shown schematically in Fig. 2.8.

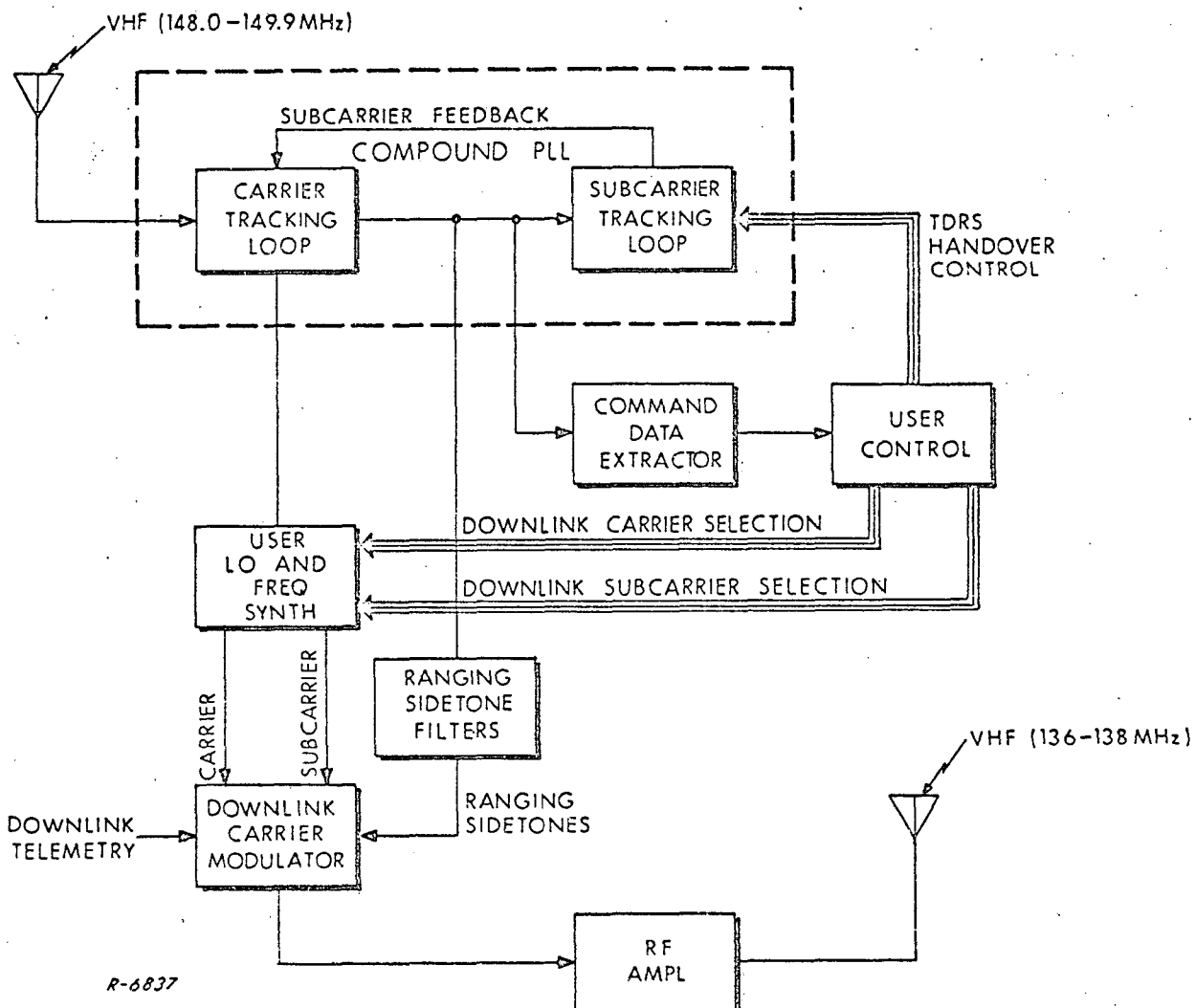

Fig. 2.8 User Transponder Functional Block Diagram

2.5.2 User Transponder Compound PLL Receiver

The User transponder compound PLL receiver acquires, tracks, and demodulates the wideband FM uplink signal from one of the TDRS's in view. A block diagram of the tracking portion of the receiver is shown in Fig. 2.9. This shows a receiver designed to receive the wideband FM signal from a single TDRS whose subcarrier frequency is ω_{sc}. The problems of acquisition and handover are treated in a later section.

The receiver is a compound PLL consisting of a carrier tracking phase-locked loop, a subcarrier tracking phase-locked loop, a subcarrier feedback and wideband FM reference signal generator, and a carrier phase demodulator. The VCXO output signal of the subcarrier loop is used to modulate the carrier loop VCO output signal in such a manner as to permit full compression of the wideband FM RF input signal at the RF mixer. This is accomplished by utilizing a PM modulator followed by a frequency multiplication by 24 in the feedback path. The effect is equivalent to wideband FM modulation if the phase of the subcarrier is shifted by 90° prior to PM modulation of the carrier loop VCO signal. The gain of the feedback loop is adjusted to yield full compression by making the modulation index of the wideband FM reference signal equal to 5.52 at the control input to the RF mixer.

The advantages of full compression and of using a modulation index of 5.52 are:

1) Full compression offers optimum operation in the presence of noise and interference.

2) The received wideband FM signal has no carrier component since $J_0(5.52) = 0$. This is important for proper SSMA operation since it prevents the carrier components of other User or other TDRS signals from interfering with carrier tracking or data demodulation. Also, the fact that $J_0(\delta) = 0$ when $\delta = 5.52$ makes it easy to set the modulation index at this value.

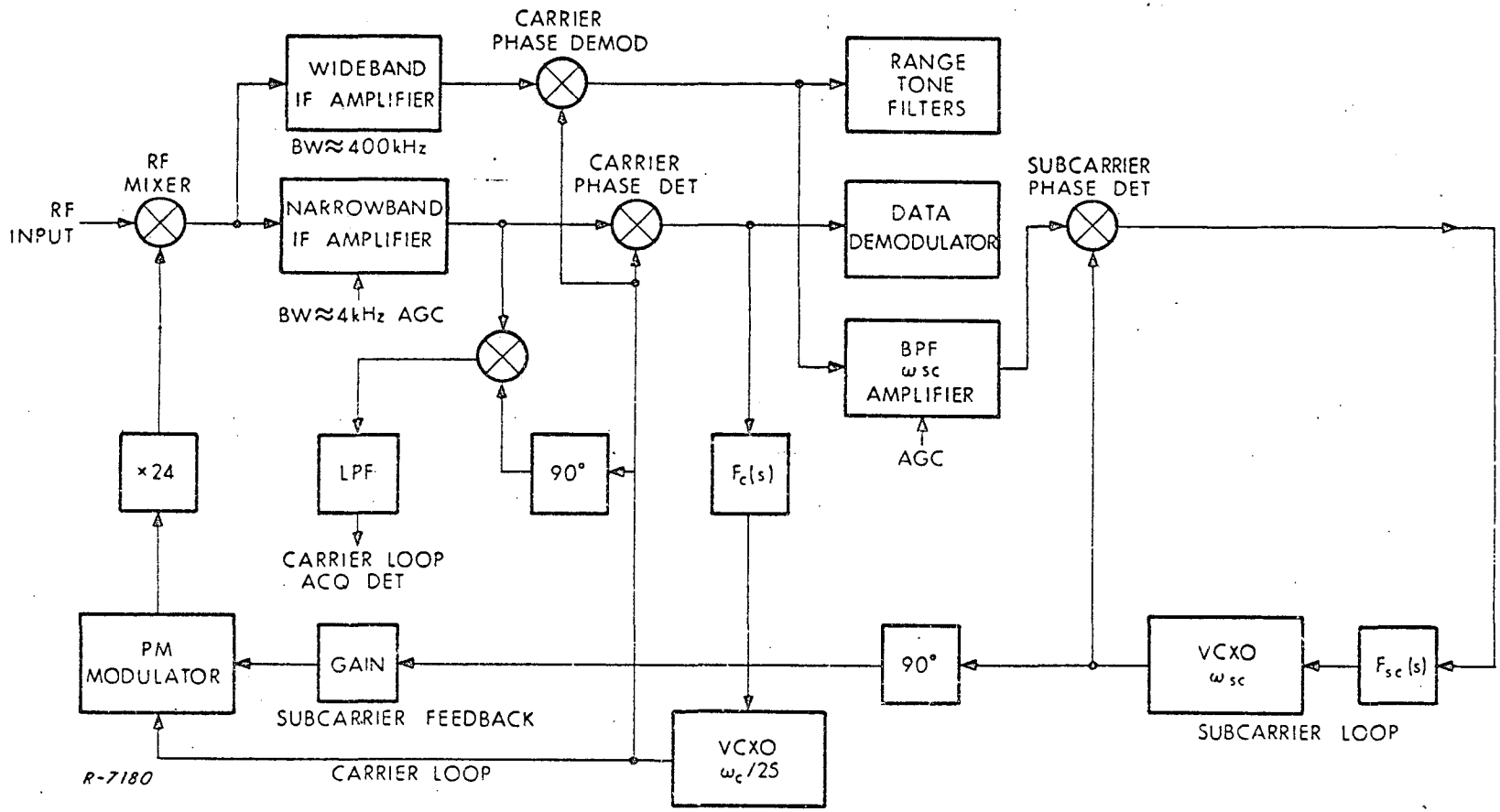

Fig. 2.9 Block Diagram of Tracking Portion of Wideband FM Compound PLL

3) Only the first six sidebands carry significant signal power. This permits utilization of the higher subcarrier frequencies as primary subcarrier frequencies. The advantage of this is that it spreads the wideband FM signal over more of the 2 MHz bandwidth. This helps reduce the effects of SSMA and RFI interference by reducing the probability of certain interference mechanisms.

4) The fourth, fifth, and first order sidebands are the three largest subcarrier sidebands. This is used to advantage in the acquisition technique as will be described.

Note that by using a carrier PLL in a "long loop" configuration with a multiply-by-24 prior to the RF mixer, the carrier loop VCO frequency is made 1/25 of the VHF uplink carrier frequency. This is a very simple way to obtain the divide-by-25 in the 23/25 turnaround ratio.

The high level of RFI which is present on the uplink necessitates the use of a separate carrier phase demodulator and phase detector. This is done because coherent AGC is used to control the gain, and hence the noise bandwidth, of the carrier loop. Consequently, a narrowband IF amplifier (BW $\approx$ 4.0 kHz) is used to amplify the compressed carrier component. By using this narrow bandwidth, RFI components which lie more than a few kHz away from any of the subcarrier sideband components will be suppressed prior to IF amplification. This prevents any of these RFI components from overloading the IF amplifier.

A wideband IF amplifier passes the ranging sidetones and first-order subcarrier sidebands. This amplifier operates at a much lower gain than the narrowband IF amplifier. Further amplification of the ranging sidetones and the residual subcarrier first-order sideband is performed after coherent demodulation by the carrier phase demodulator and subsequent narrowband filtering by ranging sidetone filters and a subcarrier bandpass filter. The amplifiers used in this connection are AGC'd from the output of an AGC detector to be described in the section on acquisition.

The data may be extracted from the output of the carrier phase detector since it's bandwidth is much less than 4.0 kHz and it is PM'd directly on the carrier. The amplitude of the data at this point in the receiver has already been amplified to a controlled signal level by the AGC'd narrow-band IF amplifier.

The data demodulator consists of a bit synchronizer and an integrate-and-dump matched filter detector. The data demodulator is common to any TDRS system concept and need not be discussed further.

The range tone filters and the ranging sidetone turnaround channel is unique to the particular system under discussion, and is described in detail in a later section. We now turn our attention to the problem of acquisition of the wideband FM signal.

2.5.3 Signal Acquisition

The problem of acquisition on the uplink differs from that on the downlink for several important reasons. These are:

1. Acquisition on the uplink must be performed with the uplink command data and ranging sidetones present, whereas on the downlink, the User can be commanded to not transmit telemetry data until the ground receiver acquires the wide-band FM signal and the ranging sidetones.
2. Depending on how handover is accomplished, the User may be able to take longer to acquire than the ground receiver.
3. It is desirable to keep the User electronics as simple as possible, whereas additional sophistication may be built into the ground receiver acquisition circuitry.
4. The User must acquire in the presence of high levels of RFI interference.
5. The ground receiver must acquire in the presence of many other-User signals (SSMA interference).
6. The doppler on the downlink carrier is essentially twice that on the uplink carrier, although the dopplers on the subcarriers are essentially the same on both the uplink and downlink.

7. The signal power to noise power density ratios are generally different on the uplink and the downlink.

8. The ground receiver can be designed to receive a signal over a single downlink channel, whereas the User receiver may have to utilize portions of the same receiver to receive signals from different TDRS's. A downlink channel is defined by the downlink subcarrier frequency and carrier band assignment. It may be easier to design separate receivers for each downlink channel than to design ground receivers capable of receiving all downlink channels.

The following restrictions are placed on the uplink signal design and system operation based on the above acquisition considerations:

1. The 400 BPS command data is not transmitted when a User spacecraft is trying to acquire the wideband FM signal from the TDRS in question during handover.

2. The final choice of uplink subcarrier frequencies for the two or three TDRS's is to be made on the basis of no RFI interference of any significance lying within ±8 kHz of the upper 4th and 5th order sidebands, and no serious RFI interference lying within ±8 kHz of any other wideband FM signal spectral component.

That is, there should be essentially no RFI interference near the upper 4th, or 5th order sidebands, and the RFI that may lie near other spectral components should not be so large as to seriously interfere with compound PLL tracking, data demodulation, or ranging sidetone turnaround when the receiver is in the track mode. Since only 2 or 3 subcarrier frequencies need be selected for the uplink, these requirements may not be as severe as might appear at first glance. As a last resort, it may be necessary to require some RFI sources to go off the air.

A block diagram of the uplink acquisition scheme is shown in Fig. 2.10. This scheme has been designed to acquire the uplink wideband FM signal in the presence of RFI and multipath with the maximum possible reliability consistent with the requirements for reasonable acquisition time, signal-to-noise ratio, and receiver complexity. In particular, the scheme was designed to acquire lock with an input SNR no higher than that required

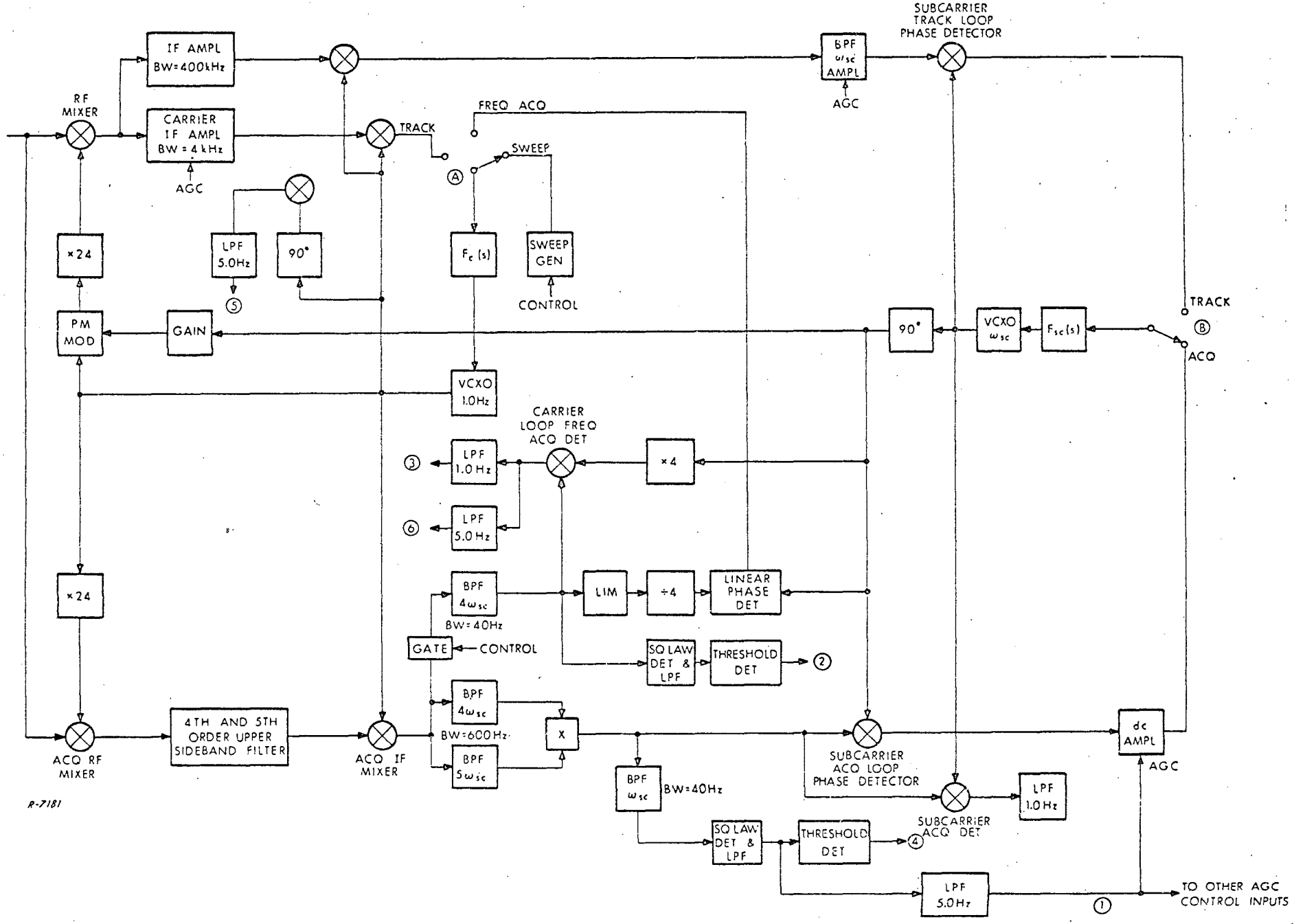

Fig. 2.10 Uplink Acquisition Scheme

for 400 BPS data demodulation and with full uplink modulation present (although with 100 BPS data). Acquisition times on the order of 10 to 12 seconds should be possible with almost no possibility of false lock.

We now describe briefly the functions of the acquisition scheme and then indicate how these functions are realized by the system of Fig. 2.10.

The functional behavior of the acquisition scheme is:

1. With the carrier and subcarrier loops unlocked, the carrier loop VCXO is swept until the error frequency is less than about 200 Hz. This is the coarse frequency search.
2. The carrier loop sweep generator continues to sweep in the same direction for a short time and is then switched to its fine frequency search mode in which the sweep is reversed and swept slowly until the error frequency is less than about 20 Hz.
3. At this time the carrier loop is switched from the sweep mode to the acquisition mode, and the carrier loop error frequency is forced to zero.
4. Meanwhile, the subcarrier loop, which is in the acquisition mode, acquires frequency lock.
5. As the carrier loop error frequency goes to zero, the phasing error on the subcarrier signal into the subcarrier acquisition becomes negligibly small, thereby enabling the subcarrier loop VCXO to acquire the proper phase for wideband FM compression.
6. With the subcarrier loop properly phased and the carrier loop frequency acquired, the carrier loop is switched to the track mode.
7. Meanwhile, the gain of the carrier loop IF amplifier is adjusted by an AGC signal derived from the acquisition subcarrier signal so that when the carrier loop is switched to the track mode, its loop noise bandwidth is already set at the proper value. This not only saves acquisition time, but also helps prevent the carrier loop from locking onto a CW RFI component that may be close to one of the subcarrier sidebands but which lies further away from the sideband than several carrier loop noise bandwidths. The carrier loop need now only acquire phase lock. The gain of the subcarrier tracking loop is adjusted in a similar fashion.

8. Phase lock is detected by a coherent carrier loop lock indicator, and is verified by checking to see that the upper 4th order subcarrier sideband lies where it should. This permits detection of false lock by the carrier loop on a CW RFI component that may fall within the carrier loop noise bandwidth but which may lie more than a few Hz away from the particular subcarrier sideband with which it interferes.

9. Finally, when proper carrier lock is verified, the subcarrier loop may be switched to the track mode.

10. The in-lock condition is constantly monitored, so that if the carrier or subcarrier tracking loop falls out of lock, a reacquisition procedure may be initiated. In particular, the subcarrier loop would be immediately switched to the acquisition mode, since, if the carrier loop VCO has not drifted too far in frequency from the frequency of the input carrier, subcarrier loop acquisition could take place rather quickly, and the carrier loop could reacquire without having to switch out of the track mode. Consequently, reacquisition could take place in one or two seconds if the in-lock condition is constantly monitored. This is important since it means that the communications link would only be out of service for a short time should loss of lock occur.

At the start of acquisition, switches A and B in the receiver shown in Fig. 2.10 are in the positions indicated. The carrier loop VCXO is swept back and forth so as to cover the input doppler range plus any small VCXO frequency instability plus a small additional guard band range. Now if a wideband FM signal whose subcarrier frequency is ω_{sc} is present at the input, its upper 4th and 5th order sidebands are mixed down to baseband by the carrier loop VCXO in the acquisition RF and IF mixers. As the carrier loop error frequency is reduced below about 200 Hz, the upper 4th and 5th order subcarrier sidebands, phase modulated by the 100 BPS data, appear at the outputs of their respective sideband bandpass filters. The outputs of these sideband filters are multiplied together, and the resulting subcarrier signal plus noise is filtered by a narrowband bandpass filter tuned to the subcarrier frequency. The subcarrier signal is generated from the product

of the 4th and 5th order subcarrier sidebands and their accompanying data sidebands. The noise is generated from the product of the noises at the outputs of the sideband filters and from the product of the subcarrier sidebands and noise.

The bandwidth of the sideband bandpass filters is chosen to be wide enough to pass the 100 BPS data sidebands, yet narrow enough so that the product of the noises at the outputs of the filters is negligible compared to the products of the sidebands and noise when the ratio of signal power to noise power density in the receiver is equal to that necessary to achieve the required BEP for the 400 BPS data. The bandwidth must also be narrow enough so that the carrier loop error frequency is not too large when the sweep is turned off. These requirements are satisfied at the above signal-to-noise-power-density ratio for the 100 BPS data with a sideband filter noise bandwidth of 600 Hz. These sideband filters are crystal filters which are designed to provide an approximately flat amplitude and linear phase over a 400 Hz bandwidth. The skirts of the filter fall off gradually enough so that the filter responds in a quasi-stationary manner to the linear sweep of the sideband through the passband, and so that the data transitions do not cause the filter to ring excessively.

The subcarrier signal at the output of the narrowband bandpass filter following the multiplier is detected by a square law detector-lowpass filter combination followed by a threshold detector. As the 4th and 5th order sidebands are swept into the sideband filters, the signal output of the narrowband subcarrier BPF builds up and rises above the noise level. When the sidebands are near the center of their respective sideband filter passbands, the output of the lowpass filter following the square law detector will exceed the threshold level of the threshold detector. The sweep rate is determined by the bandwidth of this lowpass filter, which in turn is determined by the requirement that signal-to-noise ratio at the output of the lowpass filter is large enough to assure a high probability of correct detection.

For example, if the lowpass filter is a single-pole RC filter, the time constant, τ_{LPF}, is related to the noise bandwidth of the filter, B_{LPF}, by

$$\tau_{LPF} = \frac{1}{4\,B_{LPF}} \tag{2.3}$$

If we require that the VCXO sweep rate is such that the carrier loop error frequency sweeps 50 Hz in a time equal to four time constants of the lowpass filter, the sweep rate will be $R = 50\,B_{LPF}$ Hz/sec. If B_{LPF} is 20 Hz, this corresponds to a sweep rate of 1 kHz/sec.

When the threshold detector detects the presence of the subcarrier signal it triggers a monostable which stays on for a time long enough to permit the sweep to move the subcarrier sideband components past the center of the band of the sideband filters. When the monostable turns off, the sweep is reversed and slowed down and the analog gate at the input to the narrowband 4th order sideband bandpass filter is closed. This gate is kept open during the coarse sweep to prevent this narrowband filter from ringing as a result of the presence of a fast sweeping signal at its input. As the 4th order subcarrier sideband is swept into the passband of the narrowband 4th order sideband bandpass filter, the signal level at point 2 will rise above the threshold level of the threshold detector. This disconnects the sweep by switching the carrier loop switch A from the sweep position to the acquisition position. The output of the narrowband 4th order sideband BPF is hard limited and frequency divided by 4 to produce a signal at the subcarrier frequency which is offset from the subcarrier frequency by 1/4 of the residual carrier loop error frequency. This signal is compared with the subcarrier VCXO signal in a linear phase detector, so that the output of the linear phase detector will be a ramp whose time derivative is proportional to 1/4 of the residual carrier loop error frequency plus the subcarrier loop error frequency. The carrier loop is designed so that the seize frequency in the acquisition mode is greater than the maximum value of the sum of the residual carrier loop error frequency plus 4 times the subcarrier

loop frequency error.* The carrier loop then rapidly adjusts the phase of the carrier loop VCXO so that the carrier loop frequency error is equal to minus 4 times the subcarrier loop frequency error. This, however, is very small, and the 4th and 5th order sidebands will be well centered in the passbands of their respective sideband filters. Detection of carrier loop frequency acquisition is made at point 3.

Meanwhile, the gains of the subcarrier and carrier tracking loops and the subcarrier acquisition loop are adjusted by an AGC voltage derived from the output of the lowpass filter at point 1. This adjusts the damping factor and the noise bandwidths of these loops to their design values.

Subcarrier loop acquisition is detected by the coherent subcarrier loop acquisition detector at point 4. As the subcarrier loop pulls into lock, the carrier loop frequency error goes to zero. At this time the subcarrier loop is phase-locked, the carrier loop is frequency-locked, the AGC'd amplifiers in the carrier and subcarrier loops are adjusted to their proper gain values, and wideband FM compression is taking place in the RF mixer of the carrier tracking loop. The carrier loop may now be switched to the track mode. The carrier loop will rapidly settle to the proper phase in a time on the order of the inverse of the carrier loop noise bandwidth. Depending on the initial phase error, the loop may slip one cycle before phase lock is achieved. The phase lock condition is detected by the coherent carrier loop acquisition detector at point 5. If the carrier loop locks onto the compressed carrier component, the output at point 3 will remain high. On the other hand, should the carrier loop lock onto a CW RFI component lying within the loop noise bandwidth but several Hz away from the subcarrier sideband with which it interferes in the RF spectrum, the signal level at point 3 will drop, since the 4th order sideband will no longer lie where it it supposed to be.

---

*C. J. Byrne, "Properties and Design of the Phase-Controlled Oscillator with a Sawtooth Comparator," The Bell System Technical Journal, p. 587, March 1962.

If the signals at points 5 and 3 indicate that the carrier loop is properly acquired, the subcarrier loop is switched from the acquisition to the track mode. The in-lock condition of the subcarrier loop may be monitored at point 4. If this signal level continues to indicate that the subcarrier loop is locked, the receiver is in the track mode, and the downlink wideband FM signal may be transmitted. Downlink telemetry and ranging sidetones are not transmitted until the ground receiver acquires the downlink wideband FM signal and commands the User to transmit these signals as PM modulation on the downlink carrier. Acquisition of the ground receiver is described in a later section.

We now describe the sweep system in more detail so that the mean time to acquire may be calculated. A large portion of the acquisition time is spent on the coarse and fine carrier sweep. From Fig. 2.10 it is seen that the sweep is applied to the input of the active loop filter $F_c(s)$. The transfer function of this filter is

$$F_c(s) = \frac{1 + \tau_2 s}{\tau_1 s} = \frac{\tau_2}{\tau_1} + \frac{1}{\tau_1 s} \qquad (2.4)$$

The filter behaves like a gain of τ_2/τ_1 plus an ideal integrator of gain $1/\tau_1$. (This holds down to very low frequencies at which point the active filter behaves like a gain G, where G is the dc gain of the operational amplifier used in the active filter.) Consequently, if a step is applied to the input of this filter, the output (VCXO input) would consist of a step of amplitude τ_2/τ_1 times the input amplitude, plus a range of slope $1/\tau_1$ times the input amplitude. The ramp provides the sweep, and the amplitude of the step controls the sweep rate. A small step at the VCXO input may be tolerated at the ends of the sweep which extends past where the input is known to be, but it may present a problem when the sweep is being changed from the coarse to the fine sweep mode. To circumvent this problem, the step is first applied to an RC filter circuit whose time constant is equal to τ_2,

and the output of the sweep generator is obtained from the voltage across the capacitor. This eliminates the step at the VCXO input. In addition, the analog gate at the input to the narrowband 4th order sideband filter is closed slowly enough so that the sudden application of the signal does not cause the narrowband filter to ring. In this application, the gate circuit behaves like an AGC amplifier whose gain is increased slowly from zero to its final design value as the gate is closed.

A block diagram of the sweep generator is shown in Fig. 2.11. The operation of the sweep generator is as follows. When the generator is in the coarse frequency sweep mode gates #1, 2, and 3 are all closed. These are analog gates employing FET's as variable resistors.* The output of gate #3 is connected to the carrier loop active loop filter $F_2(s)$. The squarewave generator output consists of a balanced symmetrical squarewave whose period is $2\,T_{SWEEP}$. The squarewave passes through gate #1 to the positive input of a differential amplifier. The squarewave is reduced in amplitude and passed through gate #2 to the negative input of the differential amplifier to which a "holding" capacitor is connected. This capacitor has a very short charge time when the gate is closed, and a very long discharge time when the gate is open. Consequently, when the gates are closed, the output of the differential amplifier is a squarewave whose amplitude is the difference between the squarewave amplitude at the outputs of gates #1 and #2.

The output of the differential amplifier is fed into an RC filter whose time constant, $\tau_o = R_o C_o$, is equal to the time constant τ_2 of the active loop filter. This is done so that the voltage at the input to the VCXO will be a ramp when a step of voltage is applied at the input of this RC filter.

---

*H. W. Ruegg, "An Integrated FET Analog Switch, PIEE, pp. 1572-1575, December 1964.

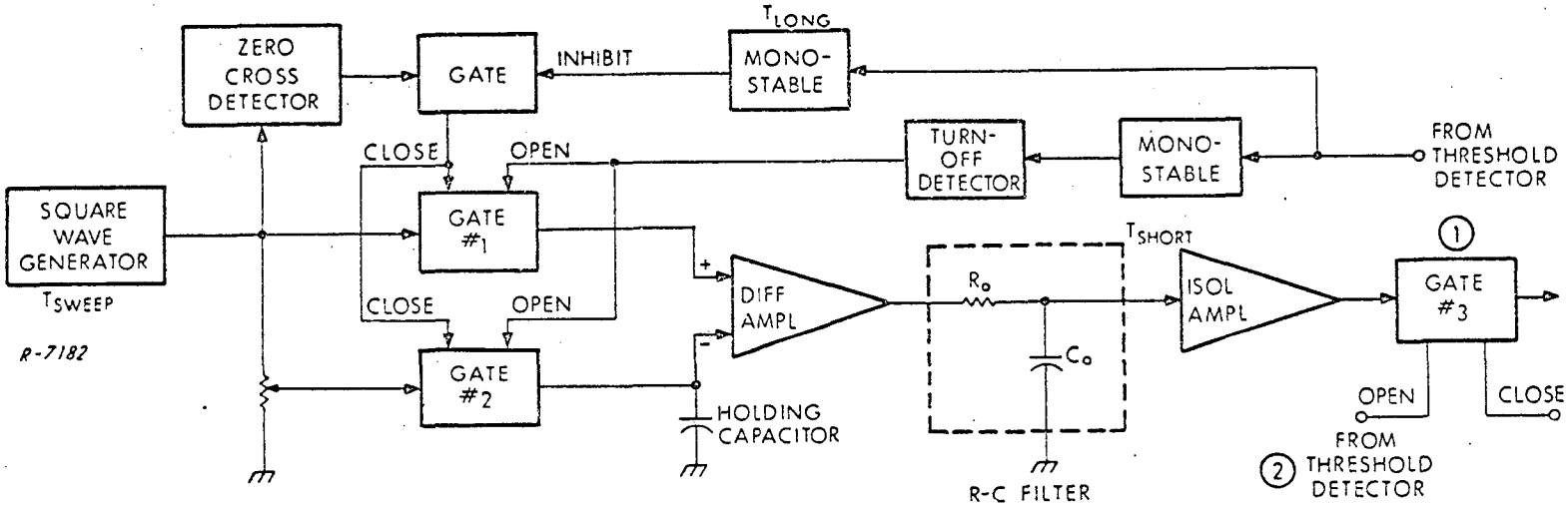

Fig. 2.11 Sweep Generator

To show that this is the case, we write the product of the filter transfer functions of the RC filter and the active loop filter as

$$\frac{1}{(1+\tau_o s)} \times \frac{(1+\tau_2 s)}{\tau_1 s} = \frac{(1+\tau_2 s)}{(1+\tau_o s)} \times \frac{1}{\tau_1 s} \qquad (2.5)$$

Observe that when $\tau_o = \tau_2$, the product of these two transfer functions is a pure integrator. Consequently, the voltage at the VCXO input will be a triangular wave with no voltage jumps when the loop filter is driven by this sweep generator.

Now, when the threshold detector at point 1 in the block diagram of Fig. 2.10 detects the presence of the subcarrier signal, it triggers two monostable multivibrators. The short duration monostable stays on long enough for the sweep circuit to sweep the subcarrier sideband components past the center frequency of the sideband filters. If the sweep rate is 1 kHz/sec in the coarse frequency sweep mode, and if a sweep of 200 Hz is sufficient to assure that the subcarrier sideband components are at least 100 Hz past the sideband filter center frequencies, the monostable period should be 0.2 sec. At the end of this time the monostable reverts to its OFF state. This is detected by a turn-off detector which then opens gates #1 and #2. The function of the long duration monostable is to prevent the next zero crossing of the squarewave generator from closing these gates if this zero crossing occurs in a time following the opening of these gates which is too short to permit fine sweep acquisition to occur. This arrangement makes it unnecessary to extend the period of the squarewave by a time long enough to permit fine sweep acquisition. This is also the reason why gate #2 is used in conjunction with a holding capacitor rather than feeding the reduced amplitude squarewave directly into the negative input of the differential amplifier.

When gates #1 and #2 are opened, the voltage at the output of the differential amplifier jumps to the negative of the voltage on the holding capacitor. This provides the voltage for the return sweep. Since this voltage is smaller than the voltage at the output of the differential amplifier during the coarse sweep mode, the return sweep will be slower. At this time the gate at the input to the narrowband 4th order sideband filter is closed.

If the single-pole lowpass filter at point 2 in Fig. 2.10 has a noise bandwidth of 20 Hz, and if we require that in 4 time constants of this filter the return sweep travels 10 Hz, the return sweep rate must be 200 Hz/sec or 1/5 of the coarse sweep rate. Consequently, if the fine sweep must return 200 Hz in order to sweep the 4th order subcarrier sideband into the passband of the narrowband 4th order sideband bandpass filter, the fine sweep portion of the wideband FM acquisition will last 1 second. If we measure the start of acquisition from a zero crossing of the squarewave generator, and if we consider the sweep range to be 8 kHz when referred to the VHF input, the maximum coarse frequency sweep time will be 8 sec.

When the threshold detector at point 2 in Fig. 2.10 detects the 4th order subcarrier sideband, it opens gate #3 in the sweep generator, thereby disconnecting the sweep, and closes a gate which connects the carrier loop filter to the output of the linear phase detector. The carrier loop error frequency is now on the order of 20 Hz or less, and the subcarrier loop error frequency is at most 3 Hz, so that the output of the linear phase detector, just prior to switching the loop to the acquisition mode, consists of a ramp whose maximum time derivative corresponds to an input error frequency of 1/4 the carrier loop error frequency plus the subcarrier loop error frequency, or about 8 Hz. The carrier loop can lock on to this signal very rapidly as we shall now show.

We choose the gain of the acquisition loop so that the damping factor is $\tau = 1$ (critical damping). This is done by adjusting the gain of the linear phase detector. The loop noise bandwidth now is 15 Hz. The response of the carrier loop phase error to a step in the phase input is * in this case

$$\theta_{ce}(t) = \Delta\theta_i\, e^{-x}(1-x) \tag{2.6}$$

where

$$x = \zeta\omega_n t = 2\zeta^2 t/\tau_2 = \frac{2t}{\tau_2} \tag{2.7}$$

The response to a step in input frequency is simply the integral of this, or

$$\theta_{ce}(t) = \Delta\omega_i \int_0^x e^{-x}(1-x)\,dx\left(\frac{\tau_2}{2}\right) \tag{2.8}$$

$$= \Delta\omega_i\left(\frac{\tau_2}{2}\right) xe^{-x} \tag{2.9}$$

The response to the sum of these inputs is then simply

$$\theta_{ce}(t) = \Delta\theta_i\, e^{-x}(1-x) + \Delta\omega_i\left(\frac{\tau_2}{2}\right) xe^{-x} \tag{2.10}$$

(We neglect the small residual phase error required to maintain frequency lock on the input frequency offset.) This may be rewritten as

$$\theta_{ce}(t) = \Delta\theta_i\, e^{-x} - \left(\Delta\theta_i - \Delta\omega_i\left(\frac{\tau_2}{2}\right)\right) xe^{-x} \tag{2.11}$$

---

*C.J. Byrne, "Properties and Design of the Phase Controlled Oscillator with a Sawtooth Comparator," BSTJ, p. 578, March 1962.

Note that the initial slope of the response is

$$\dot{\theta}_{ce}(t = 0^{+}) = \frac{2}{\tau_2} \left[-\Delta\theta_i - \left(\Delta\theta_i - \Delta\omega_i \left(\frac{\tau_2}{2} \right) \right) \right] \tag{2.12}$$

which must be negative if $\Delta\theta_i$ is > 0 and positive if $\Delta\theta_i$ is < 0 in order that the loop not slip a cycle. The requirement on $\Delta\omega_i$ is

$$|\Delta\omega_i| < \frac{4\Delta\theta_i}{\tau_2} \tag{2.13}$$

Since the maximum initial phase jump is π, the requirement on Δf_i is

$$|\Delta f_i| < \frac{2}{\tau_2} \tag{2.14}$$

With $\tau_2 = 1/12$ sec (see Appendix D) this frequency, known as the "seize" frequency, is 24 Hz. This is about 3 times as large as the maximum frequency offset that we are likely to encounter.

The carrier loop may be considered to be acquired when $x \cong 5$. Thus, from Eq. (2.7), the acquisition time is

$$t_{acq.} = \frac{5\tau_2}{2} \cong 0.20 \text{ sec} \tag{2.15}$$

During the time that this acquisition is taking place, the subcarrier loop is acquiring lock on the subcarrier signal at the output of the multiplier. The dc amplifier in the subcarrier loop is adjusted by the AGC circuit so that the damping coefficient is 2 (overdamped). In this case, the loop noise bandwidth is 2.84 Hz. This is approximately equal to the maximum subcarrier loop error frequency. In this situation the subcarrier loop should lock up without slipping cycles in a time on the order of $1/\omega_n$ sec.

Since $1/\omega_n$ is given by

$$\frac{1}{\omega_n} = \frac{\tau_2}{2\zeta_{acq.}} \tag{2.16}$$

for a second order loop with an active filter, and since τ_2 is determined by track mode considerations ($\zeta = 1/\sqrt{2}$ and $B_L = 0.5$ Hz in the track mode), and is related to the loop noise bandwidth and the damping coefficient by

$$\tau_2 = \frac{\zeta^2_{track}}{(B_L)_{track}} 1 + \frac{1}{4\zeta^2_{track}} = 1.5 \text{ sec} \tag{2.17}$$

the subcarrier loop acquisition takes place in about

$$\frac{1}{\omega_n} = \frac{1.5}{2\times 2} \approx 0.4 \text{ sec} \tag{2.18}$$

The subcarrier loop acquisition is detected by the coherent subcarrier loop acquisition detector which employs a lowpass filter having a noise bandwidth of 1.0 Hz. If this is a single pole filter, it responds in about 1 second. This is the same time that it takes to detect carrier loop frequency acquisition at point 3. When carrier frequency acquisition and subcarrier phase acquisition are detected, the carrier loop is switched to the track mode. The carrier loop gain is already adjusted to its proper value by the AGC circuit. Since the carrier loop is already frequency acquired, it need only adjust its phase. This phase acquisition occurs on the order of $1/\omega_n$ sec or approximately 0.06 sec. Phase acquisition is detected by a coherent cophasal phase detector as indicated in Fig. 2.10. This takes another 0.2 sec. If the carrier loop locks onto the compressed carrier and not onto some CW interference component that lies inside the loop noise bandwidth, there will be a signal output at point 6. It takes 0.2 sec to observe a loss of output at this point. This detection occurs simultaneously with carrier loop acquisition detection. If this output indicates

proper carrier loop lock, the subcarrier loop may be switched to the track mode. The outputs at points 5 and 6 may be monitored to make certain that the loops remain in lock.

The various times contributing to the total acquisition time are summarized in Table 2.2.

Table 2.2

User Receiver Compound PLL Acquisition Time

	Acquisition Function	Maximum Time (sec)
1.	Coarse Frequency Sweep	8.0
2.	Fine Frequency Sweep	1.0
3.	Carrier Loop Frequency Acquisition	0.2
4.	Subcarrier Loop Acquisition	0.4
5.	Carrier and Subcarrier Loop Acquisition Detection (Simultaneous)	1.0
6.	Carrier Loop Acquisition in Track Mode	0.1 (upper bound)
7.	Carrier Loop Acquisition Detection and Verification (Simultaneous)	0.2
8.	Verification of Subcarrier Loop Acquisition in Track Mode	0.2
	Total Maximum Acquisition Time	11.1 sec

The largest contribution to the acquisition time is the coarse frequency sweep. If this can be speeded up by sweeping at 1.2 kHz/sec rather than at 1.0 kHz/sec, the acquisition time can be reduced below 10 seconds.

When the compound PLL is properly locked, AGC control is obtained from the coherent carrier loop lock detector rather than from the subcarrier signal at the output of the sideband multiplier in the acquisition aid portion of the receiver. This is done so that the loops will have the proper AGC control voltages on their gain-controlled amplifiers in the event that the 400 BPS data is switched on. The output of the coherent carrier loop lock detector is lowpass filtered by a filter having a noise bandwidth on the order of 0.1 Hz in obtaining the AGC control voltage. This is done so that if the loops should fall out of lock while the 400 BPS data was on, reacquistion could take place with the gain-controlled amplifiers set to their proper gain levels. Should reacquisition fail to take place as a result of the lower SNR into the subcarrier acquisition loop during transmission of the 400 BPS data, this fact could be made known to the ground by an emergency telemetry signal which would be transmitted by the User in the event that reacquisition failed to occur within some short time after loss of lock, say 2 seconds. In this event, the ground would have to cease transmission of the 400 BPS data in order to permit this User to reacquire. With a properly designed system, such loss of lock situations should occur with very low probability so that interruption of the 400 BPS data by such a loss of lock situation will be rare.

2.5.4 The Ranging Sidetone Turnaround Channel

The functions of the ranging sidetone turnaround channel are:

1. To filter the ranging sidetones so as to remove as much noise, multipath, and RFI as possible while still preserving the relative phasing of these sidetones,
2. To amplify the sidetones to their proper level for phase modulation of the downlink carrier,

3. To detect when an excessive noise or RFI condition exists at the outputs of the ranging sidetone filters such that either excessive noise loading of the downlink carrier or insufficient SNR in the range tone demodulator would occur.

4. To disconnect the AR sidetones from the downlink demodulator when this condition exists at the output of the AR sidetone filter, and to disconnect all sidetones from the demodulator when this condition exists at the output of the fine range tone filter.

A block diagram of the ranging sidetone turnaround channel is shown in Fig. 2.12. After bandpass filtering and amplification to the proper signal level for PM modulation of the downlink carrier, the outputs of the fine range tone amplifier and the ambiguity range tone amplifier are square law detected and lowpass filtered by a very narrowband lowpass filter. As the noise level or the level of RFI in the outputs of these amplifiers rises, this is detected by the square law detector. The gain of the analog gate circuits at the output of these amplifiers is reduced from unity gain so that excessive noise loading of the downlink carrier does not occur. If the gain is reduced too much, however, the signal level in the range tone demodulator will be insufficient to permit proper range tone extraction. When this occurs there is no need to transmit the range tones on the downlink. Consequently, the analog gates are opened when the Schmitt triggers detect that the noise or interference levels have reached this point. Because of the much wider bandwidth of the AR sidetone filter, there is more chance that RFI may be present at the output of this filter than at the output of the fine range tone filter. However, the gain of the analog gate for the AR sidetones may be reduced by as much as a factor of 4 before the probability of AR tone extraction errors rise noticeably. The gain of the analog gate for the fine range tone cannot be reduced very much before the signal level of the fine range tone falls below threshold. However, because of the much narrower bandwidth of the fine range tone filter, the power density level of the RFI can increase to a much higher level than it can in the AR sidetone filter before it becomes necessary to reduce the gain of the analog gate below the threshold level. When threshold

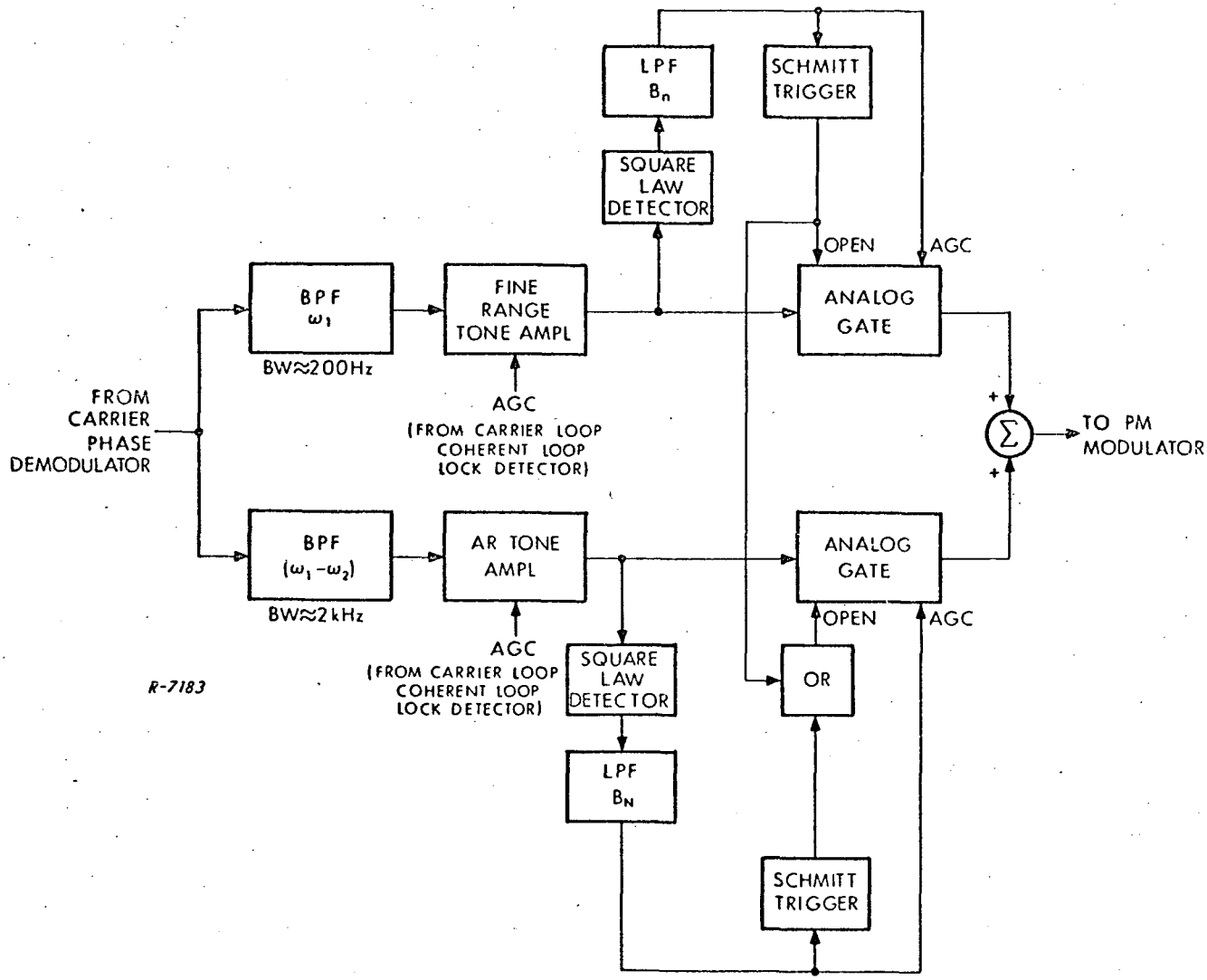

Fig. 2.12 Ranging Sidetone Turnaround Channel

is reached at the output of the fine range tone tilter, both the fine range tone and the AR sidetone analog gates are opened. Since AR demodulation cannot take place on the ground when the fine range tone is not transmitted on the downlink, there is no reason to transmit the AR sidetones under this condition.

The Schmitt trigger has a built-in hysteresis whose value is set so that when the gates are opened again the noise or RFI level will have been reduced by an amount sufficient to assure that ranging measurements can be made for a time long enough to obtain sufficient range data.

Alternate range tone schemes which reduce the problem of excessive noise loading of the downlink carrier as a result of noise and RFI turnaround are described briefly in Appendix D.

2.5.5 User Transponder Transmitter

Since as many as 30 Users may be transmitting simultaneously on the downlink, it is necessary to be able to distinguish between these various Users. This is done by assigning each User a unique wideband FM subcarrier frequency and carrier band. With 10 primary subcarrier frequencies and 3 carrier bands, 30 Users may be accommodated. With 10 additional auxiliary subcarrier frequencies, the number of simultaneous Users could be increased to 60.

The primary subcarrier frequencies are separated by 3.2 kHz, and the carrier bands by $3.2 \times 8 = 25.6$ kHz. The auxiliary subcarrier frequencies are interleaved between the primary subcarrier frequencies. All subcarriers and the 25.6 kHz carrier band separation frequency are derived from a 128 kHz crystal oscillator. This permits the effects of the local oscillator to be removed in the DAF doppler extractor as will be shown in Sec. 2.6.4. A convenient way to generate the subcarrier frequencies is shown in Fig. 2.13. In practice, a User would only be required to generate one primary subcarrier frequency and the adjacent auxiliary frequency.

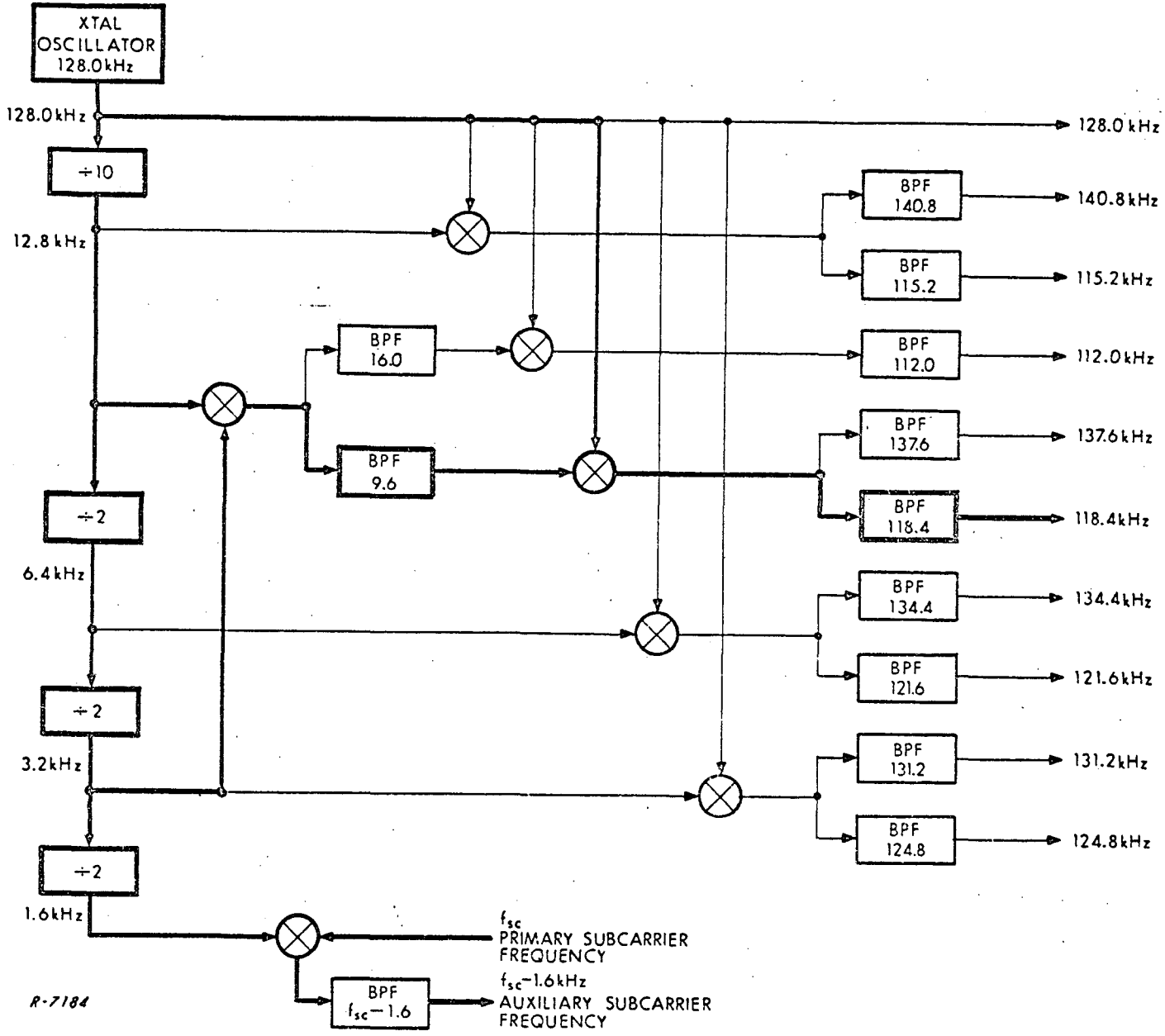

Fig. 2.13 Subcarrier Frequency Generation Scheme

The block diagram in Fig. 2.13 shows how any of the frequencies listed in Table 2.3 below can be generated. If a User were assigned a frequency of 118.4 kHz, for example, only the circuitry shown in bold lines in Fig. 2.13 would be used in this User's transponder.

Table 2.3

Downlink Subcarrier Frequencies

Primary (kHz)	Auxiliary (kHz)
112.0	110.4
115.2	113.6
118.4	116.8
121.6	120.0
124.8	123.2
128.0	126.4
131.2	129.6
134.4	132.8
137.6	136.0
140.8	139.2

The User transponder uses a turnaround ratio of 23/25 = 0.92. This ratio was chosen because:

1. It is very close to the desired ratio of 137/148.95 = 0.9197717355, and
2. It is a very convenient ratio to use.

With an uplink frequency of 148.9255 MHz, the downlink frequency will be 137.01146 MHz. Both are sufficiently close to the desired center band frequencies so as to cause no problem in that regard.

2

As in the DAF transmitter, the PM modulation of the downlink carrier by the filtered ranging sidetones and the telemetry data, and the wideband FM modulation by the subcarrier are performed in separate channels. The outputs of these channels are mixed in an output mixer which combines the modulations and achieves the desired downlink VHF carrier frequency.

The "divide-by-25" is achieved in the User transponder receiver by using a "long loop" carrier tracking PLL as shown in Fig. 2.9 in which the multiplier following the PM modulator multiplies the PM modulated VCO signal by 24. In this way the VCO frequency will be 1/25 of the input carrier frequency.

The "multiply-by-23" is achieved in the User transponder transmitter by using the fact that 23 = 48-25, so that a mixing operation can be utilized in which two separate signals from two multiplier-modulation chains are mixed together to form the desired output multiplication factor. As in the DAF transmitter, the PM modulator is followed by a multiply-by-48 multiplication chain as shown in Fig. 2.14. The factor of 25 is obtained by utilizing the fact that $25 = 24 + 1 = 8 \times (3 + \frac{1}{8})$. The coherent FM modulator is a phase-locked loop similar to that used in the DAF transmitter.

The carrier band may either be selected in accordance with instructions from the DAF or else simply designed into the transponder. The center band involves nothing more than a simple turnaround as described above. The two outer bands, one on either side of the carrier, are obtained by adding or subtracting 3.2 kHz to the frequency at the output of the divide-by-eight frequency divider as shown in Fig. 2.14. The frequency multiply-by-eight of the coherent FM modulator VCO signal increases the carrier band separation to 25.6 kHz.

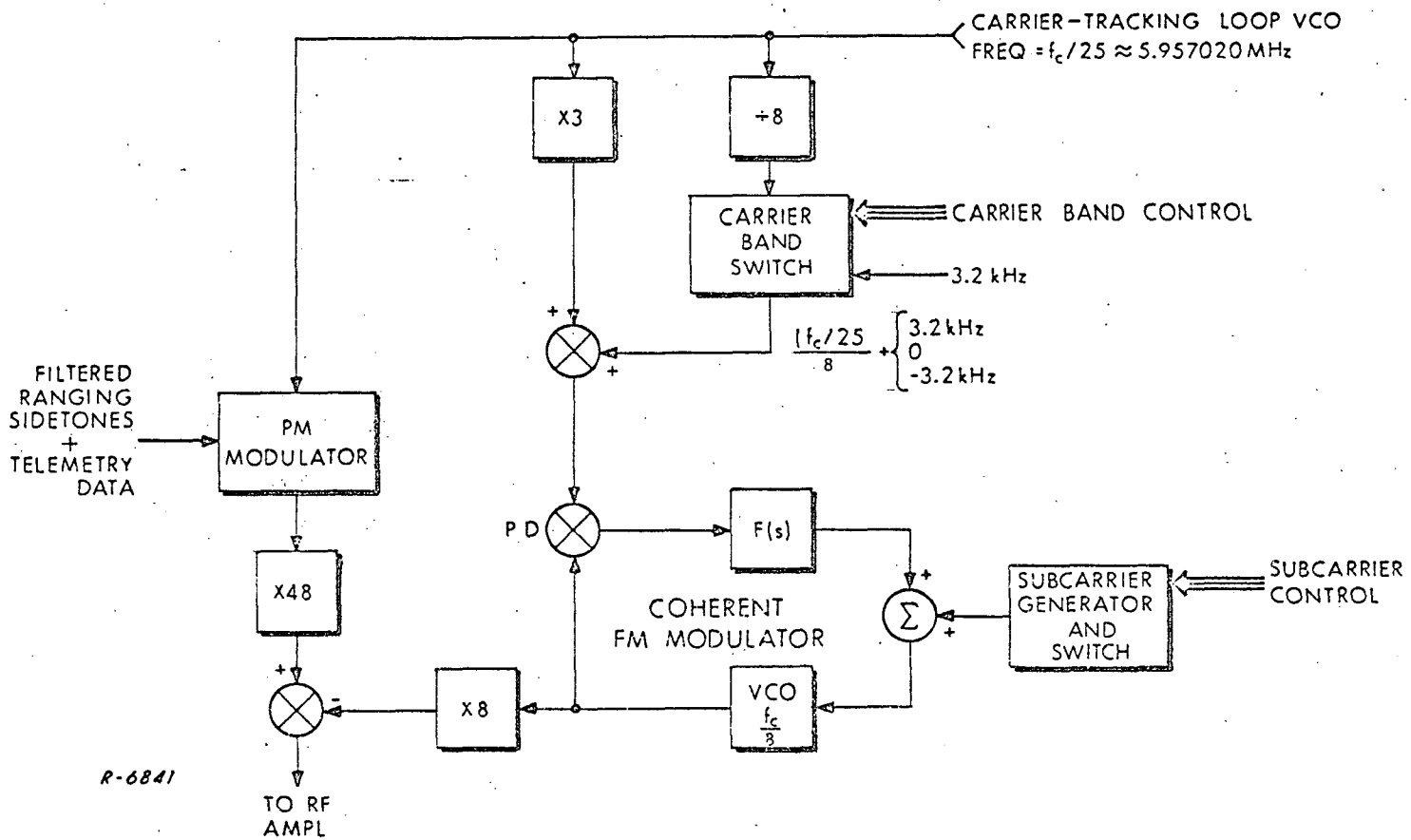

Fig. 2.14 User Transponder Transmitter

2.5.6 Handover

Two types of handover operations need be considered. These are 1) TDRS handover on the uplink and 2) SSMA channel handover on the downlink. TDRS handover occurs when it is desired to have a particular User cease tracking the signal from one TDRS and commence tracking the signal from another TDRS. SSMA channel handover occurs when it is desired to switch the User transmitter from one downlink channel to another.

Various options of differing degrees of complexity are possible insofar as TDRS handover operation is concerned. The simplest of these is to permit a User to receive from only one TDRS. This means that this User has the capability of receiving only the uplink signal which is wideband PM modulated with the subcarrier having the particular subcarrier frequency that his receiver is designed to acquire and track.

If the User is to receive signals from more than one TDRS, his receiver must be modified from the simple receiver design shown in Fig. 2.10. Two levels of complexity are possible for the case of multiple TDRS reception capability. The next simplest receiver utilizes a single carrier loop, a multiple frequency subcarrier loop and multiple acquisition aids as indicated in Fig. 2.15, which shows a receiver capable of sequentially receiving signals from two relay satellites. To understand the operation of this receiver, assume that the User is tracking the TDRS signal having subcarrier frequency f_{sc1}. In this case the subcarrier bandpass filter switch, the VCXO switch, the feedback switch, and the acquisition aid switch are all set to the state which passes the signals which correspond to the subcarrier at frequency f_{sc1}. The subcarrier loop mode switch is in the track position. If the DAF desires to switch the User from TDRS #1 to TDRS #2, it sends the appropriate command to the User via TDRS #1. Upon reception of this command, the User-control switches all the above switches to the state which passes the signals corresponding to the subcarrier at

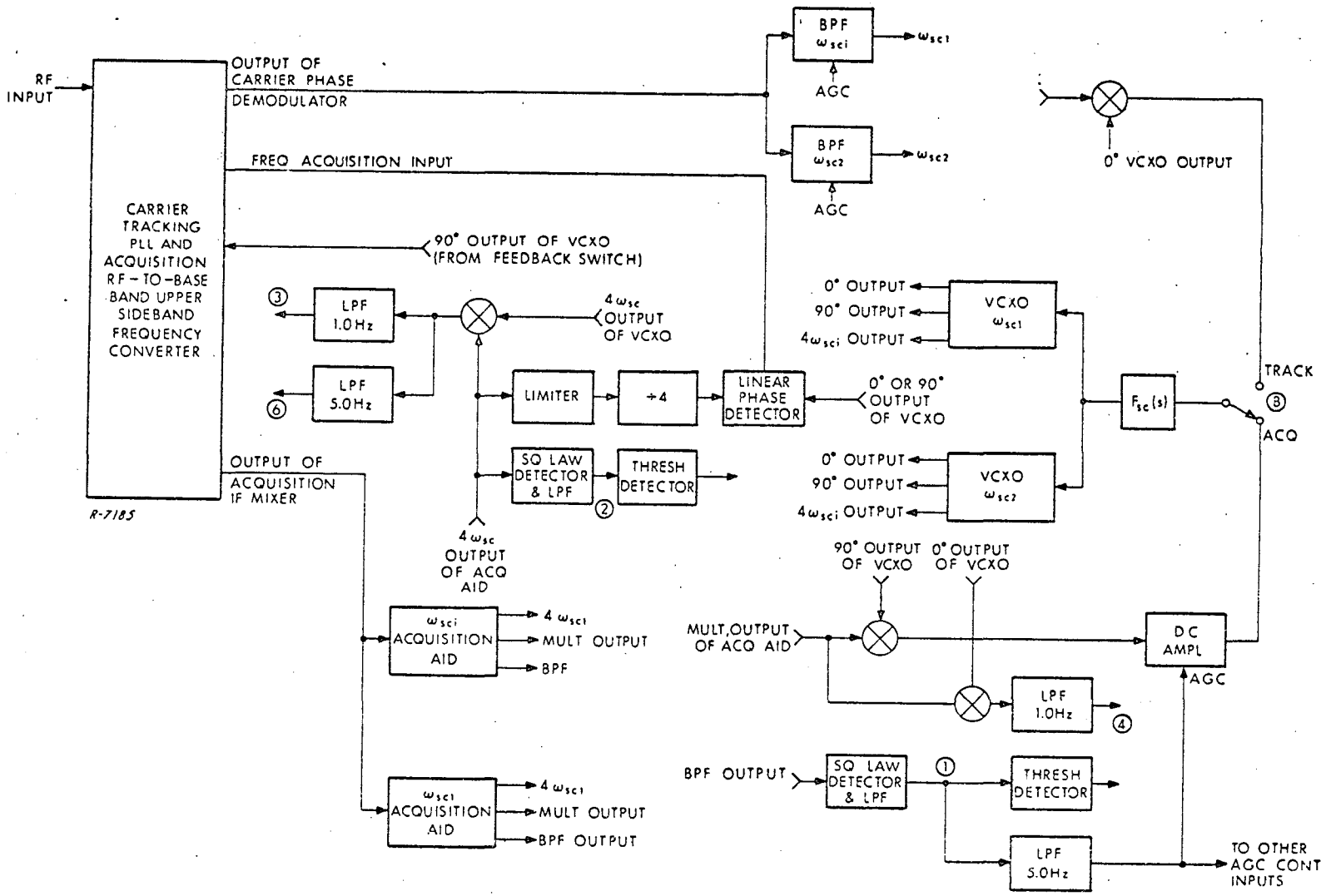

Fig. 2.15 User Receiver with Multi-TDRS Reception Capability

frequency f_{sc2}, and switches the subcarrier loop mode switch to the acquisition position and initiates carrier loop sweeps. The receiver then acquires the signal from TDRS #2 as described in the section on acquisition. The switches are not shown in Fig. 2.15.

The box labeled "ω_{sc} ACQ. AID" in Fig. 2.15 consists of the 4th and 5th order subcarrier sideband bandpass filters, the multiplier, the subcarrier signal bandpass filter, and the narrowband 4th order sideband BPF and its gate. The box labeled "VCXO ω_{sc}" in Fig. 2.15 consists of the subcarrier VCXO, the 90° phase shifter, and the frequency multiply-by-4. Refer to Fig. 2.10 for comparison.

If signals are to be sequentially received from more than two relay satellites, the User receiver is simply modified by adding additional acquisition aids, subcarrier loop VCXO's, and subcarrier bandpass filters. Additional transmission gate switches are simply added to accommodate the additional subcarrier frequencies.

The next level of complexity utilizes a separate receiver for each TDRS, but only a single transmitter. The User continually tracks the signals from all relay satellites in its view, but transmits the turned around carrier and ranging sidetones from only one receiver at a time in accordance with command instructions from the DAF. This permits more rapid sequential range and range rate measurements to be made to different relay satellites than is possible in the previous case.

Finally, the highest level of complexity utilizes essentially a separate complete transponder for each TDRS. The transmitter in each transponder uses a different downlink channel. This permits simultaneous ranging through several relay satellites.

SSMA channel handover is required when there are more Users than available channels but not all Users are in view simultaneously. In SSMA channel handover, the problem is to switch the User from its

present downlink channel, defined by its downlink subcarrier frequency and carrier band, to an unoccupied channel which the User has the capability of utilizing. The assignment of downlink channel capability to the various classes of Users and the procedure for distributing the Users among the various downlink channels so as to minimize the frequency of channel handover is an operational problem that can only be attacked when the communications requirements of each class of User, their number, and their orbital configurations are known. The capability that some Users will have of utilizing one of several different downlink channels permits this operational problem to be solved in a reasonably efficient and flexible manner.

The simplest level of User complexity provides the User with the capability of using only the center downlink carrier band and a single primary downlink subcarrier frequency. This User must switch to his auxiliary subcarrier frequency when another User must use this channel, or else must simply turn off his transmitter.

The next level of User complexity provides the User either with the capability of using all downlink carrier bands but only one downlink primary subcarrier frequency, or of using only the center downlink carrier band but several downlink primary subcarrier frequencies.

The highest level of User complexity provides the User with the capability of using all downlink carrier bands and several primary subcarrier frequencies.

The subcarrier generation technique and the carrier band selection technique were described in Sec. 2.5.5 and illustrated in Figs. 2.13 and 2.14. Transmission gate switches, controlled by the User-control, switch the User transponder transmitter to the downlink carrier band and subcarrier frequency commanded by the DAF.

2.6 DAF Receiving System

2.6.1 Functions

The DAF receiving system must perform the following functions:

1) Coherent translation of the downlink TDRS X-band signal to VHF.
2) Acquisition of the VHF wideband FM signal.
3) Coherent carrier tracking and phase demodulation of the VHF wideband FM signal by a compound PLL.
4) Extraction of the downlink telemetry.
5) Extraction of the range tones and range measurement.
6) Extraction of the two-way VHF carrier doppler and range rate measurement.

A functional block diagram of the DAF receiving system is shown in Fig. 2.16.

2.6.2 DAF Compound PLL Receiver

A block diagram of the DAF receiver compound PLL is shown in Fig. 2.17. This particular receiver receives the signal on the downlink channel corresponding to the downlink subcarrier frequency f'_{sc} and the downlink carrier frequency f'_c. In general, f'_c may be written as $(23/25)f_c + k\Delta f$, where k is either -1, 0, or +1, depending on which downlink carrier band is involved, and Δf is 25.6 kHz. The above frequencies are nominal frequencies and don't include the VHF doppler offset.

A comparison of this receiver with the User transponder receiver reveals that the structure of the compound PLL in the two receivers is identical. For the situation where $k \neq 0$, i.e., the downlink carrier band involved is not the center band, it is necessary to derive the carrier offset frequency Δf from the subcarrier tracking loop VCXO frequency. This is

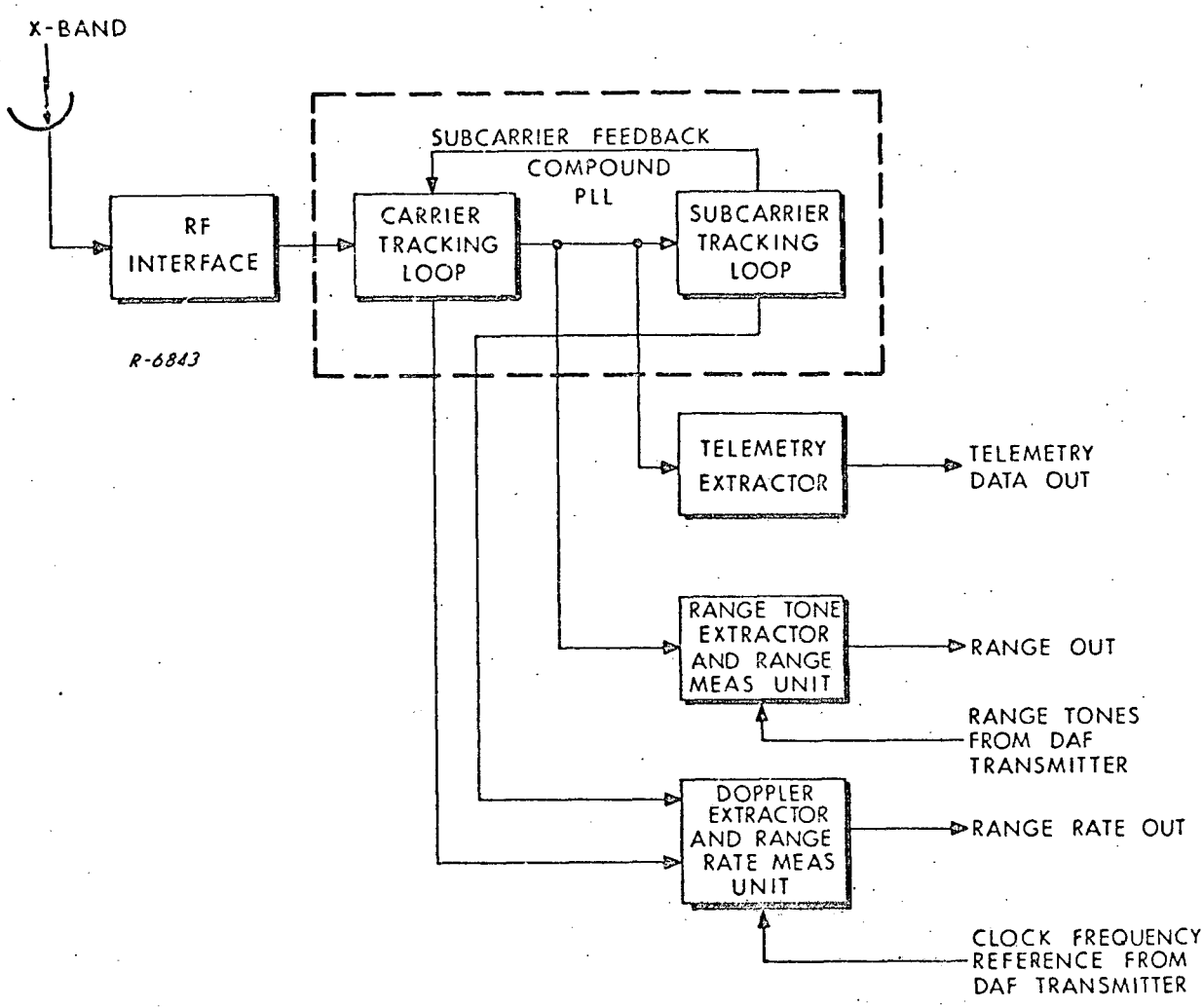

Fig. 2.16 DAF Receiving System Functional Block Diagram

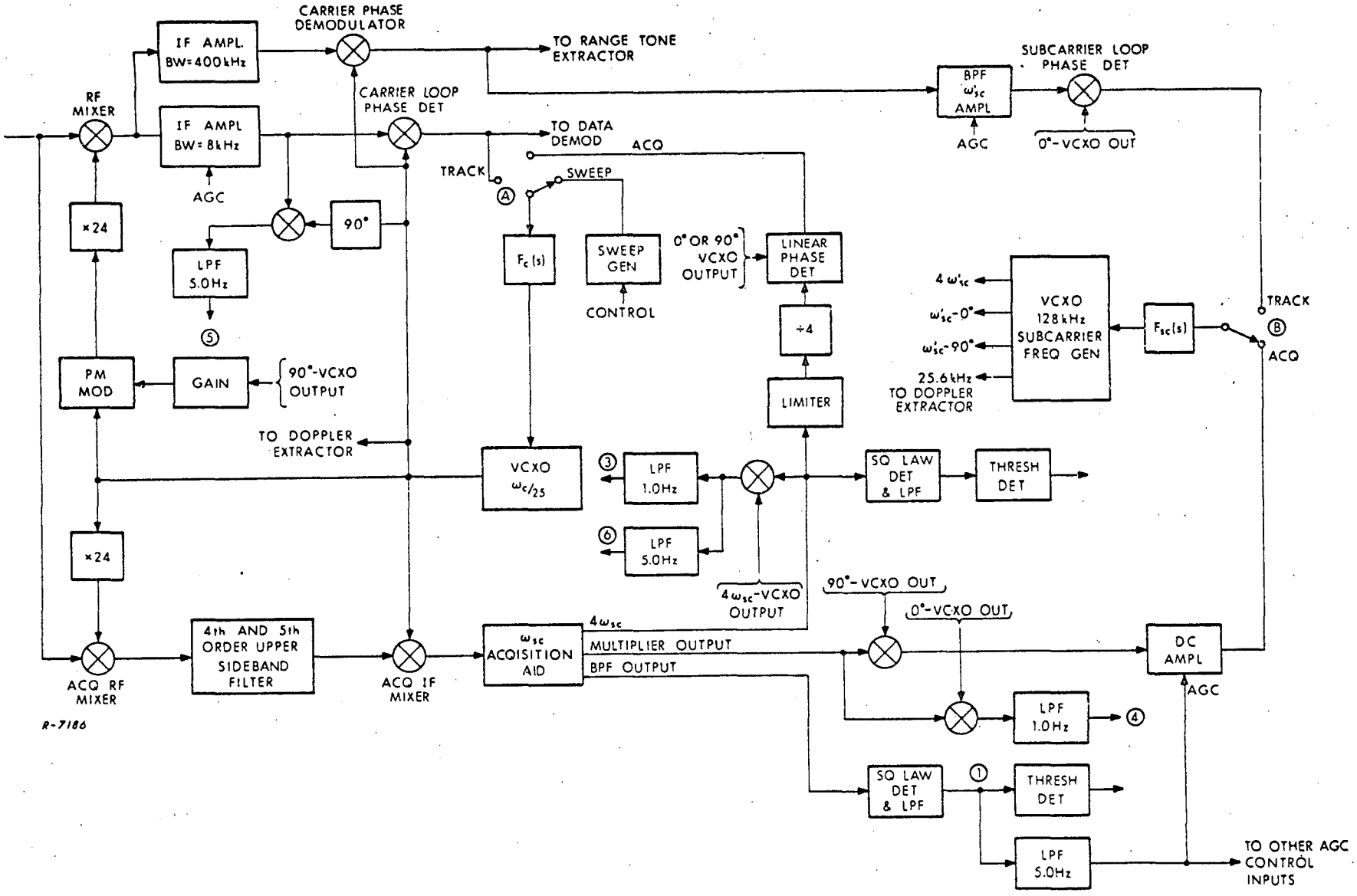

Fig. 2.17 Ground Receiver Compound PLL

so because the two frequencies are coherently related, both having been generated in the User transponder from the common 128 kHz crystal oscillator. The simplest way to do this is to use a subcarrier loop VCXO whose frequency is 128 kHz followed by a frequency synthesizer which generates the frequency 25.6 kHz and the subcarrier frequency f'_{sc} in the manner indicated in Fig. 2.13.

Acquisition is very similar to that of the User transponder except that data is not transmitted on the downlink during acquisition. Since the power that would have been robbed from the subcarrier sideband components by the data is now back in the subcarrier sidebands, the sideband filters in the acquisition aid can be narrowed to about 200 Hz, thereby helping to provide some discrimination against SSMA interference. The lowpass filter at the output of the square law detector at point 1 in the block diagram of Fig. 2.17 may be widened as a consequence of the higher downlink signal-to-noise power density ratio (required by proper demodulation of the 1000 BPS data). This means that the sweep rate may be essentially doubled in the coarse frequency sweep mode. Since the sweep range is essentially twice that of the uplink, the coarse frequency sweep time should be essentially the same as for the User receiver. The fine sweep time should be essentially the same as for the uplink case, as should the other acquisition times, so that the total acquisition time for the downlink should be about 10 seconds as in the uplink.

Range tone extraction may now be performed with the downlink telemetry data still not turned on. This means that the range tones may be acquired more rapidly and with less probability of error than if the data were present.

The receiver shown in Fig. 2.17 is capable of receiving the downlink signal from a single downlink channel. It would be desirable to design the receiver to be able to receive either the primary or corresponding auxiliary subcarrier frequency and with any of the three

carrier bands. In this way a User could be commanded to switch his downlink signal between any of these channels, in order to avoid an SSMA problem for example, and the same receiver could be used to track the signal. For the two subcarrier frequencies, the receiver would be modified as in Fig. 2.15. For the three carrier bands, the VCXO in the carrier loop could simply be designed to run at the center band frequency and could be pulled into either the upper or the lower carrier bands. During coarse frequency acquisition this is accomplished by applying a postive or negative dc voltage to the input of the loop filter for a preset time sufficient to drive the VCXO to the center frequency of either the upper or the lower carrier band. The sweep generator then sweeps the VCXO over the range of input doppler in that band. If the VCXO is in the center of the band when the sweep is applied, care must be taken not to sweep the VCXO out of the band. This means that the first sweep should sweep the VCXO only to the edge of the band with subsequent sweeps moving the VCXO back across the band. To prevent the VCXO from sweeping too far, or not far enough, the voltage on the VCXO may be monitored and compared to reference voltages which represent the desired end points of the sweep in each direction. During the search mode, the sweep can be controlled so as to sweep between these desired end points. Similar remarks apply to the sweep generator in the User transponder.

With these minor modifications, the receiver is capable of receiving a signal from any one of three primary channels and three auxiliary channels corresponding to a single primary subcarrier frequency with any of the three carrier bands and its associated auxiliary subcarrier frequency with any of the three carrier bands.

2.6.3 Range Tone Extraction and Range Measurement

A block diagram of the range tone extractor is shown in Fig. 2.18. A phase-locked loop is used to track the fine range tone. The fine range tone VCXO signal is then used to coherently demodulate the other ranging sidetones as indicated. A bandpass filter centered at 96 kHz ensures that noise and interference centered around the missing upper sideband frequency of 108.8 kHz does not appear at the output of the first coherent detector. The fine range tone VCXO signal is frequency divided by 16 and compared in phase with the coherently detected 6.4 kHz range tone. Logic circuitry determines whether to advance or retard the divide-by-16 counter. This process continues until the coarse range tone is acquired.

The fine range is measured by comparing the phase of the received fine range tone VCXO signal with that of the fine range tone from the DAF clock and frequency synthesizer. A digital phasemeter of 9 bit accuracy is required in this phase measurement.

Coarse range is measured by simply subtracting the contents of the divide-by-16 counter in the DAF range tone generator from the contents of the divide-by-16 counters in the DAF range tone extractor. The simplicity of this range extraction technique is one of the advantages of this ranging system.

2.6.4 Doppler Extraction and Range Rate Measurement

Range rate is determined by measuring the two-way VHF carrier doppler contained in the DAF receiver carrier-tracking loop VCO frequency. The function of the doppler extractor is to extract this doppler from the VCO frequency and add it to a convenient bias frequency. The range rate measurement unit then measures this doppler plus bias frequency, and determines the range rate. Any X-band doppler between the DAF and the TDRS is assumed to have been removed prior to the DAF VHF receiver.

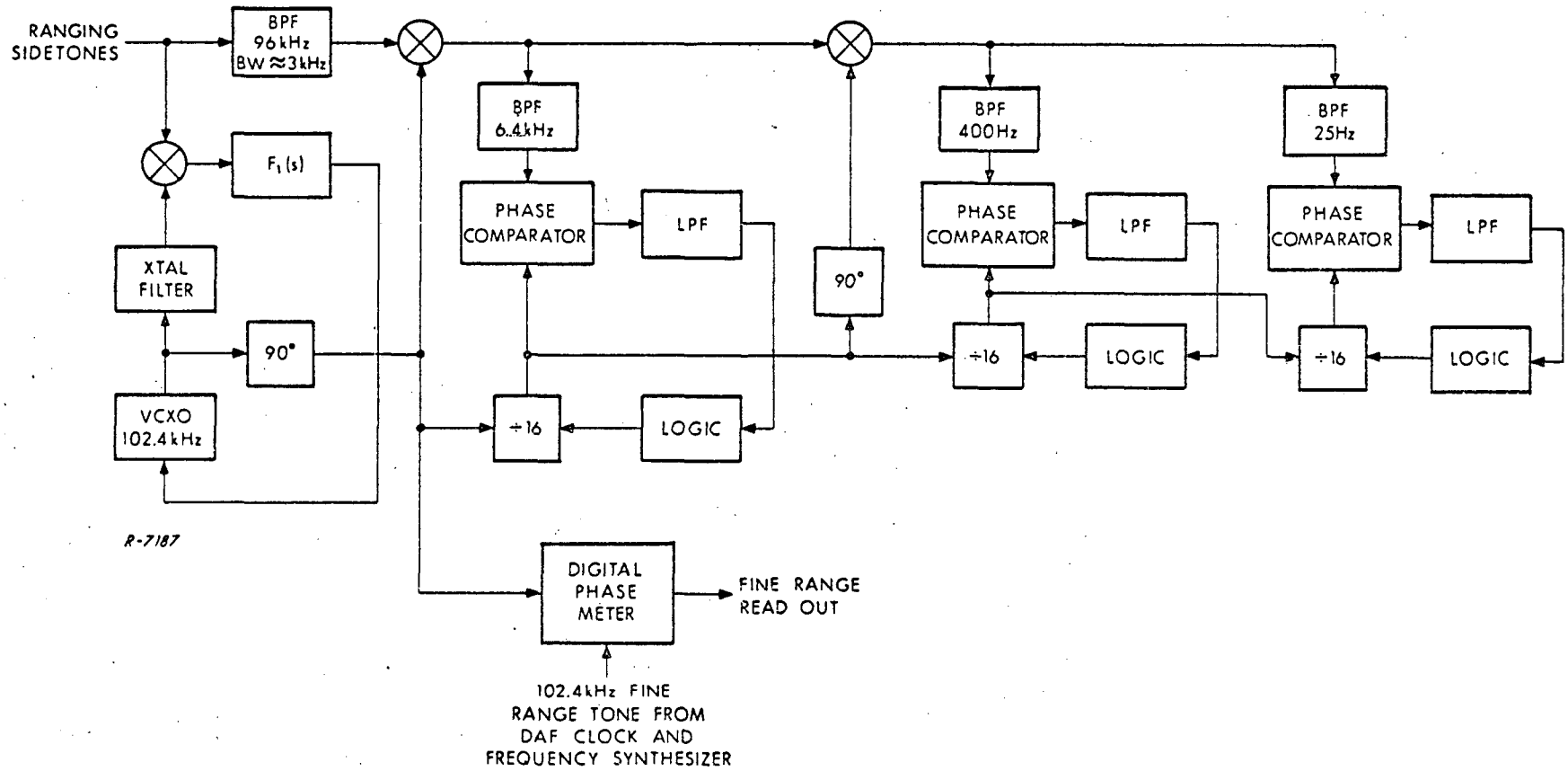

Fig. 2.18 Range Tone Extractor

The DAF receiver carrier loop VCO frequency, including doppler, is

$$f_{VCO} = \frac{f'_c}{25} = \frac{1}{25}\left\{\left(\frac{23}{25}\right)f_c + k\Delta f(1-\dot{\tau}_d) - \left(\frac{23}{25}\right)f_c\, 2\dot{\tau}_d\right\} \qquad (2.19)$$

where $\dot{\tau}_d$ is the doppler factor v_d/c. The doppler extractor must remove the carrier band offset frequency term $k\Delta f(1-\dot{\tau}_d)$ and the downlink center band carrier frequency term $\left(\frac{23}{25}\right)f_c$, and must add an appropriate bias frequency. How this is done is shown in Fig. 2.19.

The carrier loop VCO frequency is mixed with the frequency $(23/25)6f_o$ in mixer #1. This serves to remove the center band carrier frequency term and add an intermediate bias frequency. To see how this comes about, recall that the uplink carrier frequency is $f_c = 149\, f_o = 150\, f_o - f_o = 25(6\, f_o - f_o/25)$. Consequently, $6\, f_o$ is $f_c/25 + f_o/25$. The multiplication of the frequency $6\, f_o$ by the transponder turnaround ratio 23/25 yields the frequency

$$\frac{1}{25}\left\{\frac{23}{25}\, f_c + \frac{23}{25}\, f_o\right\} \qquad (2.20)$$

This is seen to be the sum of the center band carrier frequency term which must be removed from the carrier loop VCO plus an intermediate bias frequency. The difference frequency at the output of mixer #1 is

$$\frac{1}{25}\left\{\frac{23}{25}\, f_c - k\Delta f(1-\dot{\tau}_d) + \frac{23}{25}\, f_c\, 2\dot{\tau}_d\right\} \qquad (2.21)$$

This frequency is then multiplied by 25 to yield

$$\frac{23}{25}\, f_o - k\Delta f(1-\dot{\tau}_d) + \frac{23}{25}\, f_c\, 2\dot{\tau}_d \qquad (2.22)$$

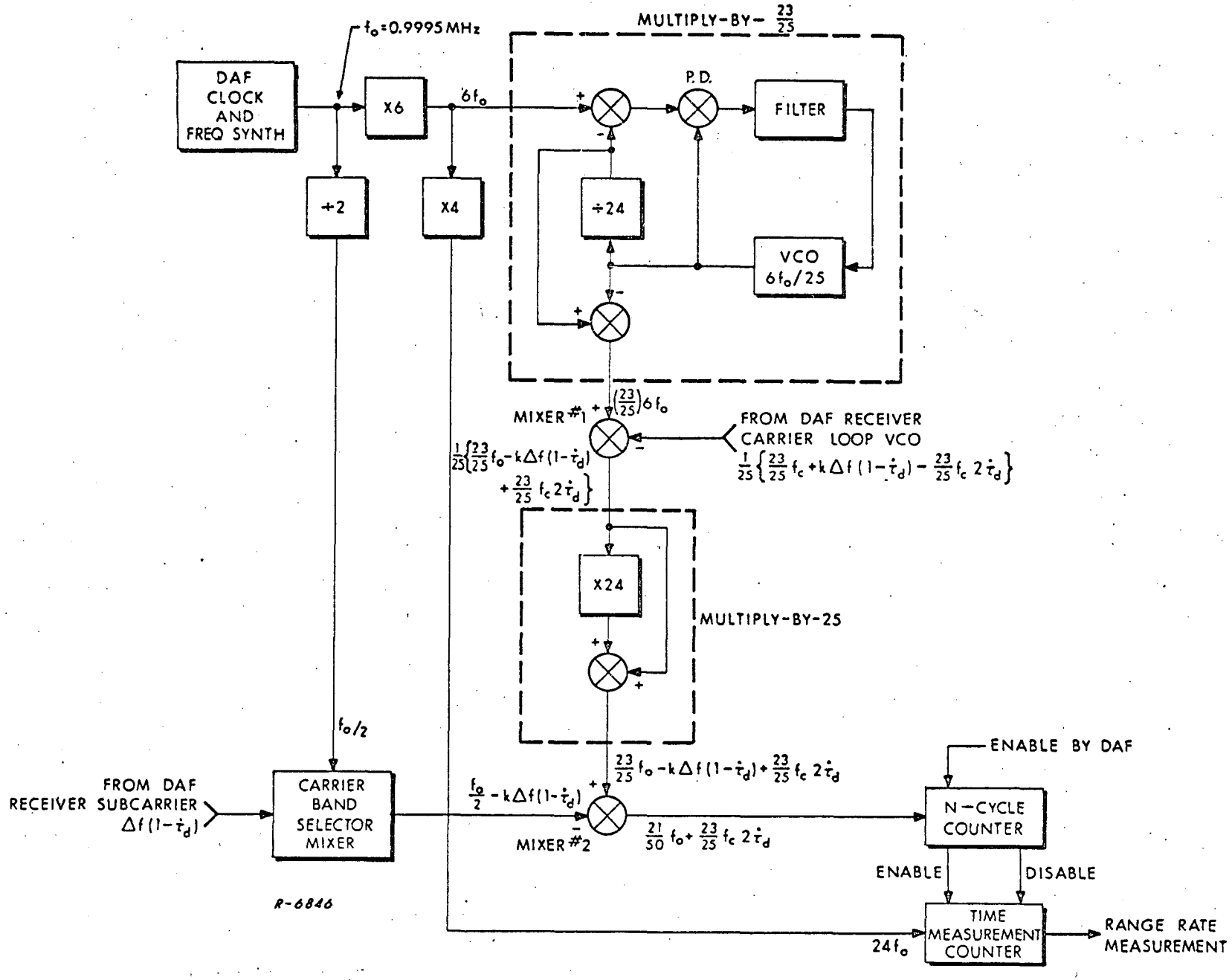

Fig. 2.19 Doppler Extractor and Range Rate Measurement Unit

The carrier offset term is removed by first mixing the frequency $f_o/2$ with the frequency $\Delta f(1-\dot{\tau}_d)$ obtained from the subcarrier loop in the carrier band selector mixer to produce the frequency

$$\frac{f_o}{2} - k\Delta f(1-\dot{\tau}_d) \tag{2.23}$$

and then mixing this in mixer #2 with the frequency at the output of the multiply-by-25 to obtain

$$\frac{23}{25} f_o - \frac{f_o}{2} + \frac{23}{25} f_c 2\dot{\tau}_d = \frac{21}{50} f_o + \frac{23}{25} f_c 2 \dot{\tau}_d \tag{2.24}$$

The frequency $(21/50) f_o$ is the final bias frequency at 419.79 kHz.

The range rate measurement is made with an N-counter system which measures the time required to accumulate N cycles of the doppler plus bias frequency. The clock frequency used in the N-counter range rate measurement system is $24 f_o \approx 24$ MHz. This frequency is both simple to generate, and ensures that the rms quantization error in the range rate measurement is much less than the permissible rms range rate error.

The N-counter range rate measurement system shown in Fig. 2.19 is enabled by the DAF. The first positive-going zero crossing of the doppler plus bias signal enables the time measurement counter which counts cycles of the clock frequency at $24 f_o$. When N-cycles of doppler plus bias are counted, the time measurement counter is disabled. The range rate is computed from the measured number of cycles of clock counted during the time required to accumulate N-cycles of doppler plus bias.

3. APPROACH TO PERFORMANCE EVALUATION

3.1 Disturbances

Any TDRS multiple-access system will be subjected to a variety of disturbances and interference threats. These include:

a) Additive Random Noise received from radiating noise sources such as the galactic plane, or generated in the receiver itself.

b) CW Interference received from terrestrial radiating sources. By CW is meant any interference signal consisting exclusively of discrete spectral components, i.e., perfectly periodic signal.

c) Narrowband RFI received from terrestrial radiating sources. This category is meant to include signals modulated by intelligence, such as voice-modulated or data-modulated signals. The term narrowband is relative to the spread-spectrum (2 MHz wide) of the TDRS signal. This RFI bandwidth is typically 10-20 kHz. Narrowband RFI is to be distinguished from CW RFI in that its spectrum does not consist exclusively of discrete components, but rather contains substantial amounts of continuous-spectrum components arising from nonperiodic signal components.

d) SSMA Interference. This is interference resulting from the use of Spread-Spectrum Multiple-Access techniques. At the User receiver, this interference results from the presence in the same band as the desired relay satellite signal of signals from other (undesired) relay satellites. At the relay satellite receiver, and hence at the ground receiver, this interference results from the presence in the same band as the desired User signal of signals from other (undesired) User spacecraft.

e) Multipath Interference arising from signal reflections off the earth's surface. This includes both specular and diffuse components, depending on the roughness and physics of the reflecting surface and the parameters of the TDRS-earth-User geometry.

The effects of each of these disturbances on the wideband FM system are analyzed in succeeding chapters, in terms of the basic communications functions performed by the system.

3.2 Basic System Functions

In order for the system to satisfactorily perform its intended functions of communications and tracking, it must successfully accomplish a set of more basic functions peculiar to the wideband-FM concept. The most important of these are:

a) Signal Acquisition including the locking of the various control loops and initiation of tracking and data extraction functions.

b) Compound PLL Tracking involving the tracking of both carrier and subcarrier with acceptably small phase errors.

c) Data Demodulation - the extraction of data-carrying waveforms with sufficient fidelity to permit bit detection, and bit and frame synchronization.

d) Ranging Sidetone Turnaround by the User transponder without undue degradation.

e) Ranging Sidetone Demodulation by the ground receiver, with sufficiently low phase errors to permit accurate ranging.

f) Doppler Extraction at the ground receiver, again with sufficiently low phase errors to permit accurate range rate measurement.

The effect of each disturbance type on each of these basic system functions is analyzed in the appropriate chapter in this report.

3.3 Performance Evaluation

The performance of the wideband FM technique in the presence of various disturbances is more difficult to evaluate analytically than other spread-spectrum techniques, such as the pseudo-noise technique. This is because the technique is not "uniformly" susceptible to most disturbances: the efffects of a disturbance are usually negligible over large segments of the range of variation of its parameters, and significant only over a small segment of the range. Thus the significant disturbance effects do not accumulate to degrade system performance except in the relatively rare occasions when the respective disturbances simultaneously fall within the "worst case" regions of their parameters.

Instead of attempting to determine the combinations of signal and disturbance radiation conditions that would yield significant system degradation, an unnecessarily cumbersome and speculative process at best, we chose a parametric approach to performance evaluation. Each disturbance is treated separately in terms of each of the basic system functions listed in Sec. 3.2, and the ranges of disturbance parameters that would impair the function were determined.

From this treatment emerged the particular function most vulnerable to the particular disturbance. This then set the "threshold" values of the disturbance parameters that could be tolerated in the worst case. Generally speaking, these worst case disturbance conditions did not occur simultaneously, so that the consideration of one disturbance at a time was justified as a meaningful evaluation procedure.

4. ADDITIVE RANDOM NOISE EFFECTS

4.1 Introduction

The function of a noise analysis of the TDRS wideband FM system is to 1) determine which of the various system functions: compound PLL acquisition and tracking, data demodulation, ranging, and range-rate measurement is the limiting factor in the determination of the required system signal to noise power density level on the uplink and the downlink, and 2) determine what modifications may be made in either the signal format or the receiver design to improve system performance.

The uplink is considered first. Uplink compound PLL tracking and command data demodulation depend only on the received uplink signal power and uplink noise power density. Range and range-rate measurements are made on the ground, and consequently both uplink and downlink received signal powers and noise power densitites enter into the computations. This requires a judicious apportionment of the uplink and downlink powers in the computation.

4.2 Uplink Analysis

The received wideband FM signal on the uplink may be written as

$$e_u(t) = \sqrt{2S_u}\,\sin\left\{\omega_{cu}t + \theta_{cu}(t) + \delta\sin\left[\omega_{su}t + \theta_{su}(t)\right] + \phi_{mu}(t)\right\} \tag{4.1}$$

where

S_u is the received uplink power

ω_{cu} is the uplink VHF carrier frequency (rad/sec)

θ_{cu} is the carrier phase which contains the uplink VHF doppler and doppler dynamics

δ is the wideband FM subcarrier modulation index, and is equal to 5.52

ω_{su} is the uplink subcarrier frequency (rad/sec) which is used to distinguish the particular TDRS

θ_{su} is the subcarrier phase which contains the uplink subcarrier doppler and doppler dynamics

$\phi_{mu}(t)$ is the uplink PM modulating signal consisting of split-phase command data $\beta x_u(t)$ and ranging sidetones

$$\rho_1 \sin\left[\omega_1 t + \theta_1(t)\right] + \rho_2 \cos\left[(\omega_1 - \omega_2)t + \theta_1(t) - \theta_2(t)\right]$$

$$+ 2\rho_A \left(\sin\left[\omega_3 t + \theta_3(t)\right] + \sin\left[\omega_4 t + \theta_4(t)\right]\right)$$

$$\cos\left[(\omega_1 - \omega_2)t + \theta_1(t) - \theta_2(t)\right] .$$

The data phase deviation β is 1 radian. The phase deviation of the fine range tone, ρ_1, is 0.5 radians. The phase deviations ρ_2 and ρ_A are to be determined from the noise analysis, but they are presumed to be less than ρ_1.

With the compound PLL in the track mode, the equivalent wideband FM reference signal which effectively multiplies the received signal may be written as

$$e_{ref}(t) = \sqrt{2} \cos\left\{\omega_{cu} t + \hat{\theta}_{cu}(t) + \delta \sin\left[\omega_{su} t + \hat{\theta}_{su}(t)\right]\right\} \qquad (4.2)$$

where

$\hat{\theta}_{cu}(t)$ and $\hat{\theta}_{su}(t)$ are estimates of $\theta_{cu}(t)$ and $\theta_{su}(t)$.

If white Gaussian noise of single-sided noise power density N_u is also present at the input, the output of the carrier loop phase detector is, in normalized form,

$$e_{PD}(t) = \sin\left\{\theta_{cu}(t) - \hat{\theta}_{cu}(t) + \delta\sin\left[\omega_{su}t + \theta_{su}(t)\right]\right.$$

$$\left. - \delta\sin\left[\omega_{su}t + \hat{\theta}_{su}(t)\right] + \phi_{mu}(t)\right\}$$

$$+ \text{Gaussian white noise of single-sided power density } N_u/S_u \qquad (4.3)$$

This output may be expanded and renormalized as

$$\sin\left\{\theta_{cu}(t) - \hat{\theta}_{cu}(t) + \delta\sin\left[\omega_{su}t + \theta_{su}(t)\right] - \delta\sin\left[\omega_{su}t + \hat{\theta}_{su}(t)\right]\right\}$$

$$\overline{+\cos\left\{\theta_{cu}(t) - \hat{\theta}_{cu}(t) + \delta\sin\left[\omega_{su}t + \theta_{su}(t)\right]\right.}$$

$$\left.\overline{- \delta\sin\left[\omega_{su}t + \hat{\theta}_{su}(t)\right]\right\}}\left[\tan\beta\chi_u(t) + \bar{\rho}_1\sin\left[\omega_1 t + \theta_{1u}(t)\right]\right.$$

$$+ \bar{\rho}_2\cos\left[(\omega_1 - \omega_2)t + \theta_{1u}(t) - \theta_{2u}(t)\right] + 2\bar{\rho}_A\left(\sin\left[\omega_3 t + \theta_{3u}(t)\right]\right.$$

$$\left.\left. + \sin\left[\omega_4 t + \theta_{4u}(t)\right]\right)\cos\left[(\omega_1 - \omega_2)t + \theta_{1u}(t) - \theta_{2u}(t)\right]\right]$$

$$+ \text{Gaussian white noise of single-sided power density } N_u/S_u M_u^2$$

where

$$M_u = \overline{\cos\phi_{mu}(t)} \quad \text{and} \quad \bar{\rho}_R = \frac{2J_1(\rho_R)}{J_o(\rho_R)} \approx \rho_R \quad \text{for } \rho_R \le 0.5. \qquad (4.4)$$

The first term in Eq. (4.4) is the compound PLL tracking error. The second term represents the data and ranging sidetones which are suppressed slightly by the fact that there are carrier and subcarrier loop tracking errors. The third term is the Gaussian white noise of single-sided noise power density $N_u/S_u M_u^2$.

4.2.1 Compound PLL Tracking Threshold

The value of the ratio $S_u M_u^2/N_u$ required for the compound PLL to operate approximately as linear independent carrier and subcarrier loops in the presence of worst-case doppler dynamics is computed in Appendix A. The carrier loop presents the more severe problem as a result of the wider loop noise bandwidth required to track the worst-case carrier doppler dynamics. The results of the analysis conducted in Appendix A are summarized in Table 4.1.

Table 4.1

Compound PLL Parameters

Quantity	Value	Significance
$\left[\ddot{\theta}_{cu}(t)\right]_{maximum}$	30 rad/sec^2	worst-case carrier doppler dynamics
$\left(B_{cu}\right)_{optimum}$	9 Hz	optimum carrier loop noise bandwidth
$\left(\rho_{threshold}\right)_{cu} = \left(S_u M_u^2/N_u\right)$	462	corresponds to a peak carrier loop phase error of 30°.
$\left(B_{su}\right)_{optimum}$	~0.5 Hz	optimum subcarrier loop noise bandwidth
$\left(\sqrt{\overline{\theta_{cuen}^2}}\right)_{threshold}$	8°	carrier loop rms phase noise error at threshold

4.2.2 Data Demodulator Threshold

If the carrier and subcarrier loop phase errors are small, their effects on slight suppression of the PM modulation may be neglected. In this case the results of Appendix C may be applied with $\mu = T\tan\beta$ $\sigma^2 = \frac{1}{2} N_u T/S_u M_u^2$, so that the condition for achieving the required BEP becomes

$$T\tan^2\beta\left(\rho_{\text{threshold}}\right)_{xu} = 15.85 \qquad (4.5)$$

With $\beta = 1$ radian and $T = 2.5 \times 10^{-3}$ sec (400 BPS data), the value of $\left(\rho_{\text{threshold}}\right)_{xu}$ is 2600. This is significantly larger than the threshold of linear operation of the compound PLL, and in fact will turn out to be the determining factor in setting the uplink signal-to-noise power density ratio.

For the 100 BPS data the value of $\left(\rho_{\text{threshold}}\right)_{xu}$ is 650, which is just slightly higher than the threshold of linear operation of the compound PLL.

4.2.3 Ranging Sidetone Turnaround

The fine range tone at ω_1 and the ambiguity resolution sidetones clustered around $(\omega_1 - \omega_2)$ are bandpass filtered as indicated in Fig. 4.1.

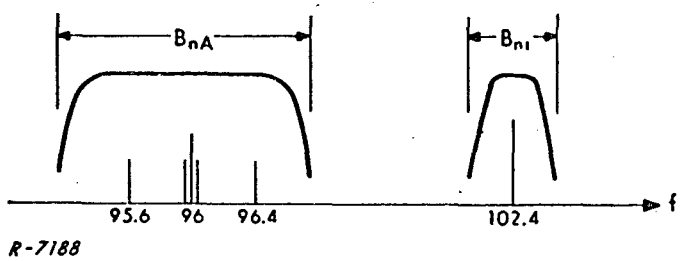

Fig. 4.1 Bandpass Filtering of Ranging Sidetones

The noise bandwidth of the fine range tone filter may be on the order of 200 Hz, whereas the noise bandwidth of the ambiguity resolution sidetone filter is on the order of 2000 Hz.

The filtered sidetones phase modulate the downlink carrier with approximately the same deviations as on the uplink. As will be shown, it is more advantageous to use a larger phase deviation for the ambiguity resolving tones on the uplink than on the downlink. Noise which is contained in these filter bandwidths also phase modulates the downlink modulation. The modulation suppression caused by the retransmitted noise will now be evaluated.

The noise in these filter bandwidths is considered to be divided into noises whose spectral components lie within several Hz of each ranging sidetone, plus the remaining noise. That is, the total noise passed by the filters, $n_F(t)$, is written as

$$n_F(t) = n_1(t) + n_{1R}(t) + n_2(t) + n_3^+(t) + n_3^-(t) + n_4^+(t) + n_4^-(t) + n_{AR}(t) \tag{4.6}$$

where $n_1(t)$ is the noise whose spectral components lie within several Hz of the fine range tone, and $n_{1R}(t)$ is the remaining noise passed by the fine range tone bandpass filter. Similar definitions apply to the other noises in Eq. (4.6). The single-sided noise power density of $n_F(t)$ is $N_u/S_u M_u^2$.

The downlink transmitted signal is of the form

$$e_T(t) = \sqrt{2S_T}\sin\left\{\frac{23}{25}\left(\omega_{cu}t + \hat{\theta}_{cu}(t)\right) + k\Delta\omega t + \delta\sin[\omega_{sd}t] + \beta\chi_d(t)\right.$$
$$+ \bar{\rho}_1\sin\left(\omega_1 t + \theta_{1u}(t)\right) + n_1(t) + \bar{\rho}_2\cos[(\omega_1-\omega_2)t + \theta_{1u}(t) - \theta_{2u}(t) + n_2(t)$$
$$\left. + \bar{\rho}_A\sin[(\omega_1-\omega_2)t + \omega_3 t + \theta_{1u}(t) - \theta_{2u}(t) + \theta_{3u}(t)] + n_3^+(t)\right.$$

$$- \bar{\rho}_A \sin[(\omega_1 - \omega_2)t - \omega_3 t + \theta_{1u}(t) - \theta_{2u}(t) - \theta_{3u}(t)] + n_3^-(t)$$

$$+ \bar{\rho}_A \sin[(\omega_1 - \omega_2)t + \omega_4 t + \theta_{1u}(t) - \theta_{2u}(t) + \theta_{4u}(t)] + n_4^+(t)$$

$$- \bar{\rho}_A \sin[(\omega_1 - \omega_2)t - \omega_4 t + \theta_{1u}(t) - \theta_{2u}(t) - \theta_{4u}(t)] + n_4^-(t)$$

$$+ n_{1R}(t) + n_{AR}(t) \Big\} \qquad (4.7)$$

The noises $n_{1R}(t)$ and $n_{AR}(t)$ suppress the amplitude of the desired modulation by the factor

$$M_n = \overline{\cos\left(n_{1R}(t) + n_{AR}(t)\right)} = e^{-\frac{1}{2}\left(\overline{n_{1R}^2} + \overline{n_{AR}^2}\right)} \qquad (4.8)$$

The variances $\overline{n_{1R}^2}$ and $\overline{n_{AR}^2}$ are approximately

$$\overline{n_{1R}^2} = \frac{1}{\rho_u} B_{n1} \quad \text{and} \quad \overline{n_{AR}^2} = \frac{1}{\rho_u} B_{nA} \qquad (4.9)$$

where B_{n1} and B_{nA} are the noise bandwidths of the fine range tone filter and the ambiguity resolution sidetone filter, respectively. The power in the desired modulation is suppressed by the factor

$$M^2 = e^{-\left(\overline{n_{1R}^2} + \overline{n_{AR}^2}\right)} = e^{-\left(B_{n1} + B_{nA}\right)/\rho_u} \qquad (4.10)$$

If $B_{n1} + B_{nA} = 2.2 \times 10^3$ Hz, and if ρ_u is equal to the value required by the 400 BPS data BEP requirement, then $M_n^2 = 0.429$. This means that the retransmitted noise will suppress the desired downlink signal components by approximately 3.7 dB in power.

4.3 Downlink Analysis

The received downlink signal may be written as

$$
\begin{aligned}
e_d(t) = \sqrt{2S_d}\,\sin\Big\{ & \frac{23}{25}\left(\omega_{cu}t + \hat{\theta}_{cu}(t)\right) + k\Delta\omega t + \theta_{cd}(t) + \delta\sin\left[\omega_{sd}t + \theta_{sd}(t)\right] \\
& + \beta\chi_d(t) + \bar{\rho}_1\sin\left(\omega_1 t + \theta_{1d}(t)\right) + {}_1(t) + \bar{\rho}_2\cos\left[(\omega_1-\omega_2)t + \theta_{1d}(t) - \theta_{2d}(t)\right] \\
& + n_2(t) + \bar{\rho}_A\sin\left[(\omega_1-\omega_2)t + \omega_3 t + \theta_{1d}(t) - \theta_{2d}(t) + \theta_{3d}(t)\right] + n_3^+(t) \\
& - \bar{\rho}_A\sin\left[(\omega_1-\omega_2)t - \omega_3 t + \theta_{1d}(t) - \theta_{2d}(t) - \theta_{3d}(t)\right] + n_3^-(t) \\
& + \bar{\rho}_A\sin\left[(\omega_1-\omega_2)t + \omega_4 t + \theta_{1d}(t) - \theta_{2d}(t) + \theta_{4d}(t)\right] + n_4^+(t) \\
& - \bar{\rho}_A\sin\left[(\omega_1-\omega_2)t - \omega_4 t + \theta_{1d}(t) - \theta_{2d}(t) - \theta_{4d}(t)\right] + n_4^-(t) \\
& + n_{1R}(t) + n_{AR}(t)\Big\}
\end{aligned}
\tag{4.11}
$$

where

S_d is the received wideband FM downlink signal power.

23/25 is the transponder turnaround ratio.

$\Delta\omega$ is the carrier offset frequency, and k may be either +1, 0, or -1.

$\theta_{cd}(t)$ is the carrier phase which contains the downlink carrier doppler and doppler dynamics.

δ is the wideband FM subcarrier modulation index and is equal to 5.52.

ω_{sd} is the downlink subcarrier frequency.

$\theta_{sd}(t)$ is the subcarrier phase which contains the downlink subcarrier doppler and doppler dynamics.

$\chi_{kd}(t)$ is the downlink split-phase telemetry data.

$\theta_{kd}(t)$ is the k^{th} range tone phase containing the <u>two-way</u> range tone doppler and doppler dynamics.

The equivalent wideband FM reference signal which effectively multiplies the received signal is

$$e_{REF}(t) = \sqrt{2}\cos\left\{\frac{23}{25}\omega_{cu}t + k\Delta\omega t + \hat{\theta}_c(t) + \delta\sin\left[\omega_{sd}t + \hat{\theta}_{sd}(t)\right]\right\} \qquad (4.12)$$

where $\hat{\theta}_c(t)$ is the estimate of $\theta_c(t) = \left(\theta_{cd}(t) + \left(\frac{23}{25}\right)\hat{\theta}_{cu}(t)\right)$, and $\hat{\theta}_{sd}(t)$ is the estimate of the subcarrier phase $\theta_{sd}(t)$.

Rewriting the phase $\theta_c(t)$ as

$$\theta_c(t) = \left(\theta_{cd}(t) + \left(\frac{23}{25}\right)\theta_{cu}(t) - \left(\frac{23}{25}\right)\left(\theta_{cu}(t) - \hat{\theta}_{cu}(t)\right)\right) \qquad (4.13)$$

it is readily seen that the carrier loop must essentially track the two-way doppler dynamics on the downlink VHF carrier, and will also track the phase-jitter on the transmitted downlink carrier.

If white Gaussian noise of single-sided noise power density N_d is also present at the input, the output of the carrier loop phase detector is, in normalized form

$$e_{PD}(t) = \sin\left\{\theta_c(t) - \hat{\theta}_c(t) + \delta\sin\left[\omega_{sd}t + \theta_{sd}(t)\right] - \delta\sin\left[\omega_{sd}t + \hat{\theta}_{sd}(t)\right] + \beta\chi_d(t)\right.$$

$$\left. + \text{turned-around range tones and noise}\right\}$$

$$+ \text{Gaussian white noise of single-sided power density } \frac{N_d}{S_d} \qquad (4.14)$$

As was done in the uplink analysis, this output is expanded and renormalized as

$$\sin\left\{\theta_c(t) - \hat{\theta}_c(t) + \delta\sin\left[\omega_{sd}t + \theta_{sd}(t)\right] - \delta\sin\left[\omega_{sd}t + \hat{\theta}_{sd}(t)\right]\right\}$$

$$+ \cos\left\{\theta_c(t) - \hat{\theta}_c(t) + \delta\sin\left[\omega_{sd}t + \theta_{sd}(t)\right] - \delta\sin\left[\omega_{sd}t + \hat{\theta}_{sd}(t)\right]\right\}\left[\tan\beta\,\chi_d(t)\right.$$

$$\left. + \tilde{\rho}_1\sin\left[\omega_1 t + \theta_{1d}(t)\right] + \tilde{\rho}_2\cos\left[(\omega_1 - \omega_2)t + \theta_{1d}(t) - \theta_{2d}(t)\right] + n_1(t) + n_2(t)\right.$$

$$+ \tilde{\rho}_A \sin[(\omega_1 - \omega_2)t + \omega_3 t + \theta_{1d}(t) - \theta_{2d}(t) + \theta_{3d}(t)] + n_3^+(t)$$

$$- \tilde{\rho}_A \sin[(\omega_1 - \omega_2)t - \omega_3 t + \theta_{1d}(t) - \theta_{2d}(t) - \theta_{3d}(t)] + n_3^-(t)$$

$$+ \tilde{\rho}_A \sin[(\omega_1 - \omega_2)t + \omega_4 t + \theta_{1d}(t) - \theta_{2d}(t) + \theta_{4d}(t)] + n_4^+(t)$$

$$- \tilde{\rho}_A \sin[(\omega_1 - \omega_2)t - \omega_4 t + \theta_{1d}(t) - \theta_{2d}(t) - \theta_{4d}(t)] + n_4^-(t) \Big]$$

$$+ \text{Gaussian white noise of single-sided power density } \frac{N_d}{S_d M_d^2 M_n^2} \tag{4.15}$$

where $M_d^2 \approx M_u^2$ if $\beta = 1$ radian and if $\bar{\rho}_R = \dfrac{2J_1(\rho_R)}{J_o(\rho_R)} \approx \rho_R$, and M_n^2 is given in Eq. (4.10).

The first term in Eq. (4.15) is the compound PLL tracking error. The second term represents the data and ranging sidetones plus the noises lying within several Hz of the ranging sidetones, and the third term is the Gaussian white noise of single-sided power density $N_d/S_d M_d^2 M_n^2$.

4.3.1 Compound PLL Tracking Threshold

If we assume that the carrier loop tracks the phase-jitter on the transmitted downlink carrier with negligible error, the carrier loop-phase error $\theta_c(t) - \hat{\theta}_c(t)$ will consist of the dynamic tracking error plus phase jitter resulting from the presenece of the Gaussian white noise at the receiver input. Consequently, the results of Appendix A may be applied here with $\ddot{\theta}_c$ increased to

$$\ddot{\theta}_c = 30 \times 2 \times \frac{23}{25} = 55.2 \text{ rad/sec}^2 \tag{4.16}$$

The optimum carrier loop noise bandwidth in the ground receiver is 12.2 Hz, and the threshold value of $\rho_d \equiv S_d M_d^2 M_n^2 / N_d$ for carrier threshold, $\left(\rho_{\text{threshold}}\right)_{cd}$, is 622. The subcarrier loop noise bandwidth in the ground receiver need not differ from that of user receiver since only one-way doppler dynamics are involved in subcarrier tracking on the down-link. Also, the carrier loop is the critical loop in the compound PLL. Consequently, the subcarrier loop noise bandwidth will be set at 0.5 Hz for all downlink subcarrier frequencies.

4.3.2 Data Demodulator Threshold

As in the uplink case, the results of Appendix C may be applied with $\mu = T \tan\beta$ and $\sigma^2 = \frac{1}{2} N_d T / S_d M_d^2 M_n^2$, so that the condition for achieving the required BEP becomes

$$T \tan^2\beta \left(\rho_{\text{threshold}}\right)_{xd} = 15.85 \qquad (4.17)$$

With $\beta = 1$ radian and $T = 10^{-3}$ sec, the value of $\left(\rho_{\text{threshold}}\right)_{xd}$ is 6500. This is considerably higher than the value required by the compound PLL, and in fact determines the threshold on the downlink.

4.3.3 Range Tone Demodulation

The signals and noises into the range tone demodulator may be written as

$$\tilde{\rho}_1 \sin[\omega_1 t + \theta_{1d}(t)] + n_1(t) + \tilde{\rho}_2 \cos[(\omega_1 - \omega_2)t + \theta_{1d}(t) - \theta_{2d}(t)] + n_2(t)$$

$$+ \tilde{\rho}_A \sin[(\omega_1 - \omega_2)t + \theta_{1d}(t) - \theta_{2d}(t) + \omega_3 t + \theta_{3d}(t)] + n_3^+(t)$$

$$- \tilde{\rho}_A \sin[(\omega_1 - \omega_2)t + \theta_{1d}(t) - \theta_{2d}(t) - \omega_3 t - \theta_{3d}(t)] + n_3^-(t) + \ldots .$$

+ Gaussian white noise of single-sided noise power density $N_d / S_d M_d^2 M_n^2$ — (4.18)

It is convenient to write the downlink noise as the sum of noises which lie within several Hz of each sidetone plus the remaining noise. If the range tone demodulator is linear, only the noises that lie within several Hz of each sidetone will contribute to the ranging errors. Consequently, the above expression for the signals and noises into the range tone demodulator is modified by replacing $n_1(t)$, $n_2(t)$, etc., with noises $\tilde{n}_1(t)$, $\tilde{n}_2(t)$, etc., which all have single-sided noise power densitites around each sidetone given by the sum

$$\frac{N_u}{S_u M_u^2} + \frac{N_d}{S_d M_d^2 M_n^2} = \Phi_R = \frac{1}{\rho_u} + \frac{1}{\rho_d} \tag{4.19}$$

In the fine range tone loop the fine range tone input signal and noise is effectively multiplied by a VCO signal of the form

$$e_{1VCO}(t) = \sqrt{2}\cos[\omega_1 t + \hat{\theta}_{1d}(t)] \tag{4.20}$$

where $\hat{\theta}_{1d}(t)$ is an estimate of $\theta_{1d}(t)$. The output of this multiplier is

$$\frac{\tilde{\rho}_1}{\sqrt{2}}\sin[\theta_{1d}(t) - \hat{\theta}_{1d}(t)] + \text{Gaussian "white" noise of single-sided power density } \Phi_R \tag{4.21}$$

The noise is "white" over the fine range tone loop noise bandwidth.

The fine range tone loop is linear if the error $\theta_{1d}(t) - \hat{\theta}_{1d}(t)$ is small. Under the small phase error resumption, the linear phase model of the loop shown in Fig. 4.2 may be used.

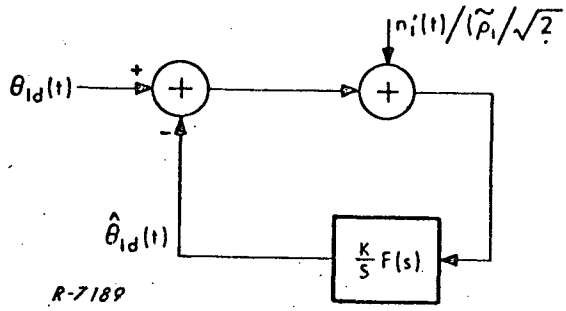

Fig. 4.2 Linear Phase Model of the Fine Range Tone PLL

The noise $n_1'(t)$ is the noise $\tilde{n}_1(t)$ multiplied down to baseband so that its single-sided power density is Φ_R.

The phase error $\theta_{1R} = \theta_{1d}(t) - \hat{\theta}_{1d}(t)$ consists of a dynamic tracking error and a noise error. TDRS system specifications require that the one-way rms range error be less than 15 meters. For a fine range tone frequency of 102.4 kHz, this requires that the rms phase error, $\sqrt{\theta_{1e}^2}$, be less than 0.0645 radians or 3.7°. This means that the total rms phase error

$$\sqrt{\theta_{1e}^2} = \sqrt{\theta_{1et}^2 + \theta_{1en}^2} \tag{4.22}$$

must be less than 0.0645 radians even for the worst-case doppler dynamics.

The dynamic tracking error, θ_{1et}, is given by

$$\theta_{1et} = \frac{\ddot{\theta}_{1d}}{\omega_{n1}^2} \tag{4.23}$$

where the loop natural frequency, ω_{n1}, is related to the loop noise bandwidth, B_1, by

$$B_1 = \frac{\omega_{n1}}{2}\left(\zeta + \frac{1}{4\zeta}\right) = k_1\omega_{n1} \tag{4.24}$$

The mean square phase noise error, $\overline{\theta_{1en}^2}$, is

$$\overline{\theta_{1en}^2} = \frac{2}{\tilde{\rho}_1^2} \Phi_R B_1 \tag{4.25}$$

If the loop is optimized by selecting the noise bandwidth so that Φ_R is maximum when the rms phase error is at its threshold value, the following results are obtained:

$$\left(B_1\right)_{\text{optimum}} = \frac{\sqrt{5}\,\ddot{\theta}_{1d}\,k_1^2}{\left(\sqrt{\overline{\theta_{1e}^2}}\right)_p} \tag{4.26}$$

$$\left(\Phi_R\right)_{\text{threshold}} = \left(\frac{4}{5}\right)\frac{\left(\overline{\theta_{1e}^2}\right)_p}{\left(B_1\right)_{\text{opt.}}}\,\frac{\tilde{\rho}_1^2}{2} \tag{4.27}$$

For $\zeta = 1/\sqrt{2}$, $\tilde{\rho}_1 \cong 0.5$, $\ddot{\theta}_{1d} \cong 4.1 \times 10^{-2}$ rad/sec^2, and $\left(\sqrt{\overline{\theta_{1e}^2}}\right)_p = 0.0645$ radians, $\left(B_1\right)_{\text{optimum}}$ and $\left(\Phi_R\right)_{\text{threshold}}$ are

$$\left(B_1\right)_{\text{optimum}} = 0.635 \text{ Hz} \tag{4.28}$$

$$\left(\Phi_R\right)_{\text{threshold}} = 0.655 \times 10^{-3} \tag{4.29}$$

If $\rho_u = S_u M_u^2 / N_u$ is equal to 2600 (the value required for uplink data, and which makes M_n^2 equal to 0.429), ρ_d must be greater than 3700 for thi s threshold value of Φ_R to be realized. For larger values of ρ_u the value of ρ_d may be decreased. It must, however, be larger than $1528 = \left(\Phi_R\right)_{th}^{-1}$. We now consider the requirements of proper range ambiguity resolution.

The ambiguity resolution sidetones clustered around $\omega_1 - \omega_2$ are coherently mixed down to the medium fine range tone frequency, ω_2, by a signal of the form $\sqrt{2}\sin[\omega_1 t + \hat{\theta}_{1d}(t)]$ which is obtained by phase shifting the fine range tone VCO signal by 90°. The output of this mixer is

$$\frac{\tilde{\rho}_2}{\sqrt{2}}\sin\left[\omega_2 t - \left(\theta_{1d}(t) - \hat{\theta}_{1d}(t)\right) + \theta_{2d}(t)\right] + \left(\tilde{n}_2(t)\right)'$$
$$+\frac{\tilde{\rho}_A}{\sqrt{2}}\cos\left[\omega_2 t - \left(\theta_{1d}(t) - \hat{\theta}_{1d}(t)\right) + \theta_{2d}(t) - \left(\omega_3 t + \theta_{3d}(t)\right)\right] + \left(\tilde{n}_3^+(t)\right)'$$
$$-\frac{\tilde{\rho}_A}{\sqrt{2}}\cos\left[\omega_2 t - \left(\theta_{1d}(t) - \hat{\theta}_{1d}(t)\right) + \theta_{2d}(t) + \left(\omega_3 t + \theta_{3d}(t)\right)\right] + \left(\tilde{n}_3^-(t)\right)'$$
$$+\frac{\tilde{\rho}_A}{\sqrt{2}}\cos\left[\omega_2 t - \left(\theta_{1d}(t) - \hat{\theta}_{1d}(t)\right) + \theta_{2d}(t) - \left(\omega_4 t + \theta_{4d}(t)\right)\right] + \left(\tilde{n}_4^+(t)\right)'$$
$$-\frac{\tilde{\rho}_A}{\sqrt{2}}\cos\left[\omega_2 t - \left(\theta_{1d}(t) - \hat{\theta}_{1d}(t)\right) + \theta_{2d}(t) + \left(\omega_4 t + \theta_{4d}(t)\right)\right] + \left(\tilde{n}_4^-(t)\right)' \tag{4.30}$$

The single-sided noise power densitites of the noises around the medium fine range tone and the other ranging side tone frequencies are all equal to Φ_R.

The phase shifted signal $\sqrt{2}\sin[\omega_1 t + \hat{\theta}_{1d}(t)]$ is frequency divided by 16 to form the medium-fine range tone ambiguity loop VCO signal. This VCO signal may be written as

$$e_{2VCO}(t) = \sqrt{2}\cos\left[\omega_2 t + \frac{\hat{\theta}_1}{16} + \theta_{2A}\right] \tag{4.31}$$

where θ_{2A} is ambiguity resolution phase error.

This VCO signal multiplies the medium fine range tone and noise $\left(\tilde{n}_2(t)\right)'$ to produce the error signal and noise given by

$$\frac{\tilde{\rho}_2}{2}\sin\left[-\theta_{1e} + \frac{\theta_{1e}}{16} - \theta_{2A}\right] + n_2'(t) \tag{4.32}$$

Here use has been made of the facts that $\theta_{2d} = \theta_{1d}/16$ and that $\theta_{1e} = \theta_{1d} - \hat{\theta}_{1d}$. The single-sided noise power density of the noise $n_2'(t)$ is Φ_R.

The ambiguity resolution phase error θ_{2A} is driven to zero by the action of the medium fine range tone ambiguity PLL. A linear phase model of the loop is valid when the phase $\left(\theta_{2A} + \frac{15}{16}\theta_{1e}\right)$ is small. The phase $-\theta_{2A}$ may be considered as the loop phase error, with $n_2'(t)$ and $-\frac{15}{16}\theta_{1e}$ representing additive noises. If the noise plus the phase error $(15/16)\theta_{1e}$ is too large, it may cause θ_{2A} to settle at + or $-22\frac{1^\circ}{2}$ thereby causing an ambiguity resolution error. We there <u>define</u> a "peak" phase error θ_{p2} as

$$\theta_{p2} = \sigma\sqrt{\frac{4}{\tilde{\rho}_2^2}\Phi_R B_2} + \left(\frac{15}{16}\right)\sigma\sqrt{\frac{2}{\tilde{\rho}_1^2}\Phi_R B_2} + \left(\frac{15}{16}\right)\theta_{1et} \qquad (4.33)$$

and require that $\tilde{\rho}_2$ be chosen so that for $B_2 \cong 0.02$ Hz, $\sigma = 3$, and Φ_R equal to the fine range tone threshold value, the "peak" phase error is $\pi/16$.

For the manner in which the noise bandwidth of the fine range tone loop was optimized, $\theta_{1et} = \frac{1}{\sqrt{5}}\left(\sqrt{\theta_{1e}^2}\right)_p$. Under these conditions the value of $\tilde{\rho}_2$ is found to be approximately 0.16.

The VCO signal of the medium-fine range tone ambiguity loop is phase-shifted by 90° to provide the reference signal for the coherent demodulation of the medium-coarse and coarse range tones. The output of this coherent demodulator when $\theta_{2A} = 0$ is

$$\tilde{\rho}_A \cos\left[\frac{15}{16}\theta_{1e}\right] \sin\left(\omega_3 t + \theta_3(t)\right) + \left(n_3^+\right)'' + \left(n_3^-\right)''$$
$$+ \tilde{\rho}_A \cos\left[\frac{15}{16}\theta_{1e}\right] \sin\left(\omega_4 t + \theta_4(t)\right) + \left(n_4^+\right)'' + \left(n_4^-\right)'' \qquad (4.34)$$

where $\left(n_3^+\right)''$ and $\left(n_3^-\right)''$ are the noises around ω_3 from the upper and lower sidebands respectively, and similarly for $\left(n_4^+\right)''$ and $\left(n_4^-\right)''$. For $\sqrt{\overline{\theta_{1e}^2}} \leq 0.0645$, $\cos\left[\frac{15}{16}\theta_{1e}\right]$ may be approximated by 1.

The medium-coarse range tone ambiguity loop reference signal is obtained from the reference signal used for the coherent demodulation of the medium-coarse and coarse range tones by a digital divide by 16. This reference signal may be written as

$$e_{3VCO}(t) = \sqrt{2}\cos\left[\omega_3 t + \frac{\hat{\theta}_1}{(16)^2} + \theta_{3A}\right] \tag{4.35}$$

so that the output of the medium-coarse range tone ambiguity loop phase detector is

$$\frac{\tilde{\rho}_A}{\sqrt{2}}\sin\left(\frac{\theta_{1e}}{(16)^2} - \theta_{3A}\right) + n_3'(t) \tag{4.36}$$

where θ_{3A} is the ambiguity resolution phase error, and the single-sided noise power density of $n_3'(t)$ is $2\Phi_R$.

Neglecting $\theta_{1e}/(16)^2$, our criterion for correct ambiguity resolution is that the "peak" error defined by

$$\theta_p = \sigma\sqrt{\frac{4\Phi_R B_3}{\tilde{\rho}_A^2}} \tag{4.37}$$

be less than $\pi/16$. We select $\tilde{\rho}_A$ so that for $B_3 \cong 0.02$ Hz, Φ_R equal to the threshold value for fine range tone tracking, and $\sigma = 3$, the peak error, θ_p, is $\pi/16$. The value of $\tilde{\rho}_A$ so obtained is approximately 0.110 radians. Analysis of the coarse range tone ambiguity loop yields the same result.

The results of the ranging analysis are summarized below.

For $\tilde{\rho}_1 \approx \rho_1 = 0.5$ radians, the maximum value of Φ_R that may be tolerated is 0.655×10^{-3} when the fine range tone loop is optimized so that the rms phase error is 0.0645 radians (or 3.7°). The optimum noise bandwidth of the fine range tone loop, (B_1), is 0.635 Hz.

Correct ambiguity resolution will be achieved with high probability for the above value of Φ_R for ambiguity resolution range tone loop noise bandwidths of 0.02 Hz if $\tilde{\rho}_2 \approx \rho_2 = 0.16$ radians and $\tilde{\rho}_A \approx \rho_A = 0.11$ radians.

4.3.4 Range-Rate Analysis

Range-rate measurement specifications call for an rms range-rate error of less than 10 cm/sec for a 1 second measurement time. For an N-cycle counter doppler measurement unit, the rms one-way range rate error $(\overline{\Delta\dot{R}^2})^{1/2}$, is related to the rms phase jitter on the tracked downlink carrier $(\overline{\theta_{cn}^2})^{1/2}$ by the expression

$$\left(\overline{\Delta\dot{R}^2}\right)^{1/2} = \frac{c}{\sqrt{2}\, 2\pi f_c \left(\frac{23}{25}\right) T} \left(\overline{\theta_{cn}^2}\right)^{1/2} \tag{4.38}$$

where f_c is the uplink carrier frequency, T is the measurement duration, and c is the velocity of light. This expression assumes that the phase jitter is uncorrelated over a time duration of length T. The phase jitter on the tracked downlink carrier consists of phase jitter on the tracked uplink carrier which is retransmitted by the User spacecraft, plus phase jitter arising from noise (or other sources of interference) at the DAF receiver input which falls within the carrier loop noise bandwidth after wideband FM compression. That is, $\left(\overline{\theta_{cn}^2}\right)^{1/2}$ is given by

$$\left(\overline{\theta_{cn}^2}\right)^{1/2} = \left[\left(\frac{23}{25}\right)^2 \left(\overline{\theta_{cen}^2}\right)_u + \left(\overline{\theta_{cen}^2}\right)_d\right]^{1/2} \tag{4.39}$$

For T = 1 sec and f_c = 148.925 MHz, the 19 cm/sec range-rate error corresponds to an rms phase jitter $\left(\overline{\theta^2_{c\eta}}\right)^{1/2}$ equal to 0.405 radians.

For the carrier loop threshold values of ρ_u and ρ_d

$$\left(\overline{\theta^2_{cen}}\right)_u = \left(\frac{(B_c)_{opt.}}{\rho_{th}}\right)_u = \frac{9.0}{462} = .0195$$

$$\left(\overline{\theta^2_{cen}}\right)_d = \left(\frac{(B_c)_{opt.}}{\rho_{th}}\right)_d = \frac{12.2}{622} = .0195$$

so that

$$\left[\left(\frac{23}{25}\right)^2 \left(\overline{\theta^2_{cen}}\right)_u + \left(\overline{\theta^2_{cen}}\right)_d\right]^{1/2} = \left[(1.847)(.0195)\right]^{1/2} = 0.190 \qquad (4.40)$$

Since this is less than the threshold value of the range rate measurement, the range-rate measurement specifications will be met if the compound PLL's are operating above threshold.

4.3.5 Uplink and Downlink S/N Tradeoff

Of real interest in the TDRS system analysis are the values of S_u/N_u and S_d/N_d. Now that M^2 can be computed, the values of S_u/N_u and S_d/N_d may be determined in terms of required values of ρ_u and ρ_d.

With β = 1 radian, ρ_1 = 0.5 radian, ρ_2 = 0.16 radian, and ρ_A = 0.11 radian, M^2 is

$$M^2 = \cos^2\beta J_0^2(\rho_1) J_0^2(\rho_2) J_0^8(\rho_A) = (.54)^2(.9385)^2(.9936)^2(.997)^8$$

$$= 0.245 \qquad (4.41)$$

The most stringent requirement on both the uplink and downlink S/N occurs for the data demodulation. On the uplin $\rho_u > 2600$, whereas on the downlink $\rho_d > 6500$. Because of the turned-around noise on the downlink, ρ_d is

$$\rho_d = \left(\frac{S_d}{N_d}\right) M^2 e^{-(B_{n1} + B_{nA})/\rho_u} \tag{4.42}$$

and

$$\rho_u = \left(\frac{S_u}{N_u}\right) M^2$$

For $\rho_d = 6500$, ρ_u may be increased over its required value of 2600 thereby permitting (S_d/N_d) to lie between 26,400 and 61,500. The noise bandwidth of the ranging sidetone turn-around filter, $(B_{n1} + B_{nA})$, is taken to be 2.2 kHz. A plot of (S_d/N_d) as a function of (S_u/N_u) for $\rho_d = 6500$ is shown in Fig. 4.3. This plot shows the reduction in required downlink (S/N) that may be realized by reducing the effects of the suppression of the downlink signal by turn-around noise.

4.3.6 An Alternative Technique for Reducing the Effects of Turned-Around Noise

In Fig. 4.3 it was shown how the value of (S_d/N_d) required to meet the downlink data BEP requirement may be decreased at the expense of an increase in the value of (S_u/N_u). This effect is a result of reducing the suppression of the downlink desired-signal modulation power by the re-transmitted phase noise as the uplink S/N is increased. An alternative way of accomplishing this is to increase the deviations of the ambiguity resolving ranging sidetones on the uplink and decrease them on the downlink. The increased modulation suppression on the uplink is compensated for by an increase in (S_u/N_u).

For example, if ρ_2 on the uplink is increased to 0.48 radians and ρ_A is increased to 0.375 radians, the value of $M_u^2 = \cos^2\beta J_0^2(\rho_1) J_0^2(\rho_2) J_0^8(\rho_A)$ is 0.170. In order that $\rho_u = S_u M_u^2/N_u$ be greater than 2600, as required by

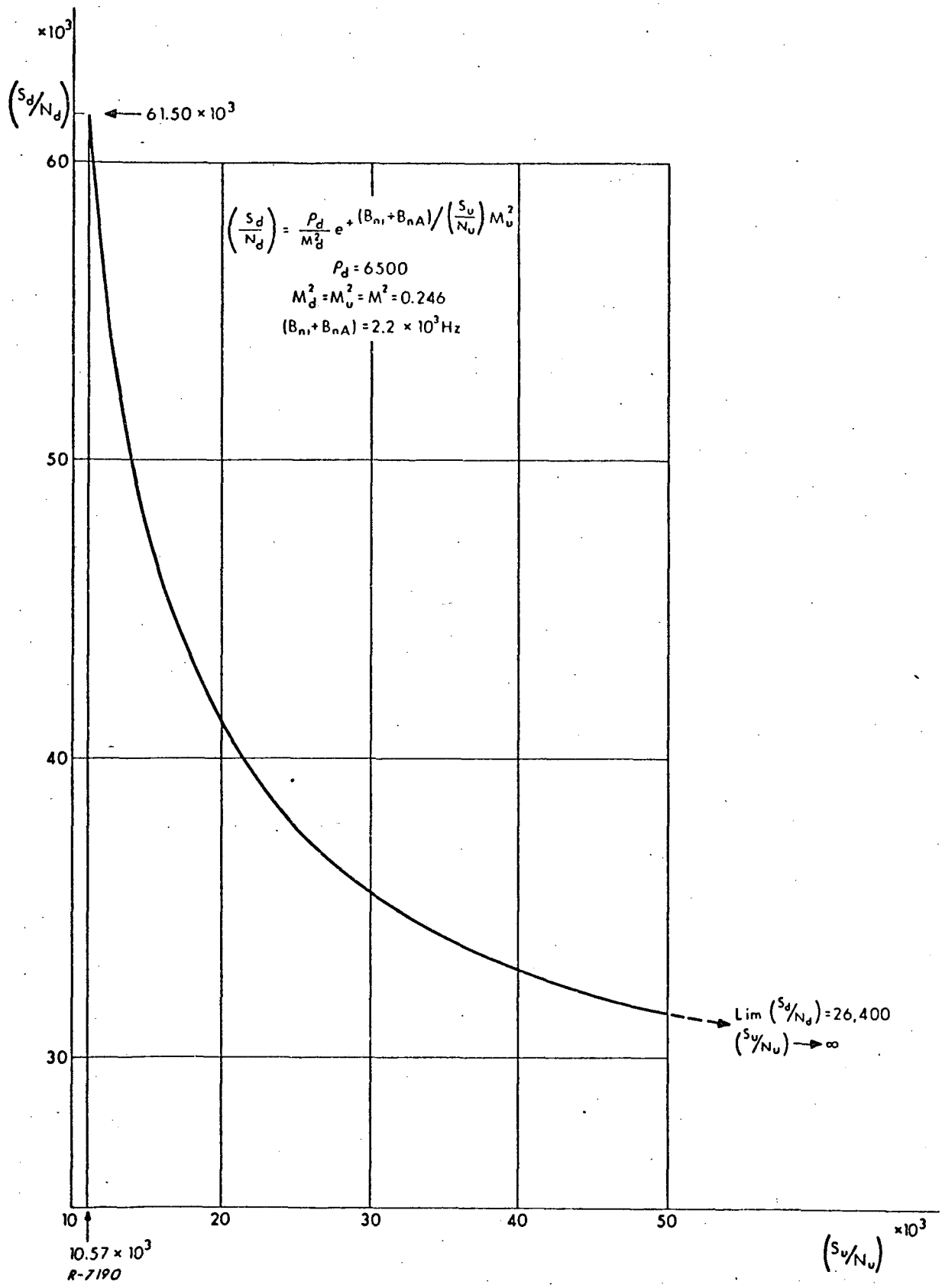

Fig. 4.3 Downlink vs. Uplink Signal-to-Noise-Power-Density Ratio for Fixed Downlink Data Error Rate

the uplink data BEP, (S_u/N_u) must be increased from the previous minimum value of 10,570 to 15,280. If on the downlink ρ_2 is made equal to 0.12 radians and ρ_A is made equal to 0.094 radians, a reduction from the uplink deviations by a factor of 4, proper ambiguity resolution will still occur. The modulation suppression arising from retransmitted noise is now

$$M_n^2 = e^{-B_{n1}/\rho_u} \; e^{-B_{nA}/(4)^2\rho_u} \tag{4.43}$$

This factor is now only 0.8825 when $\rho_u = 2600$, $B_{N1} = 0.2 \times 10^3$ Hz and $B_{NA} = 2.0 \times 10^3$ Hz rather than 0.429 as was the case previously. This means that this technique can result in a decrease in (S_d/N_d) from 61.50×10^3 to 29.30×10^3. (Note that $M_d^2 = 0.251$ rather than 0.246 as previously.) This is a significant reduction, and required only a relatively small increase if (S_u/N_u) were increased without changing the uplink and downlink deviations.

5. C. W. INTERFERENCE EFFECTS

The effects of C.W. interference on the TDRS wideband FM system performance depend on 1) the location of the C.W. interference in the wideband FM signal spectrum at the receiver input, and 2) the relative strength of the C.W. interference. The analyses of these effects are divided into several sections: 1) compound PLL demodulation, 2) data demodulation, and 3) ranging and ranging sidetone turn-around. The probability of the various interference effects in terms of the percentage of the 2 MHz bandwidth which is vulnerable to C.W. interference is also considered.

5.1 Compound PLL Demodulation

If the C.W. interference falls very close to one of the wideband FM subcarrier sidebands it may interfere with the compound PLL demodulation. If it lies within both the carrier and subcarrier loop noise bandwidths, it can interfere with both carrier and subcarrier tracking. Since the subcarrier loop noise bandwidth is much smaller than the carrier loop noise bandwidth (0.5 Hz vs. 9 Hz single-sided), the likelihood is that it will interfere only with carrier tracking, if it all.

To analyze the situation, we write the received uplink signal plus interference as

$$
\begin{aligned}
e_u(t) &= \sqrt{2S_u}\ \sin\left\{\omega_c t + \theta_c(t) + \delta\sin\left[\omega_{sc} t + \theta_{sc}(t)\right] + \phi_m(t)\right\} \\
&\quad + \sqrt{2S_I}\ \sin\left\{\omega_I t + \theta_I(t)\right\} \\
&= \sqrt{2S_u}\ \sum_{n=-N}^{+N} J_n(\delta)\sin\left\{\omega_c t + \theta_c(t) + n\left[\omega_{sc} t + \theta_{sc}(t)\right] + \phi_m(t)\right\} \\
&\quad + \sqrt{2S_I}\ \sin\left\{\omega_{ct} + \theta_c(t) + m\left[\omega_{sc} t + \theta_{sc}(t)\right] + \Delta\omega_I t + \Delta\theta_I(t)\right\}
\end{aligned}
\tag{5.1}
$$

where ω_I is the nominal frequency of the interference and $\theta_I(t)$ is the carrier doppler phase of the received interference. The frequency of the interference lies near the sideband for which n = m. That is,

$$\omega_I t + \theta_I(t) = \omega_c t + \theta_c(t) + m[\omega_{sc} t + \theta_{sc}(t)] + \Delta\omega_I t + \Delta\theta_I(t) \qquad (5.2)$$

with $\Delta\omega_I + \Delta\dot{\theta}_I$ being small.

The received signal plus interference is effectively multiplied by the wideband FM reference signal

$$e_{REF}(t) = \sqrt{2}\left\{\cos\omega_c t + \hat{\theta}_c(t) + \delta\sin[\omega_{sc} t + \hat{\theta}_{sc}(t)]\right\} \qquad (5.3)$$

where $\hat{\theta}_c(t)$ and $\hat{\theta}_{sc}(t)$ are estimates of the received phases $\theta_c(t)$ and $\theta_{sc}(t)$. This may be expanded as

$$e_{REF}(t) = \sqrt{2}\sum_{\ell=-\infty}^{\infty} J_\ell(\delta)\cos\left\{\omega_c t + \hat{\theta}_c(t) + \ell[\omega_{sc} t + \hat{\theta}_{sc}(t)]\right\} \qquad (5.4)$$

The output of the multiplier (carrier loop phase detector) is (in normalized form)

$$\begin{aligned}
\left(e_o(t)\right)_c &= \sin\left\{\theta_{ce}(t) + \delta\sin[\omega_{sc} t + \theta_{sc}(t)] - \delta\sin[\omega_{sc} t + \hat{\theta}_{sc}(t)] + \phi_m(t)\right\} \\
&+ \sqrt{\frac{S_I}{S_u}}\, J_m(\delta)\sin\left\{\theta_{ce}(t) + m\theta_{sce}(t) + \Delta\omega_I t + \Delta\theta_I(t)\right\} \\
&+ \sqrt{\frac{S_I}{S_u}}\left(J_{m+1}(\delta)\sin\left\{\theta_{ce}(t) + m\theta_{sce}(t) + \Delta\omega_I t + \Delta\theta_I(t) - [\omega_{sc} t + \hat{\theta}_{sc}(t)]\right\}\right. \\
&\left. + J_{m-1}(\delta)\sin\left\{\theta_{ce}(t) + m\theta_{sce}(t) + \Delta\omega_I t + \Delta\theta_I(t) + [\omega_{sc} t + \hat{\theta}_{sc}(t)]\right\}\right) \\
&= J_o(\Delta_{sc})[M_u \sin\theta_{ce}(t) + \cos\theta_{ce}(t)\sin\phi_m(t)] \\
&+ \sqrt{\frac{S_I}{S_u}}\, J_m(\delta)\sin\left\{\theta_{ce}(t) + m\theta_{se}(t) + \Delta\omega_I t + \Delta\theta_I(t)\right\}
\end{aligned}$$

$$+ M_u \cos\theta_{ce}(t) 2J_1(\Delta_{sc}) \sin[\omega_{sc} t + \theta_{sc}(t) + \phi_{sc}(t)]$$

$$+ \sqrt{\frac{S_I}{S_u}} \left(+ J_{m+1}(\delta) \sin\left\{ -[\omega_{sc} t + \hat{\theta}_{sc}(t)] + \theta_{ce}(t) + m\theta_{sce}(t) + \Delta\omega_I t + \Delta\theta_I(t) \right\} \right.$$

$$\left. + J_{m-1}(\delta) \sin\left\{ [\omega_{sc} t + \hat{\theta}_{sc}(t)] + \theta_{ce}(t) + m\theta_{sce}(t) + \Delta\omega_I t + \Delta\theta_I(t) \right\} \right) \tag{5.5}$$

Here

$$\delta \sin[\omega_{sc} t + \theta_{sc}(t)] - \delta \sin[\omega_{sc} t + \hat{\theta}_{sc}(t)]$$

$$= \Delta_{sc} \sin[\omega_{sc} t + \theta_{sc}(t) + \phi_{sc}(t)] \tag{5.6}$$

where

$$\Delta_{sc} = 2\delta \sin\left(\frac{\theta_{sce}}{2}\right) \tag{5.7}$$

and

$$\delta \sin\theta_{sce} = \Delta_{sc} \sin(\theta_{sce} + \phi_{sc}) \tag{5.8}$$

Also

$$M_u = \langle \cos\phi_m(t) \rangle \tag{5.9}$$

So far as carrier tracking is concerned, the signal and noise components of interest are

$$\sin\theta_{ce}(t) + \frac{\sqrt{\frac{S_I}{S_u}} J_m(\delta)}{J_o(\Delta_{sc}) M_u} \sin\left\{ \theta_{ce}(t) + m\theta_{sc}(t) + \Delta\omega_I t + \Delta\theta_I(t) \right\} \tag{5.10}$$

For small $\theta_{ce}(t)$, this may be linearized by making the approximation $\sin\theta_{ce} \approx \theta_{ce}$. The results of Appendix B may be applied here with

$$\sqrt{\frac{S_i}{S_o}} = \frac{\sqrt{\frac{S_I}{S_u}} J_m(\delta)}{J_o(\Delta_{sc}) M_u} \tag{5.11}$$

Thus, if the frequency $\Delta\omega_I + \Delta\dot{\theta}_I$ lies within the carrier loop noise bandwidth, the maximum phase error resulting from the presence of this C.W. interference is

$$\left(\theta_{ce}\right)_{max} = \frac{\sqrt{\frac{S_I}{S_u}}\, J_m(\delta)}{J_o(\Delta_{sc})M_u} \qquad (5.12)$$

The worst-case occurs for m = 4 when $\delta = 5.52$, for which $J_4(5.52) = 0.3960$. With $M_u \cong 0.41$ and $J_o(\Delta_{sc}) \approx 1$, $\left(\theta_{ce}\right)_{max} \approx \sqrt{\frac{S_I}{S_u}}$. The value of $\left(\theta_{ce}\right)_{max}$ should be on the order of 0.1 radian for any single C.W. interference in order that the loop operate in the linear region when both interference and noise are present.

We can say that a C.W. interference may cause a problem with carrier tracking if it is within 3 loop noise bandwidths of a subcarrier sideband of non-negligible value. For $\delta = 5.52$, the carrier component (m = o) is zero, and sidebands for $m \geq 7$ are negligible. There are therefore 12 subcarrier sidebands to consider. For a single-sided carrier loop noise bandwidth of 9 Hz, the total bandwidth of the RF spectrum which is vulnerable to C.W. interference with carrier tracking is 3 x 2 x 9 x 12 = 648 Hz. This is a small fraction of the 2 MHz RF bandwidth. In addition, the high doppler dynamics between the user and the RFI will mean that the C.W. RFI component will sweep right through the loop noise bandwidth.

Turning now to subcarrier tracking, the output of the subcarrier loop phase detector is

$$\left(e_o(t)\right)_{sc} = \frac{M_u}{\sqrt{2}} \cos\theta_{ce}(t) 2J_1(\Delta_{sc}) \sin[\theta_{sce}(t) + \phi_{sc}(t)]$$

$$+ \frac{1}{\sqrt{2}} \sqrt{\frac{S_I}{S_u}} \left(J_{m+1}(\delta) + J_{m-1}(\delta)\right) \sin[\theta_{ce}(t) + m\theta_{sce}(t) + \Delta\omega_I + \Delta\theta_I(t)] \tag{5.13}$$

$$= M_u \cos\theta_{ce} \frac{\delta}{\sqrt{2}} \frac{2J_1(\Delta_{sc})}{\Delta_{sc}} \sin\theta_{sce}(t)$$

$$+ \sqrt{\frac{S_I}{S_u}} \frac{2m}{\sqrt{2}\,\delta} J_m(\delta) \sin[\theta_{ce}(t) + m\theta_{sce}(t) + \Delta\omega_I t + \Delta\theta_I(t)]$$

For $\Delta_{sc} \approx 0$, and θ_{sce} and θ_{ce} are small, this may be approximated

$$\frac{1}{\sqrt{2}} \delta\theta_{sce} + \frac{\sqrt{\frac{S_I}{S_u}} J_m(\delta)}{\sqrt{2}\, M_u(\delta/2m)} \sin[\theta_{ce}(t) + m\theta_{sce}(t) + \Delta\omega_I t + \Delta\theta_I(t)] \tag{5.14}$$

For $m = 4$ and $\delta = 5.52$, and with $M_u \cong 0.41$, $\left(\delta\theta_{sce}\right)_{max}$ is

$$\left(\frac{\delta}{\sqrt{2}}\theta_{sce}\right)_{max} = \frac{\sqrt{\frac{S_I}{S_u}} J_m(\delta)}{\sqrt{2}\, M_u(\delta/2m)} \approx \frac{S_I}{S_u} \tag{5.15}$$

where use has been made of the results of Appendix B. The maximum error occurs if $\Delta\omega_I + \Delta\dot{\theta}_I$ lies within the subcarrier loop noise bandwidth.

For a subcarrier loop noise bandwidth of 0.5 Hz, only $3 \times 2 \times (.5) \times 12 = 36$ Hz of the 2 MHz RF bandwidth is vulnerable to C.W. interference with subcarrier tracking. Of course a C.W. interference that interferes with subcarrier tracking will also interfere with carrier tracking.

C.W. interference with acquisition may occur if the C.W. interference lies very close to the 4th or 5th order upper sideband. However, by choosing the uplink subcarrier frequencies such that the upper 4th and 5th

order subcarrier sidebands lie in RFI free parts of the uplink VHF band, this problem may be completely eliminated.

5.2 Data Demodulation

C.W. interference may cause an error in data demodulation if it overlaps the spectrum of the data around any of the subcarrier sidebands at the RF input of the receiver.

If the C.W. interference lies near the subcarrier sideband corresponding to n = m, Eq. (5.5) may be used to determine the effects of the interference on data demodulation with $\phi_m(t)$ given by

$$\phi_m(t) = \beta\chi_u(t) + \rho_1 \sin[\omega_1 t + \theta_1(t)] + \rho_2 \cos[(\omega_1 - \omega_2)t + \theta_1(t) - \theta_2(t)]$$
$$+ 2\rho_A \left(\sin[\omega_3 t + \theta_3(t)] + \sin[\omega_4 t + \theta_4(t)]\right) \cos[(\omega_1 - \omega_2)t + \theta_1(t) - \theta_2(t)] \quad (5.16)$$

$\sin \phi_m(t)$ may be written as

$$\sin\phi_m(t) = M_u \Big[\tan\beta\chi_u(t) + \bar{\rho}_1 \sin[\omega_1 t + \theta_1(t)] + \bar{\rho}_2 \cos[(\omega_1 - \omega_2)t + \theta_1(t) - \theta_2(t)]$$
$$+ 2\bar{\rho}_A \left(\sin[\omega_3 t + \theta_3(t)] + \sin[\omega_4 t + \theta_4(t)]\right) \cos[(\omega_1 - \omega_2)t + \theta_1(t) - \theta_2(t)]\Big] \quad (5.17)$$

Focusing attention on the data, the normalized input to the data demodulator is

$$\left(e_i(t)\right)_{data} = \chi_u(t) + \left(\frac{\sqrt{\frac{S_I}{S_u}}\, J_m(\delta)}{M_u \tan\beta}\right) \sin\left\{\theta_{ce}(t) + m\theta_{sce}(t) + \Delta\omega_I t + \Delta\theta_I(t)\right\} \quad (5.18)$$

The results of Appendix C may now be applied. The variance of the interference at the output of the data demodulator was shown to be given by

$$\sigma_i^2 = S_i T^2 \frac{\sin^4(\omega_i T/4)}{(\omega_i T/4)^2} \tag{5.19}$$

where S_i is the amplitude of the C.W. interference at the input to the data demodulator, ω_i is the frequency of the interference, and T is the bit period of the data. Here S_i and ω_i are

$$S_i = \frac{1}{2}\left(\frac{\sqrt{\frac{S_I}{S_u}}\, J_m(\delta)}{M_u \tan\beta}\right)^2 \tag{5.20}$$

and

$$\omega_i = \Delta\omega_I + \Delta\dot{\theta}_I \tag{5.21}$$

The phases $\theta_{ce}(t) + m\theta_{sce}(t)$ are essentially constant over the duration of one bit period.

The worst-case variance occurs for $\omega_i T/4 \approx \pm\frac{3\pi}{8}$, for which $\sin^4(\omega_i T/4)/(\omega_i T/4)^2$ is approximately 0.525. The minus sign means that the frequency $\omega_i = \Delta\omega_I + \Delta\dot{\theta}_I$ may be negative, corresponding to the C.W. interference RF frequency lying below the sideband frequency rather than above it.

The BEP requirement states that the ratio

$$\left(\frac{\mu^2}{2\sigma^2}\right) \geq 15.85 \quad (12\ \text{dB}) \tag{5.22}$$

for a BEP of 10^{-6}. Here $\mu = T$, and σ^2 is the variance of the Gaussian noise at the output of the demodulator. We require that σ_i^2 be an order of magnitude less than the critical value of σ^2 in order that the sum of the Gaussian noise plus C.W. interference not cause excessive errors. In other words, we require that

$$\sigma_i^2 << (\sigma^2)_{critical} = \frac{\mu^2}{(2 \times 15.85)} = \frac{T^2}{31.7} \qquad (5.23)$$

or, in the worst-case,

$$(0.525)S_i << \frac{1}{31.7} = 0.0315 \qquad (5.24)$$

For $\delta = 5.52$, the worst case occurs for m = 4. With $\beta = 1$ radian and $M_u \cong 0.41$, the requirement on $\sqrt{\frac{S_I}{S_u}}$ is

$$\sqrt{\frac{S_I}{S_u}} << (0.346)\ \frac{M_u \tan\beta}{J_4(5.52)} \cong 0.56 \qquad (5.25)$$

For $|\omega_i T/4| \gtrsim 3\pi/4$, $\sin^4(\omega_i T/4)/(\omega_i T/4)^2$ is less than approximately 0.0450. The "bandwidth" of the data may therefore be defined as the bandwidth for which $\sin^4(\omega_i T/4)/(\omega_i T/4)^2$ is greater than 0.0450*, and is B = 3/T Hz = $3f_B$, where f_B is the bit rate. The uplink bit rates are 100 BPS and 400 BPS, so that the largest uplink data bandwidth is 1200 Hz. With 12 sidebands of significance, the total frequency RF bandwidth which is susceptible to C.W. interference with data demodulation is 14.4 kHz.

Because the data is split-phase, there is very little data power near d.c. This means that a C.W. interference that is not too large may interfere with either carrier tracking or data demodulation, but not both at the same time. Also, because of the different dopplers between Users and the TDRS and between Users and the interference sources, only a few Users are likely to be affected by a strong C.W. interference on the uplink. This differs from PN spread spectrum techniques in which a strong interference can cause a serious disruption in communications for all Users. Finally, the doppler rate between the User and an earth based interference

* The value of 0.0450 corresponds to the height of the next highest maximum of $\sin^4 x/x^2$.

source is much greater than between the User and the TDRS, so that a C.W. interference would not stay long inside the small loop noise bandwidth.

5.3 Ranging and Ranging Sidetone Turn-Around

A C.W. interference which lies near the ranging sidetones in the RF input spectrum may interfere with ranging and/or may rob power from the desired downlink signal components by phase modulating the downlink carrier in the ranging sidetone turn-around channel. Interference with ranging may occur in several ways. The C.W. interference may be small, but may lie sufficiently close to a ranging sidetone to directly interfere with range tone demodulation on the ground. The C.W. interference may not lie very close to a ranging sidetone, but if it is turned around with the ranging sidetones, it will rob power from the desired signal components, thereby making them more susceptible to other noise and interference on the downlink. Finally, the ranging sidetones turn-around channel is designed so that AGC amplifiers in the User transponder prevent a strong interference from phase modulating the downlink carrier with a large deviation. Consequently, a strong C.W. interference that gets through either the fine range tone filter or the ambiguity resolving sidetone filter, and which causes the AGC amplifier at the output of that filter to reduce the amplitude of the sum of the ranging sidetone (or sidetones), the C.W. interference, and the noise, will make the ranging sidetone (or sidetones) more susceptible to downlink noise and interference in the range tone demodulator. The turn-around channel is designed so that if the AGC amplifier at the output of the ambiguity resolving sidetone filter would have too small a gain as a result of the presence of RFI, the ambiguity resolving sidetones do not phase modulate the downlink carrier. This prevents the transmission of ambiguity resolving tones which are too weak, because of suppression by C.W. (or other interference), to yield proper ambiguity resolution on the ground. With the transmission of these ranging sidetones discontinued, the noise and interference which would also phase modulate the downlink

carrier no longer does so, and therefore ceases to rob power from the desired signal components. If the AGC amplifier at the output of the fine range tone filter has too small a gain, no ranging sidetones are transmitted on the downlink.

We now examine the ranging situation mathematically. For the case where a C.W. interference lies near one of the fine range tone sidebands in the RF spectrum, we write

$$\omega_I t + \theta_I(t) = \omega_c t + \theta_c(t) + m[\omega_{sc} t + \theta_{sc}(t)] + k[\omega_1 t + \theta_1(t)]$$

$$+ \Delta\omega_I t + \Delta\theta_I(t) \qquad (5.26)$$

with $\Delta\omega_I + \Delta\dot{\theta}_I$ being small, and k = +1 or -1 depending upon whether the interference lies near the upper or lower range tone sideband associated with the m^{th} (n=m) subcarrier sideband.

The signal plus interference of interest is written in normalized form as

$$e_1(t) = \bar{\rho}_1 \sin[\omega_1 t + \theta_1(t)] + \frac{\sqrt{\frac{S_I}{S_u}}\, J_m(\delta)}{M_u} \sin[k(\omega_1 t + \theta_1(t)) + \theta_{ce}(t) + m\theta_{sce}(t)$$

$$+ \Delta\omega_I t + \Delta\theta_I(t)] \qquad (5.27)$$

where the assumption of small compound PLL tracking errors has enabled us to approximate $J_o(\Delta_{sc}(\theta_{sce}))$ and $\cos\theta_{ce}$ by 1. The amplitude of the range tone, $\bar{\rho}_1$, is related to the uplink phase deviation, ρ_1, by

$$\bar{\rho}_1 = \frac{2J_1(\rho_1)}{J_o(\rho_1)} \approx \rho_1 \quad \text{for } \rho_1 \lesssim 0.5 \text{ radian} \qquad (5.28)$$

If $\Delta\omega_I + \Delta\dot{\theta}_I$ is sufficiently small so that it lies within the fine range tone loop noise bandwidth, and if the amplitude $\sqrt{\frac{S_I}{S_u}}\, J_m(\delta)/M_u$ is <u>small</u> compared to $\bar{\rho}_1$, the effect of the C.W. interference will be to cause a phase error in the fine range tone loop whose maximum value (assuming the fine range tone loop is approximately linear) is

$$\left(\theta_{1e}\right)_{max.} = \frac{\sqrt{\frac{S_I}{S_u}}\, J_m(\delta)}{M_u\, \bar{\rho}_1} \qquad (5.29)$$

This must be less than 0.0645 radians if the ranging specifications are to be met. In the worst case situation where $m = 4$, $\sqrt{\frac{S_I}{S_u}}$ must be less than approximately 0.03 for $\bar{\rho}_1 \approx 0.5$ radians when the C.W. interference lies within the fine range tone loop noise bandwidth.

The fine range tone loop noise bandwidth is approximately 0.6 Hz (single-sided). Consequently, if we assume that a C.W. interference which is within 3 times the noise bandwidth of the fine range tone may cause interference with ranging, the frequency bandwidth at RF which is susceptible to this C.W. interference is $3 \times 2 \times (0.6) \times 2 \times 6 = 43.2$ Hz. This is a very small percentage of the total RF bandwidth. Also, because of changing doppler conditions such an interference situation would be very short-lived.

If $\Delta\omega_I + \Delta\dot{\theta}_I$ is not so small that it lies within the fine range tone loop noise bandwidth, the C.W. interference may still cause a problem, if it is sufficiently large, by robbing power from the desired downlink signal components. The signal suppression factor for a retransmitted C.W. interference is simply $J_o(\bar{\rho}_{I1})$, where $\bar{\rho}_{I1}$ is the phase deviation of the C.W. interference on the downlink carrier. The power suppression is

simply the square of this. In our case, $\bar{\rho}_I 1$ is

$$\bar{\rho}_{I1} = \frac{\sqrt{\frac{S_I}{S_u}}\, J_m(\delta)}{M_u} \tag{5.30}$$

since the downlink phase deviation of the fine range tone on the carrier is the same as that on the uplink.

An AGC amplifier prevents this suppression factor from becoming too small by limiting the total phase deviation of the fine range tone, C.W. interference, and noise (and other interference) on the downlink carrier. Excessive suppression of the fine range tone to the extent that serious degradation in ranging performance would occur, would be detected, and under these circumstances the ranging sidetones would not be turned around.

If the bandwidth of the fine range tone filter in the User transponder is on the order of 200 Hz, the total RF frequency bandwidth that is susceptible to this C.W. interference effect is $200 \times 2 \times 6 = 2.4$ kHz.

Turning now to the ambiguity resolving sidetones, we may write the C.W. interference RF phase as

$$\omega_I t + \theta_I(t) = \omega_c t + \theta_c(t) + m[\omega_{sc} t + \theta_{sc}(t)] + k[(\omega_1 - \omega_2)t + \theta_1(t) - \theta_2(t)]$$

$$+ \Delta\omega_I t + \Delta\theta_I(t) \tag{5.31}$$

where $\Delta\omega_I + \Delta\dot{\theta}_I$ is small, and $k = +1$ or -1 depending on whether the C.W. interference lies near an upper or a lower sideband of the ambiguity resolving tones cluster.

As with the fine range tone, there is a small probability that the C.W. interference may lie sufficiently close to one of the ambiguity resolving sidetones to cause an incorrect ambiguity resolution on the ground.

However, by far the greater problem is the suppression of the desired downlink signal modulation by the retransmission of C.W. interference (as well as other noise and interference) that lies within the bandwidth of the ambiguity resolving tones filter. The normalized signal plus C.W. interference at the output of the filter may be written as

$$e_2(t) = \bar{\rho}_2 \cos[(\omega_1 - \omega_2)t + \theta_1(t) - \theta_2(t)] + 2\bar{\rho}_A \Big(\sin[\omega_3 t + \theta_3(t)] + \sin[\omega_4 t + \theta_4(t)] \Big) \cos[(\omega_1 - \omega_2)t + \theta_1(t) - \theta_2(t)] + \frac{\sqrt{\frac{S_I}{S_u}}\, J_m(\delta)}{M_u} \sin\Big\{ k[(\omega_1 - \omega_2)t + \theta_1(t) - \theta_2(t)] + \theta_{ce}(t) + m\theta_{sce}(t) + \Delta\omega_I t + \Delta\theta_I(t) \Big\} \qquad (5.32)$$

The amplifier at the output of this filter has its gain set so that the phase deviations of the ambiguity resolving tones on the downlink carrier are 1/K times those on the uplink carrier, where K is approximately 4 (See Sec. 4.3.6). Therefore, the signal suppression factor for a retransmitted C.W. interference is $J_o(\rho_{I2})$, where ρ_{I2} is

$$\rho_{I2} = \frac{\sqrt{\frac{S_I}{S_u}}\, J_m(\delta)}{M_u K} \qquad (5.33)$$

and the power suppression is simply the square of this. It is clear that ρ_{I2} (and ρ_{I1} of Eq. (5.30)) should be on the order of at most 1 radian.

If the bandwidth of the ambiguity resolving tones filter is on the order of 2 kHz, the total RF frequency bandwidth that is susceptible to this C.W. interference effect is $(2 \times 10^3) \times 2 \times 6 = 24$ kHz. The total RF

bandwidth that is susceptible to C.W. interference with ranging sidetone turn-around is 26.4 kHz when both the fine range tone and the ambiguity resolving sidetones are considered.

The modifications in the ranging sidetone format suggested in Appendix D would alleviate this problem to a great degree if not eliminate it altogether.

6. NARROWBAND RFI EFFECTS

Narrowband RFI is considered as having a bandwidth on the order of 15 kHz. It may be either AM or FM interference and either continuous or intermittent in nature. In general, this type of RFI may be written as

$$e_I(t) = a(t) \sin[\omega_I t + \theta_I(t) + \alpha(t)]$$

where a(t) is a generalized AM modulation and $\alpha(t)$ is a generalized angle modulation, and $\theta_I(t)$ is the interference carrier doppler phase.

Since the bandwidths of the desired signal components are much smaller than the bandwidth of the narrowband RFI, the effects of the narrowband RFI may be taken into account by replacing it by colored Gaussian noise whose power spectrum is identical to that of the narrowband RFI. To simplify matters further, we assume that the variation of the equivalent noise power density over the small desired signal components bandwidths may be neglected.

We consider the effects of narrowband RFI on 1) compound PLL tracking, 2) data demodulation, and 3) ranging and ranging sidetone turnaround.

6.1 Compound PLL Tracking

Narrowband RFI may interfere with compound PLL tracking if it overlaps one of the subcarrier sidebands. If the single-sided equivalent narrowband RFI noise power density at the sideband corresponding to n=m is N_m, the normalized output of the carrier loop phase detector is

$$\left(e_o(t)\right)_c = J_o(\Delta_{sc})[M_u \sin\theta_{ce} + \cos\theta_{ce}\sin\phi_m(t)] + \text{RFI noise of single-sided power density } \left(\frac{N_m J_m^2(\delta)}{S_u}\right) \text{ around d.c.}$$

$$+ M_u \cos\theta_{ce}\, 2J_1(\Delta_{sc})\sin[\omega_{sc}t + \theta_{sc}(t) + \phi_{sc}(t)] + \text{RFI noise of single-sided power density } \left(\frac{N_m\left(J^2_{m-1}(\delta) + J^2_{m+1}(\delta)\right)}{2S_u}\right) \qquad (6.1)$$

If the subcarrier and carrier phase errors are small, the compound PLL is uncoupled in the sense indicated in Appendix A, and the carrier and subcarrier loops are approximately linear and independent. In this case $J_o(\Delta_{sc}) \approx 1$, $\cos\theta_{ce} \approx 1$, and $\sin\theta_{ce} \approx \theta_{ce}$.

From Appendix A, the component of the carrier loop phase error variance arising from the presence of this narrowband RFI is

$$\overline{\theta^2_{ce}} = \frac{B_c N_m J^2_m(\delta)}{S_u M_u^2} \qquad (6.2)$$

where B_c is the single-sided carrier loop noise bandwidth. If the RFI power is assumed to be distributed uniformly over a bandwidth B_I ($B_I \approx 15$ kHz is typical), the single-sided equivalent narrowband RFI noise power density N_m may be written as

$$N_m = \frac{S_I}{B_I} \qquad (6.3)$$

so that Eq. (6.2) becomes

$$\overline{\theta^2_{ce}} = \frac{B_c}{B_I}\left(\frac{S_I}{S_u}\right)\frac{J^2_m(\delta)}{M_u^2} \qquad (6.4)$$

The rms error is

$$\sqrt{\overline{\theta_{ce}^2}} = \frac{\sqrt{\frac{S_I}{S_u}}\, J_m(\delta)}{M_u} \sqrt{\frac{B_c}{B_I}} \qquad (6.5)$$

This should be much less than about 0.1 radian if the total carrier tracking phase error, which considers all sources of noise and interference, is to be small.

If the location of the narrowband RFI in the RF spectrum is designated by the location of its center frequency, such narrowband RFI located anywhere within $\pm B_I/2$ of a significant subcarrier sideband can interfere with compound PLL tracking. For B_I = 15 kHz, this means that $15 \times 10^3 \times 12 = 180$ kHz of the RF spectrum is susceptible to this type of interference with compound PLL demodulation.

Turning now to subcarrier tracking, the output of the subcarrier loop phase detector is

$$\left(e_o(t)\right)_{sc} = \frac{M_u}{\sqrt{2}}\, 2J_1(\Delta_{sc}) \sin[\theta_{sce} + \phi_{sc}] + \text{RFI noise of single-sided}$$

$$\text{power density} \left(\frac{N_m\left(J^2_{m-1}(\delta) + J^2_{m+1}(\delta)\right)}{2S_u}\right)$$

$$= \frac{M_u}{\sqrt{2}}\, \delta\left(\frac{2J_1(\Delta_{sc})}{\Delta_{sc}}\right) \sin\theta_{sce} + \text{RFI noise of single-sided power}$$

$$\text{density} \left(\frac{N_m\left(J^2_{m-1}(\delta) + J^2_{m+1}(\delta)\right)}{2S_u}\right) \text{around d.c.} \qquad (6.6)$$

If θ_{sce} is small, $\sin\theta_{sce} \approx \theta_{sce}$ and $2J_1(\Delta_{sc})/\Delta_{sc} \approx 1$, so that the normalized output of the subcarrier loop phase detector becomes

$$\frac{1}{\sqrt{2}}\,\delta\theta_{sce} + \text{RFI noise of single-sided power density}$$

$$\left(\frac{N_m\left(J^2_{m-1}(\delta) + J^2_{m+1}(\delta)\right)}{2S_u M_u^2}\right)\text{around d.c.} \qquad (6.7)$$

From Appendix A, the component of the mean-square subcarrier loop error, $\frac{1}{2}\delta^2\,\overline{\theta^2_{sce}}$, resulting from the presence of the narrowband interference is

$$\frac{1}{2}\delta^2\,\overline{\theta^2_{sce}} = \frac{B_s N_m}{S_u M_u^2}\left(\frac{J^2_{m-1}(\delta) + J^2_{m+1}(\delta)}{2}\right) \qquad (6.8)$$

$$= \left(\frac{B_s}{B_I}\right)\left(\frac{S_I}{S_u}\right)\frac{1}{M_u^2}\left(\frac{J^2_{m-1}(\delta) + J^2_{m+1}(\delta)}{2}\right)$$

The rms error is

$$\frac{1}{\sqrt{2}}\delta\sqrt{\overline{\theta^2_{sce}}} = \sqrt{\frac{S_I}{S_u}}\;\frac{1}{M_u}\sqrt{\frac{J^2_{m-1}(\delta) + J^2_{m+1}(\delta)}{2}}\sqrt{\frac{B_s}{B_I}} \qquad (6.9)$$

This should be much less than about 0.1 radian if the total subcarrier tracking error, which considers all sources of noise and interference, is to be small.

6.2 Data Demodulation

For the data demodulation case, use may be made of Eqs. (6.1) and (5.17) so that the input to the data demodulator becomes

$$\left(e_i(t)\right)_{\text{data}} = \chi_u(t) + \text{RFI noise of single-sided power density } \left(\frac{N_m J_m^2(\delta)}{S_u M_u^2 \tan^2\beta}\right) \text{around d.c.} \qquad (6.10)$$

when the carrier and subcarrier tracking errors are small. Applying the results of Appendix C, the energy per bit divided by the single-sided noise power density is

$$\mu^2/2\sigma^2 = \frac{TS_u M_u^2 \tan^2\beta}{N_m J_m^2(\delta)} = \left(\frac{B_I}{f_B}\right)\left(\frac{S_u}{S_I}\right) \frac{M_u^2 \tan^2\beta}{J_m^2(\delta)} \qquad (6.11)$$

where $f_B = 1/T$ is the bit frequency. This must be much greater than 15.85 (12 dB) if the required BEP is to be achieved in the presence of noise and RFI.

As with compound PLL tracking, 180 kHz of the RF spectrum is susceptible to narrowband RFI interference with data demodulation. This is so because the data lies in a relatively narrow bandwidth about each subcarrier sideband in the RF spectrum.

6.3 Ranging and Ranging Sidetone Turnaround

If narrowband RFI overlaps one of the sidebands of the ranging sidetones cluster in the received RF spectrum, interference with ranging and ranging sidetone turn-around will occur.

If the narrowband RFI overlaps the k^{th} fine range tone sideband ($k = +1, -1$) around the m^{th} subcarrier sideband, the output of the fine range tone filter in the User transponder may be written in normalized form as

$$e_1(t) = \bar{\rho}_1 \sin[\omega_1 t + \theta_1(t)] + \text{narrowband RFI of single-sided noise power density} \left(\frac{\frac{1}{2} J_m^2(\delta) N_{m,k,1}}{S_u M_u^2}\right) \text{ around } \omega_1 \tag{6.12}$$

where $N_{m,k,1}$ denotes the single-sided narrowband RFI power density at the frequency of the k^{th} fine range tone sideband around the m^{th} subcarrier sideband.

Likewise, the output of the ambiguity resolving tones filter may be written as

$$e_2(t) = \bar{\rho}_2 \cos[(\omega_1 - \omega_2)t + \theta_1(t) - \theta_2(t)] + 2\bar{\rho}_A \left(\sin[\omega_3 t + \theta_3(t)] + \sin[\omega_4 t + \theta_4(t)]\right) \cos[(\omega_1 - \omega_2)t + \theta_1(t) - \theta_2(t)] + \text{narrowband RFI of single-sided noise power density} \left(\frac{\frac{1}{2} J_m^2(\delta) N_{m,k,2}}{S_u M_u^2}\right) \text{around } \omega_2 \tag{6.13}$$

where $N_{m,k,2}$ is the single-sided RFI power density at the frequency of the k^{th} ambiguity resolving sidetone cluster sideband around the m^{th} subcarrier sideband.

The normalized noise power density $\left(\frac{1}{2} J_m^2(\delta) N_{m,k,p} / S_u M_u^2\right)$ $(p=1, 2)$ must be small compared to $(N_u / S_u M_u^2)$ if the ranging specifications are to be met. If the noise plus narrowband and C.W. RFI at the outputs of the ranging sidetone filters is excessive, the gates following the AGC amplifiers at the outputs of these filters will open and the ranging sidetones will not be transmitted on the downlink.

7. SSMA INTERFERENCE EFFECTS

On the downlink there may be as many as 30 Users transmitting simultaneously in the 136-138 MHz band. Each of these User transmissions represents a potential source of interference to every other User and vice-versa. To reduce the extent of this interference, each User is assigned a unique combination of subcarrier frequency and carrier band (lower, center, or upper). In this way the spectral overlap between any two Users is kept as low as possible consistent with other system considerations.

Since each User RF downlink signal contains both C.W. and narrowband spectral components, both of these types of interference may be encountered on the downlink from other User transmission. Table 7.1 lists the various types of SSMA interference effects from a single other User. The following sections treat 1) compound PLL demodulation, 2) data demodulation, and 3) ranging.

7.1 Compound PLL Demodulation

To determine the effects of other-User interference on carrier and subcarrier tracking on the downlink, we begin by writing the downlink received signal as

$$e_d(t) = \sqrt{2S_d}\,\sin\Big\{\omega_c t + \theta_c(t) + \delta\sin[\omega_{sc}t + \theta_{sc}(t)] + \beta\chi_d(t)$$

$$+ \tilde{\rho}_1\,\sin\big(\omega_1 t + \theta_1(t)\big) + \phi_{AR}(t)\cos[(\omega_1-\omega_2)t + \theta_1(t) - \theta_2(t)]$$

$$+ \phi_{n1}(t) + \phi_{nAR}(t)\Big\} \qquad (7.1)$$

where

$$\omega_c t + \theta_c(t) = \frac{23}{25}\left(\omega_{cu}t + \hat{\theta}_{cu}(t)\right) + k\Delta\omega t + \theta_{cd}(t)$$

Table 7.1

SSMA Interference Effects from a Single Other-User

Interference With	Interference From	Type	Seriousness
1a. Compound PLL Demodulation	other-user subcarrier sideband	CW	potentially serious
b. (Same)	other-user data	narrowband	negligible
c. (Same)	other-user ranging sidetone plus retransmitted noise	CW plus narrowband	possible problem from fine range tone
d. (Same)	other-user retransmitted noise	narrowband	negligible
2a. Data Demodulation	other-user subcarrier sideband plus data	CW plus narrowband	potentially serious
b. (Same)	other-user ranging sidetone plus retransmitted noise	CW plus narrowband	negligible
3a. Ranging	other-user subcarrier sideband	CW	serious when it occurs, but unlikely to last too long
b. (Same)	other-user data	narrowband	not serious
c. (Same)	other-user ranging sidetone	CW	serious when it occurs, but unlikely to last too long
d. (Same)	other-user retransmitted noise	narrowband	negligible

ω_{cu} = uplink carrier frequency

$\dot{\hat{\theta}}_{cu}$ = carrier loop estimate of uplink carrier doppler phase

k = -1, 0, +1 depending on whether the carrier band is lower, center, or upper

$\Delta\omega$ = carrier band offset frequency

$\theta_{cd}(t)$ = carrier doppler phase on the downlink

$\chi_d(t)$ = downlink split-phase telemetry data

$\tilde{\rho}_1$ = downlink fine range tone phase deviation

$\theta_1(t)$ = two-way fine range tone doppler phase

$\phi_{AR}(t) = \tilde{\rho}_2 + 2\tilde{\rho}_A \sin\left(\omega_3 t + \theta_3(t)\right) + \sin\left(\omega_4 t + \theta_4(t)\right)$ is the ambiguity resolving sidetone cluster AM modulation

$\phi_{n1}(t)$ = the noise and uplink interference, if any, retransmitted on the downlink from the output of the fine range tone limiting amplifer

$\phi_{nAR}(t)$ = the noise and uplink interference, if any, retransmitted on the downlink from the output of the ambiguity resolving sidetone limiting amplifer

ω_{sc} = the downlink subcarrier frequency for the User in question

$\theta_{sc}(t)$ = the downlink (one-way) subcarrier doppler phase

δ = downlink subcarrier modulation index of 5.52 radians

Note that if the noise and interference at the output of the ambiguity resolving sidetones filter is excessive, the ambiguity resolving sidetones and its accompanying noise and interference will not phase modulate the downlink carrier. Likewise, if the noise and interference at the output of the fine range tone filter is excessive, neither the fine range tone nor the ambiguity resolving sidetones and their accompanying noise and interference will phase modulate the downlink carrier. When the ranging

sidetones do modulate the downlink carrier, the downlink phase deviations are related to the uplink phase deviations by

$$\begin{aligned}\tilde{\rho}_1 &= \bar{\rho}_1 \approx \rho_1 \\ \tilde{\rho}_2 &= \frac{1}{K}\bar{\rho}_2 \approx \frac{1}{K}\rho_2 \\ \tilde{\rho}_A &= \frac{1}{K}\bar{\rho}_A \approx \frac{1}{K}\rho_A \end{aligned} \tag{7.2}$$

where K is the attenuation of the ambiguity resolving ranging sidetones by the AGC amplifier, and is equal to 4.

We consider the interference with the i^{th} User by the j^{th} User, and use the subscripts i and j to designate them. The significant spectral components of the RF received signal of the j^{th} User at the input of the receiver tuned to receive the signal from the i^{th} User may be written approximately as

$$\begin{aligned}\left(e_d(t)\right)_j \cong \sqrt{2Sd_j} \sum_{n_j=-N}^{+N} J_{nj}(\delta)\Big\{ & M_1 M_{AR} M_{n1} M_{nAR} \sin\Big\{\omega_{cjt} + \theta_{cj}(t) \\ & + n_j[\omega_{scj} + \theta_{scj}(t)] + B\chi_{dj}(t)\Big\} + \frac{\tilde{\rho}_1}{2} M_1 M_{AR} M_{n1} M_{nAR}\Big[\sin\Big\{\omega_{cjt} \\ & + \theta_{cj}(t) + n_j[\omega_{scj}t + \theta_{scj}(t)] + \left(\omega_1 t + \theta_{1j}(t)\right) + \beta\chi_{dj}(t)\Big\} \\ & - \sin\Big\{\omega_{cj}t + \theta_{cj}(t) + n_j[\omega_{scj}(t) + \theta_{scj}(t)] - \left(\omega_1 t + \theta_{1j}(t)\right) + \beta\chi_{dj}(t)\Big\}\Big] \\ & + \frac{\phi_{AR}(t)}{2} M_1 M_{AR} M_{n1} M_{nAR}\Big[\cos\Big\{\omega_{cj}t + \theta_{cj}(t) + n_j[\omega_{scj}t + \theta_{scj}(t)] \\ & + [(\omega_1 - \omega_2)t + \theta_{1j}(t) - \theta_{2j}(t)] + \beta\chi_{dj}(t)\Big\} + \cos\Big\{\omega_{cj}t + \theta_{cj}(t) \\ & + n_j[\omega_{scj}t + \theta_{scj}(t)] - [(\omega_1 - \omega_2)t + \theta_{ij}(t) - \theta_{2j}(t)] + \beta\chi_{dj}(t)\Big\}\Big]\end{aligned}$$

$$+ M_1 M_{AR}[\phi_{n1j}(t) + \phi_{nAR_j}(t)] \cos\left\{\omega_{cj} t + \theta_{cj}(t)\right.$$

$$\left. + n_j[\omega_{scj} t + \theta_{scj}(t)] + \beta \chi_{dj}(t)\right\}\Big\} \qquad (7.3)$$

where $M_1 = J_o(\tilde{\rho}_1)$, $M_{AR} = J_o(\tilde{\rho}_2) J_o^4(\tilde{\rho}_A)$, $M_{n1} = \langle \cos \phi_{n1} \rangle$, and $M_{nAR} = \langle \cos \phi_{nAR} \rangle$ are modulation suppression factors.

The first term in Eq. (7.3) is recognized as the subcarrier sidebands modulated with the split-phase telemetry data. The second and third terms are the upper and lower fine range tone sidebands around the subcarrier sidebands. The telemetry data phase modulates these spectral components in the RF spectrum. The fourth and fifth terms are the upper and lower ambiguity resolving sidetones cluster sidebands around the subcarrier sidebands. The telemetry data phase modulates these components also. Finally, the last term is seen to contain the upper and lower sidebands of the retransmitted noise and interference around the subcarrier sidebands. The telemetry data phase modulates these components as well. The assumption is made here that the noise and interference asre sufficiently small to permit the approximations.

$$\sin \phi_{n1}(t) \approx \phi_{n1}(t)$$

and

$$\sin \phi_{nAR}(t) \approx \phi_{nAR}(t) \qquad (7.4)$$

to be made.

The desired-User signal and the other-User interference are effectively mulitplied in the ground receiver by the desired-User reference signal given by

$$\left(e_{REF.}(t)\right)_i = \sqrt{2} \cos\left\{\omega_{ci} t + \hat{\theta}_{ci}(t) + \delta \sin[\omega_{sci} t + \hat{\theta}_{sci}(t)]\right\} \qquad (7.5)$$

$$= \sqrt{2} \sum_{n_i=-\infty}^{\infty} J_{ni}(\delta) \cos\left\{\omega_{ci} t + \hat{\theta}_{ci}(t) + n_i[\omega_{sci} t + \hat{\theta}_{sci}(t)]\right\}$$

The output of the carrier loop phase detector is

$$
\begin{aligned}
\left(e_o(t)\right)_c &= \sqrt{S_{di}}\,\sin\Big\{\theta_{cei}(t) + \Delta_{sci}\sin\big[\omega_{sci}t + \theta_{scei}(t) + \phi_{sci}(t)\big] \\
&+ \beta\chi_{di}(t) + \tilde{\rho}_1\sin\left(\omega_1 t + \theta_{1i}(t)\right) + \phi_{AR}(t)\cos\big[(\omega_1-\omega_2)t + \theta_{1i}(t) - \theta_{2i}(t)\big] \\
&+ \phi_{n1}(t) + \phi_{nAR}(t)\Big\} + \sqrt{S_{dj}}\sum_{n_j=-N}^{+N}\sum_{n_i=-\infty}^{\infty} J_{n_j}(\delta) \\
&\Bigg\{M_1 M_{AR} M_{n1} M_{nAR}\sin\Big\{(\omega_{cj}-\omega_{ci})t + \theta_{cj}(t) - \hat{\theta}_{ci}(t) + (n_j\omega_{scj} - n_i\omega_{sci})t \\
&+ \left(n_j\theta_{scj}(t) - n_i\hat{\theta}_{sci}(t)\right) + \beta\chi_{dj}(t)\Big\} \\
&+ \frac{\tilde{\rho}_1}{2}M_1 M_{AR} M_{n1} M_{nAR}\Big[\sin\Big\{(\omega_{cj}-\omega_{ci})t + \theta_{cj}(t) - \hat{\theta}_{ci}(t) + \left(\omega_1 t + \theta_{1j}(t)\right) \\
&+ (n_j\omega_{scj} - n_i\omega_{sci})t + \left(n_j\theta_{scj}(t) - n_i\hat{\theta}_{sci}(t)\right) + \beta\chi_{dj}(t)\Big\} \\
&- \sin\Big\{(\omega_{cj}-\omega_{ci})t + \theta_{cj}(t) - \hat{\theta}_{ci}(t) - \left(\omega_1 t + \theta_{1j}(t)\right) + (n_j\omega_{scj} - n_i\omega_{sci})t \\
&+ \left(n_j\theta_{scj}(t) - n_i\hat{\theta}_{sci}(t)\right) + \beta\chi_{dj}(t)\Big\}\Big] \\
&+ \frac{\phi_{AR}(t)}{2}M_1 M_{AR} M_{n1} M_{nAR}\Big[\cos\Big\{(\omega_{cj}-\omega_{ci})t + \theta_{cj}(t) - \hat{\theta}_{ci}(t) \\
&+ (n_j\omega_{scj} - n_i\omega_{sci})t + \left(n_j\theta_{scj}(t) - n_i\hat{\theta}_{sci}(t)\right) + \beta\chi_{dj}(t) + \big[(\omega_1-\omega_2)t \\
&+ \theta_{1j}(t) - \theta_{2j}(t)\big]\Big\} + \cos\Big\{(\omega_{cj}-\omega_{ci})t + \theta_{cj}(t) - \hat{\theta}_{ci}(t) + (n_j\omega_{scj} - n_i\omega_{sci})t \\
&+ \left(n_j\theta_{scj}(t) - n_i\theta_{sci}(t)\right) + \beta\chi_{dj}(t) - \big[(\omega_1-\omega_2)t + \theta_{1j}(t) - \theta_{2j}(t)\big]\Big\}\Big] \\
&+ M_1 M_{AR} M_{n1} M_{nAR}\big[\phi_{n1j}(t) + \phi_{nARj}(t)\big]\cos\Big\{(\omega_{cj}-\omega_{ci})t + \theta_{cj}(t) \\
&- \hat{\theta}_{ci}(t) + (n_j\omega_{scj} - n_i\omega_{sci})t + \left(n_j\theta_{scj}(t) - n_i\hat{\theta}_{sci}(t)\right) + \beta\chi_{dj}(t)\Big\}\Bigg\} \qquad (7.6)
\end{aligned}
$$

Consider now the case where the other-User subcarrier sideband components for which $n_j = m_j$ lies very close to the desired-User subcarrier sideband component for which $n_i = m_i$. That is,

$$\omega_{cj} t + \theta_{cj}(t) + m_j[\omega_{scj} t + \theta_{scj}(t)] = \omega_{ci} t + \theta_{ci}(t) + m_i[\omega_{sci} t + \theta_{sci}(t)] + \Delta\omega_{ij} t + \theta_{ij}(t) \qquad (7.7)$$

where $\Delta\omega_{ij} + \dot{\theta}_{ij}(t)$ is small.

Then the C.W. interference with compound PLL demodulation arising from the other-User subcarrier sideband for which $n_j = m_j$ comes from the terms

$$\sqrt{S_{dj}}\, J_{m_j}(\delta) J_{m_i}(\delta) M_1 M_{AR} M_{n1} M_{nAR} \sin\left\{\theta_{cei}(t) + \beta\chi_{dj}(t) + \Delta\omega_{ij} t + \theta_{ij}(t)\right\}$$

$$+ \sqrt{S_{dj}}\, J_{m_j}(\delta) J_{m_i+1}(\delta) M_1 M_{AR} M_{n1} M_{nAR} \sin\left\{\theta_{cei}(t) + \beta\chi_{dj}(t) - \left(\omega_{sci} t + \hat{\theta}_{sci}(t)\right)\right.$$

$$\left. + \Delta\omega_{ij} t + \theta_{ij}(t)\right\} + \sqrt{S_{dj}}\, J_{m_j}(\delta) J_{m_i-1}(\delta) M_1 M_{AR} M_{n1} M_{nAR} \sin\left\{\theta_{cei}(t)\right.$$

$$\left. + \beta\chi_{dj}(t) + \left(\omega_{sci} t + \hat{\theta}_{sci}(t)\right) + \Delta\omega_{ij} t + \theta_{ij}(t)\right\} \qquad (7.8)$$

in Eq. (7.6). If $\Delta\omega_{ij} + \Delta\dot{\theta}_{ij}$ lies within the carrier loop noise bandwidth, the carrier component of the first term in Eq. (7.8) interferes with carrier tracking. If $\Delta\omega_{ij} + \Delta\dot{\theta}_{ij}$ lies within the subcarrier loop noise bandwidth, the carrier components of the second and third terms in Eq. (7.8) interfere with subcarrier tracking. If $\Delta\omega_{ij} + \Delta\dot{\theta}_{ij}$ is larger than the carrier loop noise bandwidth, the data components in Eq. (7.8) will interfere with carrier and subcarrier tracking.

If the carrier and subcarrier tracking loop phase errors are small, and $\Delta\omega_{ij} + \Delta\dot{\theta}_{ij}$ lies within the carrier loop noise bandwidth, the maximum phase error, $\left(\theta_{cei}\right)_{max}$, from this C.W. interference is

$$\left(\theta_{cei}\right)_{max} = \sqrt{\frac{S_{dj}}{S_{di}}}\, J_{m_j}(\delta) J_{m_i}(\delta) \frac{\left(M_{n1} M_{nAR}\right)_j}{\left(M_{n1} M_{nAR}\right)_i} \tag{7.9}$$

for the case where the ranging sidetones and telemetry data are being transmitted on both the desired-User and other-User downlinks. In general $\left(\theta_{cei}\right)_{max}$ may be written as

$$\left(\theta_{cei}\right)_{max} = \sqrt{\frac{S_{dj}}{S_{di}}}\, \frac{J_{m_j}(\delta) J_{m_i}(\delta)(\cos\beta_j)\left(M_1 M_{AR} M_{n1} M_{nAR}\right)_j}{(\cos\beta_i)\left(M_1 M_{AR} M_{n1} M_{nAR}\right)_i} \tag{7.10}$$

where $\beta_i = \beta$ or 0 depending on whether or not telemetry data is being transmitted, and similarly for β_j.

The important factor in Eq. (7.10) is the product $J_{m_i}(\delta) J_{m_i}(\delta)$. With $\delta = 5.52$, the largest value $J_m(\delta)$ is 0.3960 for $m = \pm 4$. If a sideband for which $m_j = \pm 4$ lies near the sideband for which $m_i = \pm 4$, then the product $J_4(\delta) J_4(\delta)$ is 0.157. This is large enough so that if the other-User signal is stronger than the desired-User signal, the worst-case condition may cause a problem with carrier tracking. It is for this reason that the TDRS system should be designed so that the downlink received signal powers are approximately equal.

To compute the probability of SSMA C.W. interference from an other-User subcarrier sideband component, the locations in the RF spectrum of the subcarrier sidebands for each combination of subcarrier frequency and carrier band are computed for the zero doppler case. Then the

various potential interference threats from other Users can be computed for each User by considering the full range of relative carrier dopplers and seeing which other-User subcarrier sidebands can overlap desired-User subcarrier sidebands. Since the carrier loop noise bandwidth is approximately 25 Hz double-sided, the probability of a serious SSMA interference problem with carrier tracking from an other-User subcarrier sideband is fortunately not large in view of the relatively large relative carrier doppler spread on the downlink.

The probability of interference with subcarrier tracking is even smaller in view of the much smaller subcarrier loop noise bandwidth. If the interference does lie within the subcarrier loop noise bandwidth, the maximum subcarrier tracking error is in general

$$\left(\frac{1}{\sqrt{2}}\,\delta\theta_{\text{scei}}\right)_{\max} = \sqrt{\frac{S_{dj}}{S_{di}}}\;\frac{J_{m_j}(\delta)J_{m_i}(\delta)(\cos\beta_j)\left(M_1 M_{AR} M_{n1} M_{nAR}\right)_j}{\sqrt{2}\,(\delta/2m_i)(\cos\beta_i)\left(M_1 M_{AR} M_{n1} M_{nAR}\right)_i} \tag{7.11}$$

For $\delta = 5.52$ and for $m_i = m_j = 4$, the factor $J_{m_j}(\delta)J_{m_i}(\delta)2m_i/\delta\sqrt{2}$ is 0.161.

We now consider the case where the data around the other-User subcarrier sideband for which $n_j = m_j$ interferes with carrier tracking and subcarrier tracking by overlapping the desired-User subcarrier sideband for which $n_i = m_i$. Since the noise bandwidths of the carrier and subcarrier loops are much less than the downlink data bit rate, the power density of the other User data interference may be assumed uniform across the noise bandwidths of these loops.

The normalized output of the carrier tracking phase locked loop phase detector is

$$\theta_{cei} + \sqrt{\frac{S_{dj}}{S_{di}}} \frac{J_{m_j}(\delta)J_{m_i}(\delta)\sin\beta_j \left(M_1 M_{AR} M_{n1} M_{nAR}\right)_j}{\cos\beta_i \left(M_1 M_{AR} M_{n1} M_{nAR}\right)}$$

$$\times \chi_{dj}(t)\cos[\Delta\omega_{ij} t + \theta_{ij}(t) + \theta_{cei}] \qquad (7.12)$$

The power density spectrum of the other-User data in Eq. (7.12) is approximately

$$\frac{S_{dj}}{S_{di}} \frac{J^2_{m_j}(\delta)J^2_{m_i}(\delta)\sin^2\beta_j \left(M_1 M_{AR} M_{n1} M_{nAR}\right)^2_j}{\cos^2\beta_i \left(M_1 M_{AR} M_{n1} M_{nAR}\right)^2_i}$$

$$\times \frac{1}{2} \times \frac{1}{2} \times \left(\Phi_{x_j}(\omega - \Delta\omega_{ij} - \dot{\theta}_{ij}) + \Phi_{x_j}(\omega + \Delta\omega_{ij} + \dot{\theta}_{ij})\right) \qquad (7.13)$$

where $\Phi_{x_j}(\omega) = T \frac{\sin^4(\omega T/4)}{(\omega T/4)^2}$ (7.14)

if the successive data bits are assumed statistically independent. The power density (double-sided) at d.c. is

$$\frac{S_{dj}}{S_{di}} \frac{J^2_{m_j}(\delta)J^2_{m_i}(\delta)\sin^2\beta_j}{\cos^2\beta_i} \frac{\left(M_1 M_{AR} M_{n1} M_{nAR}\right)^2_j}{\left(M_1 M_{AR} M_{n1} M_{nAR}\right)^2_i} \left(\frac{T}{2}\right) \frac{\sin^4(\Delta\omega_{ij} - \dot{\theta}_{ij})\frac{T}{4}}{(\Delta\omega_{ij} - \dot{\theta}_{ij})^2 \frac{T^2}{16}}$$

(7.15)

The peak of this power density spectrum occurs where $\sin^4 x/x^2 = 0.525$. The worst-case rms phase error from this interference source is

$$\sqrt{\theta^2_{cei}} = \sqrt{(0.525)}\sqrt{\frac{B_c}{f_B}}\sqrt{\frac{S_{dj}}{S_{di}}}\ \frac{J_{m_j}(\delta)J_{m_i}(\delta)\sin\beta_j\left(M_1 M_{AR} M_{n1} M_{nAR}\right)_j}{\cos\beta_i\left(M_1 M_{AR} M_{n1} M_{nAR}\right)_i} \tag{7.16}$$

Since the ratio of B_c to f_B is $12.4/10^3 = .0124$, this insures that the carrier tracking phase error from this source of SSMA interference will be negligible even under worst-case conditions. For $m_j = \pm 4$ and $m_i = \pm 4$, $(0.525)^{1/2}(B_c/f_B)^{1/2}J_{m_j}(\delta)J_{m_i}(\delta) \cong 0.0127$.

Likewise, the normalized output of the subcarrier loop phase detector is

$$\frac{1}{\sqrt{2}}\delta\theta_{scei} + \frac{1}{\sqrt{2}}\sqrt{\frac{S_{dj}}{S_{di}}}\left(\frac{2m_i}{\delta}\right)\ \frac{J_{m_j}(\delta)J_{m_i}(\delta)\sin\beta_j\left(M_1 M_{AR} M_{n1} M_{nAR}\right)_j}{\cos\beta_i\left(M_1 M_{AR} M_{n1} M_{nAR}\right)_i}$$

$$\times\ \chi_{dj}(t)\cos[\Delta\omega_{ij}t + \theta_{ij}(t) + \theta_{cei}] \tag{7.17}$$

The worst-case rms subcarrier tracking error from this interference source is

$$\frac{1}{\sqrt{2}}\delta\sqrt{\theta^2_{scei}} = \frac{\sqrt{0.525}}{\sqrt{2}}\sqrt{\frac{S_{dj}}{S_{di}}}\sqrt{\frac{B_{sc}}{f_B}}\ \frac{(2m_i/\delta)J_{m_j}(\delta)J_{m_i}(\delta)\sin\beta_j\left(M_1 M_{AR} M_{n1} M_{nAR}\right)_j}{\cos\beta_i\left(M_1 M_{AR} M_{n1} M_{nAR}\right)_i} \tag{7.18}$$

Since the ratio B_{sc}/f_B is 0.5×10^{-3}, this error contribution to subcarrier tracking should be quite negligible.

Finally, we consider the interference with compound PLL demodulation from an other-User rnaging sidetone and/or turned-around noise. Assume that a fine range tone sideband associated with the other-User

subcarrier sideband for which $n_j = m_j$ lies very close to a desired-User subcarrier sideband for which $n_i = m_i$ in the RF spectrum. As far as the C.W. interference is concerned, the maximum carrier and subcarrier tracking errors are simply $\tilde{\rho}_1/2$ times the errors for the case of interference with compound PLL demodulation by the corresponding other-User subcarrier sideband. Since $\tilde{\rho}_1 \approx 0.5$ radians, the maximum error is approximately 1/4 of that for the other-User subcarrier sideband interference case. Similar remarks apply for the AR ranging sidetones, except that $\tilde{\rho}_2$ and $\tilde{\rho}_{AR}$ are much smaller than $\tilde{\rho}_1$. Turned-around noise will also interfere with compound PLL demodulation in this case. To estimate the seriousness of this interference source, write $\phi_{n1j}(t)$ and $\phi_{nARj}(t)$ as

$$\phi_{n1j}(t) = n_{1jc}(t)\cos\omega_1 t + n_{1js}(t)\sin\omega_1 t \tag{7.19}$$

and

$$\phi_{nARj}(t) = n_{ARjc}(t)\cos(\omega_1-\omega_2)t + n_{ARjs}(t)\sin(\omega_1-\omega_2)t \tag{7.20}$$

where $n_{1jc}(t)$, $n_{1js}(t)$, $n_{ARjc}(t)$, and $n_{ARjs}(t)$ are Gaussian noises of zero mean and variances σ^2_{n1j}, σ^2_{n1j}, σ^2_{nARj}, and σ^2_{nARj}. The noise power densities may be assumed constant across the noise bandwidths of the fine range tone and ambiguity resolving ranging sidetone filters. Then the final term in Eq. (7.3) may be written as

$$\sqrt{2S_{dj}} \sum_{n_j=-N}^{+N} J_{n_j}(\delta)\left(M_1 M_{AR}\right)_j \frac{1}{2}\Big[n_{1jc}(t)\cos\Big\{\omega_{cj}t + \theta_{cj}(t) + n_j\big[\omega_{scj}t + \theta_{scj}(t)\big] + \omega_1 t + \beta_j \chi_{dj}(t)\Big\} + n_{1js}(t)\sin\Big\{\omega_{cj}t + \theta_{cj}(t) + n_j\big[\omega_{scj}t + \theta_{scj}(t)\big] + \omega_1 t + \beta_j\chi_{dj}(t)\Big\}$$

$$+ n_{ARjc}(t)\cos\Big\{\omega_{cj}t + \theta_{cj}(t) + n_j\big[\omega_{scj}t + \theta_{scj}(t)\big] + (\omega_1-\omega_2)t + \beta_j\chi_{dj}(t)\Big\}$$

$$+ n_{ARjs}(t)\sin\Big\{\omega_{cj}t + \theta_{cj}(t) + n_j\big[\omega_{scj}t + \theta_{scj}(t)\big] + (\omega_1-\omega_2)t + \beta_j\chi_{dj}(t)\Big\}$$

$$+ n_{1jc}(t)\cos\left\{\omega_{cj}t + \theta_{cj}(t) + n_j\left[\omega_{scj}t + \theta_{scj}(t)\right] - \omega_1 t + \beta_j \chi_{dj}(t)\right\}$$

$$- n_{1js}(t)\sin\left\{\omega_{cj}t + \theta_{cj}(t) + n_j\left[\omega_{scj}t + \theta_{scj}(t)\right] - \omega_1 t + \beta_j \chi_{dj}(t)\right\}$$

$$+ n_{ARjc}(t)\cos\left\{\omega_{cj}t + \theta_{cj}(t) + n_j\left[\omega_{scj}t + \theta_{scj}(t)\right] - (\omega_1-\omega_2)t + \beta_j \chi_{dj}(t)\right\}$$

$$- n_{ARjs}(t)\sin\left\{\omega_{cj}t + \theta_{cj}(t) + n_j\left[\omega_{scj}t + \theta_{scj}(t)\right] - (\omega_1-\omega_2)t + \beta_j \chi_{dj}(t)\right\}\Bigg] \quad (7.21)$$

If the noise around the upper fine range tone sideband around the $n_j=m_j$ subcarrier sideband overlaps the subcarrier sideband for which $n_i=m_i$, the normalized output of the carrier tracking PLL phase detector may be written as

$$\theta_{cei} + \sqrt{\frac{S_{dj}}{S_{di}}}\, J_{m_j}(\delta) J_{m_i}(\delta)\, \frac{1}{2}\, \frac{\left(M_1 M_{AR}\right)_j}{\cos\beta_i \left(M_1 M_{AR} M_{n1} M_n AR\right)_i}$$

$$\times \left[n_{1jc}(t)\cos\left[\Delta\omega_{ij}t + \theta_{ij}(t) + \beta_j \chi_{dj}(t)\right] + n_{1js}(t)\sin\left[\Delta\omega_{ij}t + \theta_{ij}(t) + \beta_j \chi_{dj}(t)\right]\right] \quad (7.22)$$

The noise terms may be expanded as

$$\left[n_{1jc}(t)\left(\cos\beta_j \cos\left(\Delta\omega_{ij}t + \theta_{ij}(t)\right) - \sin\beta_j \chi_{dj}(t)\sin\left(\Delta\omega_{ij}t + \theta_{ij}(t)\right)\right)\right.$$

$$\left. + n_{1js}(t)\left(\cos\beta_j \sin\left(\Delta\omega_{ij}t + \theta_{ij}(t)\right) + \sin\beta_j \chi_{dj}(t)\cos\left(\Delta\omega_{ij}t + \theta_{ij}(t)\right)\right)\right] \quad (7.23)$$

The autocorrelation function of this noise is approximately

$$\Psi_{n1j}(\tau)\cos\left[\left(\Delta\omega_{ij} + \dot{\theta}_{ij}\right)\tau\right]\cos^2\beta_j + \Psi_{n1j}(\tau)\Psi_{xj}(\tau)\cos\left[\left(\Delta\omega_{ij} + \dot{\theta}_{ij}\right)\tau\right]\sin^2\beta_j \quad (7.24)$$

which corresponds to a power density spectrum

$$\frac{1}{2}\left[\Phi_{n1j}(\omega - \Delta\omega_{ij} - \dot{\theta}_{ij}) + \Phi_{n1j}(\omega + \Delta\omega_{ij} + \dot{\theta}_{ij})\right]\cos^2\beta_j$$

$$+ \frac{1}{2}\left[\int_{-\infty}^{\infty} \frac{d\zeta}{2\pi}\,\Phi_{n1j}(\zeta)\Phi_{xj}(\omega - \Delta\omega_{ij} - \dot{\theta}_{ij} - \zeta) + \int_{-\infty}^{\infty} \frac{d\zeta}{2\pi}\,\Phi_{n1j}(\zeta)\Phi_{xj}(\omega + \Delta\omega_{ij} + \theta_{ij} - \zeta)\right]\sin^2\beta$$

(7.25)

Since the noise bandwidth (double-sided) of the fine range tone bandpass filter is on the order of 1/10 the data bit rate, we may approximate $\frac{1}{2\pi}\Phi_{n1j}(\zeta)$ by an impulse of area σ_{n1}^2 in the convolution integral in Eq. (7.25). When we do this, the power density spectrum at $\omega = 0$ becomes

$$\left[\cos^2\beta_j\,\Phi_{n1j}(\Delta\omega_{ij} + \dot{\theta}_{ij}) + \sigma_{n1}^2\sin^2\beta_j\,\Phi_{xj}(\Delta\omega_{ij} + \dot{\theta}_{ij})\right] \qquad (7.26)$$

Note also that for the range of frequencies, $\Delta\omega_{ij} + \dot{\theta}_{ij}$, for which $\Phi_{nij}(\Delta\omega_{ij} + \dot{\theta}_{ij})$ is non-zero, $\Phi_{xj}(\Delta\omega_{ij} + \dot{\theta}_{ij})$ is essentially negligible. Consequently, if $\Delta\omega_{ij} + \dot{\theta}_{ij}$ is smaller than the range tone filter bandwidth, the rms carrier tracking error from this source of interference is

$$\sqrt{\overline{\theta_{cei}^2}} = \sqrt{\frac{S_{dj}}{S_{di}}}\,J_{m_j}(\delta)J_{m_i}(\delta)\,\frac{1}{2}\,\frac{\left(M_1 M_{AR}\right)_j}{\cos\beta_i\left(M_1 M_{AR} M_{n1} M_{nAR}\right)_i} \times \cos\beta_j\sqrt{\frac{\sigma_{n1}^2 2B_c}{B_{n1}}}$$

(7.27)

where B_{n1} is the double-sided range tone BP filter noise bandwidth. With σ_{n1} on the order of at most 0.5 radians (The noise cannot be much larger than this without robbing too much downlink signal power from the other modulation components and thereby causing the limiting amplifier excess noise detector to cease transmitting the ranging sidetones on the downlink.), the factor

$$J_{m_j}(\delta)J_{m_i}(\delta)\,\frac{1}{2}\,\sigma_{n1}\sqrt{\frac{2B_c}{B_{n1}}}$$

is, in the worst-case where m_j and m_i are both either -4 or +4, approximately equal to 0.014. The noise bandwidths were taken as $2B_c = 25$ Hz and $B_{n1} = 200$ Hz. This factor is sufficiently small so that the interference from this source may be considered negligible.

For $\Delta\omega_{ij} + \dot{\theta}_{ij}$ such that the peak of the data spectrum falls in the center of the carrier loop noise bandwidth, the rms carrier phase error will be

$$\sqrt{\overline{\theta^2_{cei}}} = \sqrt{\frac{S_{dj}}{S_{di}}} J_{m_j}(\delta) J_{m_i}(\delta) \frac{1}{2} \frac{\left(M_1 M_{AR}\right)_j}{\cos\beta_i \left(M_1 M_{AR} M_{n1} M_{nAR}\right)_i} \times \sin\beta_j \sqrt{\frac{\sigma^2_{n1}(0.525)2B_c}{f_B}} \tag{7.28}$$

Since $f_B/(0.525)$ is approximately 10 times B_{n1}, this interference is even more negligible than the interference from the turned-around noise.

Likewise, it may be readily seen that the carrier phase error from the turned-around noise from the output of the ambiguity ranging sidetone filter is even smaller than that from the turned-around noise from the output of the fine range tine bandpass filter. This is so simply because the noise power density at the output of the limiting amplifier following the AR sidetone filter is less than that at the output of the limiting amplifier following the fine range tone filter. This is so in part because of the attenuation factor 1/K which reduces the amplitude of the white noise. Also, since the excess noise detector ceases transmission of the AR tones on the downlink when σ_{nAR} exceeds approximately 0.5 radians, the larger noise bandwidth B_{nAR} results in a smaller value of noise power density Φ_{nAR} prior to the excess noise limit being reached.

In summary, the most potentially serious problem of SSMA interference with compound PLL demodulation arises from C.W. interference with carrier tracking from an other-User subcarrier sideband.

The probability of this occurring is small, however, and if it does occur it should not last too long.

7.2 Data Demodulation

In the case of data demodulation, other-User SSMA interference arises from either the other-User subcarrier sideband plus data or from the other-User ranging sidetone plus data and turned-around noise. The data bandwidth is much wider than the carrier loop bandwidth, and consequently if an other-User subcarrier sideband overlaps the data around one of the desired-User subcarrier sidebands in the received RF signal spectrum, the data around the other-User subcarrier sideband will also interfere with desired-User data demodulation.

To analyze the situation for the case of interference with data demodulation from an other-User subcarrier sideband and data, we make use of the results of the previous section to write the normalized input to the data demodulator as

$$\left(e_i(t)\right)_{data} = \chi_{di}(t) + \sqrt{\frac{S_{dj}}{S_{di}}}\,\frac{J_{m_j}(\delta)J_{m_i}(\delta)\left(M_1 M_{AR} M_{n1} M_{nAR}\right)_j}{\sin\beta_1\left(M_1 M_{AR} M_{n1} M_{nAR}\right)_i}$$

$$\times\left\{\cos\beta_j \sin[\Delta\omega_{ij}t + \theta_{ij}(t) + \theta_{cei}(t)] + \sin\beta_j\,\chi_{dj}(t)\cos[\Delta\omega_{ij}t + \theta_{ij}(t) + \theta_{cei}(t)]\right\} \tag{7.29}$$

From Appendix C the variance of the interference at the output of the data demodulator is approximately

$$S_j T^2 \cdot \frac{\sin^4(\omega_{ij} + \dot{\theta}_{ij})T/4}{\left(\omega_{ij}+\dot{\theta}_{ij}\right)^2 T^2/16}\cos^2\beta_j + S_j\sin^2\beta_j \int_{-\infty}^{\infty}\frac{d\zeta}{2\pi}\,\frac{1}{4}\left[T\,\frac{\sin^4(\zeta - \omega_{ij} - \dot{\theta}_{ij})T/4}{\left(\zeta-\omega_{ij}-\dot{\theta}_{ij}\right)^2 T^2/16}\right.$$

$$\left. + T\,\frac{\sin^4(\zeta + \omega_{ij} + \dot{\theta}_{ij})T/4}{\left(\zeta+\omega_{ij}+\dot{\theta}_{ij}\right)^2 T^2/16}\right] T^2\,\frac{\sin^4(\zeta T/4)}{(\zeta T/4)^2} \tag{7.30}$$

where

$$S_j = \frac{1}{2}\frac{S_{dj}}{S_{di}}\frac{J^2_{m_j}(\delta)J^2_{m_i}(\delta)\left(M_1 M_{AR} M_{n1} M_{nAR}\right)^2_j}{\sin^2\beta_i\left(M_1 M_{AR} M_{n1} M_{nAR}\right)^2_i} \tag{7.31}$$

The worst-case interference from the C.W. subcarrier sideband of the other-User occurs for $\omega_{ij} + \dot{\theta}_{ij}$ such that $[\sin^4(\omega_{ij}+\dot{\theta}_{ij})T/4]/[(\omega_{ij}+\dot{\theta}_{ij})^2T^2/16]$ is at its peak of 0.525. The variance of the C.W. interference in that case is

$$(0.525)\, S_j \cos^2\beta_j T^2 \tag{7.32}$$

This must be much less than $T^2/31.7$, or

$$S_j \cos^2\beta_j \ll 0.06 \tag{7.33}$$

In the worst-case where $m_j = m_i = \pm 4$, $J^2_{m_j}(\delta)J^2_{m_i}(\delta) = 0.0247$.

This is sufficiently large so that this source of interference may present a problem if the other-User signal power is significantly larger than that of the desired User, or if the other-User is not transmitting telemetry and/or ranging sidetones (as during acquisition of the other-User, for example). If the other-User is transmitting data, the factor $\cos^2\beta_j/\sin^2\beta_i$, which equals $\cos^2\beta = 0.41$ for $\beta = 1$ radian, reduces the C.W. SSMA interference problem somewhat.

The worst-case interference from the other-User data occurs for $\omega_{ij} + \dot{\theta}_{ij} = 0$. In this case the variance of the other-User data interference becomes

$$\frac{1}{2}T^2 S_j \sin^2\beta_j \int_{-\infty}^{\infty}\frac{dx}{2\pi}\left(\frac{\sin^2 x/4}{x/4}\right)^4 = \frac{1}{2}T^2 S_j \sin^2\beta_j \left(\frac{25}{12}\right) \approx T^2 S_j \sin^2\beta_j \tag{7.34}$$

This must be much less than $T^2/31.7$, or

$$S_j \sin^2 \beta_j \ll 0.0316 \tag{7.35}$$

or

$$\frac{S_{dj}}{S_{di}} J^2_{m_j}(\delta) J^2_{m_i}(\delta) \frac{\left(M_1 M_{AR} M_{n1} M_{nAR}\right)^2_j}{\left(M_1 M_{AR} M_{n1} M_{nAR}\right)^2_i} \tag{7.36}$$

Again, since $J^2_{m_i}(\delta) J^2_{m_i}(\delta)$ can be as high as 0.0247 for $m_i = m_j = \pm 4$, this source of interference may pose a problem if the other-User signal power is significantly larger than that of the desired User, or if several other-User interference components of this type are simultaneously present.

Turning now to the problem of interference with data demodulation from an other-User ranging sidetone plus retransmitted noise, the input to the data demodulator for the case where an other-User fine range tone sideband plus retransmitted noise overlaps the desired-User data may be written as

$$\left(e_i(t)\right)_{data} = \chi_{di}(t) + \sqrt{\frac{S_{dj}}{S_{di}}} \frac{J_{m_j}(\delta) J_{m_i}(\delta) \left(M_1 M_{AR} M_{n1} M_{nAR}\right)_j}{\sin\beta_i \left(M_1 M_{AR} M_{n1} M_{nAR}\right)_i}$$

$$\times \left\{ \frac{\tilde{\rho}_1}{2} \sin\left\{\omega_{ij} t + \theta_{ij}(t) + \theta_{cei}(t) + \beta_j \chi_{dj}(t)\right\} + \frac{1}{2} \frac{1}{\left(M_{n1} M_{nAR}\right)_j} \left[n_{1jc}(t) \cos\left\{\Delta\omega_{ij} t \right.\right.\right.$$

$$\left.\left.\left. + \theta_{ij}(t) + \theta_{cei}(t) + \beta_j \chi_{dj}(t)\right\} + n_{1js}(t) \sin\left\{\Delta\omega_{ij} t + \theta_{ij}(t) + \theta_{cei}(t)\, \beta_j \chi_{dj}(t)\right\} \right] \right\} \tag{7.38}$$

As far as the interference from the other-User fine range tone and data is concerned, the results are identical to the case for interference from the other-User subcarrier sideband and data except that the variance

of interference is reduced by the factor $\frac{1}{4}\tilde{\rho}_1^2 \cong 0.0625$. Consequently, the interference with data demodulation from an other-User fine range tone plus data is sufficiently small to be considered negligible.

The variance of the retransmitted noise component of the output of the data demodulator is, from Appendix C,

$$\int_{-\infty}^{\infty} \frac{d\omega}{2\pi}\, \Phi_n(\omega)\, |E_{sp}(\omega)|^2 \tag{7.39}$$

where $\Phi_n(\omega)$ is given approximately by

$$\Phi_n(\omega) = S'_j \cos^2\beta_j \frac{1}{8}\left[\Phi_{n1j}(\omega+\Delta\omega_{ij}+\dot{\theta}_{ij}) + \Phi_{n1j}(\omega-\Delta\omega_{ij}-\dot{\theta}_{ij})\right]$$

$$+ S'_j \sin^2\beta_j \frac{1}{8}\left[\int_{-\infty}^{\infty}\frac{d\zeta}{2\pi}\,\Phi_{n1j}(\zeta)\,\Phi_{xj}(\omega+\Delta\omega_{ij}+\dot{\theta}_{ij}-\zeta) + \int_{-\infty}^{\infty}\frac{d\zeta}{2\pi}\,\Phi_{n1j}(\zeta)\Phi_{xj}(\omega-\Delta\omega_{ij}-\dot{\theta}_{ij}-\zeta)\right] \tag{7.40}$$

where

$$S'_j = \frac{S_{dj}}{S_{di}}\,\frac{J^2_{m_i}(\delta)J^2_{m_j}(\delta)\left(M_1 M_{AR}\right)^2_j}{\sin^2\beta_i\left(M_1 M_{AR} M_{n1} M_{nAR}\right)^2_i} \tag{7.41}$$

As before, we may approximate $\frac{1}{2\pi}\Phi_{n1j}(\zeta)$ by an impulse of area σ^2_{n1}, so that the convolution integrals in Eq. (7.40) become

$$\sigma^2_{n1}\left[\Phi_{xj}(\omega+\Delta\omega_{ij}+\dot{\theta}_{ij}) + \Phi_{xj}(\omega-\Delta\omega_{ij}-\dot{\theta}_{ij})\right] \tag{7.42}$$

With this approximation, the variance becomes

$$S'_j \cos^2\beta_j \frac{T^2}{8}\int_{-\infty}^{\infty}\frac{d\omega}{2\pi}\left(\Phi_{n1j}(\omega+\Delta\omega_{ij}+\dot{\theta}_{ij}) + \Phi_{n1j}(\omega-\Delta\omega_{ij}-\dot{\theta}_{ij})\right)\frac{\sin^4(\omega T/4)}{(\omega T/4)^2}$$

$$+ S'_j \sin^2\beta_j \frac{T^2}{8}\sigma^2_{n1}\int_{-\infty}^{\infty}\frac{d\omega}{2\pi}\left(\Phi_{xj}(\omega+\Delta\omega_{ij}+\dot{\theta}_{ij}) + \Phi_{xj}(\omega-\Delta\omega_{ij}-\dot{\theta}_{ij})\right)\frac{\sin^4(\omega T/4)}{(\omega T/4)^2} \tag{7.43}$$

The first integral is maximum when $\Delta\omega_{ij} + \dot{\theta}_{ij}$ is near the peak of $\sin^4(\omega T/4)/(\omega T/4)^2$, whereas the second integral is maximum when $\Delta\omega_{ij} + \dot{\theta}_{ij} = 0$. In the first integral $\frac{1}{2\pi}\Phi_{n1j}\left(\omega \pm (\Delta\omega_{ij} + \dot{\theta}_{ij})\right)$ is approximated by an impulse of area σ_{n1}^2, so that the maximum of the first component of Eq. (7.43) is

$$S_j' \cos^2\beta_j \frac{T^2}{8} \sigma_{n1}^2 \, 2(0.525) \cong S_j' \cos^2\beta_j \, T^2 \sigma_{n1}^2 (0.13) \tag{7.44}$$

The maximum of the second component of Eq. (7.43) is

$$S_j' \sin^2\beta_j \frac{T^2}{8} \sigma_{n1}^2 \, 2 \int_{-\infty}^{\infty} \frac{dx}{2\pi} \left(\frac{\sin^2 x/4}{x/4}\right)^4 = S_j' \sin^2\beta_j \frac{T^2}{8} \sigma_{n1}^2 \, 2\left(\frac{25}{12}\right)$$

$$\cong S_j' \sin^2\beta_j \, T^2 \sigma_{n1}^2 (0.521) \tag{7.45}$$

The variances of Eqs. (7.44) and (7.45) must be much less than $T^2/31.7$ if the required BEP is to be realized. This condition may be written as

$$\frac{S_{dj}}{S_{di}} \frac{\left(M_1 M_{AR}\right)_j^2 \cos^2\beta_j}{\left(M_1 M_{AR} M_{n1} M_{nAR}\right)_i^2} \frac{J_{m_i}^2(\delta) J_{m_j}^2(\delta)}{\sin^2\beta_i} \sigma_{n1}^2 (0.13) \ll 0.0316 \tag{7.46}$$

and

$$\frac{S_{dj}}{S_{di}} \frac{\left(M_1 M_{AR}\right)_j^2 \sin^2\beta_j}{\left(M_1 M_{AR} M_{n1} M_{nAR}\right)_i^2} \frac{J_{m_i}^2(\delta) J_{m_j}^2(\delta)}{\sin^2\beta_i} \sigma_{n1}^2 (0.521) \ll 0.0316 \tag{7.47}$$

The more difficult condition is that of Eq. (7.47). In the worst-case situation where $m_i = m_j = \pm 4$, $J_{m_i}^2(\delta) J_{m_j}^2(\delta) \sigma_{n1}^2 (0.521)$ is 0.00322 which is approximately 1/10 of the critical value of 0.0316. Consequently, if the

other-User signal power is not significantly larger than that of the desired-User, the interference with data demodulation from retransmitted noise around an other-User range tone is essentially negligible.

We now examine the case of interference with data demodulation from an other-User AR sidetone cluster plus retransmitted noise and accompanying data. Since the amplitudes of the AR sidetones are much smaller than the amplitude of the fine range tone, the interference with data demodulation from an other-User AR sidetone is entirely negligible.

As for the turned-around noise around the AR sidetone cluster, recognition of the fact that the noise power denisty $\Phi_{nAR_j}(\omega)$ is much less than the noise power density $\Phi_{n1_j}(\omega)$, even though σ^2_{nAR} may be on the same order as σ^2_{n1}, leads one to realize that this source of interference with data demodulation is negligible.

In summary, only interference with desired-User data demodulation from an other-User subcarrier sideband plus data may present a problem.

7.3 Ranging

In this section we examine the case of other-User interference with the desired-User range measurement. The worst-case SSMA interference should occur for the situation where one of the other-User subcarrier sidebands overlaps one of the desired-User fine range tone sidebands. Of course, since the fine range tone loop noise bandwidth is so small, the probability of the C.W. interference is small, and should it occur, it would not last long because of the relative carrier doppler dynamics.

The input to the fine range tone PLL phase detector may be written approximately as

$$\left(e_i(t)\right)_1 = \tilde{\rho}_1 \sin\left(\omega_1 t + \theta_1(t)\right) + \sqrt{\frac{S_{dj}}{S_{di}}} \frac{J_{m_j}(\delta) J_{m_i}(\delta) \cos\beta_j \left(M_1 M_{AR} M_{n1} M_{nAR}\right)_j}{\cos\beta_i \left(M_1 M_{AR} M_{n1} M_{nAR}\right)_i}$$

$$\times \sin[\omega_1 t + \theta_1(t) + \Delta\omega_{ij} t + \theta_{ij}(t) + \theta_{cei}(t)]$$

$$+\sqrt{\frac{S_{dj}}{S_{di}}} \frac{J_{m_j}(\delta) J_{m_i}(\delta) \sin\beta_j \left(M_1 M_{AR} M_{n1} M_{nAR}\right)_j}{\cos\beta_i \left(M_1 M_{AR} M_{n1} M_{nAR}\right)_i}$$

$$\times \chi_{dj}(t) \cos[\omega_1 t + \theta_1(t) + \Delta\omega_{ij} t + \theta_{ij}(t) + \theta_{cei}(t)] \qquad (7.48)$$

If $\Delta\omega_{ij} + \dot{\theta}_{ij}$ is less than the bandwidth of the fine range tone PLL only the C.W. interference is important. In this case, the maximum fine range tone phase error from this C.W. interference alone is

$$\left(\theta_{ie}\right)_{max} = \sqrt{\frac{S_{dj}}{S_{di}}} \frac{\cos\beta_j \left(M_1 M_{AR} M_{n1} M_{nAR}\right)_j}{\cos\beta_i \left(M_1 M_{AR} M_{n1} M_{nAR}\right)_i} \frac{J_{m_j}(\delta) J_{m_i}(\delta)}{\tilde{\rho}_1} \qquad (7.49)$$

For $m_j = m_i = \pm 4$, $J_{m_j}(\delta) J_{m_i}(\delta)/\tilde{\rho}_1 = 0.314$. Since the peak phase error must be less than 0.0645 radians, it is clear that ranging may be disrupted when this interference occurs. Fortunately, the probability of its occurrence is small, and the duration of the disruption is likely to be short. In fact, if the relative carrier doppler dynamics is large enough, the interference will sweep through the loop noise bandwidth too fast for any significant error to build up.

Turning now to the data interference component of Eq. (7.48), the rms phase error from this source of SSMA interference is

$$\sqrt{\overline{\theta_{1e}^2}} = \frac{\sin\beta_j}{\cos\beta_i} \frac{\left(M_1 M_{AR} M_{n1} M_{nAR}\right)_j}{\left(M_1 M_{AR} M_{n1} M_{nAR}\right)_i} \sqrt{\frac{S_{dj}}{S_{di}}} \sqrt{B_1 \Phi_{xj}(\Delta\omega_{ij} + \dot{\theta}_{ij})} \frac{J_{m_j}(\delta) J_{m_i}(\delta)}{\tilde{\rho}_1} \tag{7.50}$$

where B_1 is the single-sided loop noise bandwidth, and

$$\Phi_{xj}(\omega) = T \frac{\sin^4(\omega T/4)}{(\omega T/4)^2} \tag{7.51}$$

The worst-case occurs for $\Delta\omega_{ij} + \dot{\theta}_{ij}$ at the peak of $\Phi_{xj}(\omega)$. For this situation, $\sqrt{\overline{\theta_{1e}^2}}$ is

$$\left(\sqrt{\overline{\theta_{1e}^2}}\right)_{max} = \frac{\sin\beta_j}{\cos\beta_i} \frac{\left(M_1 M_{AR} M_{n1} M_{nAR}\right)_j}{\left(M_1 M_{AR} M_{n1} M_{nAR}\right)_i} \sqrt{\frac{S_{dj}}{S_{di}}} \left(\sqrt{\frac{B_1}{f_B}(0.525)} \frac{J_{m_j}(\delta) J_{m_i}(\delta)}{\tilde{\rho}_1}\right) \tag{7.52}$$

With $B_1 \cong 0.6$ Hz, $f_B = 10^3$ Hz, $\tilde{\rho}_1 = 0.5$, and $m_j = m_i = \pm 4$, the factor

$$\tan\beta \left(\sqrt{\frac{B_1}{f_B}(0.525)} \frac{J_{m_j}(\delta) J_{m_i}(\delta)}{\tilde{\rho}_1}\right) \cong 1.56 \times 0.00567 = 0.00885 \tag{7.53}$$

is sufficiently less than the critical value of 0.0645 radians, so that it is unlikely that this source of interference will be serious.

For the case of interference with ranging from an other-User ranging sidetone, consider the other-User fine range tone sideband to be the source of the SSMA C.W. interference. When the other-User fine range tone sideband falls inside the loop noise bandwidth of the desired-User fine range tone PLL the maximum phase error is $\tilde{\rho}_1/2$ times the value in Eq. (7.49). This means that the maximum fine range tone phase error will be 0.25 times the value for the case where the SSMA interference

with ranging is from the other-User subcarrier sideband. This is still large enough to cause a serious disruption of ranging if the other-User fine range tone dwells inside the loop noise bandwidth for any significant length of time. This, however, is highly unlikely.

Similarly, interference from an other-User AR sidetone may also cause a momentary problem, although a less serious one than for the case of SSMA interference from an other-User fine range tone.

Since the fine range tone rms phase error arising from SSMA interference by an other-User data component around a subcarrier sideband was already shown to be negligible, it follows that the error from the data components around the other-User rnaging sidetones sidebands will also be negligible. This is so because the error in this case is less than the above error by a factor equal to one-half the ranging sidetone phase deviations which are all less than or equal to 0.25.

The remaining source of SSMA interference with range tone tracking arises from other-User turned-around noise. We consider the turned-around noise around an other-User fine range tone sideband first. If the error from this source is neglgible, the interference from the turned-around noise around an other-User AR sidetone cluster sideband will also be negligible. The input to the fine range tone PLL for this case is

$$\left(e_i(t)\right)_1 = \tilde{\rho}_1 \sin\left(\omega_1 t + \theta_1(t)\right) + \sqrt{\frac{S_{dj}}{S_{di}}} \frac{J_{m_j}(\delta) J_{m_i}(\delta) \left(M_1 M_{AR}\right)_j}{2\cos\beta_i \left(M_1 M_{AR} M_{n1} M_{nAR}\right)_i}$$

$$\times \left[n_{1jc}(t) \cos\left(\omega_1 t + \theta_1(t) + \Delta\omega_{ij} t + \theta_{ij}(t) + \theta_{cei}(t) + \beta_j \chi_{dj}(t)\right) \right.$$

$$\left. + \; n_{1js}(t) \sin\left(\omega_1 t + \theta_1(t) + \Delta\omega_{ij} t + \theta_{ij}(t) + \theta_{cei}(t) + \beta_j \chi_{dj}(t)\right) \right] \qquad (7.54)$$

The normalized output of the fine range tone loop phase detector is approximately

$$\left(e_o(t)\right)_1 = \theta_{1ei} + \sqrt{\frac{S_{dj}}{S_{di}}} \frac{\left(M_1 M_{AR}\right)_j}{\left(M_1 M_{AR} M_{n1} M_{nAR}\right)_i} \frac{J_{m_j}(\delta) J_{m_i}(\delta)}{2\tilde{\rho}_1 \cos\beta_i}$$

$$\times \left\{ \cos\beta_j \left[n_{1jc}(t) \cos\left(\Delta\omega_{ij} t + \theta_{ij}(t)\right) + n_{1js}(t) \sin\left(\Delta\omega_{ij} t + \theta_{ij}(t)\right) \right] \right.$$

$$\left. + \sin\beta_j \chi_{dj}(t) \left[-n_{1jc}(t) \sin\left(\Delta\omega_{ij} t + \theta_{ij}(t)\right) + n_{1js}(t) \cos\left(\Delta\omega_{ij} t + \theta_{ij}(t)\right) \right] \right\} \tag{7.55}$$

We proceed as in Eqs. (7.24), (7.25), (7.26) and (7.27) to obtain the result that

$$\sqrt{\overline{\theta_{1ei}^2}} = \sqrt{\frac{S_{dj}}{S_{di}}} \frac{J_{m_j}(\delta) J_{m_i}(\delta)}{2\tilde{\rho}_1 \cos\beta_i} \frac{\left(M_1 M_{AR}\right)_j}{\left(M_1 M_{AR} M_{n1} M_{nAR}\right)_i} \cos\beta_j \sigma_{n1} \sqrt{\frac{2B_1}{B_{n1}}} \tag{7.56}$$

when $\Delta\omega_{ij} + \dot{\theta}_{ij}$ is less than the fine range tone BP filter bandwidth, and

$$\sqrt{\overline{\theta_{1ei}^2}} = \sqrt{\frac{S_{dj}}{S_{di}}} \frac{J_{m_j}(\delta) J_{m_i}(\delta)}{2\tilde{\rho}_1 \cos\beta_i} \frac{\left(M_1 M_{AR}\right)_j}{\left(M_1 M_{AR} M_{n1} M_{nAR}\right)_i} \sin\beta_j \sigma_{n1} \sqrt{\frac{2B_1(0.525)}{f_B}} \tag{7.57}$$

when $\Delta\omega_{ij} + \dot{\theta}_{ij}$ is near the peak of the $\Phi_{xj}(\omega)$ curve.

From Eq. (7.56), the factor

$$\frac{J_{m_j}(\delta) J_{m_i}(\delta)}{2\tilde{\rho}_1} \sigma_{n1} \sqrt{\frac{2B_1}{B_{n1}}} \cong \frac{0.157}{2(0.5)} (0.5) \sqrt{\frac{2(0.6)}{200}} = 0.0061 \tag{7.58}$$

is sufficiently less than the critical value of 0.0645 so that this source of SSMA interference with ranging may be considered not serious if the other-User received signal power is not significantly larger than that of the desired-User.

From Eq. (7.57), the factor

$$\frac{J_{m_j}(\delta)J_{m_i}(\delta)}{2\gamma_1}\,\sigma_{n1}\sqrt{\frac{2B_1(0.525)}{f_B}} \cong \frac{0.157}{2(0.5)}\,(0.5)\sqrt{\frac{2(0.6)(0.525)}{10^3}} \cong 0.002 \tag{7.59}$$

This is even smaller than the above case, and therefore this source of SSMA interference is essentially negligible.

Since the noise power density of the turned-around noise around an other-User AR sidetone-cluster sideband is much less than that around the other-User fine range tone sideband, this source of SSMA interference with ranging should be truly negligible.

Concerning range ambiguity resolution, we realize that the very small effective noise bandwidths of the AR tone loops make serious C.W. SSMA interference unlikely in the sense that the relative carrier doppler dynamics should prevent an other-User C.W. component from remaining for any significant length of time within a fraction of a Hz of a desired-User AR sidetone sideband. As far as other-User narrowband SSMA interference with range ambiguity resolution is concerned, recall that the AR tone phase deviations were chosen in Sec. (4) on the basis that the value of the effective noise power density, Φ_R, for fine range tone tracking threshold and AR range tone phase acquisition threshold are identical. Consequently, if the SSMA narrowband interference was negligible for the case of fine range tone tracking, it should be equally negligible for AR range tone phase acquisition.

8. MULTIPATH INTEFERENCE EFFECTS

8.1 Introduction

Three types of multipath interference are considered. At low grazing angles, the earth refelected multipath interference is likely to be primarily specular at VHF. As the grazing angle increased, flat-fading diffuse multipath interference predominates. Finally, at large grazing angles the fading of the diffuse multipath interference becomes non-coherent as the time delay spread of the multipath interference increases. By multipath interference is meant the earth reflected signals. The desired direct line-of-sight signal is referred to as the direct-path signal.

8.2 Uplink Multipath Models

The mathematical models that we shall use to represent the received signals for the three cases of multipath interference are developed below.

We consider the uplink first. The received direct-path signal is written as

$$\left(e_u(t)\right)_d = \sqrt{2S_u}\ \sin\Big\{\omega_c t + \theta_c(t) + \delta \sin[\omega_{sc} t + \theta_{sc}(t)] + \beta\chi_u(t) + \rho_1 \sin\left(\omega_1 t + \theta_1(t)\right) + \phi_{AR}(t)\cos\left((\omega_1 - \omega_2)t + \theta_1(t) - \theta_2(t)\right)\Big\} \qquad (8.1)$$

Then the specular multipath interference may be written as

$$\left(e_u(t)\right)_s = a_u\sqrt{2S_u}\ \sin\Big\{\omega_c t + \theta_c(t) + \theta_{cs}(t) + \delta \sin[\omega_{sc} t + \theta_{sc}(t) + \theta_{scs}(t)] + \beta\chi_u(t-t_s) + \rho_1 \sin\left(\omega_1 t + \theta_1(t) + \theta_{1s}(t)\right) + \phi_{AR}(t-t_s)\cos\left((\omega_1 - \omega_2)t + \theta_1(t) - \theta_2(t) + \theta_{1s}(t) - \theta_{2s}(t)\right)\Big\} \qquad (8.2)$$

where a_u is the relative amplitude of the specular multipath component, and

$$\begin{aligned}\theta_{cs}(t) &= -\omega_c t_s(t)\\ \theta_{scs}(t) &= -\omega_{sc} t_s(t)\\ \theta_{1s}(t) &= -\omega_1 t_s(t)\\ \theta_{2s}(t) &= -\omega_2 t_s(t)\end{aligned} \tag{8.3}$$

and where $t_s(t)$ is the relative specular multipath time-varying time delay.

The flat-fading dffuse multipath interference may be represented by

$$\begin{aligned}\left(e_u(t)\right)_{ffd} = {} & \chi_c(t)\sqrt{2S_u}\,\sin\Big\{\omega_c t + \theta_c(t) + \theta_{cs}(t) + \delta\sin\big[\omega_{sc} t + \theta_{sc}(t) + \theta_{scs}(t)\big]\\ & + \beta\chi_u(t-t_s) + \rho_1\sin\Big(\omega_1 t + \theta_1(t) + \theta_{1s}(t)\Big) + \phi_{AR}(t-t_s)\cos\Big((\omega_1-\omega_2)t + \theta_1(t)\\ & - \theta_{1s}(t) - \theta_{2s}(t)\Big)\Big\} + \chi_q(t)\sqrt{2S_u}\,\cos\Big\{\omega_c t + \theta_c(t) + \theta_{cs}(t) + \delta\sin\big[\omega_{sc} t + \theta_{sc}(t)\\ & + \theta_{scs}(t)\big] + \beta\chi_u(t-t_s) + \rho_1\sin\Big(\omega_1 t + \theta_1(t) + \theta_{1s}(t)\Big) + \phi_{AR}(t-t_s)\cos\Big((\omega_1-\omega_2)t\\ & + \theta_1(t) - \theta_2(t) + \theta_{1s}(t) - \theta_{2s}(t)\Big)\Big\}\end{aligned} \tag{8.4}$$

where $\chi_{cu}(t)$ and $\chi_{qu}(t)$ are independent zero mean Gaussian random fluctuations with identical variances and power density spectra. The autocorrelation function of $\chi_{cu}(t)$ and $\chi_{qu}(t)$ is assumed to be

$$\langle\chi_{cu}(t)\chi_{cu}(t+\tau)\rangle = \langle\chi_{qu}(t)\chi_{qu}(t+\tau)\rangle = \sigma^2\exp\big[-(\tau/\tau_o)^2\big] \tag{8.5}$$

where τ_o is the "decorrelation time." The Fourrier transform of this is

$$\frac{\sigma^2}{\sqrt{2\pi}\,B_f}\,e^{-f^2/2B_f^2} \tag{8.6}$$

where B_f is the "fading bandwidth," and is related to the "decorrelation time" by

$$B_f = \frac{1}{\sqrt{2}} \frac{1}{2\pi \tau_o} \tag{8.7}$$

The fading bandwidth is approximately given by

$$B_f \approx \frac{\nu_o}{\lambda_c} \Psi_w \sin\gamma \tag{8.8}$$

where ν_o is the User satellite orbital velocity, λ_c is the wavelength of the VHF carrier, Ψ_w is the rms slope of the isotropic, Gaussian-distributed undulating scattering surface, and γ is the grazing angle of the scattering.

For the case of non-coherent fading of the multipath interference, the assumption is made that spectral components separated in frequency by an amount on the order of the subcarrier frequency fade independently, whereas spectral components separated in frequency by several kHz or less fade coherently. This is a valid assumption for diffuse multipath interference at large grazing angles and for User spacecraft at altitudes between approximately 500 and 4000 miles. If the rms slope of the scattering surface undulations is on the order of 4°, the coherence bandwidth is on the order of 10 kHz.* This justifies the above assumption.

In the time-delay-spread representation, the non-coherent fading diffuse multipath interference may be written as

$$\left(e_u(t)\right)_{n\text{-}cfd} = \sum_k \chi_{ck}(t)\sin\Big\{\omega_{ct} + \theta_c(t) + \theta_{cs}(t) + \delta\sin[\omega_{sc}t + \theta_{sc}(t) + \theta_{scs}(t)$$

$$- \omega_{sc}t_k] + \beta\chi_u(t-t_s) + \rho_1\sin\left(\omega_1 t + \theta_1(t) + \theta_{1s}(t) - \omega_1 t_k\right) + \phi_{AR}(t-t_s)\cos\Big((\omega_1-\omega_2)t$$

$$+ \theta_1(t) - \theta_2(t) + \theta_{1s}(t) - \theta_{2s}(t) - (\omega_1-\omega_2)t_k\Big)\Big\} + \chi_{qk}(t)\cos\Big\{\omega_c t + \theta_c(t) + \theta_{cs}(t)$$

*Durrani & Staras - Multipath Problems in Communications Between Low-Altitude Spacecraft and Stationary Satellites. RCA Review, March 1968, p. 95.

$$+ \delta \sin[\omega_{sc} t + \theta_{sc}(t) + \theta_{scs}(t) - \omega_{sc} t_k] + \beta \chi_u(t-t_s) + \rho_1 \sin\Big(\omega_1 t + \theta_1(t) + \theta_{1s}(t) - \omega_1 t_k$$
$$+ \phi_{AR}(t-t_s) \cos\Big((\omega_1 - \omega_2)t + \theta_1(t) - \theta_2(t) + \theta_{1s}(t) - \theta_{2s}(t) - (\omega_1 - \omega_2)t_k\Big)\Big\} \qquad (8.9)$$

An alternative, and more useful representation, considers only the important spectral components of the received non-coherent diffuse multipath interference. For simplicity in representation, we use the amplitude-phase representation of the cophasal and quadrature random signal components. That is

$$a(t)\sin\Big(\omega_o t + \phi(t)\Big) = \chi_c(t)\sin\omega_o t + \chi_q(t)\cos\omega_o t \qquad (8.10)$$

where

$$\text{and} \qquad \begin{aligned} \chi_c(t) &= a(t)\cos\phi(t) \\ \chi_q(t) &= a(t)\sin\phi(t) \end{aligned} \qquad (8.11)$$

Then, to a good approximation, the non-coherent fading diffuse multipath interference may be written as

$$\Big(e_u(t)\Big)_{n\text{-}cfd} \cong M_1 M_{AR} \sqrt{2S_u} \sum_{n=-N}^{+N} J_n(\delta)\Big\{a_{n0}(t)\sin\Big\{\omega_c t + \theta_c(t) + \theta_{cs}(t) + \phi_{n0}(t)$$
$$+ n[\omega_{sc} t + \theta_{sc}(t) + \theta_{scs}(t)] + \beta\chi_u(t-t_s)\Big\} + \frac{\rho_1}{2} a^+_{n1}(t)\sin\Big\{\omega_c t + \theta_c(t) + \theta_{cs}(t)$$
$$+ \theta^+_{n1}(t) + n[\omega_{sc} t + \theta_{sc}(t) + \theta_{scs}(t)] + \beta\chi_u(t-t_s) + \Big(\omega_1 t + \theta_1(t) + \theta_{1s}(t)\Big)\Big\}$$
$$- \frac{\rho_1}{2} a^-_{n1}(t)\sin\Big\{\omega_c t + \theta_c(t) + \theta_{cs}(t) + \phi^-_{n1}(t) + n[\omega_{sc} t + \theta_{sc}(t) + \theta_{scs}(t)] + \beta\chi_u(t-t_s)$$
$$- \Big(\omega_1 t + \theta_1(t) + \theta_{1s}(t)\Big)\Big\} + \frac{1}{2}\phi_{AR}(t-t_s)\, a^+_{nAR}(t)\cos\Big\{\omega_c t + \theta_c(t) + \theta_{cs}(t) + \phi^+_{nAR}$$
$$+ n[\omega_{sc} t + \theta_{sc}(t) + \theta_{scs}(t)] + \beta\chi_u(t-t_s) + \Big((\omega_1 - \omega_2)t + \theta_1(t) - \theta_2(t) + \theta_{1s}(t) - \theta_{2s}(t)\Big)\Big\}$$

$$+\frac{1}{2}\phi_{AR}(t-t_s)\,a^{-}_{nAR}(t)\cos\Big\{\omega_c t+\theta_c(t)+\theta_{cs}(t)+\phi^{-}_{nAR}(t)+n[\omega_{sc}t+\theta_{sc}(t)+\theta_{scs}(t)]$$

$$+\beta\chi_u(t-t_s)-\big((\omega_1-\omega_2)t+\theta_1(t)-\theta_2(t)+\theta_{1s}(t)-\theta_{2s}(t)\big)\Big\}\Big\} \qquad (8.12)$$

The fact that the fading of the fine range tone sidebands and that of the nearest AR sidetone cluster sidebands may be partially coherent is largely irrelevant. It is important to note, however, that the AM sidebands of the ω_3 and ω_4 AR tones in the AR sidetone cluster fade coherently.

8.3 Specular Multipath Case

The case of specular multipath interference was studied in Tech. Memo. G-161-7. We review the results of that memorandum and update them to include the modifications in the signal and receiver design made since that time.

The output of the carrier loop phase detector for the case of specular multipath interference is

$$\big(e_o(t)\big)_c=\sin\Big\{\theta_{ce}+\delta\sin[\omega_{sc}t+\theta_{sc}]-\delta\sin[\omega_{sc}t+\hat{\theta}_{sc}]+\beta\chi_u(t)$$

$$+\rho_1\sin\big(\omega_1 t+\theta_1(t)\big)+\phi_{AR}(t)\cos\big((\omega_1-\omega_2)t+\theta_1(t)-\theta_2(t)\big)\Big\}+a_u\sin\Big\{\theta_{ce}+\theta_{cs}(t)$$

$$+\delta\sin[\omega_{sc}t+\theta_{sc}+\theta_{scs}(t)]-\delta\sin[\omega_{sc}t+\hat{\theta}_{sc}]+\beta\chi_u(t-t_s)+\rho_1\sin\big(\omega_1 t+\theta_1(t)$$

$$+\theta_{1s}(t)\big)+\phi_{AR}(t-t_s)\cos\big((\omega_1-\omega_2)t+\theta_1(t)-\theta_2(t)+\theta_{1s}(t)-\theta_{2s}(t)\big)\Big\} \qquad (8.13)$$

With θ_{ce} small and $\theta_{sce}=\theta_{sc}-\hat{\theta}_{sc}$ also small, the compound PLL operates in the linear region.

The subcarrier differences are

$$\delta\left(\sin\left[\omega_{sc}t+\theta_{sc}\right]-\sin\left[\omega_{sc}t+\theta_{sc}-\theta_{sce}\right]\right)=\Delta\sin\left[\omega_{sc}t+\theta_{sc}+\phi_{sc}\right] \tag{8.14}$$

where

$$\Delta=2\delta\left|\sin\left(\frac{\theta_{sce}}{2}\right)\right| \tag{8.15}$$

and

$$\sin\left(\phi_{sc}+\theta_{sce}\right)=\frac{\delta}{\Delta}\sin\theta_{sce} \tag{8.16}$$

and

$$\delta\left(\sin\left[\omega_{sc}t+\theta_{sc}+\theta_{scs}(t)\right]-\sin\left[\omega_{sc}t+\hat{\theta}_{sc}\right]\right)$$

$$=\Gamma\sin\left[\omega_{sc}t+\theta_{sc}+\theta_{scs}(t)+\gamma_{sc}\right] \tag{8.17}$$

where

$$\Gamma=2\delta\left|\sin\left(\frac{\theta_{sce}+\theta_{scs}}{2}\right)\right|=2\delta\left|\sin\left(\frac{\alpha}{2}\right)\right| \tag{8.18}$$

and

$$\sin\left(\theta_{sce}+\theta_{scs}(t)+\gamma_{sc}\right)=\frac{\delta}{\Gamma}\sin\left(\theta_{sce}+\theta_{scs}(t)\right) \tag{8.19}$$

The various signal components at the output of the carrier loop phase detector are obtained by expanding Eq. (8.13) and making use of Eqs. (8.14) and (8.17).

$$\left(e_o(t)\right)_c\approx M_1M_{AR}\cos\beta\left\{J_o(\Delta)\sin\theta_{ce}\right.$$ carrier loop error signal

$$+J_o(\Delta)\cos\theta_{ce}\tan\beta\,x_u(t)$$ data signal

$$+a_uJ_o(\Gamma)\sin\left(\theta_{ce}+\theta_{cs}(t)\right)$$ C.W. multipath interference

$$+a_uJ_o(\Gamma)\cos\left(\theta_{ce}+\theta_{cs}(t)\right)\tan\beta\,x_u(t-t_s)$$ specular multipath data

$$+2J_1(\Delta)\cos\theta_{ce}\sin\left[\omega_{sc}t+\theta_{sc}+\phi_{sc}\right]$$ subcarrier

$$+ a_u 2J_1(\Gamma)\left[\cos\left(\theta_{ce}+\theta_{cs}(t)\right) - \sin\left(\theta_{ce}+\theta_{cs}(t)\right)\tan\beta\chi_u(t-t_s)\right]$$
$$\times \sin[\omega_{sc}t + \theta_{sc} + \theta_{scs}(t) + \gamma_{sc}]$$

subcarrier specular multipath interference

$$+ J_o(\Delta)\cos\theta_{ce}\,\bar{\rho}_1 \sin\left(\omega_1 t + \theta_1(t)\right)$$

fine range tone

$$+ a_u J_o(\Gamma)\left[\cos\left(\theta_{ce}+\theta_{cs}(t)\right) - \sin\left(\theta_{ce}+\theta_{cs}(t)\right)\tan\beta\chi_u(t-t_s)\right]$$
$$\times \bar{\rho}_1 \sin[\omega_1 t + \theta_1(t) + \theta_{1s}(t)]$$

fine range tone specular multipath interference

$$+ J_o(\Delta)\cos\theta_{ce}\,\phi_{AR}(t)\cos\left((\omega_1-\omega_2)t + \theta_1(t) - \theta_2(t)\right)$$

AR sidetones

$$+ a_u J_o(\Gamma)\left[\cos\left(\theta_{ce}+\theta_{cs}(t)\right) - \sin\left(\theta_{ce}+\theta_{cs}(t)\tan\beta\chi_u(t-t_s)\right]\right.$$
$$\left. + \phi_{AR}(t-t_s)\cos\left((\omega_1-\omega_2)t + \theta_1(t) - \theta_2(t) + \theta_{1s}(t) - \theta_{2s}(t)\right)\right\}$$

AR sidetones specular multipath interference

(8.20)

For small θ_{ce} and $\delta\theta_{sce}$, $\sin\theta_{ce} \approx \theta_{ce}$, $\cos\theta_{ce} \approx 1$, $J_o(\Delta) \approx 1$, and $2J_1(\Delta) \approx \Delta$.

8.3.1 Effects of Specular Multipath Interference on Compound PLL Tracking

Depending on the frequency $\dot{\theta}_{cs}(t)$, the C.W. multipath interference component will either interfere with carrier tracking or data demodulation, but not both. This is a consequence of the nature of the power density spectrum of the split-phase data. The narrowband multipath interference caused by the data component around dc can interfere with both carrier-tracking and data demodulation.

If $\dot{\theta}_{cs}/2\pi$ is less than the carrier loop noise bandwidth, the maximum carrier loop phase error arising from the "carrier" component of the specular multipath interference (after multiplication by the wideband

FM reference signal) is

$$\left(\theta_{ce}\right)_{max} \cong a_u J_o(\Gamma) \tag{8.21}$$

and the rms error is $\left(\theta_{ce}\right)_{max}/\sqrt{2}$. A sketch of $J_o(\Gamma)$ as a function of $\alpha = \theta_{sce} + \theta_{scs}$ is shown in Fig. 8.1 for $\delta = 5.52$. For $|\alpha|$ greater than approximately 20°, $J_o(\Gamma)$ will be less than 0.4.

The likelihood that $\dot{\theta}_{cs}/2\pi$ will be less than the carrier loop noise bandwidth is small, however. In the range of grazing angles for which specualr multipath interference is likely to occur (γ between 10° and 40°), $\dot{\theta}_{cs}/2\pi$ will be at least 150 Hz for near equatorial circular orbits. Consequently, the effect of the C.W. specular multipath interference on carrier tracking is negligible.

The specular multipath data may interfere with carrier tracking if the relative specular multipath doppler frequency $\dot{\theta}_{cs}/2\pi$ is such that it lies near the peak of the data power density spectrum. The rms carrier loop phase error from the specular multipath data component is approximately given by

$$\left(\overline{\theta_{ce}^2}\right)^{1/2} \cong a_u J_o(\Gamma)\tan\beta \left[B_c \Phi_{x_u}\left(\dot{\theta}_{cs}\right)\right]^{1/2} \tag{8.22}$$

where $\Phi_{x_u}(\omega) = T \sin^4(\omega T/4)/(\omega T/4)^2$. If $\dot{\theta}_{cs}$ lies at the peak of the $\Phi_{x_u}(\omega)$ spectrum, this rms error is

$$\left(\overline{\theta_{ce}^2}\right)_{max}^{1/2} \cong a_u J_o(\Gamma)\tan\beta \left[\frac{B_c}{f_B}(0.525)\right]^{1/2} \tag{8.23}$$

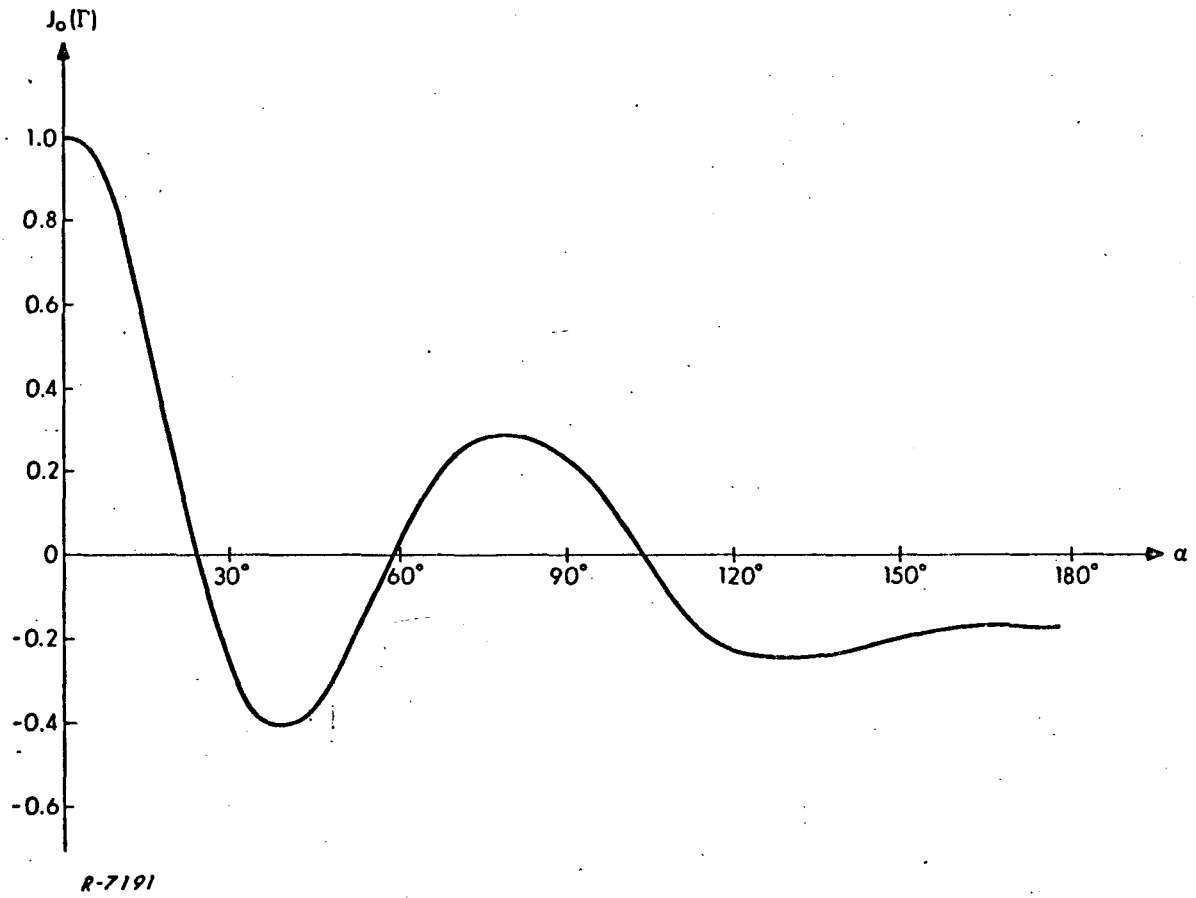

Fig. 8.1 $J_o(\Gamma)$ as a Function of α

With B_c = 9 Hz and f_B = 100 Hz, this error becomes

$$\left(\overline{\theta_{ce}^2}\right)_{max}^{1/2} = a_u J_o(\Gamma) \tan\beta\,(0.218) \tag{8.24}$$

For f_B = 400 Hz, this error is

$$\left(\overline{\theta_{ce}^2}\right)_{max}^{1/2} = a_u J_o(\Gamma) \tan\beta\,(0.109) \tag{8.25}$$

With $\dot{\theta}_{cs}/2\pi$ likely to be 150 Hz or greater, the peak of the specular multipath data component will not be shifted into the center of the carrier loop noise bandwidth. The next highest peak of $\Phi_{x_u}(\omega)$ has a value of approximately 0.045 T, and this causes a maximum rms carrier loop phase error of

$$\left(\overline{\theta_{ce}^2}\right)_{max}^{1/2} = a_u J_o(\Gamma) \tan\beta\,(0.064) \tag{8.26}$$

It is clear that the relative specular multipath carrier doppler frequency is a big factor in reducing the effects of the specular multipath interference on carrier tracking. Considering the fact that a_u is likely to be less than about 1/2, and that $J_o(\Gamma)$ is less than 0.4 for approximately 90 percent of the range of the relative specular multipath subcarrier phase θ_{scs}, it is evident that the contribution to the carrier loop phase error from specular multipath interference is essentially neglibible.

Turning now to subcarrier tracking, the output of the subcarrier loop phase detector is approximately given by

$$\left(e_o(t)\right)_{sc} \cong \frac{1}{\sqrt{2}}\, 2J_1(\delta)\sin\left(\theta_{sce} + \phi_{sc}\right) + \frac{a_u}{\sqrt{2}}\, 2J_1(\Gamma)\cos\left(\theta_{ce} + \theta_{cs}(t)\right)\sin\left(\theta_{sce}\right.$$

$$\left. + \theta_{scs}(t) + \gamma_{sc}\right) - \frac{a_u}{\sqrt{2}}\, 2J_1(\Gamma)\sin\left(\theta_{ce} + \theta_{cs}(t)\right)\tan\beta\chi_u(t-t_s)\sin\left(\theta_{sce} + \theta_{scs}(t) + \gamma_{sc}\right) \tag{8.27}$$

$$\cong \frac{\delta}{\sqrt{2}}\,\theta_{sce} + a_u\,\frac{\delta}{\sqrt{2}}\left(\frac{2J_1(\Gamma)}{\Gamma}\right)\cos\left(\theta_{ce} + \theta_{cs}(t)\right)\sin\left(\theta_{sce} + \theta_{scs}(t)\right)$$

$$- \frac{a_u\delta}{\sqrt{2}}\left(\frac{2J_1(\Gamma)}{\Gamma}\right)\sin\left(\theta_{ce} + \theta_{cs}(t)\right)\tan\beta\,\chi_u(t-t_s)\sin\left(\theta_{sce} + \theta_{scs}(t)\right) \tag{8.28}$$

The error resulting from the presence of the C. W. specular multipath interference is negligible because the relative specular multipath carrier doppler frequency $\dot{\theta}_{cs}/2\pi$ is much greater than the subcarrier loop noise bandwidth B_{sc}. The contribution to the rms error from the specular multipath data is approximately given by

$$\frac{\delta}{\sqrt{2}}\left(\overline{\theta^2_{sce}}\right)^{1/2} = a_u\,\frac{\delta}{\sqrt{2}}\left(\frac{2J_1(\Gamma)}{\Gamma}\sin\alpha\right)\tan\beta\left[\frac{B_{cs}}{f_B}\,\Phi_{x_u}\left(\dot{\theta}_{cs}\right)\right]^{1/2} \tag{8.29}$$

A sketch of $\left[2\delta J_1\left(\Gamma(\alpha)\right)\sin\alpha/\Gamma(\alpha)\right]$ is shown in Fig. 8.2 for $\delta = 5.52$. The maximum value of this factor is approximately 1.1. For $\dot{\theta}_{cs}$ at the peak of the data power spectrum $\Phi_{x_u}(\omega)$, and for $f_B = 400$ Hz and $B_{cs} = 0.5$ Hz, the worst-case rms error is

$$\frac{\delta}{\sqrt{2}}\left(\overline{\theta^2_{sce}}\right)^{1/2}_{max} = a_u\,\frac{1}{\sqrt{2}}(1.1)(1.56)\left[\frac{0.5}{400}(0.525)\right]^{1/2} = 0.031\,a_u \tag{8.30}$$

This is certainly negligible.

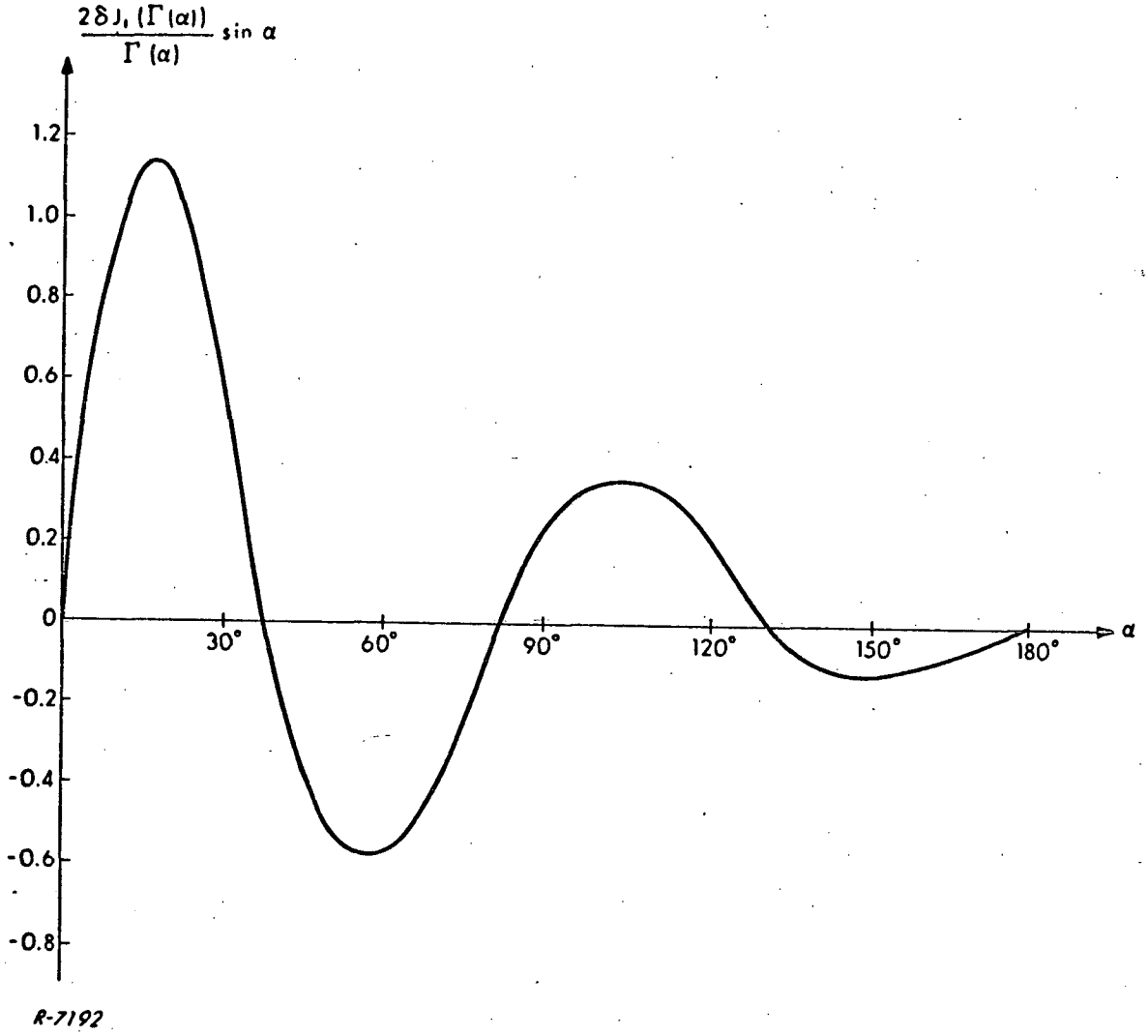

Fig. 8.2 $\dfrac{2\delta J_1\left(\Gamma(\alpha)\right) \sin\alpha}{\Gamma(\alpha)}$ as a Function of α

For f_B = 100 Hz, and $\dot{\theta}_{cs}$ at the second-highest peak, the maximum error is

$$\frac{\delta}{\sqrt{2}}\left(\overline{\theta^2_{sce}}\right)^{1/2}_{max} = a_u \frac{1}{\sqrt{2}}(1.1)(1.56)\left[\frac{0.5}{100}(0.045)\right]^{1/2} = 0.0182\, a_u \tag{8.31}$$

which is even more negligible.

In summary, the effects of specular multipath interference on compound PLL tracking are negligible.

8.3.2 Effects of Specular Multipath Interference on Data Demodulation

Turning now to the case of data demodulation, the normalized input to the data demodulation is approximately

$$\left(e_i(t)\right)_{data} = x_u(t) + a_u J_o(\Gamma)\cot\beta \sin\left(\theta_{ce} + \theta_{cs}(t)\right) + a_u J_o(\Gamma)\cos\left(\theta_{ce} + \theta_{cs}(t)\right)x_u(t-t_s) \tag{8.32}$$

The variance of the C.W. interference at the output of the phase detectoris

$$\sigma^2_{cw} = \frac{1}{2} a_u^2 J_o^2(\Gamma)\cot^2\beta\, T^2 \frac{\sin^4(\dot{\theta}_{cs}T/4)}{(\dot{\theta}_{cs}T/4)^2} \tag{8.33}$$

The worst-case situation occurs for $\dot{\theta}_{cs}$ at the peak of the split-phase power density spectrum. In this case the condition for the required BEP is

$$\sigma^2_{cw} << \frac{T^2}{31.7} \tag{8.34}$$

or

$$\frac{1}{2}(0.525)\, a_u^2 J_o^2(\Gamma)\cot^2\beta << \frac{1}{31.7}$$

With a_u less than about 1/2, and $J_o(\Gamma)$ less than 0.4 for approximately 90 percent of the range of the subcarrier relative specular multipath phase delay, θ_{scs}, this condition should be satisfied most of the time.

For the 100 BPS data rate, $\dot{\theta}_{cs}$ will more than likely lie past the peak of the split-phase power density spectrum. If $\dot{\theta}_{cs}$ lies at the next highest peak of split-phase power density spectrum, the condition on $a_u J_o(\Gamma)$ is

$$a_u J_o(\Gamma) \ll 1.84 \tag{8.36}$$

This condition will be satisfied essentially all of the time.

The specular multipath data component at the output of the data demodulator is

$$a_u J_o(\Gamma) \int_o^T \cos\left(\theta_{ce} + \dot{\theta}_{cs} t + \theta_{cs}(o)\right) \chi_u(t-t_s)\, e_{sp}(t)dt \tag{8.37}$$

Since the worst-case specular multipath interference occurs at low grazing angles ($\gamma \lesssim 20°$), and since such low grazing angles would only be encountered for low altitudes, the relative specular multipath delay, t_s, will be small compared to a bit period under conditions for which specular multipath interference is likely to be a problem. For example, for altitudes below 200 miles, and for grazing angles below 20°, the relative specular multipath time delay is less than 0.4 msec. This compares with uplink bit periods of 10 msec or 2.5 msec for the command data, and a downlink bit period of 1 msec for the telemetry data. Consequently, we make the simplifying assumption that t_s is negligible in Eq. (8.37), so that the product $\chi_u(t-t_s)e_{sp}(t) = \pm 1$ over the bit period.

The mean-square value of the specular multipath data component at the output of the data demodulator is

$$\sigma_{sd}^2 = T^2 \frac{1}{2} a_u^2 J_o^2(\Gamma) \frac{\sin^2(\dot{\theta}_{cs} T/2)}{(\dot{\theta}_{cs} T/2)^2} \tag{8.38}$$

With $\dot{\theta}_{cs}/2\pi$ greater than 150 Hz, the worst-case condition for the required BEP becomes, in the case of T = 10 msec, approximately

$$\frac{\sigma_{sd}^2}{T^2} \ll \frac{1}{31.7} \quad \text{or} \quad \frac{1}{2}\left(a_u^2 J_o^2(\Gamma)\right) \frac{1}{(3\pi/2)^2} \ll \frac{1}{31.7} \tag{8.39}$$

or

$$a_u J_o(\Gamma) \ll 1.2 \tag{8.40}$$

This condition is satisfied most of the time.

For T = 2.5 msec, the worst-case condition becomes

$$\frac{1}{2}\left(a_u^2 J_o^2(\Gamma)\right) \ll \frac{1}{31.7} \tag{8.41}$$

or

$$a_u J_o(\Gamma) \ll 0.252 \tag{8.42}$$

This condition is not satisfied very easily. However, if $\dot{\theta}_{cs}/2\pi$ is greater than 400 Hz, the worst-case condition reduces to that of Eq. (8.40).

8.3.3 Specular Multipath Ranging Sidetones Interference

Concerning the specular multipath ranging sidetones, it is seen from Eq. (8.20) that these sidetones are reduced in amplitude by the factor $J_o(\Gamma)$ and are modulated by the relative specular multipath carrier doppler frequency terms

$$\left[\cos\left(\theta_{ce}+\theta_{cs}(t)\right) - \sin\left(\theta_{ce}+\theta_{cs}(t)\right)\tan\beta\chi_u(t-t_s)\right] \qquad (8.43)$$

If $\dot{\theta}_{cs}/2\pi$ is greater than one-half the fine range tone filter noise bandwidth, the C.W. interference term will be further attenuated by the filter transfer function. If $\dot{\theta}_{cs}/2\pi$ is greater than the data bit rate, the peak of the specular multipath data spectrum in Eq. (8.43) will not overlap the direct-path fine range tone.

Similar remarks apply for the AR sidetones except that the wider AR sidetones filter bandwidth results in turn-around of most of the AR sidetone specular multipath components.

If $\dot{\theta}_{cs}/2\pi$ is such that it places the peak of the specular multipath 400 BPS data spectrum on the fine range tone, the criterion that this source of interference contributes a fine range tone rms phase error which is much less than the critical value of 0.0645 radians is that $a_u J_o(\Gamma) \ll 2.83$. This is easily satisfied since $a_u J_o(\Gamma)$ is on the order of 1/10 of this value.

8.4 Flat-Fading Diffuse Multipath Interference

We now examine the case of flat-fading diffuse multipath interference. In this case the output of the carrier loop phase detector may be written as

$$\left(e_o(t)\right)_c = \sin\Big\{\theta_{ce} + \Delta\sin[\omega_{sc}t + \theta_{sc} + \phi_{sc}] + \beta\chi_u(t) + \rho_1\sin\left(\omega_1 t + \theta_1(t)\right)$$

$$+ \phi_{AR}(t)\cos\left((\omega_1-\omega_2)t + \theta_1(t) - \theta_2(t)\right)\Big\} + a_u(t)\sin\Big\{\theta_{ce} + \theta_{cs}(t) + \phi_{sc}9t) + \Gamma\sin[\omega_{sc}t$$

$$+ \theta_{sc} + \theta_{scs}(t) + \gamma_{sc}] + \beta\chi_u(t-t_s) + \rho_1\sin\left(\omega_1 t + \theta_1(t) + \theta_{1s}(t)\right)$$

$$+ \phi_{AR}(t-t_s)\cos\left((\omega_1-\omega_2)t + \theta_1(t) - \theta_2(t) + \theta_{1s}(t) - \theta_{2s}(t)\right)\Big\} \qquad (8.44)$$

where $a_u(t)\cos\phi_u(t) = \chi_c(t)$

and $a_u(t)\sin\phi_u(t) = \chi_q(t)$ (8.45)

For small tracking errors θ_{ce} and $\delta\theta_{sce}$, this is expanded as

$$\left(e_o(t)\right)_c \approx M_1 M_{AR}\cos\beta\Big\{\theta_{ce} + \tan\beta\,\chi_u(t) + a_u(t)J_o(\Gamma)\sin\left(\theta_{cs}(t) + \phi_u(t)\right)$$

$$+ a_u(t)J_o(\Gamma)\cos\left(\theta_{cs}(t) + \phi_u(t)\right)\tan\beta\,\chi_u(t-t_s) + 2J_1(\Delta)\sin\left[\omega_{sc}t + \theta_{sc} + \phi_{sc}\right]$$

$$+ a_u(t)2J_1(\Gamma)\left[\cos\left(\theta_{cs}(t) + \phi_u(t)\right) - \sin\left(\theta_{cs}(t) + \phi_u(t)\right)\tan\beta\,\chi_u(t-t_s)\right]$$

$$\times\ \sin\left[\omega_{sc}t + \theta_{sc} + \theta_{scs}(t) + \gamma_{sc}\right] + \bar{\rho}_1\sin\left(\omega_1 t + \theta_1(t)\right) + a_u(t)J_o(\Gamma)\left[\cos\left(\theta_{cs}(t)\right.\right.$$

$$\left.\left. + \phi_u(t)\right) - \sin\left(\theta_{cs}(t) + \phi_u(t)\right)\tan\beta\,\chi_u(t-t_s)\right] \times \bar{\rho}_1\sin\left(\omega_1 t + \theta_1(t) + \theta_{1s}(t)\right)$$

$$+ \phi_{AR}(t)\cos\left((\omega_1-\omega_2)t + \theta_1(t) - \theta_2(t)\right) + a_u(t)J_o(\Gamma)\left[\cos\left(\theta_{cs}(t) + \phi_u(t)\right) - \sin\left(\theta_{cs}(t)\right.\right.$$

$$\left.\left. + \phi_u(t)\right)\tan\beta\,\chi_u(t-t_s)\right] \times \phi_{AR}(t-t_s)\cos\left((\omega_1-\omega_2)t + \theta_1(t) - \theta_2(t) + \theta_{1s}(t) - \theta_{2s}(t)\right)$$

(8.46)

The effect of the fading is to spread the spectrum of the multipath interference. For low orbit User spacecraft and for an rms scattering surface slope value of approximately 4° and a grazing angle in excess of 20°, the fading bandwidth will exceed approximately 90 Hz. This is much larger than the noise bandwidths of any of the phase-locked-loops in the system, so that the spectrum of the fading may be considered as "white" inside the various loop noise bandwidths.

8.4.1 Interference with Compound PLL Tracking

The multipath interference with carrier tracking may be written as

$$J_o(\Gamma)\,\chi_c(t)\sin\theta_{cs}(t) + J_o(\Gamma)\,\chi_q(t)\cos\theta_{cs}(t)$$

$$+ J_o(\Gamma)\,\chi_c(t)\cos\theta_{cs}(t)\tan\beta\,\chi_u(t-t_s)$$

$$- J_o(\Gamma)\,\chi_q(t)\sin\theta_{cs}(t)\tan\beta\,\chi_u(t-t_s) \qquad (8.47)$$

The autocorrelation function of this interference is

$$J_o^2(\Gamma)\left\{\Psi(\tau)\cos(\dot{\theta}_{cs}\tau) + \tan^2\beta\,\Psi(\tau)\,\Psi_{x_u}(\tau)\cos(\dot{\theta}_{cs}\tau)\right\}$$

where $$\Psi(\tau) = \langle x_c(t)x_c(t+\tau)\rangle = \langle x_q(t)x_q(t+\tau)\rangle. \qquad (8.48)$$

The power density spectrum at $\omega = 0$ is

$$J_o^2(\Gamma)\left\{\Phi(\dot{\theta}_{cs}) + \tan^2\beta \int_{-\infty}^{\infty} \frac{d\zeta}{2\pi}\,\Phi_{x_u}(\zeta)\,\Phi(\zeta - \dot{\theta}_{cs})\right\} \qquad (8.49)$$

where

$$\Phi(\omega) = \frac{\sigma^2}{\sqrt{2\pi}\,B_f}\; e^{-\omega^2/2(2\pi B_f)^2} \qquad (8.50)$$

where σ^2 is the value of $\Psi(\tau)$ at $\tau=0$, and B is the fading bandwidth.

The integral in Eq. (8.49) is

$$I = \sigma^2 T \int_{-\infty}^{\infty} \frac{d\zeta}{2\pi}\;\frac{\sin^4(\zeta\,T/4)}{(\zeta\,T/4)^2}\;\frac{1}{\sqrt{2\pi}\,B_f}\; e^{-\left(\zeta-\dot{\theta}_{cs}\right)^2/2\left(2\pi B_f\right)^2} \qquad (8.51)$$

The worst case occurs when $\dot{\theta}_{cs}$ is at the peak of the $\Phi_{x_u}(\zeta)$ curve, and the fading bandwidth, B_f, is much narrower than the width of the peak. Although this condition is unlikely, even for the 400 BPS data rate, it does represent an upper bound on the integral. The maximum value of the integral is then

$$I_{max} = (0.525T)\sigma^2 \tag{8.52}$$

and the maximum rms carrier tracking loop phase error from this diffuse multipath data component is

$$\left(\overline{\theta_{ce}^2}\right)^{1/2}_{max} = \sigma J_o(\Gamma)\tan\beta(0.109) \quad \text{for } f_B = 400 \text{ Hz} \tag{8.53}$$

and

$$\left(\overline{\theta_{ce}^2}\right)^{1/2}_{max} = \sigma J_o(\Gamma)\tan\beta(0.064) \quad \text{for } f_B = 100 \text{ Hz} \tag{8.54}$$

It is assumed that $\dot{\theta}_{cs}/2\pi$ exceeds 150 Hz in the above, so that the worst case occurs for $\dot{\theta}_{cs}/2\pi$ at the second highest peak of the data power density spectrum when $f_B = 100$ Hz.

The rms carrier loop phase error arising from the first term in Eq. (8.49), for the case where B_f exceeds 90 Hz is

$$\left(\overline{\theta_{ce}^2}\right)^{1/2} = \sigma J_o(\Gamma)\left(\frac{2B_c}{\sqrt{2\pi}\,B_f}\, e^{-\ddot{\theta}_{cs}^2/2(2\pi B_f)^2}\right)^{1/2} \tag{8.55}$$

With $B_f = 90$ Hz and $\dot{\theta}_{cs}/2\pi = 150$ Hz, this error becomes

$$\left(\overline{\dot{\theta}_{ce}^2}\right)^{1/2} = \sigma J_o(\Gamma)(0.14) \tag{8.56}$$

This is sufficiently small to be considered negligible.

A similar analysis applied to the subcarrier tracking loop reveals that, as in the specular multipath case, the subcarrier tracking error $\frac{\delta}{\sqrt{2}}\left(\overline{\theta^2_{sce}}\right)^{1/2}_{max}$ is negligible. For example, the maximum error from the diffuse multipath subcarrier component for $B_f = 90$ Hz and $\dot{\theta}_{sc}/2\pi = 150$ Hz is

$$\frac{\delta}{\sqrt{2}}\left(\overline{\theta^2_{sce}}\right)^{1/2} = \sigma\frac{\delta}{\sqrt{2}}\left(\frac{2J_1(\Gamma)}{\Gamma}\sin\alpha\right)\left[\frac{2B_{sc}}{\sqrt{2\pi}\,B_f}\,e^{-\dot{\theta}^2_{cs}/2(2\pi B_f)^2}\right]^{1/2}$$

$$\leq \frac{\sigma}{\sqrt{2}}(1.1)\left[\frac{2(0.5)}{\sqrt{2\pi}\,(90)}\,e^{-\frac{1}{2}(150/90)^2}\right]^{1/2} \qquad (8.57)$$

$$\leq 0.026\sigma$$

which is totally negligible.

8.4.2 Interference with Data Demodulation

We now consider the data demodulator. The normalized input to the data demodulator is

$$\left(e_i(t)\right)_{data} = \chi_u(t) + J_o(\Gamma)\cot\beta\left[x_c(t)\sin\theta_{cs}(t) + x_q(t)\cos\theta_{cs}(t)\right]$$

$$+ J_o(\Gamma)\,x_u(t-t_s)\left[x_c(t)\cos\theta_{cs}(t) - x_q(t)\sin\theta_{cs}(t)\right] \qquad (8.58)$$

The output of the data demodulator is

$$\left(e_o(t)\right)_{data} = T + J_o(\Gamma)\cot\beta\int_o^T\left[x_c(t)\sin\theta_{cs}(t) + x_q(t)\cos\theta_{cs}(t)\right]e_{sp}(t)dt$$

$$+ J_o(\Gamma)\int_o^T\left[x_c(t)\cos\theta_{cs}(t) - x_q(t)\sin\theta_{cs}(t)\right]x_u(t-t_s)e_{sp}(t)dt$$

(8.59)

The variances of the two interference components at the output of the demodulator are

$$\sigma_1^2 = J_o^2(\Gamma)\cot^2\beta T^2\sigma^2 \int_{-\infty}^{\infty} \frac{d\omega}{2\pi} \frac{1}{\sqrt{2\pi}\,B_f} e^{-(\omega-\dot{\theta}_{cs})^2/2(2\pi B_f)^2} \frac{\sin^4(\omega T/4)}{(\omega T/4)^2}$$

$$\sigma_1^2 \leq J_o^2(\Gamma)\cot^2\beta T^2\sigma^2\,(0.525) \qquad (8.60)$$

and

$$\sigma_2^2 = J_o^2(\Gamma)T^2\sigma^2 \int_{-\infty}^{\infty} \frac{d\omega}{2\pi} \int_{-\infty}^{\infty} \frac{d\zeta}{2\pi} \Phi_{x_u}(\zeta)\Phi(\omega-\zeta-\dot{\theta}_{cs}) \frac{\sin^4(\omega T/4)}{(\omega T/4)^2} \qquad (8.61)$$

for $t_s > T/2$ so that $x_u(t-t_s)e_{sp}(t)$ is essentially random or

$$\sigma_2^2 = J_o^2(\Gamma)T^2\sigma^2 \int_{-\infty}^{\infty} \frac{d\omega}{2\pi} \Phi(\omega-\dot{\theta}_{cs}) \frac{\sin^2(\omega T/2)}{(\omega T/2)^2} \qquad (8.62)$$

for $t_s \ll T/2$ so that $\chi_u(t-t_s)e_{sp}(t) \approx e_{sp}^2(t)$

While the integrals in the above equations are difficult to evaluate in general, the frequency spreading of the diffuse multipath reduces the variances below the corresponding ones for the case of specular multipath. Since the conditions for achieving the required BEP could be achieved in the worst-case for the specular multipath case, it can be achieved also for the flat fading diffuse multipath case.

8.4.3 Flat-Fading Diffuse Multipath Ranging Sidetones Interference

From Eq. (8.46) it is seen that the flat-fading diffuse multipath ranging sidetones are reduced in amplitude by the factor $J_o(\Gamma)$ and are modulated by the flat-fading relative specular multipath carrier doppler frequency terms

$$a_u(t)\left[\cos\left(\theta_{cs}(t) + \phi_u(t)\right) - \sin\left(\theta_{cs}(t) + \phi_u(t)\right)\tan\beta\chi_u(t-t_s)\right] \qquad (8.63)$$

For $\dot{\theta}_{cs}/2\pi$ greater than one-half the fine range tone filter noise bandwidth, the fading C.W. term will be further attenuated by the filter transfer function. Also, if $\dot{\theta}_{cs}/2\pi$ is sufficiently greater than the data bit rate, the peak of the flat-fading diffuse multipath data spectrum in Eq. (8.63) will not overlap the direct-path fine range tone. If this data peak does overlap the direct-path fine range tone, the fading will help reduce this contribution to the fine range tone loop rms phase error below that for the specular multipath case.

8.5 Non-Coherent Fading Diffuse Multipath Interference

For the case of non-coherent fading diffuse multipath interference, the output of the carrier loop phase detector may be written approximately as

$$\begin{aligned}
\left(e_o(t)\right)_c = \sin\Big\{ & \theta_{ce} + \Delta\sin[\omega_{sc}t + \theta_{sc} + \phi_{sc}] + \beta\chi_u(t) + \rho_1\sin\left(\omega_1 t + \theta_1(t)\right) \\
& + \phi_{AR}(t)\cos\left((\omega_1-\omega_2)t + \theta_1(t) - \theta_2(t)\right)\Big\} + M_1 M_{AR}\sum_{n=-N}^{+N} J_n^2(\delta)\Big\{ a_{no}(t)\sin\Big\{\theta_{ce} \\
& + \theta_{cs}(t) + \phi_{no}(t) + \beta\chi_u(t-t_s) + n\left(\theta_{sce} + \theta_{scs}(t)\right)\Big\} + \frac{\rho_1}{2} a_{n1}^{+}(t)\sin\Big\{\theta_{ce} + \theta_{cs}(t) \\
& + \phi_{n1}^{+}(t) + \beta\chi_u(t-t_s) + n\left(\theta_{sce} + \theta_{scs}(t)\right) + \left(\omega_1 t + \theta_1(t) + \theta_{1s}(t)\right)\Big\} \\
& - \frac{\rho_1}{2} a_{n1}^{-}(t)\sin\Big\{\theta_{ce} + \theta_{cs}(t) + \phi_{n1}^{-}(t) + \beta\chi_u(t-t_s) + n\left(\theta_{sce} + \theta_{scs}(t)\right) \\
& - \left(\omega_1 t + \theta_1(t) + \theta_{1s}(t)\right)\Big\} + \frac{1}{2}\phi_{AR}(t-t_s)\, a_{nAR}^{+}(t)\cos\Big\{\theta_{ce} + \theta_{cs}(t) + \theta_{nAR}^{+}(t) \\
& + \beta\chi_u(t-t_s) + n\left(\theta_{sce} + \theta_{scs}(t)\right) + \left((\omega_1-\omega_2)t + \theta_1(t) - \theta_2(t) + \theta_{1s}(t) - \theta_{2s}(t)\right)\Big\} \\
& + \frac{1}{2}\phi_{AR}(t-t_s) a_{nAR}^{-}(t)\cos\Big\{\theta_{ce} + \theta_{cs}(t) + \phi_{nAR}^{-}(t) + \beta\chi_u(t-t_s) + n\left(\theta_{sce} + \theta_{scs}(t)\right) \\
& - \left((\omega_1-\omega_2)t + \theta_1(t) - \theta_2(t) + \theta_{1s}(t) - \theta_{2s}(t)\right)\Big\}\Big\}
\end{aligned}$$

$$+ M_1 M_{AR} \sum_{n=-N}^{+N} J_n(\delta) a_{no}(t) \Big\{ + J_{n+1}(\delta) \sin\Big\{ \theta_{ce} + \theta_{cs}(t) + \phi_{no}(t) + \beta \chi_u(t-t_s) + n\big(\theta_{sce} + \theta_{scs}(t)\big) - \big(\omega_{sc} t + \theta_{sc}(t) + \theta_{scs}(t)\big) \Big\} + J_{n-1}(\delta) \sin\Big\{ \theta_{ce} + \theta_{cs}(t) + \phi_{no}(t) + \beta \chi_u(t-t_s) + n\big(\theta_{sce} + \theta_{scs}(t)\big) + \big(\omega_{sc} t + \theta_{sc}(t) + \theta_{scs}(t)\big) \Big\} \Big\} \tag{8.64}$$

where only the non-coherent fading diffuse multipath interference terms of significance are listed.

8.5.1 Compound PLL Tracking

The carrier and subcarrier loop phase errors are assumed small so that the loops may be treated as independent linear systems. Considering the carrier loop first, the terms of importance at the output of the carrier loop phase detector may be written in normalized form approximately as

$$\theta_{ce} + \sum_{n=-N}^{+N} J_n^2(\delta) \Big\{ a_{no}(t) \sin\Big\{ \theta_{cs}(t) + \phi_{no}(t) + a_{no}(t) \tan\beta \chi_u(t-t_s) \cos\Big\{ \theta_{cs}(t) + \phi_{no}(t) \Big\} \Big\} \Big\} \tag{8.65}$$

The rms carrier loop phase error is approximately

$$\sqrt{\theta_{ce}^2} = \Big\{ \sum_{n=-N}^{+N} J_n^4(\delta) \Big\}^{1/2} \Big\{ 2B_c \Phi_c(o) \Big\}^{1/2} \tag{8.66}$$

where $\Phi_c(o)$ is the value of the power density spectrum of

$$\Big\{ a_{no}(t) \sin\Big\{ \theta_{cs}(t) + \phi_{no}(t) \Big\} + a_{no}(t) \tan\beta \chi_u(t-t_s) \cos\Big\{ \theta_{cs}(t) + \phi_{no}(t) \Big\} \Big\}$$

at $\omega = 0$. This implies that the fading statistics are independent of n.

From Eqs. (8.47) and (8.49), $\Phi_c(o)$ is

$$\Phi_c(o) = \Phi(\dot{\theta}_{cs}) + \tan^2\beta \int_{-\infty}^{\infty} \frac{d\zeta}{2\pi} \Phi_{x_u}(\zeta)\, \Phi(\zeta - \dot{\theta}_{cs}) \tag{8.67}$$

where $\Phi(\dot{\theta}_{cs})$ is given by

$$\Phi(\dot{\theta}_{cs}) = \frac{\sigma^2}{\sqrt{2\pi}\, B_f}\, e^{-\ddot{\theta}_{cs}^2/2(2\pi B_f)^2} \tag{8.68}$$

and the integral is

$$I = \sigma^2 T \int_{-\infty}^{\infty} \frac{d\zeta}{2\pi} \frac{\sin^4(\zeta T/4)}{(\zeta T/4)^2} \frac{1}{\sqrt{2\pi}\, B_f}\, e^{-(\zeta - \dot{\theta}_{cs})^2/2(2\pi B_f)^2} \tag{8.69}$$

which has an upper bound of $(0.525T)\sigma^2$. This upper bound is approached when $\dot{\theta}_{cs}$ is at the peak of the $\Phi_{x_u}(\zeta)$ curve and B_f is much narrower than the width of the peak. In this case $\Phi(\dot{\theta}_{cs})$ would be negligibly small.

On the other hand, with $\dot{\theta}_{cs}/2\pi$ = 150 Hz and B_f = 90 Hz, $\Phi(\dot{\theta}_{cs})$ would be approximately equal to $1.1 \times 10^{-3}\sigma^2$. This is to be compa to $(0.525T)\sigma^2$ for $T = 2.5 \times 10^{-3}$ sec, or $1.31 \times 10^{-3}\sigma^2$. For $T = 10^{-2}$ sec, $(0.525T)\sigma^2$ is $5.25 \times 10^{-3}\sigma^2$. With $2B_c$ = 18 Hz, the upper bound on $\sqrt{\overline{\theta_{ce}^2}}$, is, with $\tan\beta = 1.56$,

$$\left(\sqrt{\overline{\theta_{ce}^2}}\right)_{max} = \left\{\sum_{n=-N}^{+N} J_n^4(5.52)\right\}^{1/2} \left\{(18)(5.25 \times 10^{-3} + 2.68 \times 10^{-3})\right\}^{1/2} \sigma$$

$$\cong 0.378\sigma \left\{\sum_{n=-N}^{+N} J_n^4(5.52)\right\}^{1/2} \cong 0.127\sigma \tag{8.70}$$

Since this is an upper bound and is negligibly small, it may be concluded that the effect of the non-coherent fading diffuse multipath on carrier tracking is negligible.

Turning now to subcarrier tracking, the output of the subcarrier loop phase detector is approximately

$$\frac{1}{\sqrt{2}}\delta\theta_{sce} + \frac{1}{\sqrt{2}}\sum_{n=-N}^{+N} a_{no}(t)J_n(\delta)\Big(J_{n+1}(\delta)+J_{n-1}(\delta)\Big)\Big[\sin\Big\{\theta_{cs}(t)+\phi_{no}(t)\Big\}$$

$$+\tan\beta\,\chi_u(t-t_s)\cos\Big\{\theta_{cs}(t)+\phi_{no}(t)\Big\}\Big] \qquad (8.71)$$

so that $\frac{1}{2}\delta\sqrt{\theta^2_{sce}}$ is

$$\frac{1}{2}\delta\sqrt{\theta^2_{sce}} = \frac{1}{2}\left\{\sum_{n=-N}^{+N}\left(\frac{2n}{\delta}J_n^2(\delta)\right)^2\right\}^{1/2}\left\{2B_{sc}\Phi_c(o)\right\}^{1/2} \qquad (8.72)$$

$$\leq \frac{1}{\sqrt{2}}\,\frac{2}{\delta\sqrt{2}}\left\{\sum_{n=1}^{N} n^2J_n^4(5.52)\right\}^{1/2}\left\{5.25\times10^{-3}+2.68\times10^{-3}\right\}^{1/2}\sigma$$

$$\leq 0.0324\sigma(0.880) \cong 0.0286\sigma$$

which is entirely negligible.

In summary, the effects of non-coherent fading diffuse multipath on compound PLL tracking are negligible if the relative specular multipath carrier doppler exceeds 150 Hz and the fading bandwidth exceeds 90 Hz.

8.5.2 Data Demodulation

The normalized input to the data demodulator is approximately

$$\Big(e_1(t)\Big)_{data} = \chi_u(t) + \sum_{n=-N}^{+N} J_n^2(\delta)\cot\beta\; a_{no}(t)\Big[\sin\Big\{\theta_{cs}(t)+\phi_{no}(t)\Big\}$$

$$+\tan\beta\,\chi_u(t-t_s)\cos\Big\{\theta_{cs}(t)+\phi_{no}(t)\Big\}\Big] \qquad (8.73)$$

The variances of the interference at the output of the data demodulator are

$$\sigma_1^2 = \left\{\sum_{n=-N}^{+N} J_n^4(\delta)\right\}\cot^2\beta\,T^2\sigma^2\int_{-\infty}^{\infty}\frac{d\omega}{2\pi}\frac{1}{\sqrt{2\pi}B_f}\,e^{-(\omega-\dot{\theta}_{cs})^2/2(2\pi B_f)^2}\,\frac{\sin^4(\omega T/4)}{(\omega T/4)^2}$$

$$\leq \left\{\sum_{n=-N}^{+N} J_n^4(\delta)\right\}\cot^2\beta\,T^2\sigma^2(0.525) \qquad (8.74)$$

and

$$\sigma_2^2 = \left\{ \sum_{n=-N}^{+N} J_n^4(\delta) \right\} T^2 \sigma^2 \int_{-\infty}^{\infty} \frac{d\omega}{2\pi} \int_{-\infty}^{\infty} \frac{d\zeta}{2\pi} \Phi_{x_u}(\omega - \zeta - \dot{\theta}_{cs}) \frac{\sin^4(\omega T/4)}{(\omega T/4)^2} \tag{8.75}$$

for $t_s > T/2$ so that $x_u(t-t_s)e_{sp}(t)$ is essentially random

or

$$\sigma_2^2 = \left\{ \sum_{n=-N}^{+N} J_n^4(\delta) \right\} T^2 \sigma^2 \int_{-\infty}^{\infty} \frac{d\omega}{2\pi} \Phi(\omega - \dot{\theta}_{cs}) \frac{\sin^2(\omega T/2)}{(\omega T/2)^2} \tag{8.76}$$

for $t_s \ll T/2$ so that $x_u(t-t_s)e_{sp}(t) \approx e_{sp}^2(t)$

where

$$\Phi(\omega) = \frac{1}{\sqrt{2\pi}\, B_f} e^{-\omega^2/2(2\pi B_f)^2}$$

For proper data demodulation σ_1^2 must be much less than $T^2/31.7$

or $$\left\{ \sum_{n=-N}^{+N} J_n^4(5.52) \right\} \cot^2\beta\, \sigma^2(0.525) \ll \frac{1}{31.7} \tag{8.77}$$

with $\beta = 1$ rad and $\left\{ \sum_{n=-N}^{N} J_n^4(5.52) \right\} = 0.113$, this reduces to $\sigma^2 \ll 1.3$. This condition should pertain almost all of the time.

If $\dot{\theta}_{cs}/2\pi$ is greater than the data bit rate, the condition $\sigma_2^2 \ll T^2/31.7$ reduces in the worst case to

$$\left\{ \sum_{n=-N}^{+N} J_n^4(5.52) \right\} \sigma^2 \frac{1}{(3\pi/2)^2} \ll \frac{1}{31.7} \tag{8.78}$$

or

$$\sigma^2 \ll 6.2$$

This condition is readily satisfied.

If the bit rate is 400 Hz, and $\dot{\theta}_{cs}/2\pi$ is much smaller than this, the worst-case condition on $\sigma_2^2 \ll T^2/31.7$, reduces to

$$\left\{ \sum_{n=-N}^{+N} J_n^4(\delta) \right\} \sigma^2 \ll \frac{1}{31.7} \tag{8.79}$$

or

$$\sigma^2 \ll 0.28$$

This condition may not be satisfied very easily. However, the likelihood that this worst-case condition will be encountered is very remote.

8.5.3 Non-Coherent Fading Diffuse Multipath Ranging Sidetones Interference

The non-coherent fading diffuse multipath ranging sidetones are, from Eq. (9.64), approximately given by

$$\begin{aligned} e_R(t) = M_1 M_{AR} \sum_{n=-N}^{+N} J_n^2(\delta) \Bigg\{ & \frac{\rho_1}{2} a_{n1}^{+}(t) \sin\Big\{\theta_{cs}(t) + \phi_{n1}^{+}(t) + \beta\chi_u(t-t_s) \\ & + \Big(\omega_1 t + \theta_1(t) + \theta_{1s}(t)\Big)\Big\} - \frac{\rho_1}{2} a_{n1}^{-}(t) \sin\Big\{\theta_{cs}(t) + \phi_{n1}^{-}(t) + \beta\chi_u(t-t_s) \\ & - \Big(\omega_1 t + \theta_1(t) + \theta_{1s}(t)\Big)\Big\} + \frac{1}{2} \phi_{AR}(t-t_s) a_{nAR}^{+}(t) \cos\Big\{\theta_{cs}(t) + \phi_{nAR}^{+}(t) \\ & + \beta\chi_u(t-t_s) + \Big((\omega_1-\omega_2)t + \theta_1(t) - \theta_2(t) + \theta_{1s}(t) - \theta_{2s}(t)\Big)\Big\} \\ & + \frac{1}{2} \phi_{AR}(t-t_s)\, a_{nAR}^{-}(t) \cos\Big\{\theta_{cs}(t) + \phi_{nAR}^{-}(t) + \beta\chi_u(t-t_s) - \Big((\omega_1-\omega_2)t + \theta_1(t) \\ & - \theta_2(t) + \theta_{1s}(t) - \theta_{2s}(t)\Big)\Big\} \Bigg\} \end{aligned} \tag{8.80}$$

The autocorrelation function of $e_R(t)$ is approximately

$$\overline{e_R(t)e_R(t+\tau)} = M_1^2 M_{AR}^2 \sum_{n=-N}^{+N} J_n^4(\delta)\left\{\left(\frac{\rho_1}{4}\right)^2\left[\psi(\tau)\left(1+\tan^2\beta\,\psi_{x_u}(\tau)\right)\cos[(\omega_1+\dot{\theta}_1+\dot{\theta}_{cs})\tau]\right.\right.$$
$$+\psi(\tau)\left(1+\tan^2\beta\,\psi_{x_u}(\tau)\right)\cos[(\omega_1+\dot{\theta}_1-\dot{\theta}_{cs})\tau]\Big]$$
$$+\frac{1}{4}\psi_{AR}(\tau)\Big[\psi(\tau)\left(1+\tan^2\beta\,\psi_{x_u}(\tau)\right)\cos[(\omega_1+\dot{\theta}_1+\dot{\theta}_{cs})\tau]$$
$$\left.\left.+\psi(\tau)\left(1+\tan^2\beta\,\psi_{x_u}(\tau)\right)\cos[(\omega_1+\dot{\theta}_1-\dot{\theta}_{cs})\tau]\Big]\right\} \qquad (8.81)$$

The various ranging sidetones add incoherently as indicated. The relative multipath carrier doppler frequency, $\dot{\theta}_{cs}$, and the diffuse multipath fading help spread the multipath interference components over a much wider bandwidth than the corresponding direct-path components, and this, plus the incoherence of the multipath fading, reduces the effects of the non-coherent fading diffuse multipath on ranging.

8.6 Downlink Multipath Models

The downlink multipath models are essentially identical to those for the uplink, except that the downlink signal of Eq. (7.1) is used in place of the uplink signal of Eq. (8.1). Also, with the downlink telemetry data, $x_d(t)$, having a bit rate of 1000 BPS, the effects of downlink multipath data components on compound PLL tracking and ranging are even more negligible than for the uplink.

The problem of other-User multipath interference is also present on the downlink. However, if the other-User signal power is not much larger than the desired-User signal power, the other-User multipath interference should be negligible. This is a consequence of the following factors: 1) the wideband FM SSMA interference suppression mechanism,

2) the generally weaker received signal power of the earth-reflected multipath interference, and 3) the frequency spreading of the diffuse multipath interference. In addition, the changing doppler conditions between the desired-User and the other-User received signals mean that the duration of a given other-User interference mechanism will be relatively short compared to the duration of the interference from the desired-User's own multipath.

Appendix A

COMPOUND PLL ANALYSIS

The wideband FM receiver employs a compound PLL which simultaneously tracks the subcarrier and the carrier, and regenerates the wideband FM signal as a coherent reference. This permits the coherent demodulation of the low deviation PM data and range tones. For the case of small carrier and subcarrier tracking phase errors, the carrier and subcarrier loops are approximately both linear and independent. Consequently, linear PLL analysis may be applied to the loops. In particular, the loops may be optimized independently in the presence of Gaussian white noise and changing doppler. This analysis is developed below.

The received wideband FM signal on the uplink may be written as

$$e_r(t) = \sqrt{2S_u}\ \sin\left\{\omega_c t + \theta_c(t) + \delta \sin\left[\omega_s t + \theta_s(t) + \phi_m(t)\right]\right\} \qquad (A.1)$$

where

S_u is the uplink received power.

ω_c is the uplink carrier frequency.

$\theta_c(t)$ is the carrier phase which contains the doppler and doppler dynamics.

δ is the modulation index of the wideband FM subcarrier, and is equal to 5.52.

ω_s is the uplink subcarrier frequency.

$\theta_s(t)$ is the subcarrier phase which contains the doppler and doppler dynamics.

$\phi_m(t)$ is the low deviation PM modulation consisting of split-phase command data and ranging sidetones.

In the track mode the received wideband FM signal is effectively multiplied by a reference signal given by

$$e_{ref}(t) = \sqrt{2}\ \cos\left\{\omega_c t + \hat{\theta}_c(t) + \delta \sin[\omega_s t + \hat{\theta}_s(t)]\right\} \tag{A.2}$$

where $\hat{\theta}_c(t)$ and $\hat{\theta}_s(t)$ are estimates of the phases $\theta_c(t)$ and $\theta_s(t)$, respectively.

The output of the multiplier (carrier loop phase detector) is

$$s_o(t) = \sqrt{S_u}\ \sin\left\{\theta_c(t) - \hat{\theta}_c(t) + \delta\sin[\omega_s t + \theta_s(t)] - \delta\sin[\omega_s t + \hat{\theta}_s(t)] + \phi_m(t)\right\} \tag{A.3}$$

If Gaussian white noise of single-sided power density N_u is also present at the input to the receiver, the noise at the output of the multiplier will also be Gaussian and white with a single-sided power density N_u. Writing the noise at the output of the multiplier as $n_c(t)$, the total output of the multiplier, appropriately normalized as is the custom in developing phase models of PLL's, may be written as

$$e_o(t) \cong \sin\left\{\theta_c(t) - \hat{\theta}_c(t) + \delta\sin[\omega_s t + \theta_s(t)] - \delta\sin[\omega_s t + \hat{\theta}_s(t)]\right\} + \overline{\cos\left\{\theta_c(t) - \hat{\theta}_c(t) + \delta\sin[\omega_s t + \theta_s(t)] - \delta\sin[\omega_s t + \hat{\theta}_s(t)]\right\}}\ \frac{\sin\phi_m(t)}{M} + \frac{n_c(t)}{\sqrt{S_u}\,M} \tag{A.4}$$

where M is the modulation suppression factor given by

$$M = \overline{\cos\phi_m(t)} \tag{A.5}$$

4

If the phase errors $\theta_{ce} = \theta_c - \hat{\theta}_c$ and $\theta_{se} = \theta_s - \hat{\theta}_s$ are small, the approximation

$$\sin\left\{\theta_{ce} + \delta\sin[\omega_s t + \hat{\theta}_s + \theta_{se}] - \delta\sin[\omega_s t + \hat{\theta}_s]\right\}$$

$$\approx \theta_{ce} + \delta\sin[\omega_s t + \hat{\theta}_s + \theta_{se}] - \delta\sin[\omega_s t + \hat{\theta}_s] \qquad \text{(A. 6)}$$

may be made. This approximation <u>linearizes</u> both the carrier and the subcarrier loop and makes them <u>independent</u> to a first approximation. There is a small high order coupling between the loops as may be seen by writing

$$\sin\left\{\theta_{ce} + \delta\sin[\omega_s t + \hat{\theta}_s + \theta_{se}] - \delta\sin[\omega_s t + \hat{\theta}_s]\right\}$$

$$= \sin\left\{\theta_{ce} + 2\,\delta\sin(\theta_{se}/2)\cos[\omega_s t + \hat{\theta}_s + \frac{\theta_{se}}{2}]\right\}$$

$$\cong \cos\left\{2\delta\sin(\theta_{se}/2)\cos[\omega_s t + \hat{\theta}_s + \frac{\theta_{se}}{2}]\right\}\sin\theta_{ce}$$

$$+ \cos\theta_{ce}\,\sin\left\{\delta\sin[\omega_s t + \hat{\theta}_s + \theta_{se}] - \delta\sin[\omega_s t + \hat{\theta}_s]\right\}$$

$$= J_o\left(2\,\delta\sin(\theta_{se}/2)\right)\sin\theta_{ce}$$

$$+ \cos\theta_{ce}\,\sin\left\{\delta\sin[\omega_s t + \hat{\theta}_s + \theta_{se}] - \delta\sin[\omega_s t + \hat{\theta}_s]\right\} \qquad \text{(A. 7)}$$

If θ_{ce} is small and if $\delta\theta_{se}$ is small, the above may be approximated by

$$J_o(\delta\theta_{se})\,\theta_{ce} + \cos\theta_{ce}\left\{\delta\sin[\omega_s t + \hat{\theta}_s + \theta_{se}] - \delta\sin[\omega_s t + \hat{\theta}_s]\right\} \qquad \text{(A. 8)}$$

Since

$$J_o(\delta\theta_{se}) \approx 1 - \frac{1}{4}(\delta\theta_{se})^2 + \ldots \quad \text{(A.9)}$$

and

$$\cos\theta_{ce} \approx 1 - \frac{1}{2}\theta_{ce}^2 + \ldots \quad \text{(A.10)}$$

the coupling, for the case of small phase errors, is a second-order fluctuation in the amplitudes of the error signals of the carrier and subcarrier loops. In the analysis which follows, this coupling is neglected.

The carrier loop may therefore be modeled as shown in Fig. A.1.

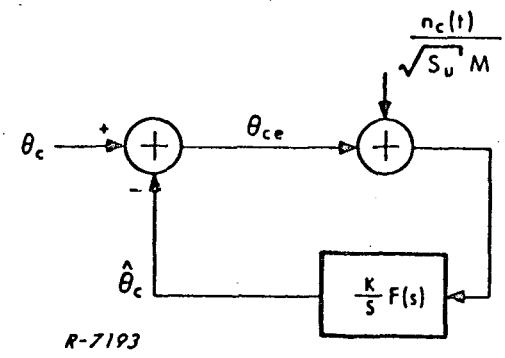

Fig. A.1 Linearized Model of Carrier PLL

The loop is designed to be a high-gain second-order loop. The error θ_{ce} consists of a dynamic tracking error and a noise error. For the case where the carrier doppler is changing at a constant rate given by $\ddot{\theta}_c$, the dynamic tracking error, θ_{cet}, is given by

$$\theta_{cet} = \ddot{\theta}_c/\omega_{nc}^2 \quad \text{(A.11)}$$

where ω_{nc} is the loop natural frequency (rad/sec). The loop natural frequency is related to the loop noise bandwidth, B_c, as

$$B_c = \frac{\omega_{nc}}{2}\left(\zeta_c + \frac{1}{4\zeta_c}\right) = k_c\omega_{nc} \quad \text{(A.12)}$$

where ζ_c is the damping factor.

The noise error variance is given by

$$\overline{\theta^2_{cen}} = \frac{B_c N_u}{S_u M^2} = \frac{B_c}{\rho} \tag{A.13}$$

Defining a "peak" phase error, $\left(\theta_{ce}\right)_p$, by

$$\left(\theta_{ce}\right)_p = |\theta_{cet}| + \sigma_c\left(\overline{\theta^2_{cen}}\right)^{1/2} \tag{A.14}$$

the noise bandwidth, B_c, is chosen so that at threshold $\rho = S_u M^2/N_u$ is minimized for a given worst case doppler rate, $\ddot{\theta}_c$, and Gaussian noise error peak factor σ_c. Threshold is defined by $\left(\theta_{ce}\right)_p = \theta_{cm}$, where θ_{cm} is a maximum tolerable "peak" phase error. For the compound PLL, this maximum tolerable "peak" phase error may be set at 30°, since the linearization approximation begins to break down for phase errors in excess of about 30°. The Gaussian noise error peak factor may be taken to be 3. The damping factor ζ_c is chosen to be $1/\sqrt{2}$.

From Eqs. (A.11), (A.12), (A.13), and (A.14), ρ is related to B_c and the other variables as

$$\rho = \left(\frac{\sigma_c}{\theta_{cm}/}\right)^2 \frac{B_c^5}{\left(B_c^2 - k_c^2 \frac{\ddot{\theta}_c}{\theta_{cm}}\right)^2} \tag{A.15}$$

The minimum value of ρ at threshold corresponds to a loop noise bandwidth given by

$$\left(B_c\right)_{optimum} = \sqrt{5k_c^2(\ddot{\theta}_c/\theta_{cm})} \tag{A.16}$$

The threshold value of ρ is then

$$(\rho)_{\text{threshold}} = \left(\frac{5}{4}\right)^2 \left(\sigma_c/\theta_{cm}\right)^2 \left(B_c\right)_{\text{optimum}} \tag{A.17}$$

The doppler rate θ_c is equal to $\omega_c(R/c)$, where R is the range between the spacecraft and the TDRS, and c is the velocity of light.

Turning now to the subcarrier loop, the error signal of Eq. (A.6) is effectively multiplied by the subcarrier loop VCO signal

$$\left(e_s(t)\right)_{\text{vco}} = \sqrt{2}\ \cos[\omega_s t + \hat{\theta}_s] \tag{A.18}$$

The output of this multiplier is

$$\frac{1}{\sqrt{2}}\ \sin\theta_{se} \approx \frac{\delta}{\sqrt{2}}\ \theta_{se} \tag{A.19}$$

plus Gaussian noise of single-sided power density $N_u/S_u M^2$. The equivalent phase model of the loop may be drawn as shown in Fig. A.2.

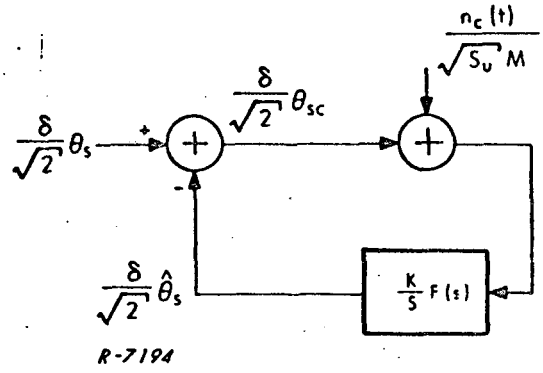

Fig. A.2 Linearized Model of Subcarrier PLL

The "effective phase error" is taken as $\frac{\delta}{\sqrt{2}}\,\theta_{se}$ because for a constant or slowly varying subcarrier loop phase error, θ_{se}, the subcarrier difference in Eq. (A.6)

$$\delta \sin[\omega_s t + \hat{\theta}_s + \theta_{se}] - \delta \sin[\omega_s t + \hat{\theta}_s] \cong \delta\theta_{se} \cos[\omega_{st} + \hat{\theta}_s + \frac{\theta_{se}}{2}] \tag{A.20}$$

has an rms value of $\frac{\delta\theta_{se}}{\sqrt{2}}$. Letting $\alpha_{se} = \frac{\delta\theta_{se}}{\sqrt{2}}$, a "peak" error, $(\alpha_{se})_p$, may be defined in a manner analogous to Eq. (A.14). That is

$$(\alpha_{se})_p = |\alpha_{set}| + \sigma_s \left(\overline{\alpha_{sen}^2}\right)^{1/2} \tag{A.21}$$

Here $\overline{\alpha_{sen}^2}$ is

$$\overline{\alpha_{sen}^2} = \frac{B_s N_u}{S_u M^2} = \frac{B_s}{\rho} \tag{A.22}$$

where B_s is the subcarrier loop noise bandwidth. The dynamic tracking error α_{set} is

$$\alpha_{set} = \ddot{\alpha}_s / \omega_{ns}^2 = \frac{\delta}{\sqrt{2}} \frac{\omega_s}{\omega_{ns}^2} \frac{\ddot{R}}{c} \tag{A.23}$$

where the loop natural frequency, ω_{ns}, is related to the loop noise bandwidth, B_s, by

$$B_s = \frac{\omega_{ns}}{2} \left(\zeta_s + \frac{1}{4\zeta_s}\right) = k_s \omega_{ns} \tag{A.24}$$

The damping factor ζ_s is chosen to be $1/\sqrt{2}$ as in the carrier loop.

Defining threshold by $\left(\alpha_{se}\right)_p = \alpha_{sm}$, where α_{sm} is a maximum tolerable "peak" error, the subcarrier loop may be optimized by selecting the loop noise bandwidth B_s so as to minimize the value of ρ at this threshold. The results are

$$\left(B_s\right)_{optimum} = \sqrt{5k_{s,\alpha_{sm}}^{2}\dot{\alpha}_s} \tag{A.25}$$

and

$$(\rho)_{threshold} = \left(\frac{5}{4}\right)^2\left(\sigma_s/\alpha_{sm}\right)^2\left(B_s\right)_{optimum} \tag{A.26}$$

If $\alpha_{sm} = \theta_{cm}$, $k_s = k_c$, and $\sigma_s = \sigma_c$, the ratio of the noise bandwidths of the subcarrier and carrier loops is

$$\frac{\left(B_s\right)_{opt.}}{\left(B_c\right)_{opt.}} = \sqrt{\frac{\ddot{\alpha}_s}{\ddot{\theta}_c}} = \sqrt{\frac{\delta}{\sqrt{2}}\frac{f_s}{f_c}} \tag{A.27}$$

For $\delta = 5.52$, $f_s = 107.2$ kHz, and $f_c \cong 149$ MHz, this ratio is approximately 0.053. This is also equal to the ratio of the threshold values of ρ. Consequently, the carrier loop clearly imposes the more stringent requirement on received signal power. This means that for a value of ρ at or above carrier loop threshold, the subcarrier loop will be well above threshold. The "peak" error, $\left(\alpha_{se}\right)_p$, at carrier loop threshold is

$$\left(\alpha_{se}\right)_p = \frac{1}{5}\alpha_{sm} + \frac{4}{5}\alpha_{sm}\sqrt{\frac{\delta}{\sqrt{2}}\frac{f_s}{f_c}} = 0.242\alpha_{sm} \tag{A.28}$$

Numerical Example

The highest doppler rate occurs for a low orbit spacecraft passing directly under the TDRS. The carrier doppler rate on the uplink in this case is approximately 30 rad/sec^2. The TDRS must radiate sufficient power to permit spacecraft with this worst-case doppler dynamics to operate above threshold in the presence of the worst-case noise power density. Consequently, this value of $\ddot{\theta}_c$ helps determine the required uplink TDRS transmitter power.

For $\ddot{\theta}_c = 30$ rad/sec^2, and with $\zeta_c = \zeta_s = 1/\sqrt{2}$, $\sigma_c = \sigma_s = 3$, and $\theta_{cm} = \alpha_{sm} = 30°$, the values of $\left(B_c\right)_{opt.}$, $(\rho)_{th}$, and $\left(B_s\right)_{opt}$ are given in Table A.1.

Table A.1

Compound PLL Parameters

$\ddot{\theta}_c$ (rad/sec^2)	30
$\left(B_c\right)_{opt.}$ (Hz)	9.0
$(\rho)_{th}$ (Hz)	462
$\left(B_s\right)_{opt.}$ (Hz)	0.48

Page intentionally left blank

Appendix B

CW INTERFERENCE WITH PLL TRACKING

In this appendix the effects of small CW interference on PLL tracking are considered. The PLL is considered to be linear, and the phase error caused by the CW interference is assumed small.

The input to the loop may be written as

$$e_{in}(t) = \sqrt{2S_o}\,\sin[\omega_o t + \theta_o(t)] + \sqrt{2S_i}\,\sin[\omega_i t + \theta_i(t)] \qquad (B.1)$$

where S_o is the signal power, S_i is the interference power, $\theta_o(t)$ is the phase to be tracked by the PLL, ω_i is the frequency of the interference, and $\theta_i(t)$ represents possible doppler dynamics on the interference.

The VCO signal which multiplies $e_{in}(t)$ may be written as

$$e_{VCO}(t) = \sqrt{2}\,\cos\,[\omega_o t + \hat{\theta}_o(t)] \qquad (B.2)$$

where $\hat{\theta}_o(t)$ is the estimate of $\theta_o(t)$.

The output of the multiplier is therefore

$$e_o(t) = \sin[\theta_o(t) - \hat{\theta}_o(t)] + \sqrt{\frac{S_i}{S_o}}\,\sin[(\omega_i - \omega_o)t + \theta_i(t) - \hat{\theta}_o(t)] \qquad (B.3)$$

The linearized loop phase model is shown in Fig. B.1.

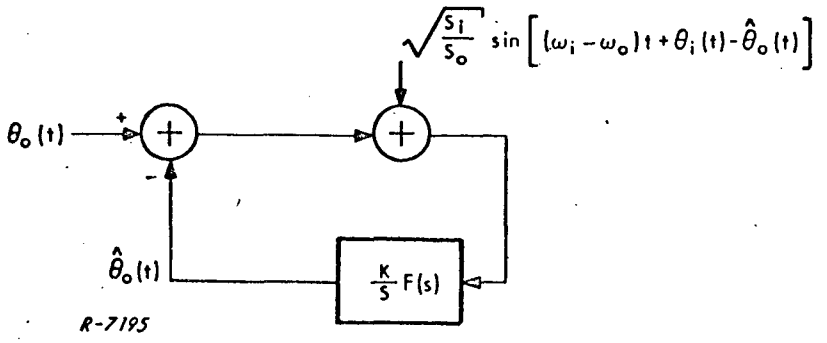

Fig. B.1 Linearized Phase Model of PLL

With the frequency $\Delta\omega_i = (\omega_i - \omega_o) + \dot{\theta}_i(t) - \dot{\theta}_o(t)$ lying well within the loop noise bandwidth, the maximum phase error arising from the presence of the interference is simply equal to $\sqrt{S_i/S_o}$. If this is small (i.e., on the order of 30° or less) the loop linearization approximation is reasonable, and the rms phase error contributed by the interference may be approximated by $\left(\frac{1}{2}S_i/S_o\right)^{1/2}$ when the interference lies within the loop noise bandwidth.

For $\Delta\omega_i$ lying outside the loop noise bandwidth, and for low doppler dynamics, the rms phase error of $\left(\frac{1}{2}S_i/S_o\right)^{1/2}$ is simply reduced by the amplitude of the loop transfer function at the frequency $\Delta\omega_i$.

Appendix C

DATA DEMODULATION

TDRS system specifications call for a BEP (bit error probability) of 10^{-6} for the uplink command data and the downlink telemetry. The uplink bit rate may be either 100 BPS or 400 BPS, whereas the downlink bit rate is 1000 BPS. The data demodulator is a coherent integrate and dump detector as shown in Fig. C.1.

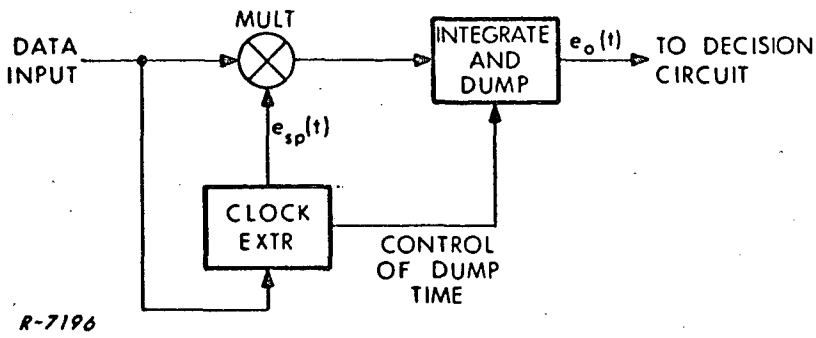

Fig. C.1 Data Demodulator

For the required BEP, the clock may be assumed to be extracted with negligible phase jitter. For a data demodulator input consisting of split-phase data $x_{sp}(t)$, and white gaussian noise, $n_w(t)$, the output, $e_o(t)$, is

$$e_o(t) = \int x_{sp}(t)\, e_{sp}(t)\, dt + \int n_w(t)\, e_{sp}(t)\, dt \qquad (C.1)$$

The first integral is simply equal to bT, where b is either +1 or -1 depending on whether the data bit was a binary 1 or 0, and T is

the bit period. The second integral is a gaussian random variable of mean zero whose variance is given by the statistical average

$$\int dt_1 \int dt_2 \, \overline{n_w(t_1)\, n_w(t_2)}\, e_{sp}(t_1)\, e_{sp}(t_2) \tag{C.2}$$

The average over the noise is equal to

$$\overline{n_w(t_1)\, n_w(t_2)} = \left(\frac{\Phi}{2}\right) \delta(t_1 - t_2) \tag{C.3}$$

where $(\Phi/2)$ is the double-sided noise power density, and $\delta(t_1 - t_2)$ is the Dirac-delta function. The variance is readily seen to be equal to

$$\sigma^2 = \left(\frac{\Phi}{2}\right) T \tag{C.4}$$

The probability of error, or BEP, is

$$P_e = \frac{1}{2}\left[1 - \operatorname{erf}\left(\sqrt{\frac{\mu^2}{2\sigma^2}}\right)\right] \tag{C.5}$$

where $\mu = T$. The ratio $\mu^2/2\sigma^2 = T/\Phi$ is recognized as the energy per bit divided by the single-sided noise power density. The required BEP is realized for values of T/Φ greater than abuut 12 dB (15.85).

For the case where the noise (or interference) is gaussian but non-white, the average over the noise is

$$\overline{n_c(t_1)\, n_c(t_2)} = \int_{-\infty}^{\infty} \frac{d\omega}{2\pi}\, \Phi_n(\omega)\, e^{j\omega(t_1 - t_2)} \tag{C.6}$$

where $\Phi_n(\omega)$ is the power density spectrum of the colored noise.

Introducing this into Eq. (C.2), the variance is seen to be equal to

$$\int_{-\infty}^{\infty} \frac{d\omega}{2\pi} \Phi_n(\omega) \left|E_{sp}(\omega)\right|^2 \tag{C.7}$$

where $E_{sp}(\omega)$ is the Fourier transform of $e_{sp}(t)$. $\left|E_{sp}(\omega)\right|^2$ is given by

$$\left|E_{sp}(\omega)\right|^2 = T^2 \frac{\sin^4(\omega T/4)}{(\omega T/4)^2} \tag{C.8}$$

If $\Phi_n(\omega)$ is essentially constant over the bandwidth of $\left|E_{sp}(\omega)\right|^2$, the variance may be approximated by $\overline{\Phi}_n$, the value of $\Phi_n(\omega)$ near the peak of $\left|E_{sp}(\omega)\right|^2$. This is a reasonable approximation for narrowband RFI whose bandwidth is much larger than the bit rate.

On the other extreme, if the interference is a sinusoid of frequency ω_i which is statistically independent of the data clock (i.e., its phase is random with respect to the phase of the data clock), the variance is

$$S_i T^2 \frac{\sin^4(\omega_i T/4)}{(\omega_i T/4)^2} \tag{C.9}$$

where S_i is the power in the sinusoid. The maximum value of this variance occurs for $\omega_i T/4 \approx 3\pi/8$ and is approximately $S_i T^2(0.525)$. With many different types of noise and interference present in addition to the white gaussian noise, and with no one noise or interference dominating, the statistics of the random portion of the data demodulator output may still be considered to be zero mean gaussian with a variance equal to the sum of the variances of the individual noise or interference contributions. The total variance must be such that the ratio $\mu^2/2\sigma^2$ is greater than 12 dB if the required BEP is to be realized.

Page intentionally left blank

Appendix D

AN IMPROVED WIDEBAND FM TDRS SYSTEM

One of the biggest advantages of the wideband FM system concept is its extreme flexibility insofar as the improvements in performance that may be attained by making minor modifications in the signal format and receiver design. The system described in this appendix is an outgrowth of the analysis conducted under this contract. By analyzing the system described in Sec. 2 of this report, as was done in Secs. 4, 5, 6, 7 and 8, we were able to see which communications functions (i.e., data, ranging, tracking, multiple access) were most susceptible to noise, CW RFI, narrowband RFI, SSMA interference, and multipath interference. This indicated where improvements could be made in the wideband FM system. In particular, the modified system offers the following improvements:

1. By PN coding the uplink command data bits with a 511 bit PN code, whose bits are split-phase, the 100 BPS data is both spread in frequency and shifted away from the carrier. This results in improved data demodulation in the presence of multipath interference of all classifications as well as CW and narrowband RFI.

2. By making the command bit rate coherent with the 100 Hz range tone, bit synchronization and PN code acquisition may be easily accomplished, as will be described.

3. By reducing the phase deviation of the command data on the uplink carrier from 1 radian to $\pi/4$ radians, the percentage of the total signal power in the carrier and the range tones is essentially doubled, with only a small loss in the percentage power in the data. This helps wideband FM acquisition, and also reduces the probability of loss of lock, as well as aiding in ranging.

4. Since the data sidebands no longer lie near the carrier they cannot be used to aid in acquisition. Consequently the wideband FM modulation index is reduced from 5.52 to 5.32 so that the 3rd and 5th order sidebands have equal power and the 4th order sideband has the maximum available power. The 4th order upper sideband is multiplied by the sum of the 3rd and 5th order upper sidebands in the acquisition aid, and similarly for the corresponding lower order sidebands. This more than makes up for the fact that the data sidebands around these subcarrier sidebands are no longer multiplied together in the acquisition aid system. With the deviation reduced to 5.32 radians the power in the carrier component is still negligibly small, but no longer zero, and the power in the second order sidebands is reduced to negligible proportions. The power in the first order sidebands is now at its maximum value. The power in the 7th and higher order sidebands is now even more negligible than before. Consequently, there are only 5 sidebands having significant power when $\delta = 5.32$ radians. This reduces the percentage of the RF band for which the wideband FM signal is susceptible to various kinds of RFI.

5. By modifying the range tone format so that the AR tones directly phase modulate the carrier, the range tone extraction problem is simplified. The fine and medium fine range tone frequencies are 102.4 kHz and 6.4 kHz as before, but the medium coarse and coarse range tone frequencies are now 800 Hz and 100 Hz. The ratios between these new frequencies is 8 rather than 16 as before. This means that more power may be put in the fine and medium fine range tones, and the power in the AR tones may be reduced. In the User transponder the fine range tone is coherently filtered and turned around. The medium fine range tone is tracked and the tracked tone drives a divide-down chain which generates the 3.2, 1.6, 800 Hz, 400 Hz, 200 Hz and 100 Hz tones. Ambiguity resolution is performed with the uplink 800 and 100 Hz range tones. The ambiguity

resolved tones from the downlink chain and the tracked 6.4 kHz are transmitted on the downlink. This totally eliminates the problem of turned-around noise and RFI associated with the AR sidetone turn-around channel in the previous system. The problem of turned-around noise and RFI in the fine range tone turnaround channel is reduced in the new system by a quasi-coherent narrowband filtering of the fine range tone prior to transmission on the downlink, as will be described. The command data clock is derived from the divider chain, thereby eliminating the need for a bit synchronizer. The downlink telemetry data clock is also generated from the divider chain, and this permits the elimination of the data clock generator in the User and the data bit synchronizer in the ground receiver. In addition, the 6.4 kHz range tone tracker generates the PN code chip rate clock, a subcarrier on which the downlink data is modulated, a signal used in the quasi-coherent narrowband filtering of the fine range tone in the User transponder, and frequencies which may be used in the downlink subcarrier frequency generator. Consequently, this additional User circuitry actually replaces much of the circuitry that would be required in the User transponder described in Sec. 2.

Although the lowest frequency range tone is now 100 Hz rather than 25 Hz, this still provides 3000 kilometers of range ambiguity. This should be more than adequate for the TDRS application.

6. The downlink data is modulated by a 51.2 kHz squarewave prior to modulation on the downlink carrier. This aids in the suppression of multipath interference with data demodulation, and still provides a high degree of immunity against SSMA interference since the data is not spread in frequency very much. It also prevents interference with tracking by the multipath data sideband components and interference with data demodulation by the multipath subcarrier sidebands. With the data modulated by the 51.2 kHz squarewave, two carrier bands separated by 25.6 kHz are used rather than three. Each User will have access to two subcarrier frequencies and either of the two carrier bands, and will select the downlink

channel in accordance with commands from the DAF. A total of 20 subcarrier frequencies ranging from 112.0 kHz to 144.0 kHz and spaced by 1.6 kHz are available (not including the frequency at 128.0 kHz) thereby providing for simultaneous transmission by 40 Users on the downlink.

Uplink Signal Format

The uplink wideband FM signal consists of a carrier PM modulated by the sum of 4 coherent range tones and 100 BPS data, and wideband FM modulated by a sinusoidal subcarrier.

The range tone frequencies are listed in Table D.1.

Table D.1

Range Tone Frequencies

Range Tone		Frequency	Phase Deviation
Fine		102.4 kHz	$\rho_1 = 0.6$ radian
Medium Fine	$\div$ 16	6.4 kHz	$\rho_2 = 0.5$ radian
Medium Coarse	$\div$ 8	800 Hz	$\rho_3 = 0.3$ radian
Coarse	$\div$ 8	100 Hz	$\rho_4 = 0.3$ radian

The data is modulated by a 511 bit PN code whose bits are split-phase. The data clock is the 100 Hz range tone frequency. The PN chip rate is 51.1 kHz. The data phase deviation is $\pi/4$ radians.

The wideband FM subcarrier frequency lies between 107 kHz and 133 kHz, the exact frequency being selected on the basis that a clear channel approximately 16 kHz wide exists at the upper 4th order subcarrier sideband frequency, with relatively clear channels around the upper and lower 3rd and 5th order sidebands and the lower 4th order sideband. The modulation index is chosen to be 5.32 radians. The power in the various sidebands is shown plotted in Fig. D.1 for the case where $\delta = 5.32$ radians. At this value the power in the 3rd and 5th order sidebands are equal, and J_4 is at a maximum,

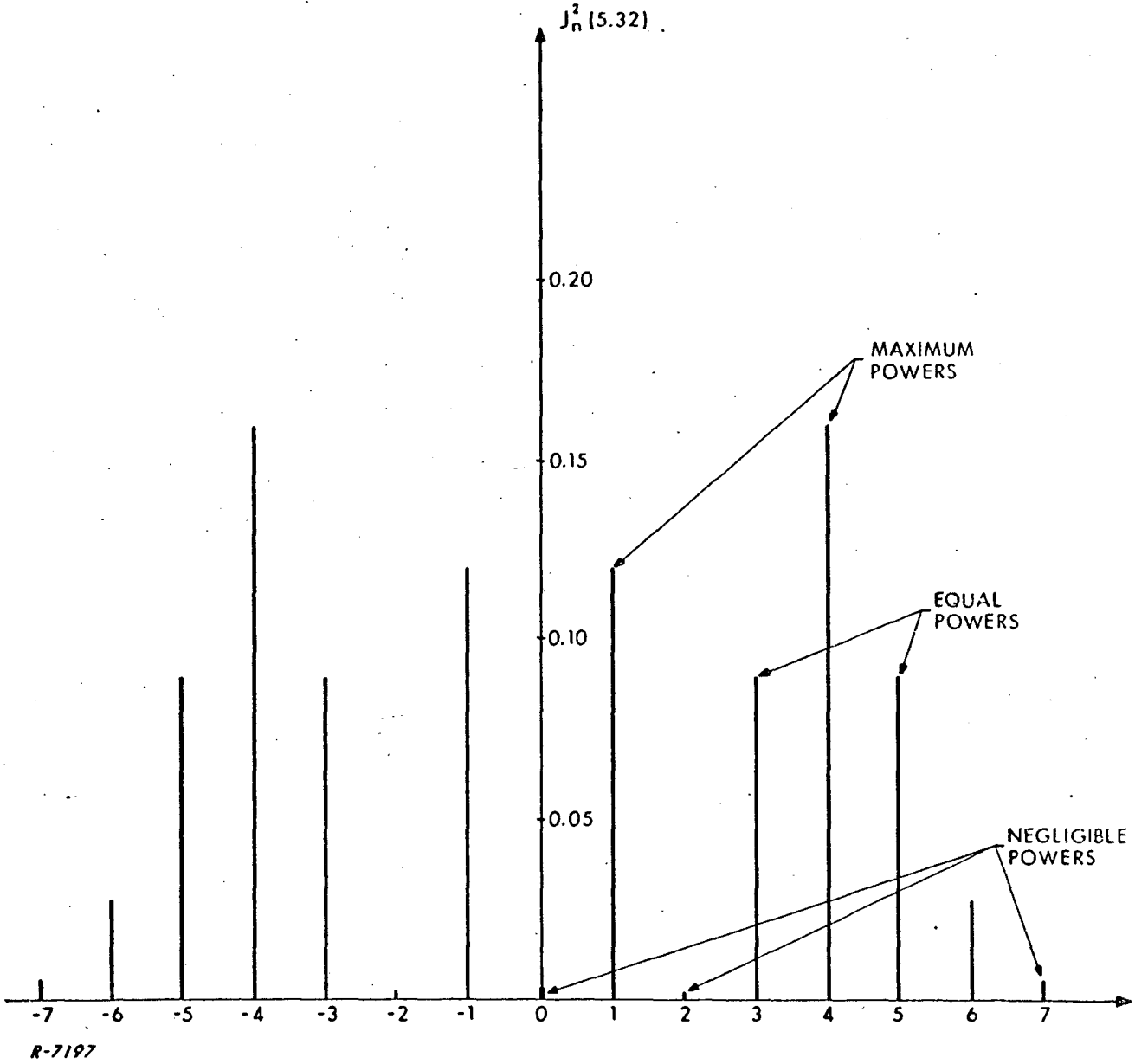

Fig. D.1 Distribution of Signal Powers in the Wideband FM Subcarrier Sidebands

as is $J_1(\delta)$. This may be seen in Fig. D.2. The value of 5.32 is not critical in that a variation of ±0.1 radian around this value would be quite acceptable. This means that no feedback circuit would be required in either the DAF transmitter or the User spacecraft compound PLL receiver to maintain the value of δ precisely at 5.32 radians.

The data and range tones around each subcarrier sideband are shown in Fig. D.3.

The uplink signal may be written as

$$e_u(t) = \sin\left\{\omega_c t + \delta \sin[\omega_{sc} t] + \beta x_d(t)\, x_{PN}(t)\, x_{c\ell}(t) + \sum_{i=1}^{4} \rho_i \sin(\omega_i t)\right\} \quad (D.1)$$

where $\delta = 5.32$ radians, $\beta = \pi/4$ radians, $\rho_1 = 0.6$, $\rho_2 = 0.5$, and $\rho_3 = \rho_4 = 0.3$ radians. Here $x_d(t)$ is the 100 BPS data, $x_{PN}(t)$ is the 511 bit PN code, and $x_{c\ell}(t)$ is the 51.1 kHz PN code clock which has the effect of making the PN code bits split-phase.

The uplink carrier frequency is now 148.9106 MHz = 149 x(1-.0006). The downlink carrier frequency is 23/25 (148.9106) = 136.99775 MHz. This is only 2.24 kHz away from the center of the downlink 136-138 MHz band. This will permit two additional subcarrier frequencies to be used on the downlink as will be explained shortly.

The User Transponder Compound PLL

A modified compound PLL is utilized in the User transponder to acquire and track the wideband FM signal, as indicated in Fig. D.4.

With the 100 BPS data no longer located immediately around the subcarrier sidebands, additional power must be provided for acquisition. This is accomplished in several ways. First, the 3rd order upper sideband is added to the 5th order upper sideband and the sum multiplies the 4th order upper sideband. This yields a higher SNR at the output of the multiplies than was the case when $\delta = 5.52$ and only the 5th order upper

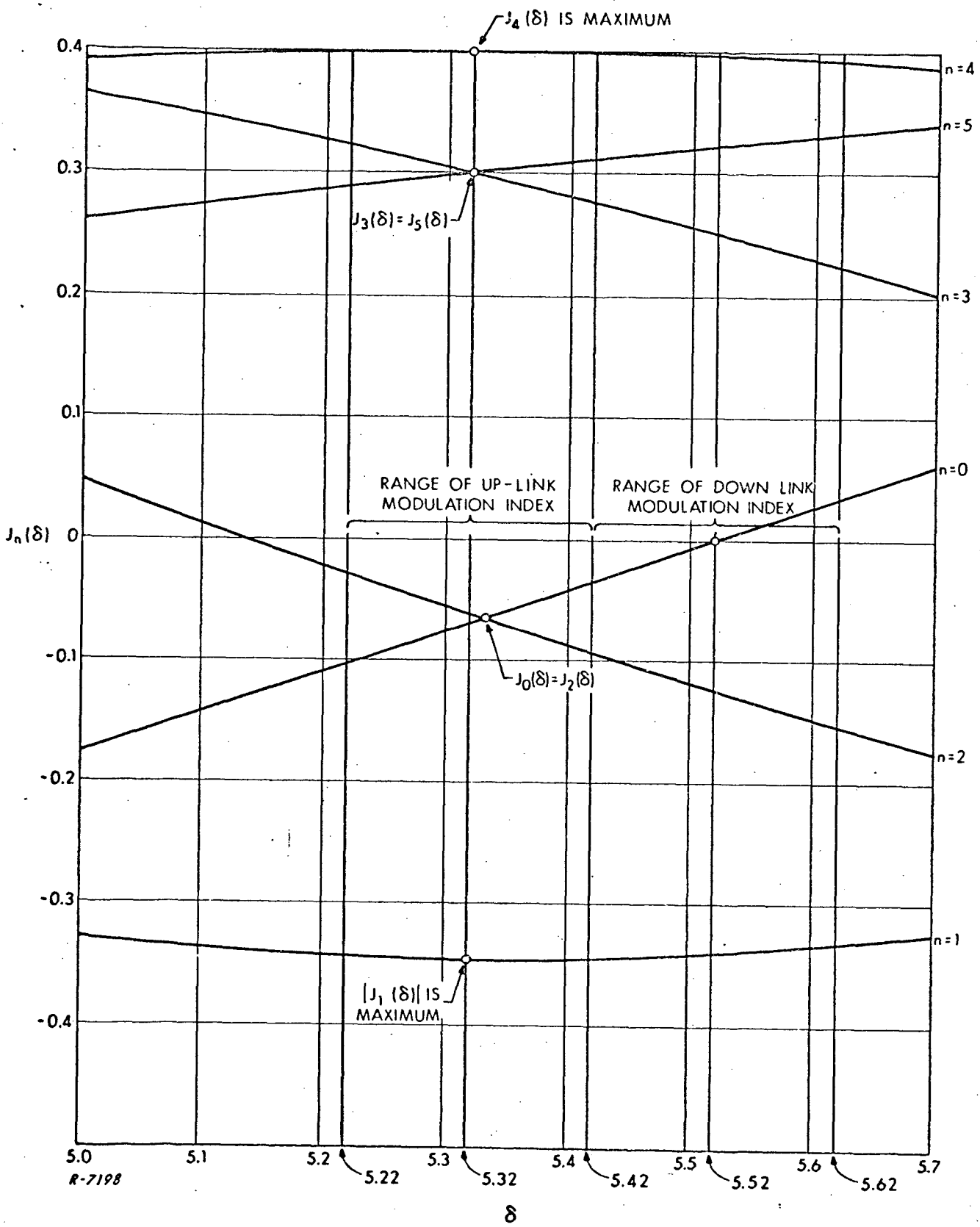

Fig. D.2 Bessel Function vs δ in the Range of Interest

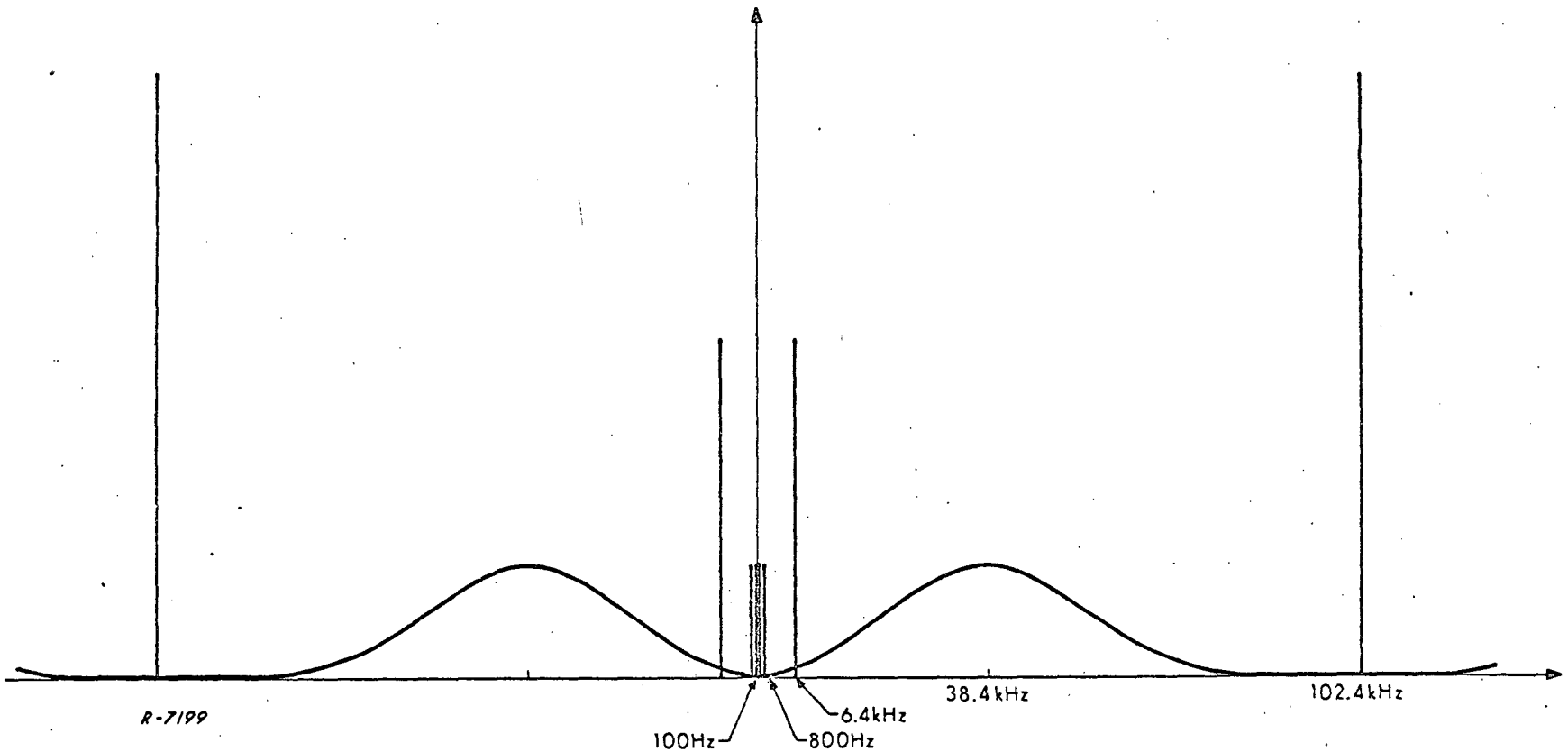

Fig. D.3 Split-Phase PN-Coded 100 BPS Data Plus Range Tones
(not to scale)

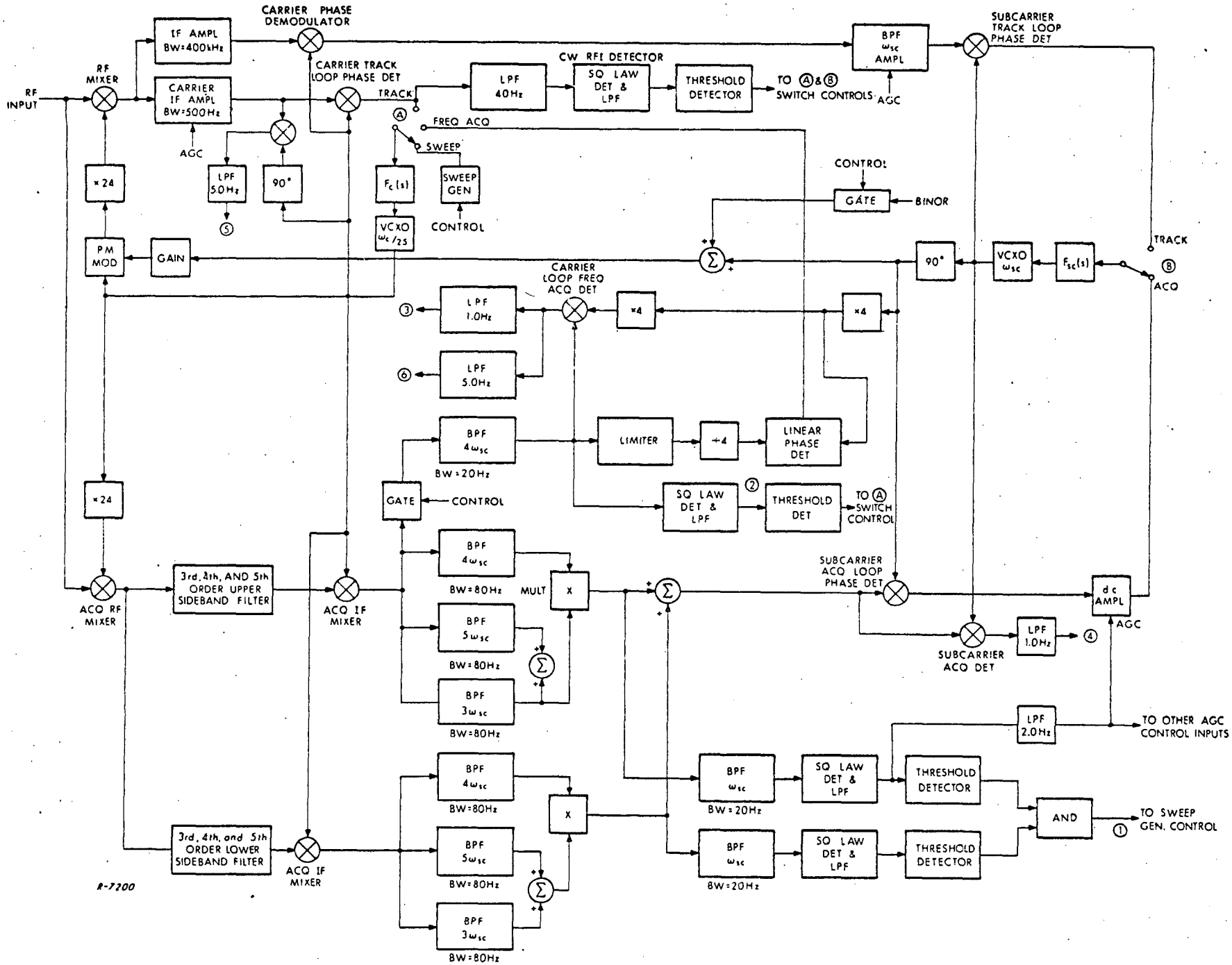

Fig. D.4 DAF Receiver Compound PLL

sideband multiplied the 4th order upper sideband. Second, the lower 3rd, 4th, and 5th order sidebands are utilized as well as the upper sidebands in the modified acquisition scheme. Third, narrower band sideband and subcarrier bandpass filters are used, with a correspondingly slower sweep rate. Fourth, reduction of β from 1 radian to $\pi/4$ radians more than doubles the power in the subcarrier sidebands. Fifth, the bandwidth of the narrowband 4th order upper sideband filter is reduced from 40 Hz to 20 Hz, with the fine sweep rate correspondingly slowed.

With the bandwidth of the sideband filters reduced from 600 Hz to 80 Hz, a degree of discrimination against multipath and RFI is achieved. Further discrimination is obtained by utilizing two coarse sweep acquisition threshold detection systems and stopping the sweep only when both the upper and lower 3rd, 4th, and 5th order sidebands lie inside their respective sideband filters.

The carrier loop frequency acquistion mode does not frequency divide the hard limited 4th order sideband by 4 and phase detect against the subcarrier VCO signal. Rather, it phase detects the hard limited 4th order sideband against the frequency-multiplied-by-4 subcarrier VCO signal. Since the narrowband 4th order sideband bandpass filter is only 20 Hz wide, the total frequency error when the carrier loop is switched to the acquisition mode should be less than the seize frequency. This modified acquisition mode also permits phase acquisition as well as frequency acquisition in this mode. In particular, should a large CW RFI component move into a band ± 40 Hz around one of the the subcarrier sidebands so that it might cause the carrier-tracking loop to lose lock, this fact could be detected by the CW RFI detector shown in Fig. D.4, and both the carrier loop and the subcarrier loop switched to the acquisition mode until the CW RFI sweeps out of this band. This will happen fairly quickly, since the doppler rate between the User and the earth-based RFI is much higher than that between the User and the TDRS. Since the carrier loop can

maintain phase lock in the acquisition mode, the communications link will not be disrupted by the CW RFI. Remember that the subcarrier frequency was selected so that the 4th order upper sideband fell in a clear channel 16 kHz wide. Consequently there is no RFI problem with it. If the RFI component should happen to lie near one of the other subcarrier sidebands used for acquisition, the narrow bandwidth of the subcarrier loop, even in the acquisition mode, will help prevent the CW RFI component from unlocking the subcarrier loop. If the gain of the subcarrier acquisition loop is adjusted so that its noise bandwidth is equal to the track loop value of 0.5 Hz instead of the acquisition value of 2.84 Hz (see Sec. 2.5.3.) during this handover to the acquisition mode, the CW RFI will have even less chance of disrupting the subcarrier loop since it will sweep in and out of the subcarrier loop noise bandwidth too quickly for the loop to respond to it. It is possible to do this since the subcarrier loop is already acquired in this situation.

When the CW RFI detector indicates that the CW RFI is no longer a threat, it switches the loops back to their track modes.

Finally the bandwidth of the carrier IF amplifier may now be reduced from 4 kHz to approximately 500 Hz, since the data sidebands do not have to be passed by this filter. Also, the IF amplifier preceding the carrier phase demodulator is widened to 500 kHz in order to pass the second spectral lobe of the split-phase bit PN-coded data spectrum.

User Transponder Range Tone Tracker

The User transponder range tone tracker replaces various subsystems presently required on board the User in the transponder described in Sec. 2. This modified system also vastly outperforms the subystems it replaces.

The subsystems replaced by this new circuitry include:

1. The uplink data bit synchronizer.
2. The AR sidetone turnaround channel.
3. The downlink telemetry clock, and
4. The downlink subcarrier frequency generator frequency-divider chain.

In addition, this new subsystem performs the functions of:

1. PN code acquisition (chip rate and code acquisition), and
2. Downlink telemetry squarewave subcarrier signal generation.

This obviates the need for a PN code matched filter code acquisition system and a separate downlink telemetry squarewave subcarrier signal generator.

The User transponder range tone tracker is shown in Fig. D.5. The range tone tracker consists of a PLL, which tracks the 6.4 kHz range tone, and associated circuitry as indicated. The 6.4 kHz reference frequency is obtained by frequency-dividing-by-eight the output of a 51.2 kHz VCXO. This approach permits us to obtain coherent signals at 51.2 kHz and at 12.8 kHz. The 51.2 kHz VCXO frequency is hard-limited and utilized as a subcarrier for the downlink telemetry data. The 12.8 kHz and the 6.4 kHz frequencies are utilized in the downlink wideband FM subcarrier frequency generator. The coherent 6.4 kHz reference frequency is successively frequency-divided-by-two down to 100 Hz. Ambiguity resolution is achieved by phase comparison of the 800 Hz and the 100 Hz divider chain frequencies with the 800 Hz and 100 Hz range tones. The dividers are advanced or retarded as necessary to achieve a phase match. The 3.2 kHz and the 1.6 kHz frequencies in the divider chain are also utilized in the downlink wideband FM subcarrier frequency generator.

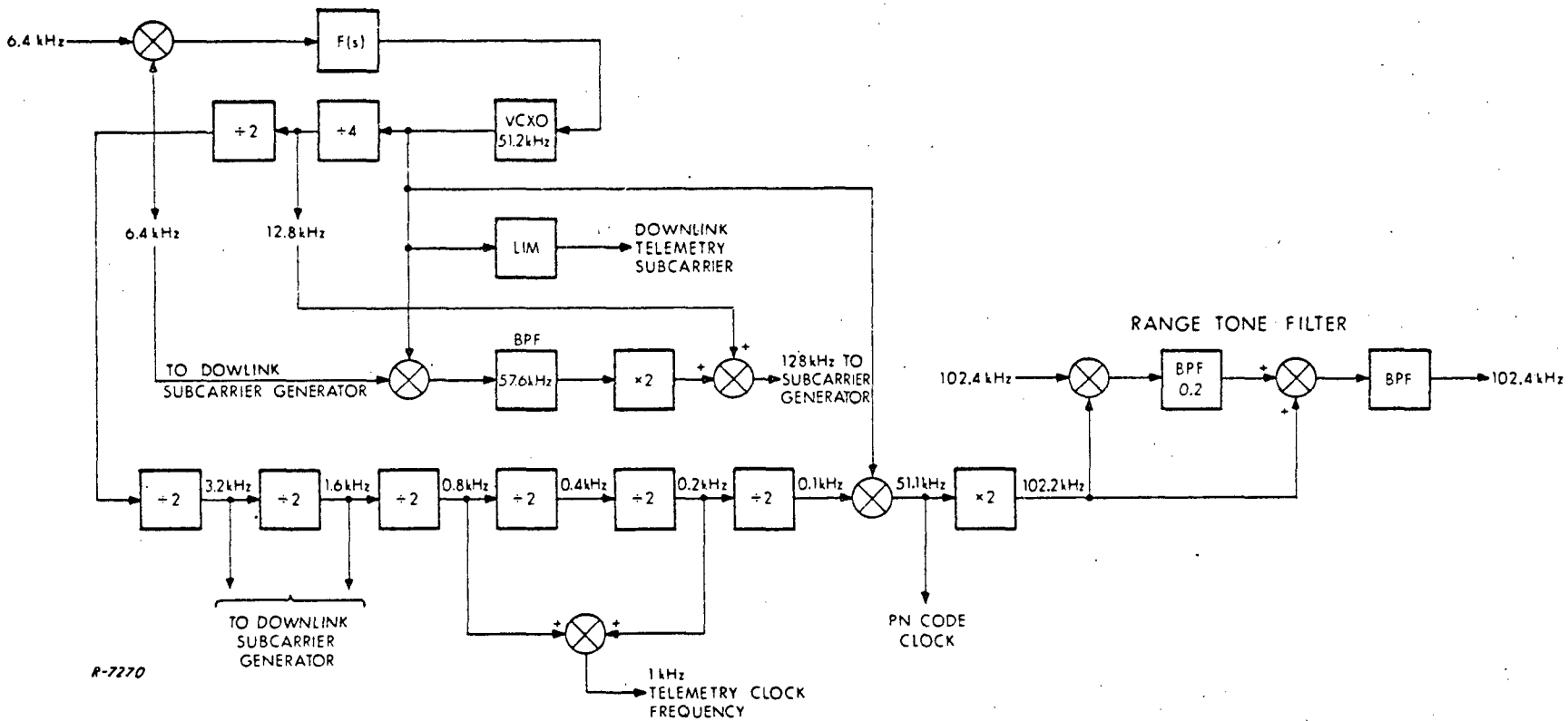

Fig. D. 5 Range Tone Tracker

The 800 Hz and the 100 Hz frequencies in the divider chain are used as the medium coarse and coarse range tones on the downlink. The 6.4 kHz coherent reference frequency is mixed with the 51.2 kHz VCXO frequency to produce a frequency at 57.6 kHz which becomes the medium fine ranging sidetone on the downlink. This frequency is also multiplied by 2 and mixed with the 12.8 kHz frequency to produce a frequency at 128 kHz used in the subcarrier frequency generator.

To demodulate the data, the 51.2 kHz VCXO frequency is mixed with the 100 Hz frequency from the divider chain to produce the 51.1 kHz PN code chip rate clock. This drives the shift register used to generate the local version of the PN code, and also multiplies the locally generated PN code so as to produce split phase bits. The 100 Hz frequency in the divider chain is phase coherent with the PN code and the data, and is used to set the shift register to the proper state so as to make the phase of the locally generated PN code match that of the received PN code. It also provides data bit sync.

The 51.1 kHz frequency is also frequency multiplied by two to produce a signal at 102.2 kHz. This is used to mix the fine range tone frequency down to 200 Hz, where, with essentially all of the doppler removed, it is filtered by a narrowband active BPF. It is then mixed back up to 102.4 kHz by the 102.2 kHz frequency. The difference frequency at 102.0 kHz is rejected by a XTAL bandpass filter centered around 102.4 kHz. The filter bandwidth is wide enough so that the phase shift introduced by the filter when doppler shifts the range tone frequency away from the filter center frequency is small, yet narrow enough to adequately suppress the frequency at 102.0 kHz. A compensating filter may be used in the ground receiver range tone demodulator to compensate for this phase shift.

Finally, the 1 kHz downlink telemetry clock is generated by mixing the 800 Hz and the 200 Hz from the divider chain as indicated in Fig. D.5.

User Transponder Transmitter

The modified User transponder transmitter utilizes a modified wideband FM subcarrier frequency generator but essentially the same downlink carrier modulator as shown in Fig. 2.14. The only difference is that the frequency into the carrier band switch is 1.6 kHz from the divider chain of the range tone tracker of Fig. D.5 rather than 3.2 kHz, and the output frequencies of the carrier band switch are $(f_c/25)/8 \pm 1.6$ kHz rather than $(f_c/25)/8 \pm 3.2$ kHz or $(f_c/25)/8$. That is, only two carrier bands rather than three are utilized. This fact, plus the modification in the uplink carrier frequency which centers the downlink carrier in the 136-138 MHz band better than had been the case previously, permits the utilization of two more subcarrier frequencies at 142.4 kHz and 144.0 kHz, and the elimination of the subcarrier frequency at 110.4 kHz. Consequently the subcarrier frequencies range from 112.0 kHz to 144.0 kHz separated by 1.6 kHz. The subcarrier reference frequency at 128.0 kHz lies at the center of this band of subcarrier frequencies. This fact is utilized in the modified, and simpler, subcarrier frequency generator.

The modified subcarrier generator starts with the frequencies 12.8 kHz, 6.4 kHz, 3.2 kHz, and 1.6 kHz obtained from the range tone tracker divider chain, and generates the frequencies at 6.4 ± 1.6 kHz and 12.8 ± 1.6 kHz and 12.8 ± 3.2 kHz. These frequencies are then mixed with the 128 kHz frequency to produce the subcarrier frequencies.

For example, if the User is assigned the subcarrier frequencies at 128.0 ± 9.6 kHz $\approx$ 137.6 kHz and 118.4 kHz, the frequency at 9.6 kHz is generated by mixing the 12.8 kHz and the 3.2 kHz frequencies to produce the difference frequency at 9.6 kHz. This is then mixed with the 128.0 kHz frequency to produce frequencies at 137.6 and 118.4 kHz.

Downlink Signal Format

The downlink wideband FM signal consists of the coherently transponded carrier PM modulated by the sum of the turned-around 102.4 kHz range tone, the medium fine ranging sidetone at 51.2 + 6.4 kHz = 57.6 kHz, the ambiguity resolution tones at 800 Hz and 100 Hz, and the 1000 BPS telemetry data which is multiplied by the 51.2 kHz squarewave, and wideband FM modulated by a sinusoidal subcarrier. The carrier is shifted to either the upper or lower carrier band by a frequency which is coherent with the range tones and the downlink subcarrier.

As a result of the higher SNR on the downlink (necessary to satisfy the BER for the 1000 BPS data), and as a consequence of the facts that

1. ranging acquisition on the downlink is performed with the telemetry data turned off,
2. the 800 Hz and 100 Hz range tones are sent down to the ground essentially noise free as a result of the ambiguity resolution performed in the User spacecraft transponder,

the downlink range tone phase deviations may be reduced somewhat. It is recommended that tentatively the phase deviations of the range tones on the downlink carrier be chosen as:

$$\rho_1 = 0.5 \text{ radians}$$
$$\rho_2 = 0.4 \text{ radians}$$
$$\rho_3 = \rho_4 = 0.2 \text{ radians}$$

It is also recommended that the phase deviation of the data on the downlink be $\pi/3$ (60°). This should leave sufficient power in the subcarrier sidebands and the fine range tone to permit the range and range rate requirements to be met, and to keep the carrier and subcarrier tracking errors small.

The wideband FM modulation index should be set at $\delta = 5.52$ in order to keep $J_o(\delta) = 0$ and thereby eliminate carrier SSMA interference. As on the uplink, a variation of ± 0.1 radian in this modulation index may be tolerated both in the User transponder transmitter and in the ground receiver wideband FM compound PLL. The distribution of signal powers in the wideband FM subcarrier sidebands for $\delta = 5.52$ is shown in Fig. 2.5.

Ground Receiver Compound PLL

The ground receiver compound PLL is very similar to that of Fig. D.4. The differences are:

1. The sweep generator must be designed to move the carrier loop VCXO into the upper or lower carrier band and sweep only in that band during acquisition.
2. The carrier loop noise bandwidth must be increased slightly to account for two-way doppler dynamics.
3. The subcarrier loop VCXO is replaced by a subcarrier frequency generator driven by a 128.0 kHz VCXO as indicated in Fig. D.6.
4. The acquisition aid circuits and the subcarrier bandpass filters are designed as plug-in units to convert the general receiver into one designed to track a specific subcarrier frequency.

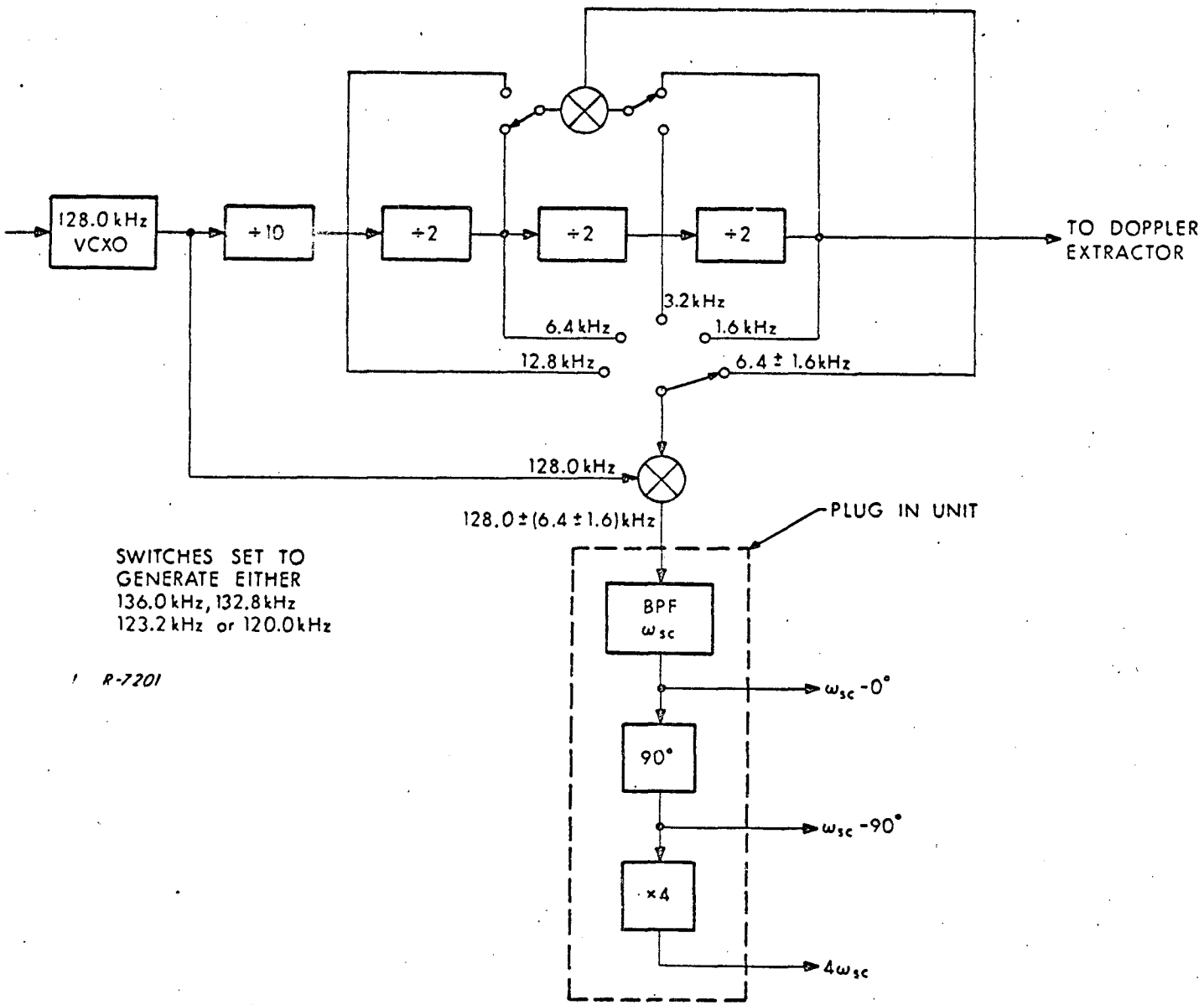
128.0 kHz
VCXO
÷10
÷2
÷2
÷2
TO DOPPLER
EXTRACTOR
6.4 kHz
3.2 kHz
1.6 kHz
12.8 kHz
6.4 ± 1.6 kHz
128.0 kHz
128.0 ± (6.4 ± 1.6) kHz
PLUG IN UNIT
SWITCHES SET TO
GENERATE EITHER
136.0 kHz, 132.8 kHz
123.2 kHz or 120.0 kHz
R-7201
BPF
ωsc
ωsc -0°
90°
ωsc -90°
×4
4ωsc

Fig D6